NASA CR-54640
MRB5007F

Final Report
STUDY OF FUEL CELLS USING STORABLE ROCKET PROPELLANTS

28 January 1964 to 29 January 1965

by

J. C. Orth, L. F. Athearn, R. E. Chute, R. F. Drake,
R. Havlin, K. W. Klunder, S. Matsuda, W. H. Power,
J. O. Smith, and P. L. Terry

prepared for

NATIONAL AERONAUTICS AND SPACE ADMINISTRATION

9 March 1965

CONTRACT NAS 3-4175

Technical Management
NASA Lewis Research Center
Cleveland, Ohio
Space Power Systems Division
Robert B. King, Technical Manager

MONSANTO RESEARCH CORPORATION
BOSTON LABORATORY
Everett, Massachusetts 02149
Tel: 617-389-0480

ABSTRACT

N66-21001

Fuel cells are described that operate with storable rocket fuels as reactants. Electrodes were developed and demonstrated for N_2H_4 and H_2 fuels and HNO_3, N_2O_4, O_2, and ClF_3 oxidizers. A full cell of the type $N_2H_4/KOH/O_2$ was operated for over 2285 hours at 25°C, 100 ma/cm^2, with a voltage of 0.6-0.7 v. Oxygen pressure was one atmosphere absolute. Another full cell of the type $N_2H_4/H_3PO_4/N_2O_4$ was operated for over 645 hours at 60°C, 100 ma/cm^2, with a voltage of 0.65-0.75 v. System designs for 1-kw units using these cells were developed. Both units were 1.3 ft^3 in volume, the alkaline-O_2 unit had an indicated weight of 45 lb; the acid-N_2O_4 system weight was 67 lb. Ion exchange membrane cells were investigated. A N_2H_4/ion exchange membrane/HNO_3 cell with both reactants dissolved in H_3PO_4 was operated for 30 hours at 60°C and 100 ma/cm^2 with a voltage of approximately 0.5 v. The feasibility of steam reforming unsymmetrical dimethyl hydrazine and monomethyl hydrazine to a H_2-rich (43 mole-%) feed stream for a fuel cell was demonstrated.

Author

TABLE OF CONTENTS

TABLE OF CONTENTS (Cont'd)

TABLE OF CONTENTS (Cont'd)

LIST OF REPORT AND APPENDIX TABLES

List of Report and Appendix Tables (Cont'd)

List of Report and Appendix Tables (Cont'd)

LIST OF REPORT AND APPENDIX FIGURES

List of Report and Appendix Figures (Cont'd)

Appendix Figures

List of Report and Appendix Figures (Cont'd)

List of Report and Appendix Figures (Cont'd)

List of Report and Appendix Figures (Cont'd)

List of Report and Appendix Figures (Cont'd)

List of Report and Appendix Figures (Cont'd)

I. INTRODUCTION

A. OBJECTIVES

This is the second stage of an investigation of fuel cells operating on storable rocket propellants as reactants.

B. PREVIOUS WORK

At the end of the initial contract (NAS3-2791), the following accomplishments were reported (ref. 1).

1. The thermodynamic properties of reactants and reaction products of interest in the project were calculated and tabulated for 25 and 90°C. The hydrazine/dinitrogen tetroxide system was found to be endothermic when operating reversibly.

2. Hydrazine was found to be an excellent electrochemical fuel on short-term tests in both acid and alkaline electrolytes. Nitrogen and water were the exclusive oxidation products. Chemically precipitated ruthenium and iridium-ruthenium were the preferred catalysts in this work.

3. Neither monomethyl nor unsymmetrical dimethyl hydrazine performed very well on any of the catalysts used in the study.

4. Both nitric acid and dinitrogen tetroxide were found to be electrochemically active oxidants. Uncatalyzed carbon was selective for the reduction of both oxidants. Nitric oxide was the exclusive reduction product with nitric acid.

5. Initial full-cell studies demonstrated the feasibility of using hydrazine as an electrochemical fuel and nitric acid, dinitrogen tetroxide, or hydrogen peroxide as oxidants.

6. The anodic oxidation of hydrazine and the cathodic reduction of chlorine trifluoride were demonstrated in anhydrous hydrogen fluoride and in melts of potassium fluoride-hydrogen fluoride. Anodic polarization in HF: 0.5 v at 5 ma/cm^2; in HF-KF, 0.5 v at 100 ma/cm^2. Cathodic polarization in HF: 0.5 v at 20 ma/cm^2; in HF-KF, 0.5 v at 5 ma/cm^2.

7. Anhydrous organic solvents with dissolved conducting salts were investigated as electrolytes for dinitrogen tetroxide/hydrazine cells. The results were not sufficiently promising to warrant follow-up. Anodic polarization: 0.5 v at 10 ma/cm^2; cathodic polarization, 0.5 v at 70 ma/cm^2.

C. SCOPE OF THIS REPORT

This report describes the development of operating fuel cells that use storable rocket propellants as reactants. System requirements are analyzed for fuel cells using these fuels and oxidants. Also described are the development of suitable electrodes and the construction and testing of full cells using storable propellants as fuels and oxidants. System designs for 1-KW units using the systems $N_2H_4/KOH/O_2$-H_2O_2 and $N_2H_4/H_3PO_4/N_2O_4$ are given. Life tests of the $N_2H_4/KOH/O_2$ and $N_2H_4/H_3PO_4/N_2O_4$ cells are reported. Results of monomethylhydrazine and dimethylhydrazine reforming studies are presented. Nonaqueous systems that use chlorine trifluoride as an oxidant and hydrazine or hydrogen as fuel are described.

D. OVER-ALL RESULTS

1. The hydrazine/oxygen alkaline electrolyte cell operates at low temperature, has demonstrated long life (over 2285 hours at 100 ma/sq cm, 25°C, 0.6-0.7 v), and operates on oxygen at atmospheric pressure with high electrode efficiencies (about 90%). (See Section IV D, page 44).

2. The hydrazine/dinitrogen tetroxide acid electrolyte cell ran over 645 hours at 100 ma/sq cm, 60°C, 0.65-0.75 v, with reproducible performance. The oxidant was at atmospheric pressure. (See Sec. IV C, page 34).

3. Reasonable weight and volume power densities appear to be obtainable from systems using these two cells. (For the alkaline cell, 45 lbs and 1.3 cu ft per kilowatt; for the acid cell, 67 lbs and 1.3 cu ft per kilowatt. Both include all accessories except oxidant supply and tankage). (See Appendixes XI, XII, pages 269 and 299).

4. The MRD-C electrodes were developed initially in other work at MRC, and have been applied to this contract. They are composed of carbon in a Teflon matrix, with or without catalysts, and are the most promising cathodes among those tested. With platinum catalyst these electrodes are active on oxygen, air, and hydrogen peroxide. Double thicknesses of uncatalyzed MRD-C electrodes have operated near reversible potentials on nitric acid and dinitrogen tetroxide, and are selective for the reduction of these oxidants in the presence of substantial amounts of hydrazine. (See Sec. III B, page 11).

5. The best anode for the oxidation of hydrazine in acid electrolytes is the MRD-A electrode, composed of platinum black in a Teflon matrix. This liquid diffusion anode is selective for the oxidation of hydrazine in the presence of as much as 1M nitric acid. (See Sec. III C, page 17).

6. Palladium catalyzed nickel plaque is the preferred liquid diffusion anode in hydrazine/oxygen alkaline electrolyte cells. This anode has operated over 2200 hours with coulombic efficiencies over 90%. (See Sec. III C, page 17

7. The best solid palladium hydrogen diffusion electrode tested was prepared by annealing, rhodium plating, and oxidizing 1-mil Pd-25% Ag foil. This anode can be used with either hydrogen or hydrazine fuel and has operated continuously on hydrogen as an anode for more than two weeks. (See Appendix III, page 119).

8. Ion exchange membranes show some promise as separators in acid electrolyte cells, but a better separator is a gel made from Santocel®FR-C colloidal silica and H_3PO_4. Cells with acid catholytes and alkaline anolytes separated by an ion exchange membrane have limited life. (See Sec. IV E, F, pages 54 and 55).

9. The catalytic reforming of monomethylhydrazine and dimethylhydrazine is a practical way to obtain hydrogen-rich feed gas for fuel cells. The reforming of monomethylhydrazine with palladium, iridium, and ruthenium-iridium catalysts in series gave a high yield of hydrogen (48%). (See Sec. V, page 59).

10. The system $ClF_3/HF(KF)/H_2$ was demonstrated as a full cell. Hydrazine and several active metals are good anodes in this new electrochemical system. Any practical cell design awaits the development of electrodes that will effectively establish electrolyte-reactant boundaries, and prevent mixing of the high-energy fuel and oxidant. (See Appendix VI, page 229).

II. ANALYSIS OF SYSTEM REQUIREMENTS AND PROJECT STATUS

A. BACKGROUND

Development of a fuel cell operable on storable rocket fuels and oxidizers necessarily proceeds through the following steps:

(1) Conception, construction, and characterization of electrodes for each potential reactant.

(2) Semi-optimization of each half-cell electrode for maximum catalytic effect and life.

(3) Integration of half cells into compatible fuel-oxidizer pairs in full-cell assemblies.

(4) Combination of multiple full cells into an operating battery system.

Under this contract, electrodes and catalysts capable of operation on several different reactants have been developed. These developments correspond to the first two steps listed above. Full cells have been constructed and successfully operated for extended periods of time, fulfilling the third step. System designs submitted for two separate nonspace applications represent a promising start on the fourth step. The following discussion will serve as a definition of problems, an exposition of storable propellant fuel cell possibilities, and a summary of project status. The details of the work done in all four areas above are covered in subsequent sections of this report.

B. POTENTIAL REACTANTS

The advantages of operating space fuel cells on storable propellants are: (1) the availability of reactants during space missions, (2) the weight and volume reduction that may be realized because separate reactant tankage is not required, (3) the potentially high power densities due to the high energy content of the reactants, and (4) the favorable heat effects caused by the endothermic nature of some of the reactions involved. It is felt that modules developed using these systems would be adaptable to a variety of space and terrestial missions where propellants are a major energy source.

The fuels and oxidizers discussed below have been evaluated on various electrode types in this work and a reasonable degree of fuel cell utilization is judged possible.

1. Hydrazine (N_2H_4)

This compound, used either as the pure monohydrate ($N_2H_4 \cdot H_2O$) or in solution with an electrolyte, is a highly reactive electrochemical fuel. It can be used in either acid or basic electrolyte systems with almost equal polarization performance. The mono- and dimethyl hydrazine derivatives are of considerable value as rocket propellants. Unfortunately, however, we have found that they oxidize electrochemically with difficulty and with considerable inefficiency. They can be used indirectly, however, when suitably reformed to a H_2-rich gas mixture.

2. Hydrogen

Hydrogen is the classic electrochemical fuel. Its use on several electrode types has been demonstrated in this laboratory.

3. Reformer Gases

These are H_2-rich gas streams of varying composition formed by catalytic and/or steam reforming of hydrocarbons, hydrocarbon derivatives, or NH_3. Because of CO_2 concentrations ordinarily associated with such mixtures, basic electrolytes are not preferred because of carbonate formation. Only with a Pd membrane anode could a basic electrolyte be employed on CO_2-containing fuel gases, unless an electrolyte regeneration system is available.

4. Oxygen

In some cases oxygen is considered a storable oxidizer and is of interest to this program. No large-scale program on O_2 cathodes has been undertaken on this contract because a Monsanto cathode (developed in other work at this laboratory) is available for use with O_2(MRD-C Pt/carbon).

5. Nitric Acid (HNO_3)

Nitric acid oxidant undergoes cathodic reduction rather easily to form NO and H_2O. This electroreduction can be accomplished on several different electrode types with only limited polarization at high current densities. Because HNO_3 is so easily reduced, its contact with the opposing anode must be prevented, or at least heavily curtailed, to prevent driving the anode to cathodic (positive) potentials. The HNO_3 catholyte can best be physically separated from the anode by use of an ion exchange membrane, or other relatively positive separator, or a HNO_3 diffusion-limiting device in the cathode itself. We believe the diffusion-controlled cathode offers the best chance for success, but is necessarily a more complicated electrode and may have to be tailored for a given mission.

6. Dinitrogen Tetroxide (N_2O_4)

In addition to HNO_3, N_2O_4 can be utilized as a fuel cell oxidizer. The same requirements of physical separation of N_2O_4-contaminated electrolyte from the anode hold; again the gas diffusion electrode affords the most logical solution.

7. Hydrogen Peroxide (H_2O_2)

Hydrogen peroxide is of some interest as a storable oxidant. Because of rapid chemical decomposition of H_2O_2 in acid and in alkaline electrolytes at fuel cell operating temperatures, the choice of a diffusion electrode in this service is indicated, utilizing the most stable pH solution as the diffusion source.

C. ELECTRODE TYPES

Seven different electrode types have been selected as usable in a storable reactant fuel cell. There are four anode and three cathode types.

1. Anodes

a. Catalyzed Ni or Stainless Steel Porous Plaque

These are sintered powder porous plaques, of the type used extensively in Ni-Cd batteries. Thickness ranges from 15 to 60 mils. Porosity varies from 25% to 75%. Catalysts are deposited by chemiplating or electroplating. Applications considered for this work were as N_2H_4-in-KOH liquid diffusion anodes in contained basic electrolyte cells. Only stainless steel plaques can be used in acid electrolyte.

b. Pd-25% Ag Solid H_2 Diffusion Anode

Thin Pd-Ag foils with special surface and heat treatments show some promise as anodes for storable reactant fuel cells. At present, because they are attacked by HNO_3, they can be used only in cells operating on O_2 or H_2O_2 oxidants. An electrode life of at least 300 hours has been established with H_2 as a fuel. Where CO_2-containing reformer gases are used as fuel, the Pd-Ag anode permits use of a basic electrolyte without the problem of carbonate formation in the electrolyte.

c. Platinized Pt Screen Anode

Solution-type anodes for use with N_2H_4 in acid electrolyte can be made by depositing Pt black on a 100 to 200 mesh screen. Low polarization is obtained at current densities up to 100 ma/cm^2. This electrode is indicated in ion exchange membrane fuel cells operating on N_2H_4 and HNO_3. Because they give only limited performance as gas electrodes, the platinized Pt screen anode is not applicable to a universal fuel cell operating on a full range of fuels and oxidizers.

d. MRD-A Type Anode

This electrode is a thin, screen-supported, membrane electrode developed at Monsanto Research Corporation. Basically it is composed of noble metal blacks in a polytetrafluoroethylene matrix. Details on construction and performance of this electrode are given in a current report (ref. 1). The MRD-A type can be formulated as a liquid or gas diffusion anode. It has been used extensively in acid full-cell work accomplished under this contract.

2. Cathodes

a. MRD-C Type Cathode

This is the cathode analog of the MRD-A type previously described. It is composed of carbon black in a polytetrafluoroethylene matrix. Various catalysts may be incorporated in the structure for special applications. With Pt catalysts we have used this electrode extensively in basic electrolyte cells as an O_2 cathode.

b. HNO_3/N_2O_4 Diffusion Limiting Cathodes

The solubility of these reactants and the polarizing effect of the dissolved contaminants on the anode dictate physical separation. Electrode structures which limit the diffusion of the reactant have helped to accomplish this requirement and several modifications have been evaluated. Double thicknesses of uncatalyzed MRD-C cathodes have performed the best.

c. Solution Type Cathode

Porous carbon block or platinized Pt screen serve as adequate solution cathodes for HNO_3 reduction. Such electrodes may be used with ion exchange membrane fuel cells.

D. CELL TYPES

Classification of fuel cells by electrolyte and electrolyte disposition is a convenient way to select the best fuel cell device for storable reactants.

1. Ion Exchange Membrane - Acidic Cathode/Basic Anode

Some work on this system, employing HNO_3 and N_2H_4 in KOH, has been done. The disadvantages of this cell type are limited life because of membrane deterioration and excessive consumption of electrolyte by the neutralization reaction.

2. Ion Exchange Membrane - Acid/Acid

In this case the N_2H_4 fuel was dissolved in 5M H_3PO_4, and the oxidant was 5M HNO_3. Various cation exchange membranes and electrodes were evaluated. The major dissadvantage is the high membrane resistivities which cause excessive IR voltage losses in operating cells. One membrane was found which performed reasonably well and it may be possible to develop it further.

3. Free Electrolyte - Acid or Base

If electrodes are available that are essentially "wet-proof" to the electrolyte (that is, permit no gross transfer of electrolyte through the electrode) free electrolyte cells offer certain advantages. Since the free electrolyte cell implies circulation of the electrolyte, heat transfer and water removal problems can be simplified. IR voltage losses can be minimized in this construction and concentration polarizations alleviated. There are problems associated with the free electrolyte--primarily cell and electrode sealing and uniform pumping of electrolyte through the very narrow electrolyte space. We believe that the MRD-A and MRD-C electrodes can be made "wet-proof" and adequately sealed in a cell. Little work has been done with this configuration under this contract.

4. Contained Electrolyte - Acid or Base

Physical stabilization of electrolyte in a gelled structure or a porous mat (asbestos, polypropylene fiber) offers advantages in fuel cell construction. By limiting the amount of electrolyte contained originally, electrodes can be started and operated without excessive flooding. With gaseous reactants, transfer and mixing of gases can be prevented by using capillary membranes such as asbestos. With gas electrodes, water must be removed by recycling the gas streams or by using an auxiliary vacuum evaporation chamber with each cell. Heat removal is somewhat more complex for a cell operating on both gaseous fuel and oxidizer.

The two cell systems most fully developed in this work use contained electrolytes: the hydrazine/oxygen system, with the KOH electrolyte contained in an asbestos membrane or polypropylene felt; and the hydrazine/dinitrogen tetroxide system, with phosphoric acid electrolyte contained in a colloidal silica gel. Both cell systems have been operated with respectable electrical performance for extended periods, at relatively low temperatures, and with little deterioration in performance.

E. SYSTEM DESIGNS

The successful construction and operation of the acid and alkaline cells described above and their subsequent characterization culminated in the submission of two nonspace NASA system designs (Appendixes X and XI).

III. ELECTRODE DEVELOPMENT

A. BACKGROUND

The general requirements for electrodes operating on storable propellant reactants are: (1) selective catalytic activity for the specific electrode reactions, (2) control of the electrode-electrolyte interface, (3) chemical stability in the operating environment, (4) adequate mechanical strength and good sealing properties, and (5) simple and reproducible fabrication. The development of electrodes with these characteristics was the key to the successful operation of full cells. For this reason a fairly broad range of electrode types were intensively investigated on this contract.

B. CATHODES

In Table 1 we have summarized the four types of cathodes investigated and have shown their activities on oxidants of interest to the program. Where possible the data refer to actual measurements of electrode potentials in operating full cells.

1. MRD-C Platinum/Carbon Cathodes

The highly successful MRD-C electrode, consisting of carbon and catalyst, dispersed in a Teflon matrix and pressed onto a metal grid (ref. 2) can be formulated for using either liquid or gaseous oxidants. These electrodes were not developed under this contract, but they proved to be the best choice among the cathodes tested. The results of operating this electrode on oxygen, hydrogen peroxide, and air in contained alkaline electrolyte full cells are given in a later section of this report, and are summarized in Table 2. In general, this cathode possesses the following advantages:

a. Simple and reproducible fabrication, rugged and durable, with good sealing properties.

b. Active electro-reduction of oxygen at room temperature at high potentials at zero psig and little purging required.

c. Demonstrated long life.

d. Capable of operating on several different oxidizers.

This electrode is the preferred cathode for the hydrazine/oxygen alkaline cell.

Table 1

CATHODE SUMMARY

Type	Structure	Activity		Life	Remarks
MRD-C Pt/Carbon	Screen-supported membrane of carbon black in Teflon matrix with approximately 10 mg Pt/in.^{2} as catalyst	O_2 in KOH electrolyte: H_2O_2 in " " Air " "	0.70-0.80 v vs SHE at 100 ma/cm^2, 25°C	> 2200 hours in KOH electrolyte on O_2, 25°C	Preferred cathode in O_2/H_2O_2 basic cells. Operates at 0 psig O_2, very light purge of O_2. Proprietary Monsanto electrode.
MRD-C Double Carbon	Screen-supported membrane of carbon black in Teflon matrix. Latest modification: Two single electrodes pressed together at 2660 psi.	N_2O_4 in H_3PO_4 electrolyte: HNO_3 in H_3PO_4 electrolyte:	0.95 v vs SHE at 100 ma/cm^2, 30°C 0.92 v vs SHE at 100 ma/cm^2, 90°C	> 600 hours in H_3PO_4 electrolyte on N_2O_4, 60°C	Preferred cathode in N_2O_4/HNO_3 acid cells. Operated at 0 psig N_2O_4, will tolerate substantial quantities of NO but requires high local gas velocities.
Solution Cathode	Porous carbon block or Platinized Pt screen	HNO_3 in acid electrolyte:	0.80-1.05 v vs SHE at 100 ma/cm^2, 90°C	--	Can be used only with ion exchange membranes to prevent reactant mixing.
Porous Teflon Vapor Diffusion Cathode	Carbon powder or block with various diffusion control barriers using Teflon powder or porous sheet	HNO_3 with H_3PO_4 electrolyte	0.80-1.05 v vs SHE at 100 ma/cm^2, 90°C	--	Problems with sealing of electrodes, fragility and reproducibility of diffusion rates.

2. MRD-C Double Carbon Cathodes

This electrode consists of double thicknesses of uncatalyzed carbon in a polytetrafluoroethylene matrix pressed onto a metal screen. It was applied as a nitric acid or dinitrogen tetroxide cathode. With these reactants it is necessary to limit the solution of the oxidant in the electrolyte by diffusion control. This is accomplished by increasing the thickness of the electrode, and in later modifications by densifying the carbon-polymer matrix by cold-pressing. The results of operating this cathode in contained acid electrolyte full cells are given in a later section of this report, and are summarized in Table 3. The advantages of this electrode are:

a. Simple and reproducible fabrication, rugged and durable with good sealing properties.

b. Near reversible electro-reduction of nitric acid and dinitrogen tetroxide at reasonable temperatures and zero psig.

c. Demonstrated long life.

This type of electrode is the preferred cathode for the hydrazine/dinitrogen tetroxide/acid electrolyte cell.

3. Solution Cathodes

These electrodes operate completely flooded with solutions containing dissolved reactants, in this case nitric acid. In the first contract much half-cell work was done with solution cathodes. In this contract, platinized platinum screen cathodes were used in ion exchange membrane full cells, and this work is described later in the report. In general, this electrode promotes the electro-reduction of nitric acid with little polarization, but there are severe practical limitations to its use in full cells. The main limitations are reactant mixing and subsequent polarization of the opposite electrode. Ion exchange membrane cells appear to offer the best application for this electrode.

4. Porous Teflon Vapor Diffusion Cathodes

Early in our work we realized the importance of limiting the amount of soluble oxidant at the electrode-electrolyte interface. Accordingly, much effort was expended to gain diffusion control. This work culminated in the application of the MRD-C double carbon electrodes for acid cells. Prior to this, we investigated electrodes employing various forms of Teflon to limit diffusion.

Table 2

PERFORMANCE OF MRD-C Pt/CARBON CATHODES IN FULL CELLS

Oxidant	Temperature	Current Density ma/cm² 0	50	100	150	200
O_2	25°C	0.97	0.88	0.78	0.65	0.52
H_2O_2	25°C	0.98	0.88	0.78	0.60	-
Air	75°C	0.98	0.82	0.70	0.50	-

Cathode: MRD-C
10 mg Pt/cm² on carbon on Pt screen
Electrolyte 5MKOH
Data are potential vs SHE

Table 3

PERFORMANCE OF MRD-C DOUBLE CARBON CATHODES IN FULL CELLS

Oxidant	Temperature	Current Density ma/cm² 0	50	100	150	200
HNO_3	90°C	1.15	0.95	0.89	0.80	0.68
N_2O_4	60°C	1.10	1.00	0.96	0.91	0.88

Electrolyte: $5MH_3PO_4$-Santocel FR-C gel
Cathode: Double carbon MRD-C
Data are potential vs SHE

a. Carbon Powder-Teflon Powder Mixture Pressed Into Porous Teflon Sheet

This structure did demonstrate vapor diffusion characteristics. The porous Teflon, distorted by the bonding operation, caused too low a diffusion rate of nitric acid vapor, and consequently too low cathodic current and poor reproducibility.

b. Porous Carbon Block-Porous Teflon Sheet Cathodes

The limiting feature of this type of construction is the formation and reproducibility of the carbon-Teflon bond. We discontinued work on this cathode, pending development of more promising structures.

c. Teflon Powder Bonded to Porous Carbon Block

The ease of construction of this cathode made it preferable to the porous Teflon sheet-carbon block electrode. Decreasing diffusion with increasing Teflon loading was demonstrated. We discontinued development work on this cathode after the more promising strength and sealing characteristics of the MRD-C type electrode became apparent.

Further details on this electrode work will be found in Appendix I.

5. Selectivity of Carbon as a Nitric Acid Catalyst

In order to operate effectively in full cells with hydrazine fuel the cathode must tolerate substantial amounts of hydrazine contaminant in the electrolyte. As shown in Table 4, carbon electrodes will tolerate at least 0.5M hydrazine without significant reduction in performance. Further details are given in Appendix I.

Table 4

ANODE AND CATHODE POLARIZATION TESTS SHOWING CATALYSTS' SELECTIVITY

Reactants		Current Density	Potential vs SHE* Electrode Material								
			FC-13		FC-14		Pt on FC-14		Ru on FC-14		
N_2H_4	HNO_3	ma/cm²	30°C	90°C	30°C	90°C	30°C	90°C	30°C	90°C	Notes
None	5M	0	1.14	1.13	1.10	--	1.11	--	1.12	--	All tests run as cathode
		10	1.10	1.11	1.08	--	1.08	--	1.07	--	
		20	1.09	1.10	1.07	--	1.07	--	1.06	--	
		50	1.07	1.09	1.05	--	1.05	--	1.05	--	
		100	1.05	1.07	1.02	--	1.03	--	1.04	--	
0.1M	5M	0	1.12	1.14	1.06	--	0.42	--	1.06	--	Pt on FC-14 tested as anode
		10	1.10	1.13	1.04	--	--	--	1.05	--	
		20	1.09	1.12	1.03	--	--	--	1.05	--	
		50	1.07	1.11	1.02	--	--	--	1.04	--	
		100	1.06	1.10	1.00	--	--	--	1.03	--	
0.3M	5M	0	--	--	1.03	1.07	0.34	0.32	0.68	0.67	Ru on FC-14 would not function as anode or cathode.
		10	--	--	1.02	1.07	0.53	0.36	--	--	
		20	--	--	1.01	1.07	--	0.43	--	--	
		50	--	--	0.98	1.06	--	0.49	--	--	
		100	--	--	0.95	1.04	--	0.59	--	--	
0.5	5M	0	1.11	1.10							
		10	1.09	1.10							
		20	1.08	1.10							
		50	1.06	1.09							
		100	1.03	1.08							

* SHE - Standard Hydrogen Electrode (a_{H^+} = 1) (SCE = 0.24 volt). This reference was used since the exact value of HE (hydrogen electrode at same temperature and pH) cannot be calculated, but should be close to SHE.

C. ANODE DEVELOPMENT

The three types of anodes investigated in this contract are summarized in Table 5, with demonstrated activities on various fuels of interest. Descriptions of each electrode type, catalyst study experiments, and hydrazine fuel cracking experiments follow:

1. MRD-A Pt Anodes

These electrodes are analogous to the MRD-C cathodes described earlier. They are screen-supported membranes of catalyst metal blacks in a Teflon matrix, and can be formulated as gas or liquid diffusion electrodes. Although these electrodes were not developed under this contract they were easily adapted for use with storable propellant fuels, and proved to be excellent electrodes in full cells. The results of operation on hydrazine fuel in both acid and alkaline full cells are given later in this report. Half-cell testing on hydrazine and hydrogen is presented in Table 6, and indicates the excellent activity of this anode. In general, this anode has been shown to possess the following advantages:

a. Simple and reproducible fabrication

b. Rugged and durable with good sealing properties

c. Active electro-oxidation of both hydrogen and hydrazine at reasonable temperatures

d. Demonstrated long life (over 600 hours).

e. Capable of operating in both acid and alkaline electrolytes.

This electrode is the preferred anode in hydrazine/dinitrogen tetroxide acid full cells.

2. Palladized Nickel Plaque Anode

These electrodes, composed of porous, sintered nickel plaques of the type commonly used in nickel-cadmium secondary batteries, were adapted specifically for use in alkaline contained electrolyte cells as liquid diffusion anodes. In the work described here palladium catalyst is deposited in the plaque by chemiplating from solution. These electrodes have been used extensively as anodes in hydrazine/oxygen alkaline cells. The results are reported in a later section of this report. A typical polarization curve is presented in Figure 1.

Table 5

ANODE SUMMARY

Type	Structure	Activity		Life	Remarks
MRD-A Pt	Screen-supported membrane of Pt black in Teflon matrix-60 mg Pt/in²	H_2 with H_3PO_4 electrolyte	0.0v vs SHE at 100 ma/cm², 90°C	>600 Hours at 60°C	Preferred anode in N_2H_4, N_2O_4 acid cells
		H_2 with KOH electrolyte	0.0 v vs HE (same solution) at 100 ma/cm², 90°C		
		N_2H_4 with H_3PO_4 electrolyte	0.1 v vs SHE at 100 ma/cm², 60°C		
		N_2H_4 with KOH electrolyte			
Pallidized Nickel Plaque	Sintered nickel plaque*, 30 mils thick, chemi-plated with palladium black 1.5-3.0 mg Pd/cm²	N_2H_4 with KOH electrolyte	0.05 v vs HE (same solution) at 100 ma/cm², 25°C	>2200 hours at 25°C	Preferred anode in N_2H_4/O_2 alkaline cells
Solid palladium diffusion anode	Pd-25% Ag foils, 1 mil thick, with special surface treatment.	N_2H_4 in KOH electrolyte	0.08 v vs HE at 100 ma/cm², 90°C	300 hours at 90°C	Stress cracking limits life
		H_2 in KOH electrolyte	0.1 v vs HE at 250 ma/cm² 90°C	300 hours at 90°C	

* Gould National Batteries, Inc.

Table 6

MRD-A Pt ANODE POLARIZATION

Fuel		Anode Potential vs SHE at Indicated Current Density (ma/cm^2)			
		0	100	300	500
100% $N_2H_4 \cdot H_2O$	85% H_3PO_4	-0.01	-0.01	+0.02	+0.09
1M N_2H_4 in 43% H_3PO_4	43% H_3PO_4	+0.17	+0.22	+0.36	+0.48
H_2	85% H_3PO_4	0	0	+0.01	+0.03
H_2	5M KOH	0	+0.01	+0.02	+0.02

Half cell testing
All potentials IR free
Temperature = 90°C
Electrode Area = 1 cm^2

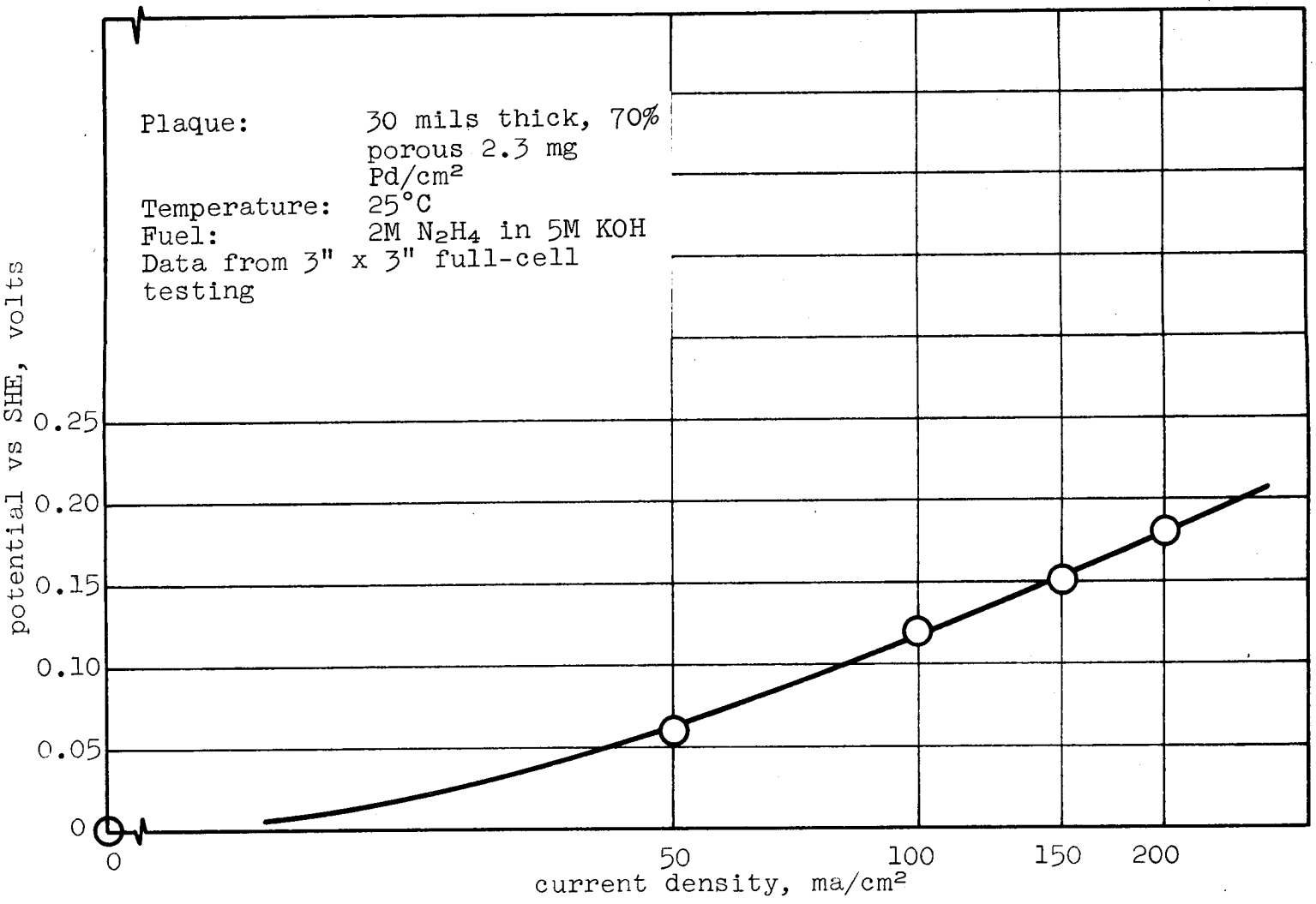

Figure 1. Polarization of Palladized Nickel Plaque Anode

The advantages of this electrode are:

a. Readily available, simple catalytic treatment, rugged with good sealing properties.

b. Active electro-oxidation of hydrazine at high coulombic efficiencies (above 90%) at room temperature.

c. Demonstrated long life (over 2200 hours).

d. Can be tailor-made for different applications; the plaques are available in thicknesses ranging from 16 to 60 mils with porosity from 25 to 75%.

Palladized plaques of 70% porosity, 30 mils thick, are the preferred electrode for the hydrazine/oxygen alkaline cell.

3. Solid Palladium Diffusion Anode

These electrodes are thin metal foils (1 mil) of Pd-25% Ag alloy specially treated for electrode activity. Since the palladium is attacked by nitric acid they are useful only in alkaline cells. However, the selective transport of hydrogen through these anodes makes them attractive for use with "dirty" hydrogen (such as are produced from the reforming of methyl hydrazines) in alkaline electrolyte cells where the carbon dioxide in the stream would ordinarily cause carbonation of the electrolyte. For this reason much work was done to adapt these foils for use as anodes, and the details are reported in Appendix III. The necessary special treatments involved annealing in argon, rhodium plating, followed by oxidation at high temperature in pure oxygen. Substantial activity with hydrogen fuel, with life of at least 300 hours, has been demonstrated with this anode. Hydrazine, however, appeared to cause stress cracking of the foil after 2-3 days of service. Typical polarization curves are presented in Figure 2, and indicate the potential utility of this type of anode.

4. Externally Decomposed Hydrazine

Hydrazine can be catalytically decomposed to hydrogen and nitrogen gases at room temperature. Such external decomposition of hydrazine is an alternate procedure to the direct use of aqueous hydrazine at a fuel electrode, by which either a hydrogen/nitrogen gas mixture or pure hydrogen could be supplied to the anode. Experimental reforming experiments are given in Appendix II.

5. Selectivity of Platinum for Hydrazine Oxidation

Because of the difficulty of entirely preventing cross contamination of oxidant and reductant in a soluble reactant fuel cell,

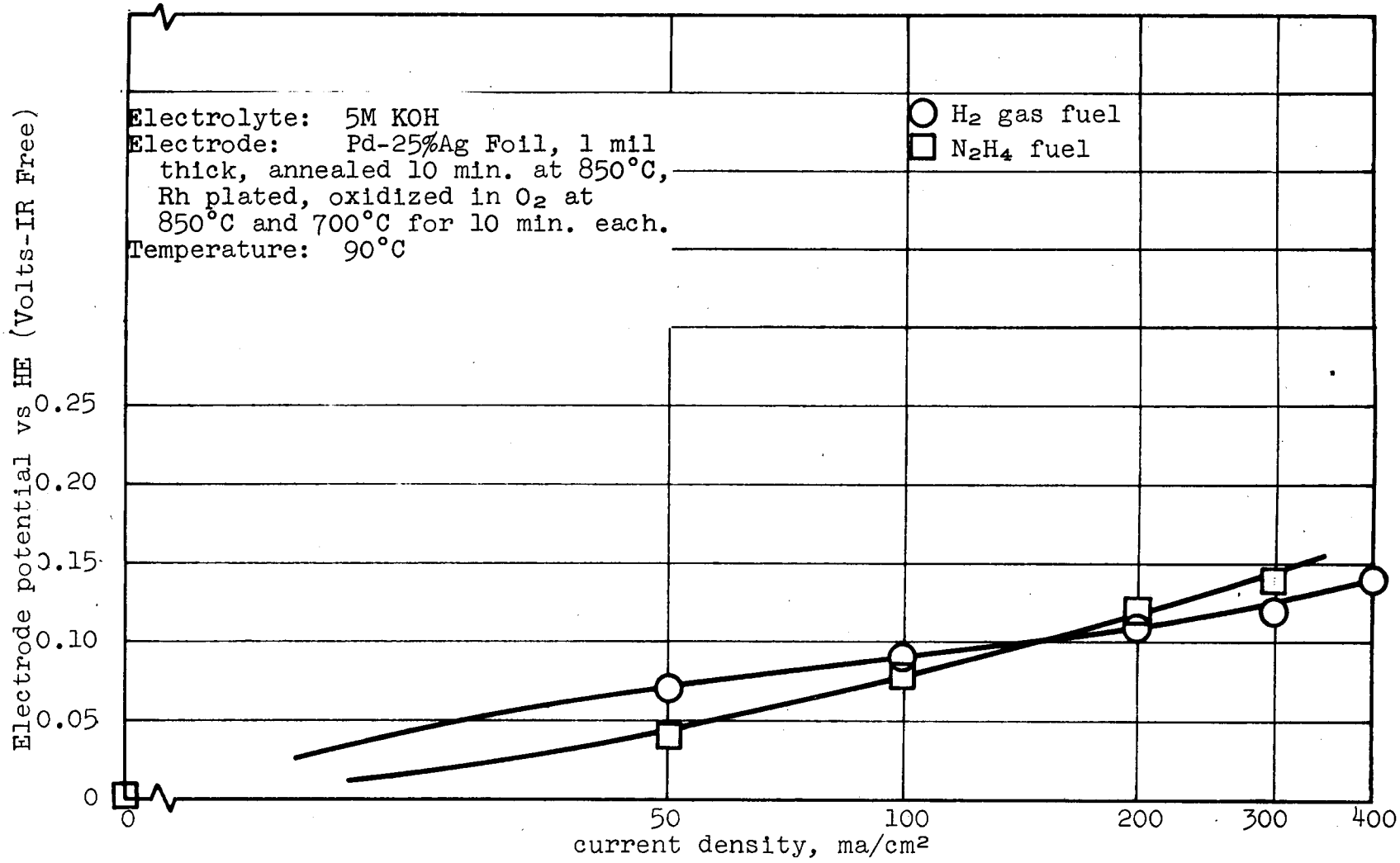

Figure 2. Polarization of Palladium Foil Anode

catalysts have been classified according to their selectivity. Platinum was found to be the most selective catalyst for the anodic oxidation of hydrazine in the presence of nitric acid. Details of this investigation are given in Appendix II.

IV. FULL-CELL DEVELOPMENT

A. BACKGROUND

Previous sections of this report have been concerned with the conception, fabrication, and optimization of electrodes. Several choices of electrode types have been developed or adapted that are capable of operation on one or more fuels or oxidants. Furthermore, a study of catalysts has indicated the best catalyst choice for each half-cell service.

The interaction of half cells when combined into a full-cell assembly has been considered. The result is that considerable effort has been given to developing electrodes selective for a single reactant with minimal deleterious effects resulting from limited concentrations of the other reactant. The use of reactants such as N_2H_4 and HNO_3, which are soluble in the electrolyte and which show a mutual polarizing effect on their counter electrode, dictated such a study.

With the availability of promising electrodes (MRD type) and specification of fuel cell system requirements for a hypothetical terrestial mission, major emphasis was placed on actual combination of various half cells into full-cell configurations. The full cells demonstrating the most promise were then fully characterized to provide data necessary for the design of a fuel cell system meeting the NASA hypothetical specifications. Two such system designs were submitted during this contract. (See Appendixes IX, X).

Four full-cell configurations were investigated during this phase of the contract:

1. Contained Acid Electrolyte

This system was designed for nitric acid or dinitrogen tetroxide oxidizers, hydrazine fuel, and phosphoric acid electrolyte. The electrolyte was immobilized between the electrodes by the use of a phosphoric acid-Santocel FR-C gel. The physical stabilization of the electrolyte offers advantages in that by limiting the amount of electrolyte the cell can be operated without flooding of the electrodes. The best electrode combination was an MRD-C diffusion cathode operating on gaseous dinitrogen tetroxide and an MRD-A platinum liquid diffusion anode, with the hydrazine fuel dissolved in a phosphoric acid solution and pumped through the anode compartment.

2. Contained Basic Electrolyte

Oxidizers for this system were oxygen or hydrogen peroxide with hydrazine as the fuel. The potassium hydroxide electrolyte was contained in an asbestos or polypropylene mat with the same

contained electrolyte advantage described above. An MRD-C carbon-platinum cathode and a palladized nickel plaque liquid diffusion anode were the electrodes. The hydrazine fuel was dissolved in potassium hydroxide solution and recirculated through the anode compartment.

3. Ion Exchange Membrane - Acid/Acid

The use of ion exchange membranes as "solid electrolytes" was of interest because of the membrane's ability to isolate soluble fuels and oxidizers. Nitric acid and dissolved hydrazine were used as reactants in the same cell construction described for contained acid electrolytes.

4. Ion Exchange Membrane - Acid/Base

This system was designed for use with nitric acid as the oxidizer, and hydrazine dissolved in potassium hydroxide solution as the fuel. If the ion exchange membrane exchanges only potassium ions the pH difference between the anolyte and catholyte will appear as part of the cell potential. Palladized nickel plaque liquid diffusion anodes were used with the anolyte pumped through the electrode. Cathodes were made of platinized platinum screen, supported on expanded stainless steel with the nitric acid recirculated through the cathode compartment.

B. METHOD

Three full-cell designs were used in this contract. An early design is shown in Figure 3; however, successful development of full cells required a more sophisticated design. Almost all full-cell testing was done with the cell shown in Figure 4, adapted for contained basic electrolyte testing. A further modification of this design is shown in Figure 5. This latter cell satisfactorily handled any of the aqueous system reactants, electrodes, or electrolyte types considered for this contract. Each half cell shown in the figure contains one electrode in the frame assembly, and a full cell is constructed by joining two such assemblies with a spacer between them. The cell parts and fittings are all stainless steel.

A test stand constructed for testing contained acid electrolyte cells operating on N_2O_4 is shown in Figure 6. Provisions are made for measurement and control of reactant flow rates, concentrations or pressures, and cell temperature. Similar test facilities were constructed for contained basic electrolyte cell testing (Figure 7), and for ion exchange or contained acid electrolyte/HNO_3 cell testing (Figure 8). Electrical measurements were made using the equipment depicted in Figure 9. Polarization measurements were made on all cells constructed and continuing life tests were made at a constant output of 100 ma/sq cm for those cells whose performance warranted it. In most cases, cell terminal voltages were measured with the cell IR drop included.

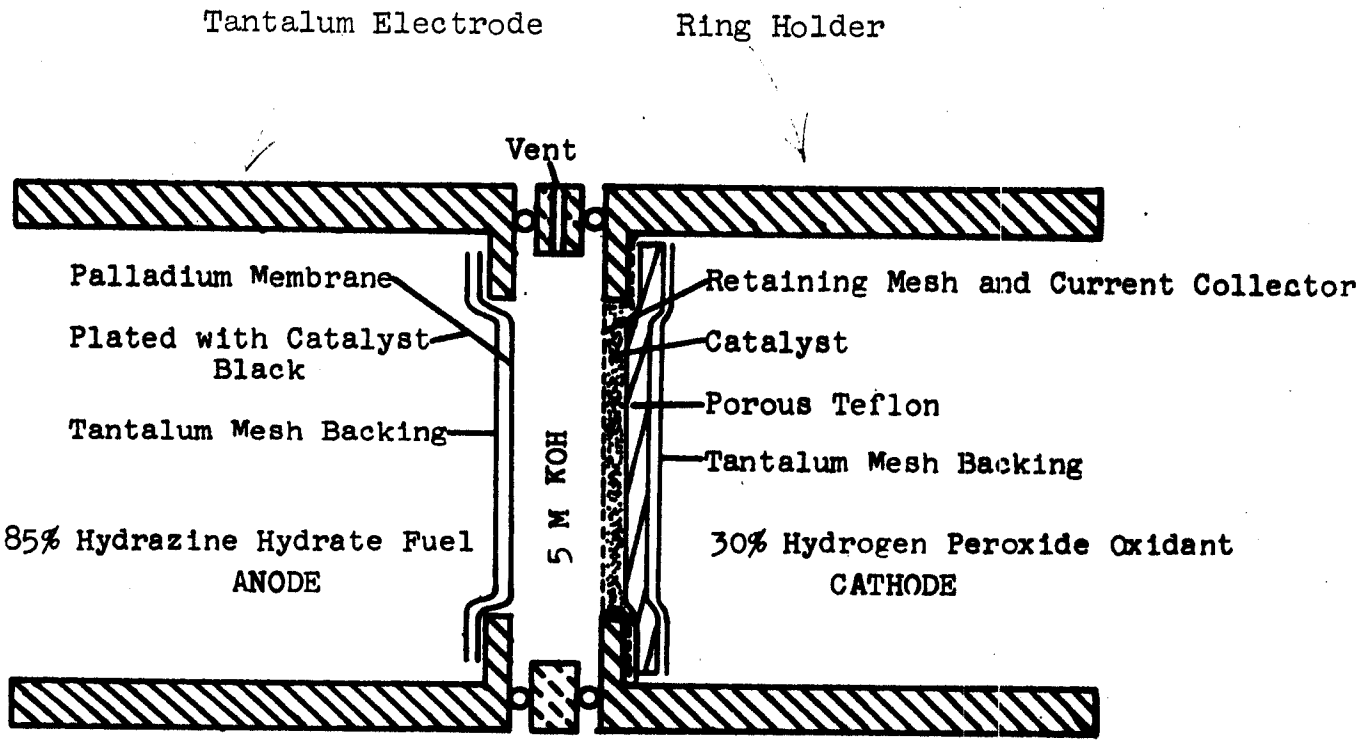

Figure 3. Complete Hydrogen Peroxide-Hydrazine Cell

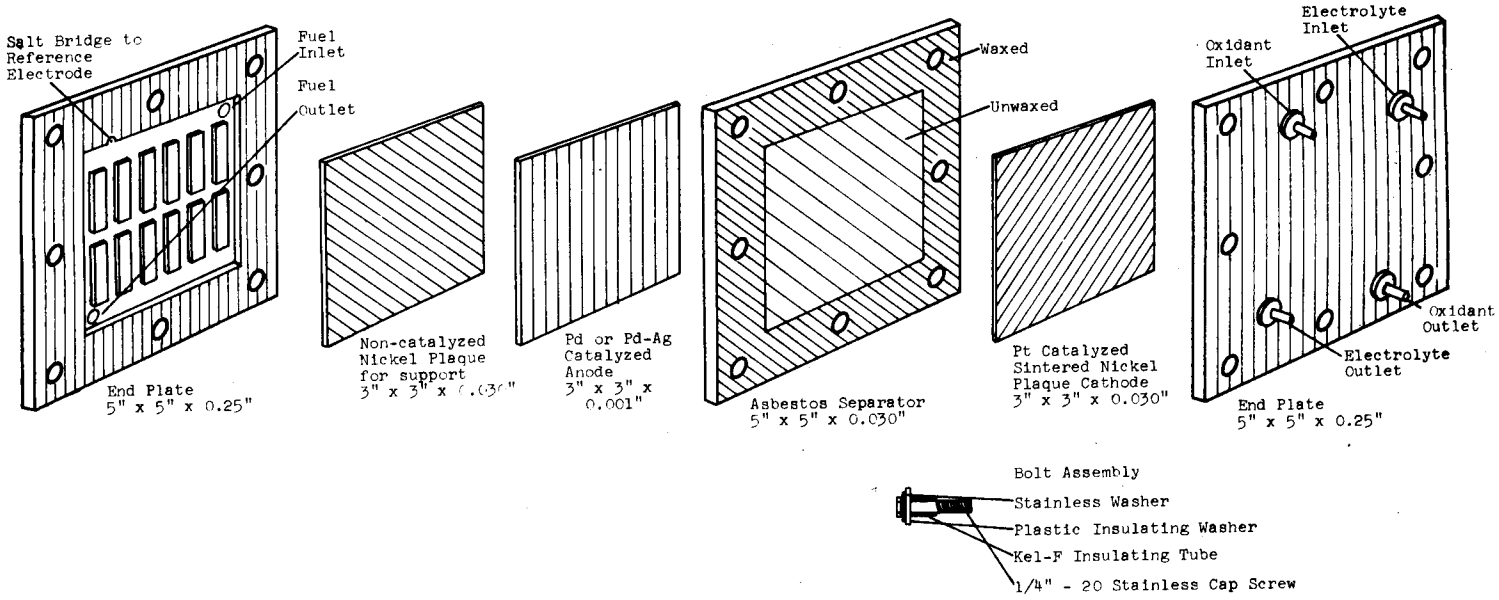

Figure 4. Exploded View of Full Cell

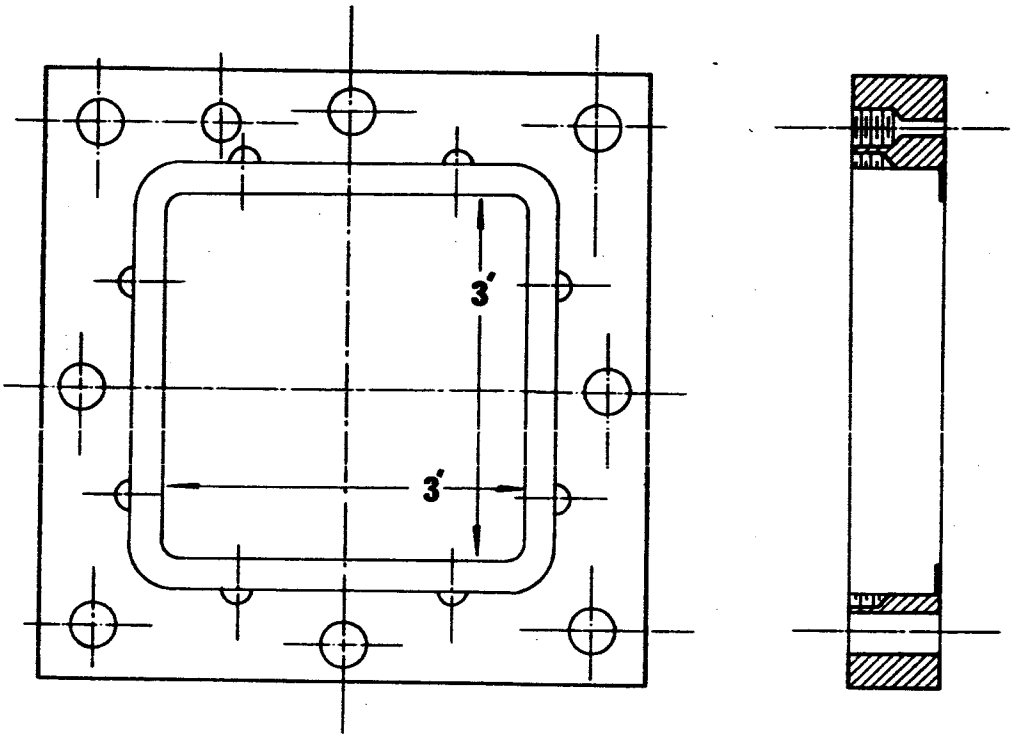

1a. Cell Frame

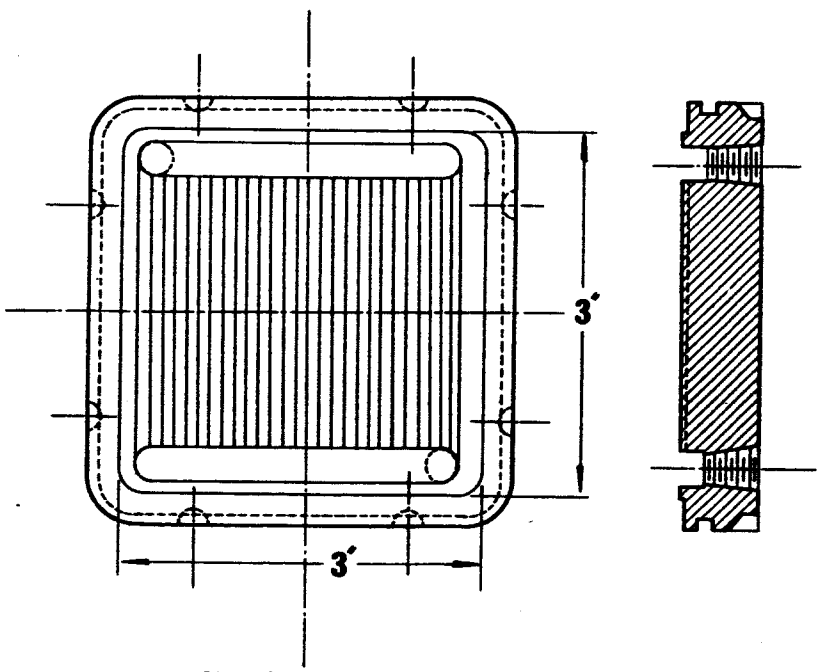

1b. Cell Insert

Figure 5. Test Cell Construction

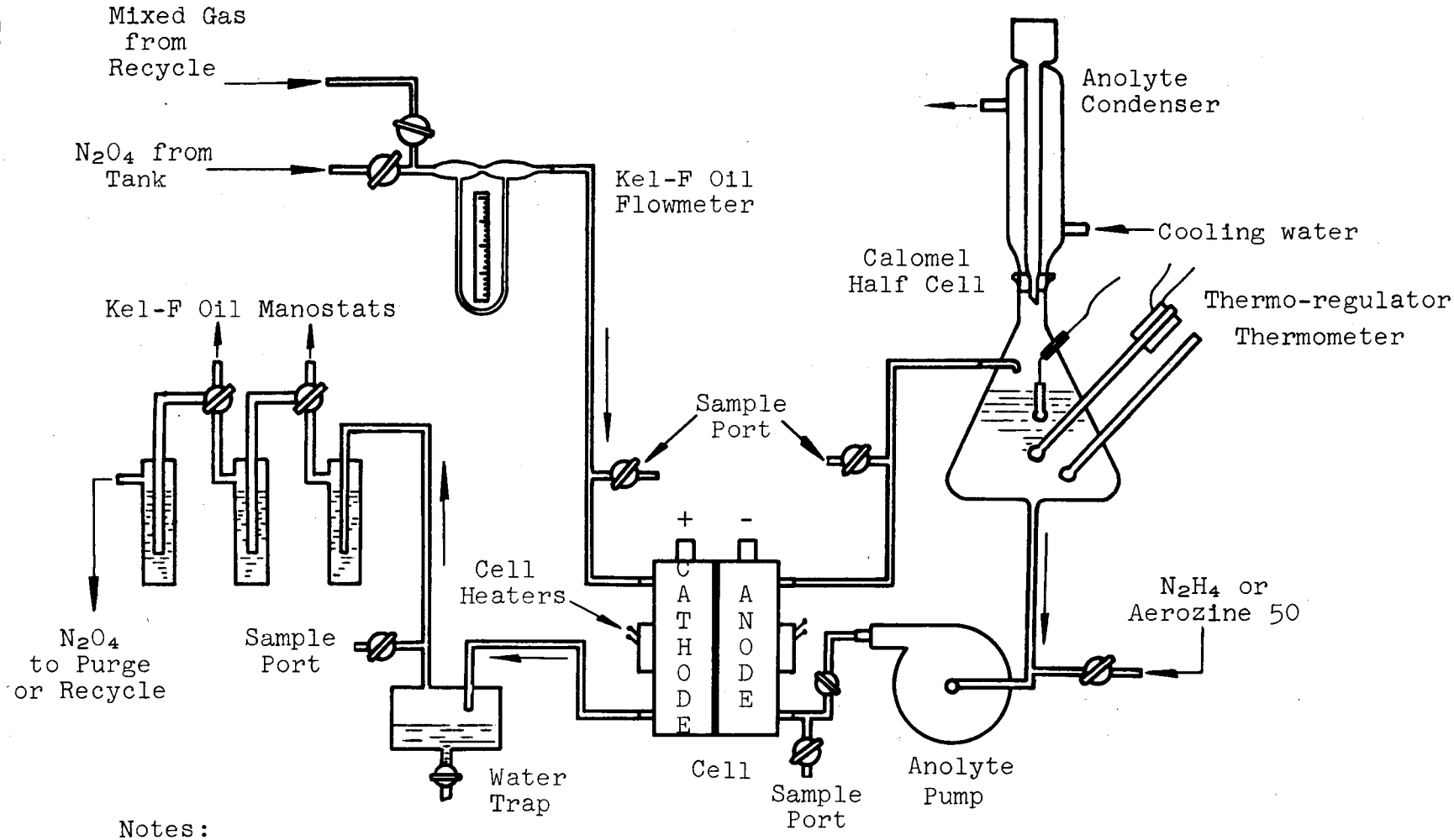

Notes:
(1) All tubing is Teflon or glass. All connections are Teflon or stainless steel Swage-Loks fittings.
(2) Anolyte pump speed controlled by variac.
(3) Heating tapes and insulation around anolyte flask. Tapes and cell heaters controlled by thermo-regulator. Glass wool insulation around cell.
(4) N_2O_4 is tank grade. Tank maintained at 40°C in water bath.

Figure 6. N_2H_4/N_2O_4 Acid Cell Test Setup

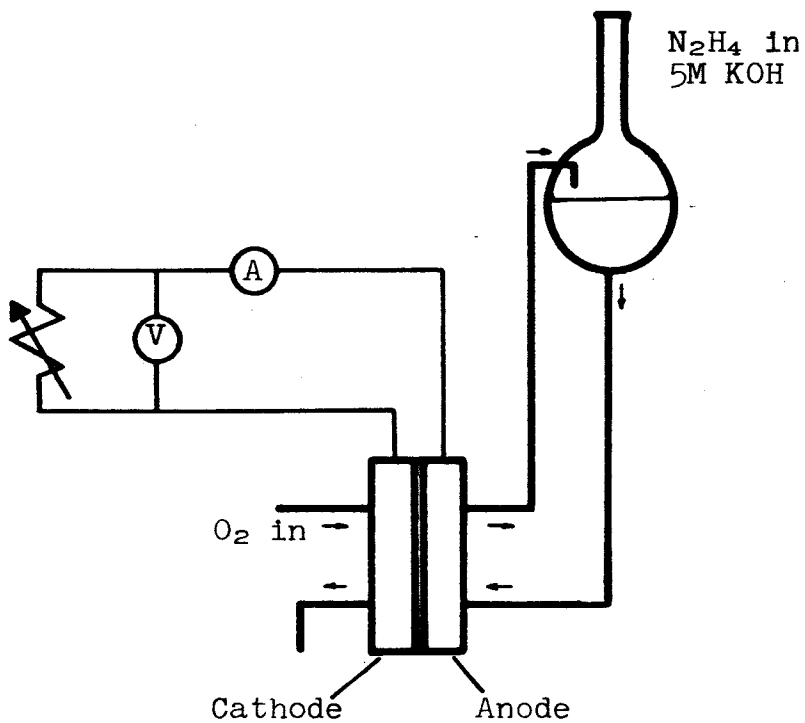

Figure 7. Contained Basic Electrolyte Full-Cell Test Setup

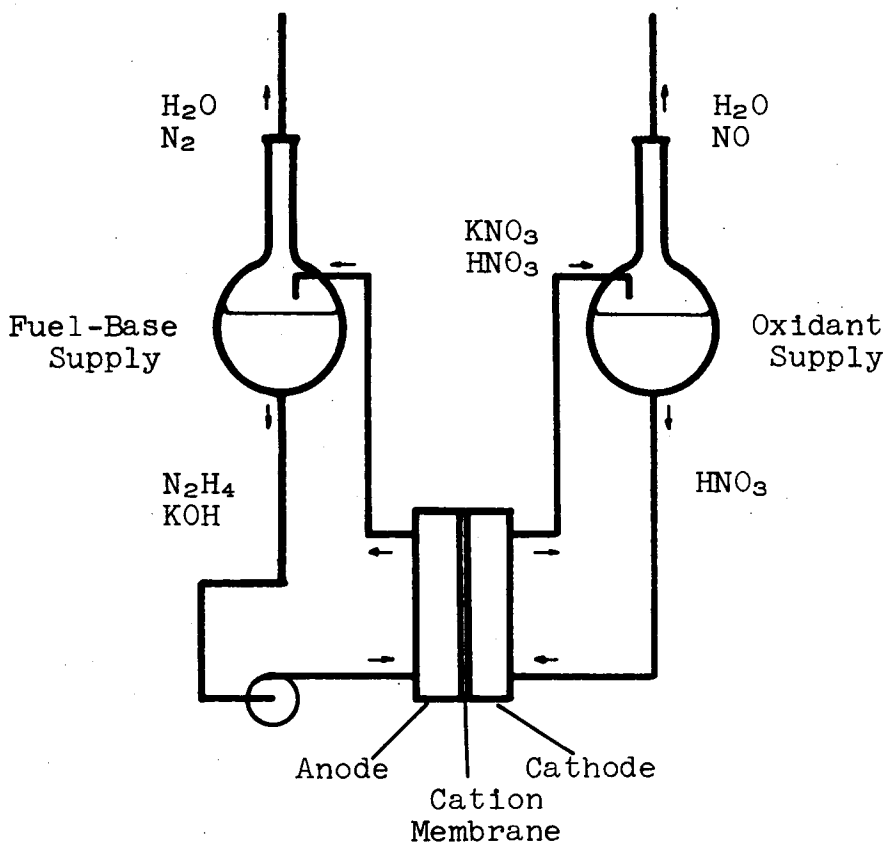

Figure 8. Fuel Cell and Pumping System

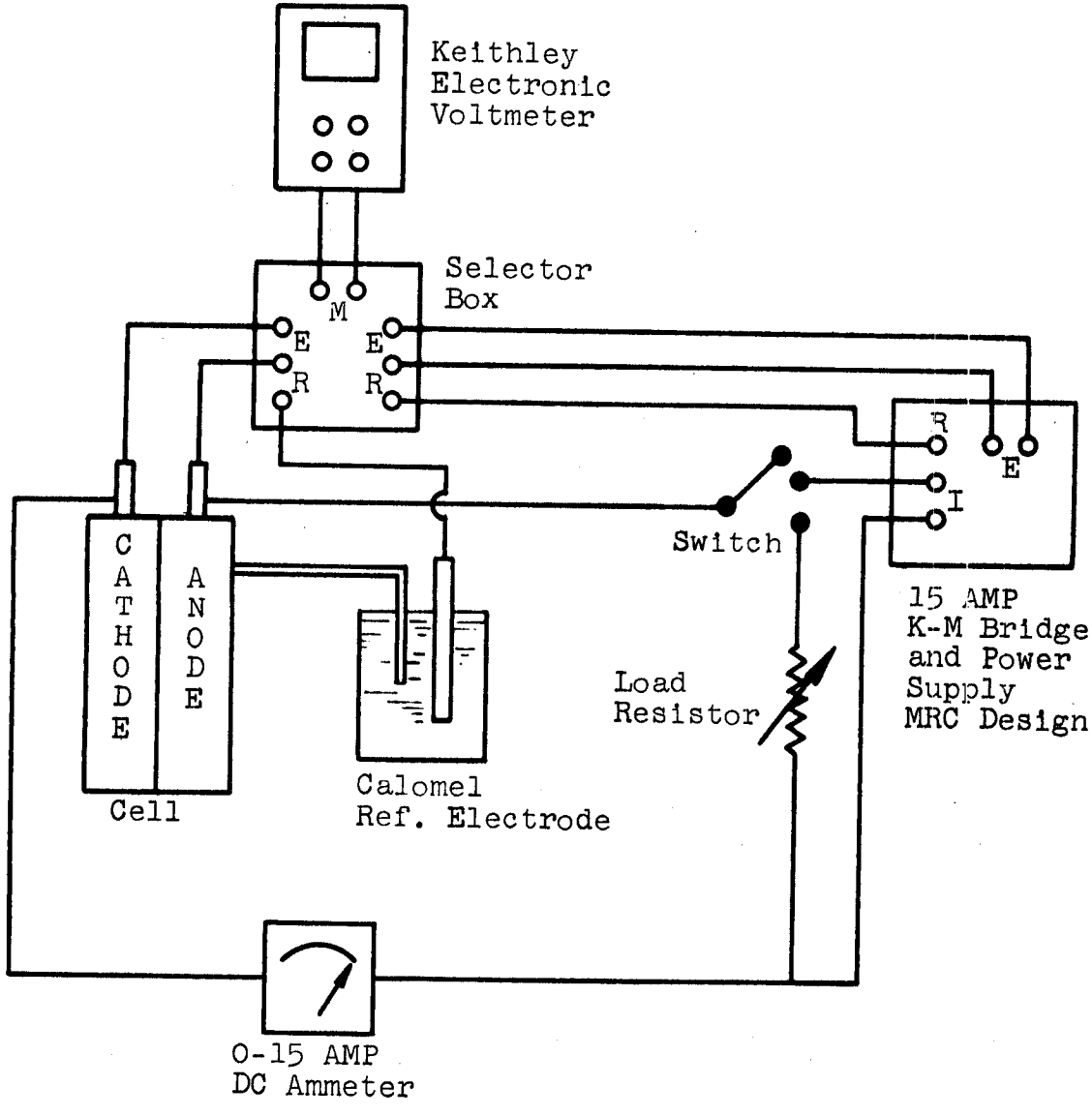

Figure 9. Electrical Measurement Diagram

C. CONTAINED ACID ELECTROLYTE CELLS

1. Cells with Nitric Acid Oxidant

The first acid full cells were constructed with porous carbon block diffusion cathodes and polypropylene mat separators. Considerable difficulty was experienced with heavy polarization and unstable potentials (Table 7). These problems were attributed to the inability of the polypropylene mat separator to restrict cross-contamination of reactants and to reactant leakage through and around the electrodes. This latter condition was especially noted with the porous carbon block HNO_3 cathods. Following this initially poor performance, the polypropylene mat separator was replaced with a thick gel or paste of H_3PO_4 and fine Santocel FR-C silica. In addition, MRD-type electrodes were prepared for the cathode with double thickness of carbon layers to obtain oxidant diffusion control with good sealing properties.

Construction of typical cells was as follows:

Cell No. 66703

Cathode: MRD-C, 20-mil double carbon layer on ss screen

Anode: MRD-A, 10 mg Pt/cm^2 on Pt screen

Fuel: 2M N_2H_4 in 5M H_3PO_4

Oxidant: 10.5M HNO_3 in 2M H_3PO_4

Electrolyte: 5M H_3PO_4

Separator: Santocel FR-C - H_3PO_4 gel

Operating Temperature: 90°C

Performance is given in Figure 10.

Hydrazine and HNO_3 pumping rates were critical for cell 66703. In general, HNO_3 circulation by gas lift was satisfactory, and slow N_2H_4 circulation over a small flow range gave the best results. Attempts to pump the HNO_3 invariably resulted in less favorable anode potentials, indicating that the HNO_3 was forced through the cathode and into contact with the anode. Cell 66703 was operated for approximately 30 hours at 100 ma/cm^2, 0.54 v, 90°C. It ultimately failed because of anode poisoning by HNO_3. Disassembly showed that turbulence in the N_2H_4 liquid manifold had caused wash-out of the H_3PO_4-silica gel separator in the vicinity of the inlet manifolds, permitting HNO_3 migration from cathode to anode.

Table 7

CONTAINED ACID ELECTROLYTE HNO_3 CELLS

Electrode Area: 9 in.^{2}

Separator: Polypropylene woven fabric
15-mil thickness

Cell No.	Anode, Fuel	Cathode, Oxidant	Temperature °C	Electrical Performance Cell Potential (volts) at Current Density Listed 0	10	15	30	40	Notes
49850A	Platinized Pt Screen 0.5M N_2H_4 in 5M H_3PO_4 (pumped)	Diffusion Type FC-13 Carbon, 125 mil thick, 10 mg/cm^2 Teflon 70% HNO_3	68* 80‡	0.60*	0.47*	0.46‡			Poor performance due to leakage of N_2H_4 and H_3PO_4 through separator.
49850B	Platinized Pt Screen 0.1M N_2H_4 in 5M H_3PO_4 (pumped)	Diffusion Type FC-13 Carbon, 125 mil thick, 10 mg/cm^2 Teflon 70% HNO_3	61	0.82				0.36	Cathode deterioration due to N_2H_4 leakage. Anode deteriorated if pumping stopped. Ineffective separator.
49850C	MRD-C Pt on Pt Screen 0.5M N_2H_4 in 5M H_3PO_4	Diffusion Type FC-13 Carbon 125 mil thick, 10 mg/cm^2 Teflon 70% HNO_3		0.78			0.35		Anode leaked. Cathode cracked after 1/2 hour.

* Fuel only pumped.

‡ Fuel and oxidant pumped.

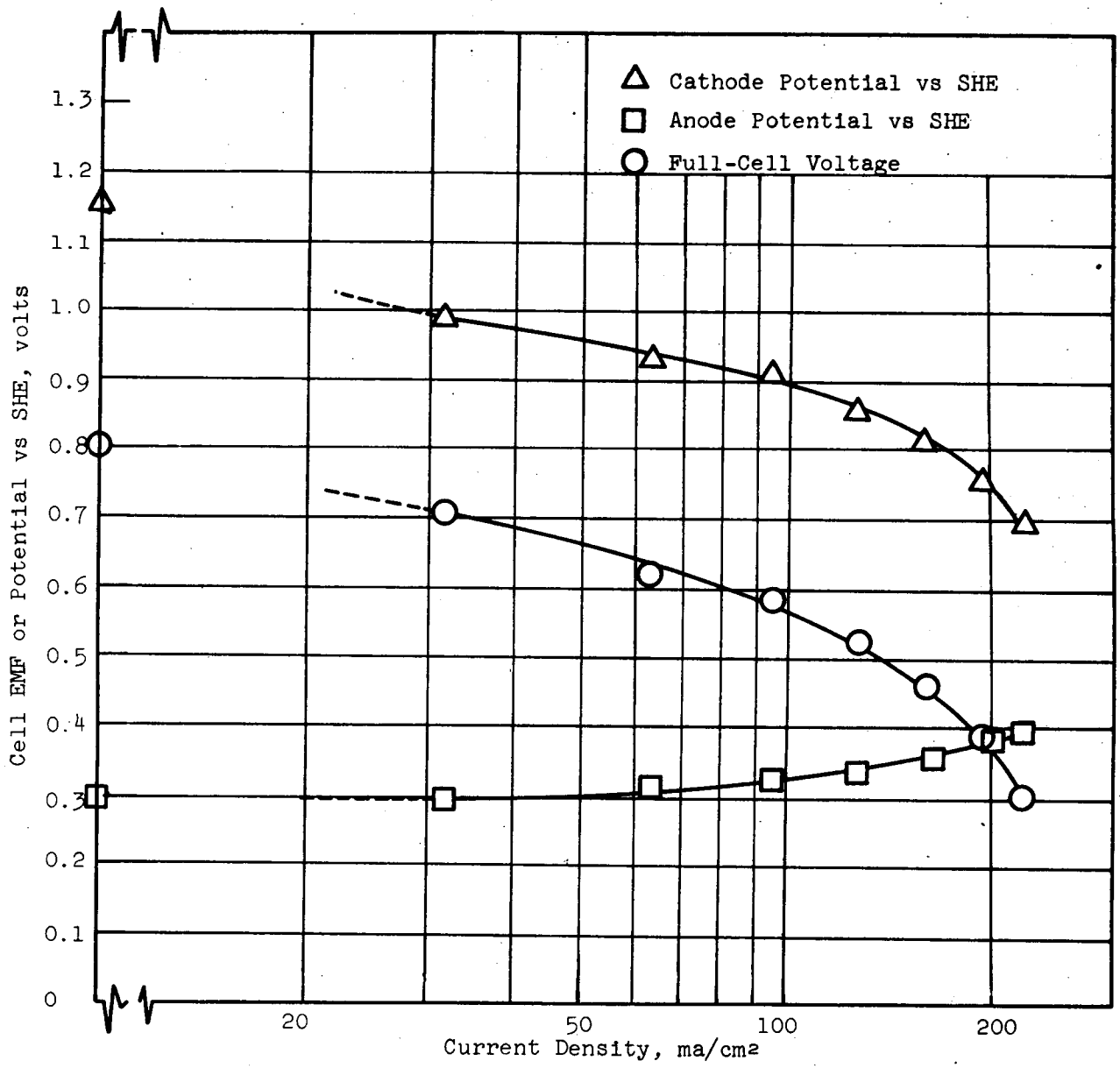

Cathode:	MD-C 20 mil Carbon Layer on Stainless Steel Screen	Oxidant:	10.5M HNO_3 in 2M H_3PO_4
Anode:	MD-A 10 mg Pt/cm² on Pt Screen	Electrolyte:	5M H_3PO_4
Fuel:	2M N_2H_4	Separator:	Santocel FRC - H_3PO_4 Gel
		Temperature:	90°C

Figure 10. Polarization Curves for Full Cell 66703

2. Cells with Dinitrogen Tetroxide Oxidant

Cells using the same type of MRD electrodes as the nitric acid cells and Santocel FR-C/phosphoric acid gel separators were operated with excellent results on gaseous dinitrogen tetroxide oxidizer and hydrazine in 5M phosphoric acid fuel. Table 8 gives a summary of full-cell testing to date. Individual cell tests are discussed fully in Appendix IV. A summary of the results achieved follows.

a. The latest cell modification (cell No. 65121) has operated for 645 hours to 1 February 1965, 30-60°C, 100 ma/sq cm, 0.68-0.75 v, with no essential change in performance over the test period to date. A polarization curve for this cell is shown in Figure 11. It demonstrates the excellent characteristics up to at least 250 ma/sq cm. The performance of this cell definitely proves that these two storable propellants can be used as reactants in an operating fuel cell to give substantial electrical output at reasonable temperatures for an extended period.

b. We have demonstrated the feasibility of a cathode gas recirculation system to improve cathode coulombic efficiencies (presently 7-8% on a single pass). The MRD-C cathodes will operate on a gas stream containing at least 50% NO with little loss in performance (see Figure 12). High local gas velocities on the gas side of the electrode are necessary for optimum performance.

c. Improvements in electrodes have allowed lower temperature operation with little loss in performance (Figure 13). Lower temperature operation tends to reduce the catalytic decomposition of hydrazine at the anode and thus improves anode coulombic efficiencies (40-50% at 60°C).

d. Preliminary data indicate that it may be feasible to use Aerozine-50 (50% by weight hydrazine, 50% UDMH) directly in the cell. However, there may be some sacrifice in anode performance (Figure 14).

e. Preliminary data also indicate a rhodium catalyst will improve anodic voltage efficiency (more nearly reversible operation); however, this catalyst is more sensitive to poisoning by dissolved nitrates from the cathode (Figure 15).

f. The phosphoric acid-Santocel FR-C gel separator has proved to be a stable, reproducible means of immobilizing the electrolyte and combines adequate reactant exclusion properties with low electrolytic resistance.

Erosion of the electrolyte gel that was experienced in some early cells was corrected by proper baffle design in the anode backing plate. This baffle change stopped the break through of the anodes at the high velocity inlet thus preventing leakage into the electrolyte compartment.

Table 8

CONTAINED ACID ELECTROLYTE FULL CELLS (LIFE TESTING)

Fuel: 3M N_2H_4 in 5M H_3PO_4
Oxidant: Tank N_2O_4
Temperature: 60-90°C*
Electrolyte: 5M H_3PO_4
Separator: Santocel FR-C/H_3PO_4 Gel

Cell No.	Anode	Cathode	Electrical Performance
61869	MRD-A No. 22-101464 20 mg Pt/cm² on 80 mesh Stainless Steel Screen	MRD-C No. 21-101364 20 mil Carbon on 30 mesh Stainless Steel screen	Approximately 150 hr, 13 November 1964, 100 ma/cm², 0.62-0.70 v at 90°C. Cathode accidentally damaged. No essential change in electrode activity at failure.
65113	Same anode as cell 61896	MRD-C No. 9(2) 20 mil Carbon on 30 mesh St inless Steel Screen	110 hr, 1 December 1964, 100 ma/cm², 0.61-0.68 v at 90°C. Cell leaked electrolyte through cathode due to rupture in unsupported section. Test was terminated.
65121	MRD-A No. 69-67240 43 mg Pt/cm² on 30 mesh Stainless Steel Screen	Two single layer carbon electrodes on 80 mesh Stainless Steel Screen pressed at 2660 lbs/in²	645 hr, 1 February 1964, 100 ma/cm², 0.66-0.74 v at 60°C. Life test continuing.
65105	MRD-A No. 50-67226 80 mg Rh/cm² on Pt screen	MRD-C No. 26-101564 20 mil Carbon on 80 mesh Stainless Steel Screen	1 hr at 100 ma/cm², 0.70-0.76 v at 90°C. Anode potential between 0.006 and 0.086 v vs SHE. Cell failed due to deterioration of cathode potential caused by separator wash-out.

* Cells 61896 and 65113 operated at 60°C overnight and 90°C during the day.
Cell 65121 operated continuously at 60°C.

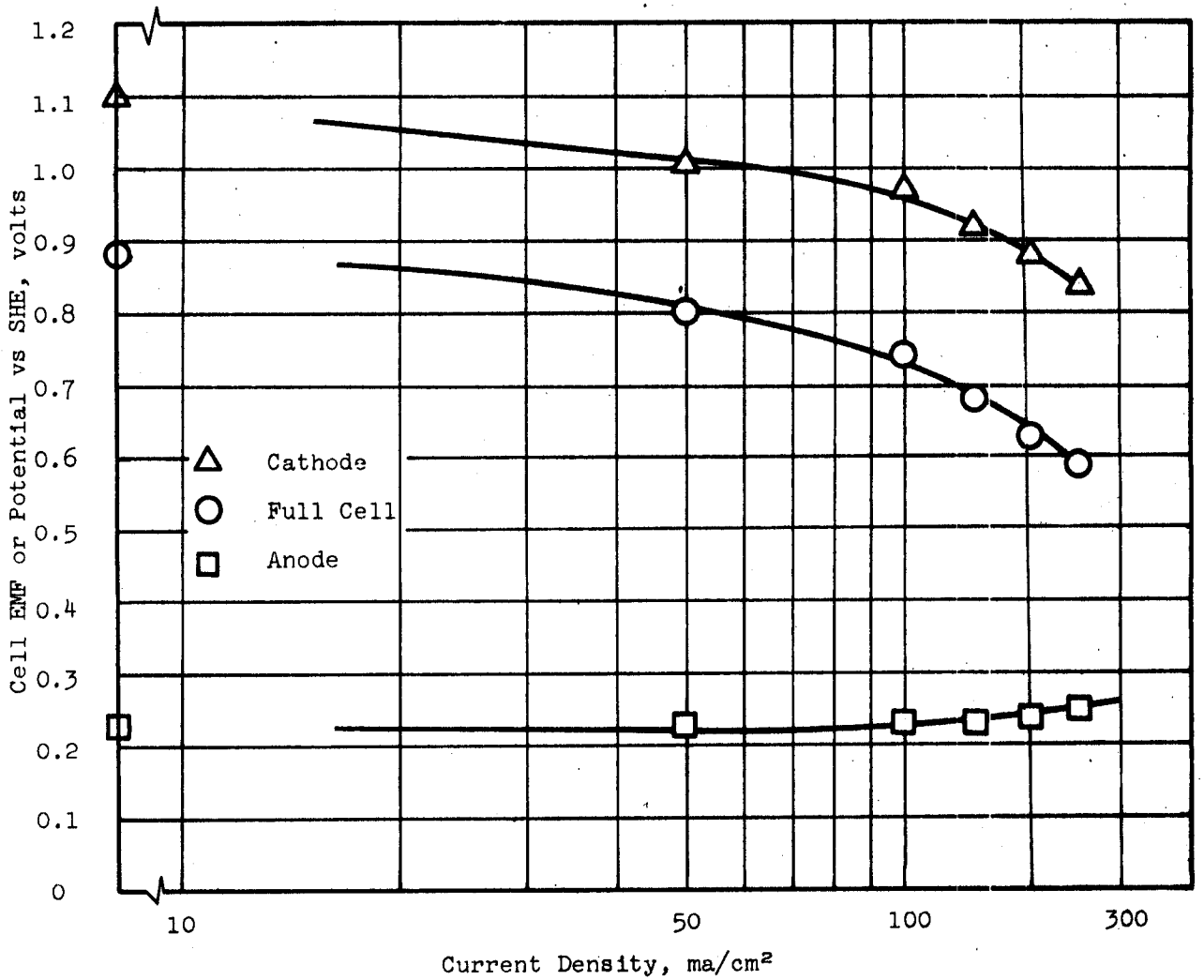

Cathode: 2 single carbon MRD-C on 80 mesh stainless steel screen, pressed back to back at 24,000 lbs.

Anode: MRD-A No.79-67240, 28 mg Pt/cm² on 30 mesh stainless steel screen

Fuel: 3M N_2H_4 in 5M H_3PO_4 anolyte

Oxidant: N_2O_4 gas at 400 ml/min, 5.4 in. H_2O

Separator: Santocel FRC-H_3PO_4 gel

Temperature: 60°C

Time: After 207 hours, 60°C, 100 ma/cm²

Figure 11. Polarization Curve, Full Cell 65121 (N_2H_4/N_2O_4)

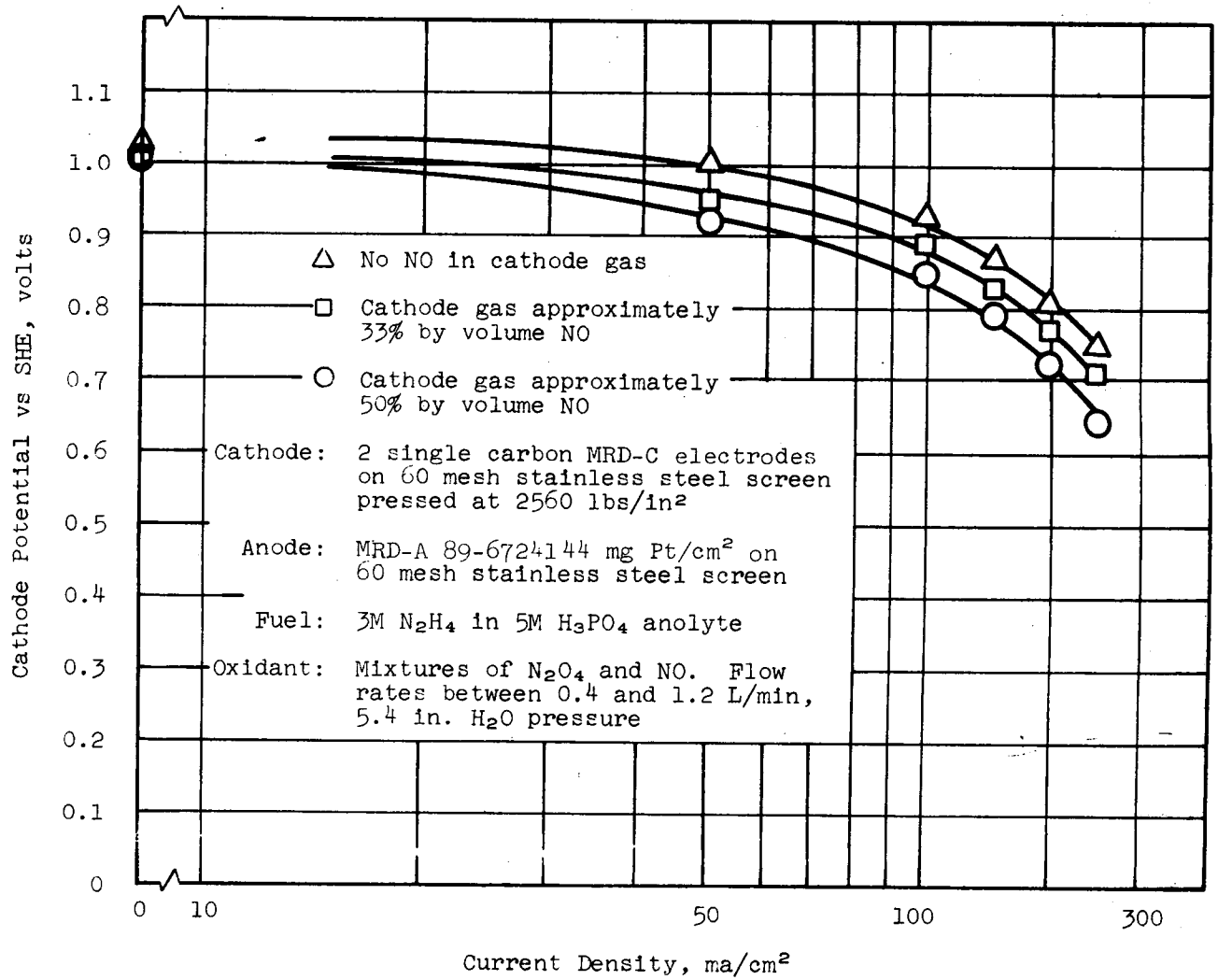

Figure 12. Effect of NO Concentration on Cathode Polarization Full Cell 65129 (N_2H_4/N_2O_4)

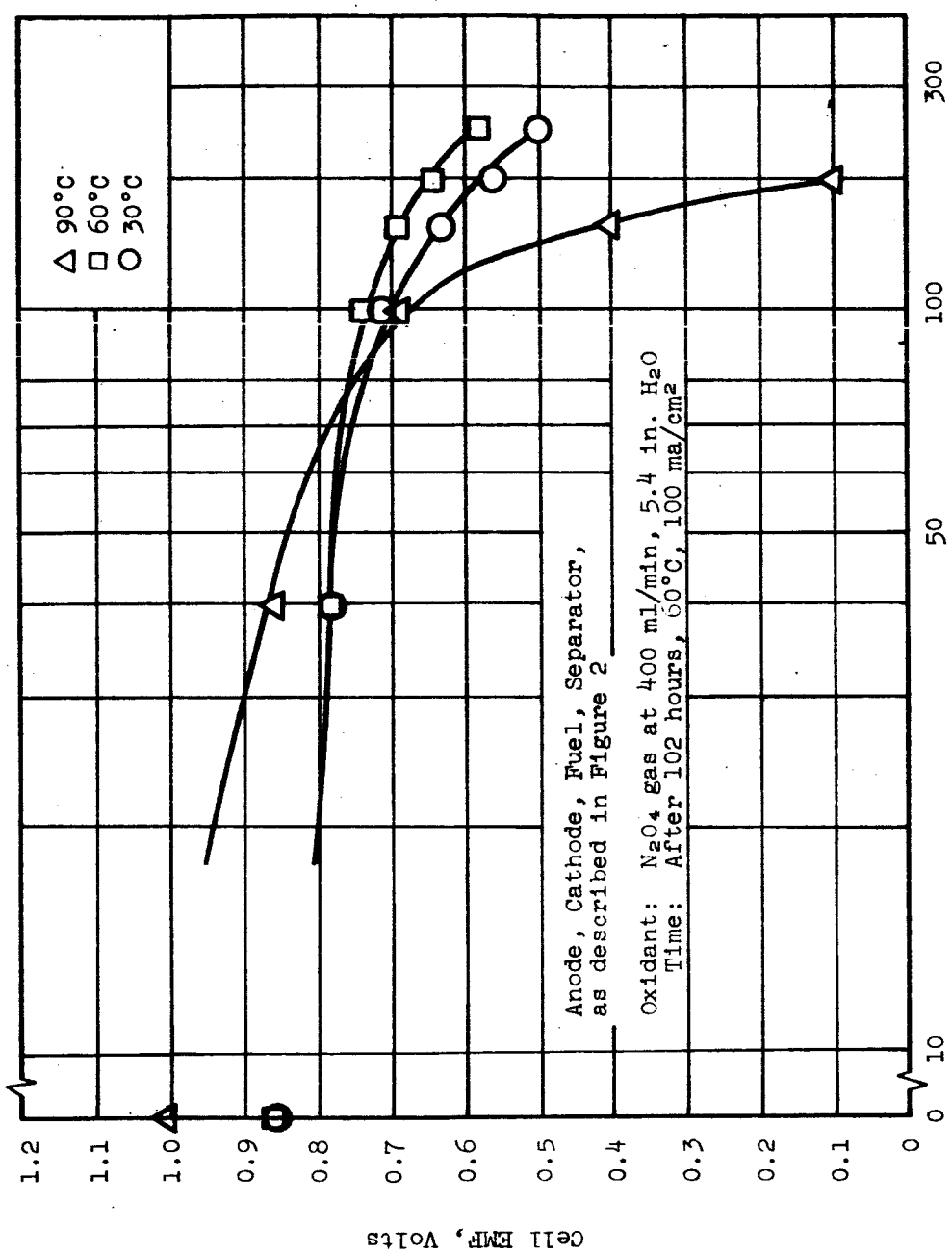

Figure 13. Effect of Temperature on Polarization
Full Cell 65121 (N_2H_4/N_2O_4)

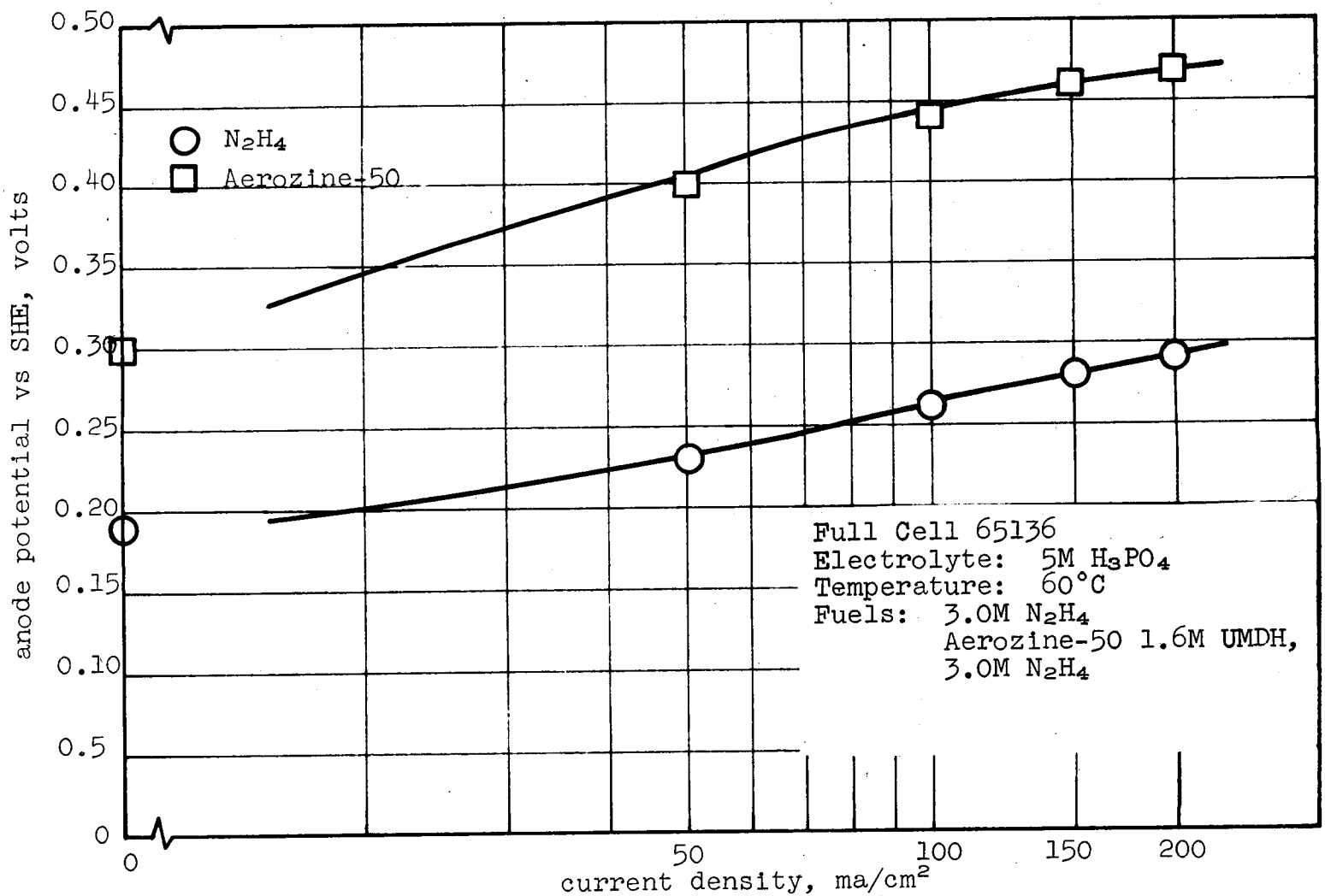

Figure 14. Polarization Characteristics of Aerozine-50 Fuel

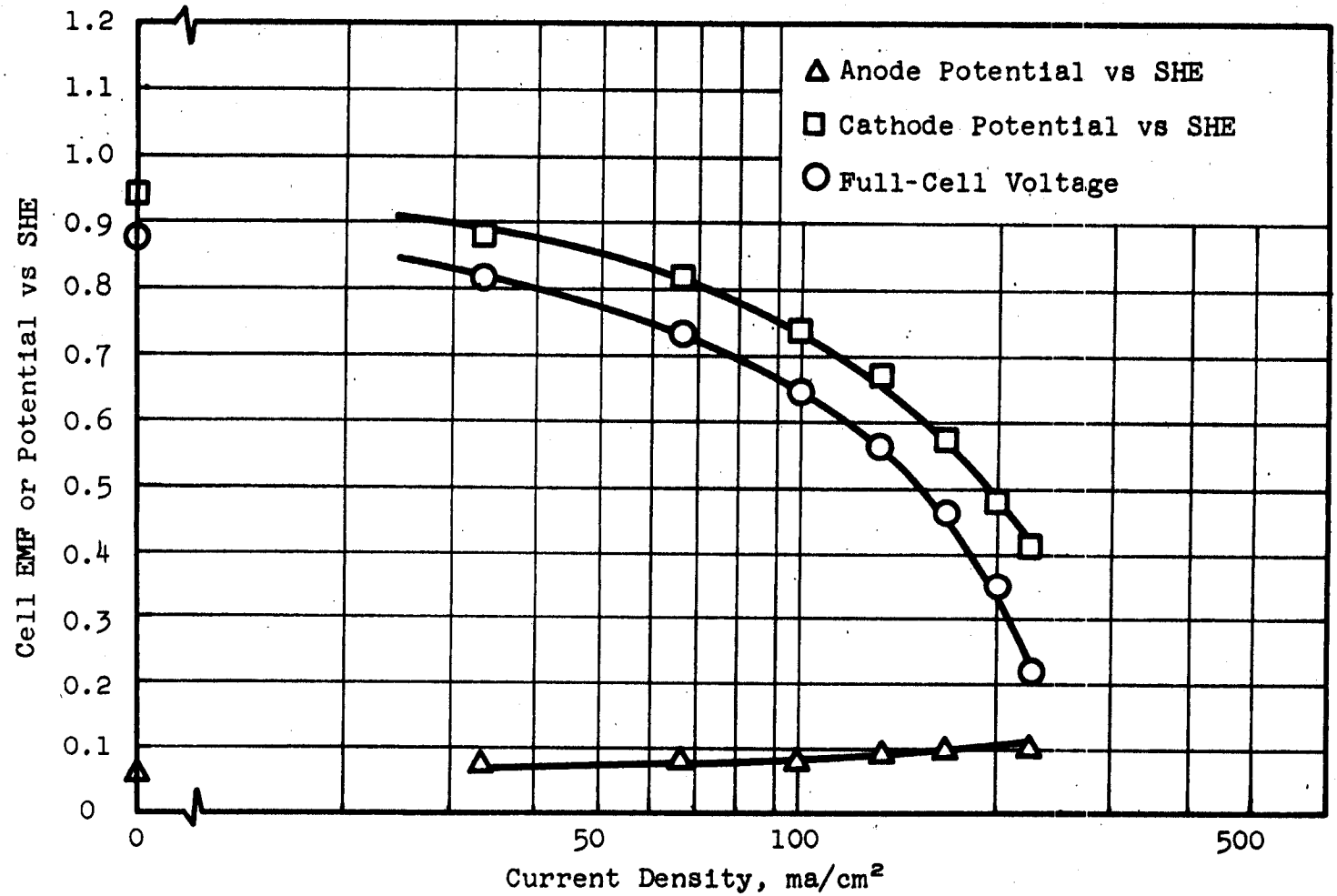

Cathode: MRD-C No. 26-101564,
20 mil Carbon on 80 mesh
Stainless Steel screen

Anode: MRD-A No. 50-67226,
80 mg Rh/cm² on Pt screen

Oxidant: N_2O_4 gas (40°C)
Separator: Santocel FRC-H_3PO_4 Gel
Electrolyte: 5M H_3PO_4
Temperature: 60°C
Fuel: 3M N_2H_4 in 5M H_3PO_4

Figure 15. Polarization Curves, Full Cell 65105

Cell development has progressed to the point where a 1-KW hypothetical system design to NASA specifications has been submitted (Appendix X). All electrical specifications were met in a unit measuring 1.3 cu ft, weighing 65 lbs, and having 100% overload capability. Improvements made since the design was submitted make the system look even more favorable, particularly with respect to required electrode areas, heat effects, operating temperature and electrode efficiencies.

D. CONTAINED BASIC ELECTROLYTE CELLS

Early work on this system concerned hydrogen/hydrogen peroxide tested in the early glass cell, and hydrogen/oxygen tested in the newer cell construction. Details are given in Appendix IV. Most subsequent work was done with hydrazine-oxygen/hydrogen peroxide. The results are given below.

1. N_2H_4-O_2 (Life Tests)

A life test program was initiated to evaluate fuel cell systems, designs, and materials on a long-term basis. The stainless steel cells with 3 in. x 3 in. electrodes were described previously. Various combinations of MRD-A anodes, nickel plaque anodes, and MRD-C cathodes were catalytically treated as shown in Table 9. The electrolyte, 5M KOH, was contained in a 15-mil thick asbestos separator or 5-mil thick polypropylene mat. All long-term full-cell tests were made with the O_2-N_2H_4 system. Tank O_2 was supplied at less than 5 psig to gently purge past the back side of the cathode.

A summary of the life test results to date is given in Table 9. The first four cells listed in Table 9, with various combinations of catalyzed nickel plaque, MRD-A, and MRD-C electrodes, had very similar current-voltage relations (0.7-0.6 v at 100 ma/cm^2 at 25°C). Cell 65608, with 2285 hours at 100 ma/cm^2 to 1 February 1965, was still in operation. Cell 65601 failed after 111 hours because of cathode leakage. The cathode was rejuvenated by heating in a vacuum at 100°C for 1 hour, and at 200°C for 16 hours. The cell was reassembled with a new nickel plaque anode, and life tests continued as cell 65608. The MRD-C cathode of cell 65608, accordingly, has been in operation for a total of 2396 hours. Polarization curves on cell 65608, taken initially and after 1628 hours of service, are presented in Figures 16 and 17, and indicate no essential change in catalytic activity. Cell 65613, with a nickel plaque anode and an MRD-C cathode, demonstrated the reproducibility of this type of cell for the O_2-N_2H_4 system for 44 hours. This run was discontinued after 44 hours to release the cell for other tests.

Table 9

CONTAINED BASIC ELECTROLYTE CELLS
(Life Test Summary)

Fuel: 1-3M N_2H_4 in 5M KOH
Oxidant: T nk O_2 at 0 psig
Temperature: 25°C

Electrolyte: 5M KOH
Separator: 15 mil Asbestos (except 67601 - 5 mil Polypropylene Mat)

Cell No.	Anode	Cathode	Electrical Performance
65601	MRD-A 10 mg Pt/cm² on Pt Screen	MRD-C 10 mg Pt/cm² on Carbon on Monel Screen	111 hr, 100 ma/cm², 0.7 to 0.6 v. Failure at 111 hr due to cathode leakage. Anodic Coulombic Efficiency - 92%.
65608 No.4	Ni Plaque (Gould) 30-mil, 0.7 mg Pt/cm², 1.5 mg Pd/cm²	Cathode from 65601 heated 1 hr in vacuum at 100°C, 16 hr in vacuum at 200°C	2285 hr to 1 Feb.'65, 100 ma/cm², 0.7 to 0.6 v. Test still running (see Fig. 3). Anodic Coulombic Efficiency - 94%. Essentially no change in electrode catalytic activity.
65611 No.5	MRD-A 10 mg Pt/cm² on Stainless Steel Screen	MRD-C 10 mg Pt/cm² on Carbon on Pt Screen	846 hr to 1 November 1964, 100 ma/cm², 0.66 to 0.60 v. Cell off test due to inadvertent rupture of separator. No essential change in electrode catalytic activity at time of failure. Anode coulombic efficiency - 93%.
65613	Ni Plaque (Gould) 30-mil, 2.3 mg Pd/cm²	MRD-C 10 mg Pt/cm² on Pt Screen	44 hr, 100 ma/cm², 0.67-0.60 v. Cell still active at end of run.
65618*	Ni Plaque (Gould) 30-mil, 2.3 Pd/cm²	MRD-C 10 mg Pt/cm² on Carbon on Pt Screen	
67601*	Ni Plaque (Gould) 25-mil, 3.0 mg Pd/cm²	MRD-C 7 mg Pt/cm² on Carbon on Stainless Steel Screen	

* This cell used for short-time polarization tests only.

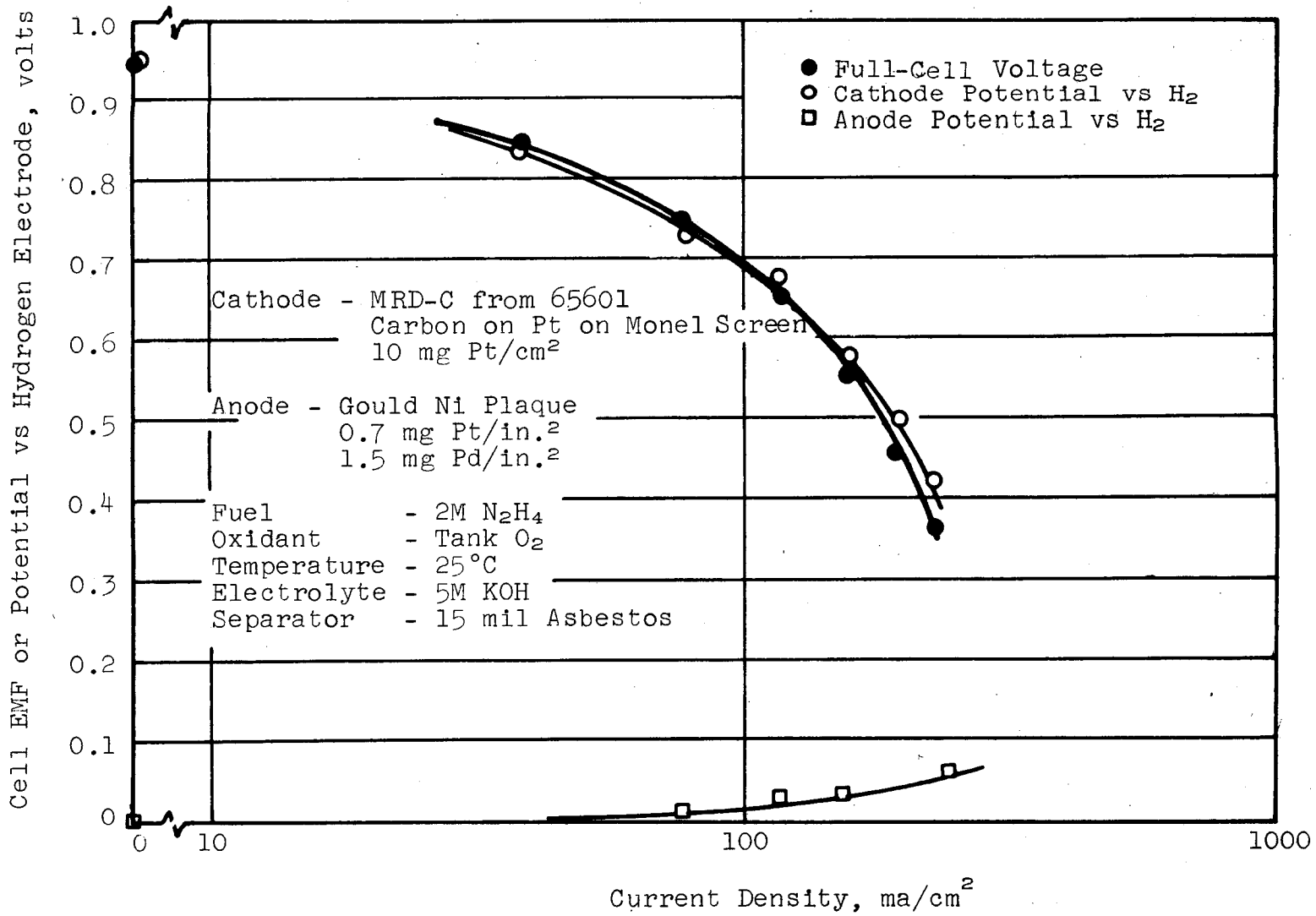

Figure 16. Initial Polarization Curves for Full Cell 65608

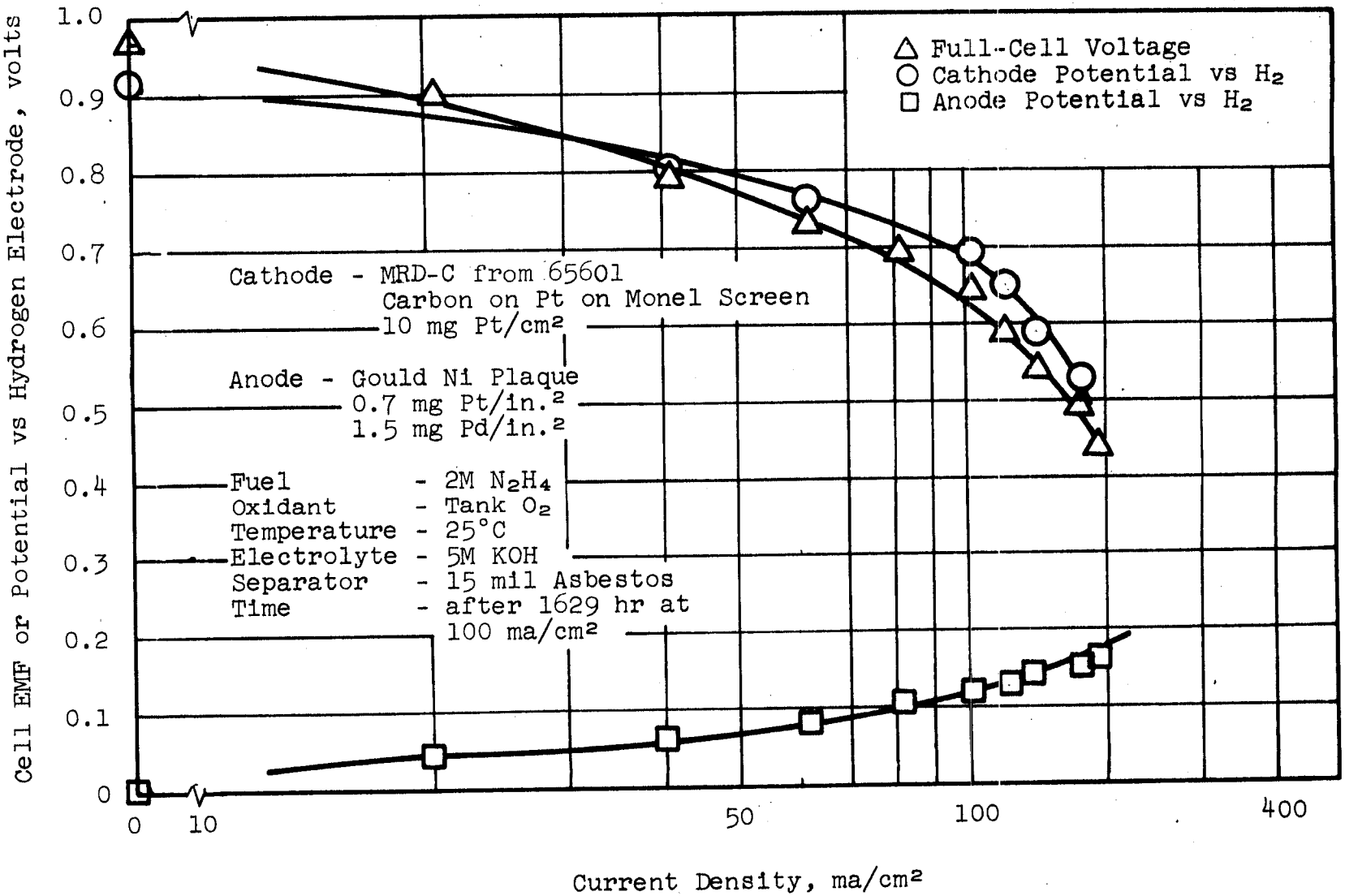

Figure 17. Polarization Curves for Full Cell 65608 (N_2H_4/O_2)

Testing of cell 65611 was terminated after 846 hours because of an accidental pressure pulse, which caused a rupture of the electrode membrane at an unsupported area and excessive electrolyte leakage through the cathode. A two-screen electrode structure has been developed that will give sufficient support to prevent similar accidents in the future. No change in catalytic activity of the electrodes was found over the entire operating life. When the cell was disassembled no evidence of corrosion or material degradation was found. The cell was performing normally prior to membrane rupture (0.66 to 0.60 v, 100 ma/cm^2, 25°C). A polarization curve for this cell is presented in Figure 18.

2. N_2H_4-H_2O_2

Cell 65617 was activated with 2M N_2H_4 in 5M KOH fuel and 1M H_2O_2 oxidant at 25°C. The current-voltage relations are plotted in Figure 19. Current-voltage relations are similar to those of a similar cell using O_2 as an oxidant (Cell 65618) up to current densities of 100 ma/cm^2 (0.70 v at 100 ma/cm^2 for both cells). At higher current densities, however, the O_2 cathode is better than the H_2O_2 cathode.

3. N_2H_4-Air

Cell 65618 with palladized nickel plaque anodes and MRD-C (Pt) cathodes was tested with both O_2-N_2H_4 and air-N_2H_4 reactants. Current-voltage relations with the O_2-N_2H_4 system are shown in Figure 20, while similar relations with the air-N_2H_4 system are shown in Figure 21. Cell voltages with O_2 and air as oxidizers at 75°C are similar at low current densities (20 ma/cm^2), but the O_2 cell is appreciably better at current densities above 100 ma/cm^2. The air cell had a voltage of 0.68 volt at 100 ma/cm^2 at 75°C, compared with the O_2 cell's voltage of 0.82 volt under similar conditions.

4. N_2H_4-O_2 with Polypropylene Mat Separator

Cell 67601, described in Table 9, was constructed to determine performance with very close electrode spacing (approximately 5 mils). The polypropylene mat was used primarily as an electrical insulator between the electrodes and, because of its open construction, approached a free electrolyte-type separator.

Figure 22 shows full-cell performance over a temperature range of 15°C to 70°C. At 30°C and at a discharge rate of 100 ma/cm^2, this cell has approximately 0.1 volt higher potential than cells with the 15-mil thick asbestos separator (compare with Figure 16 at 25°C).

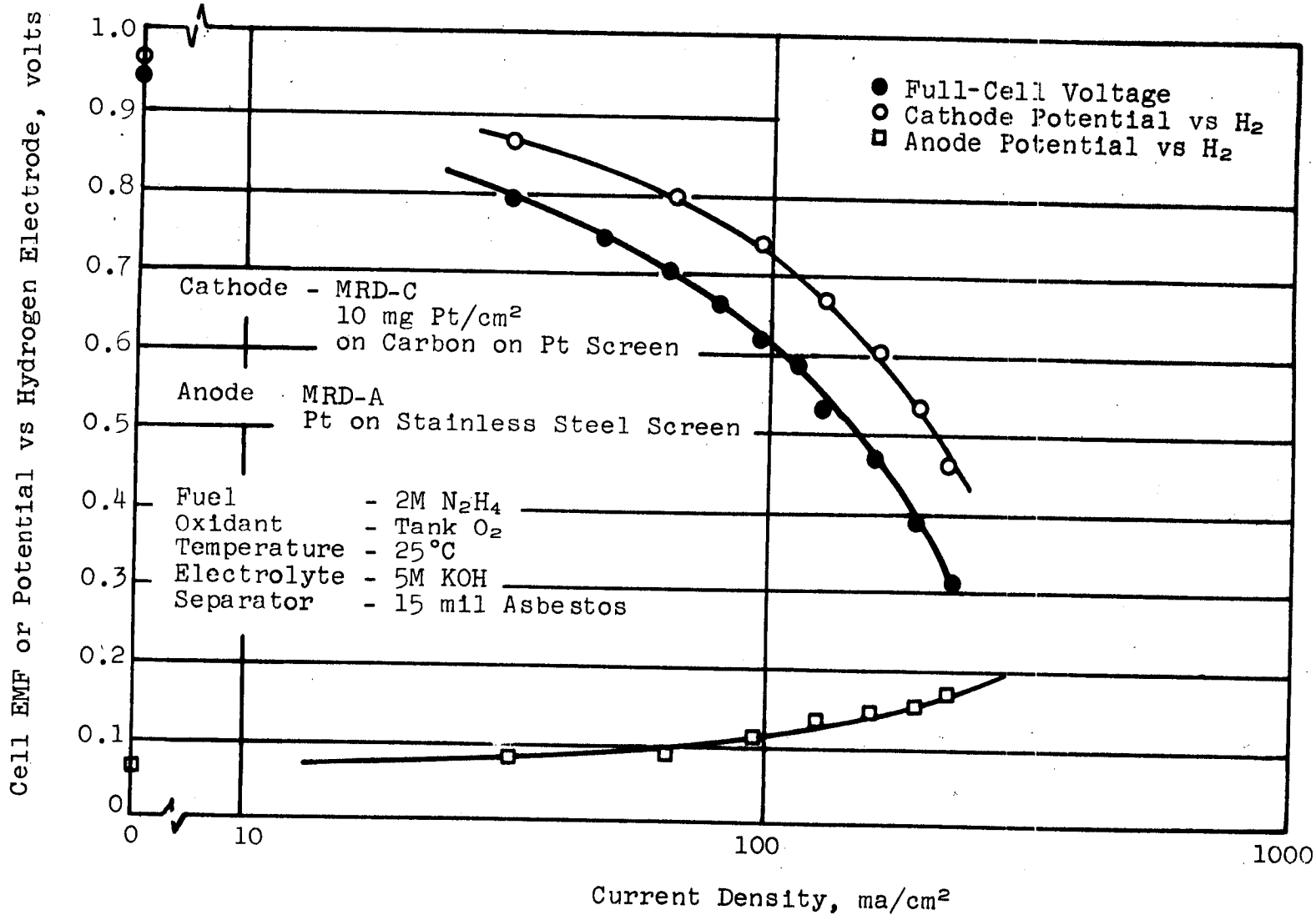

Figure 18. Polarization Curves for Full Cell 65611

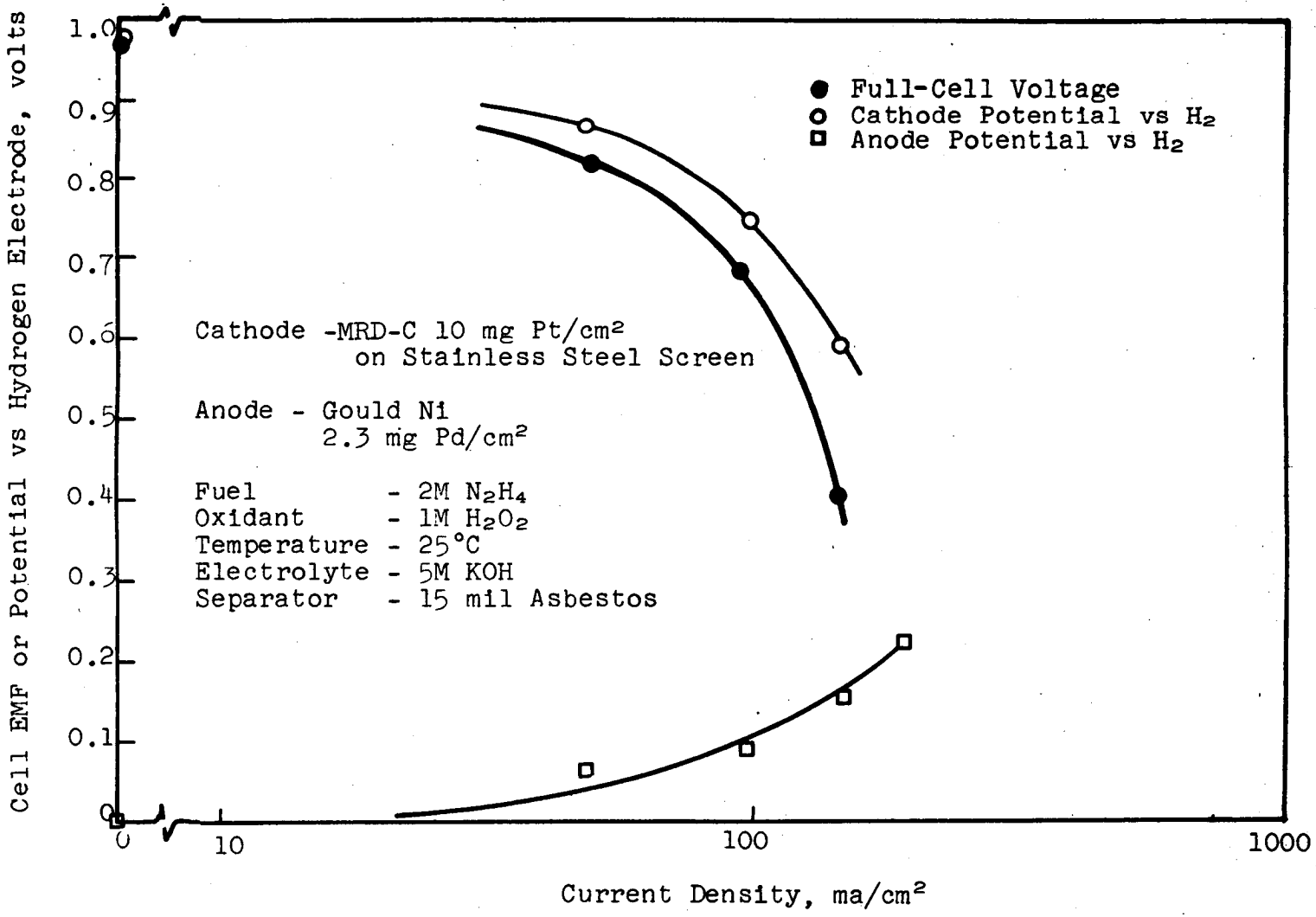

Figure 19. Polarization Curves for Full Cell 65617

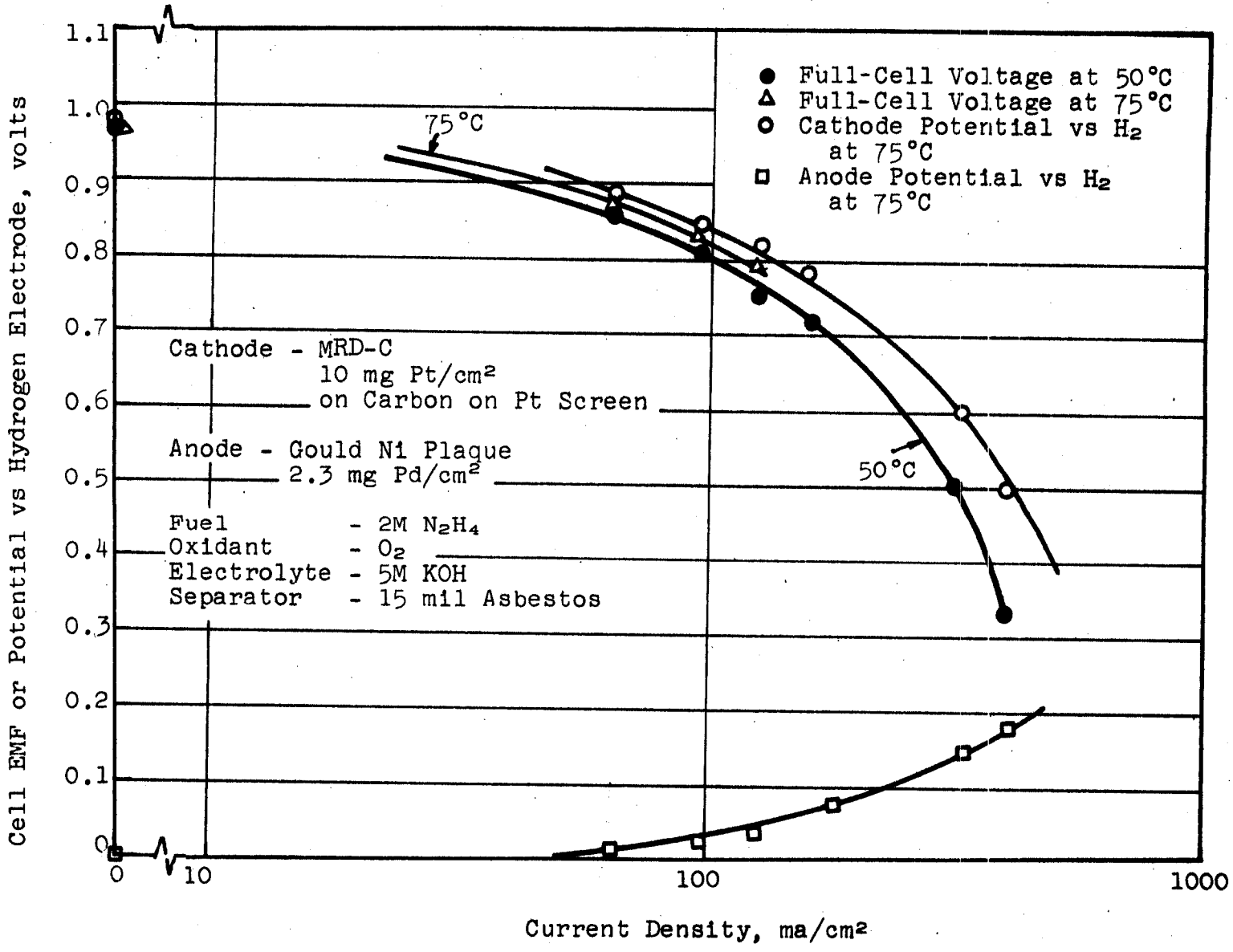

Figure 20. Polarization Curves for Full Cell 65618

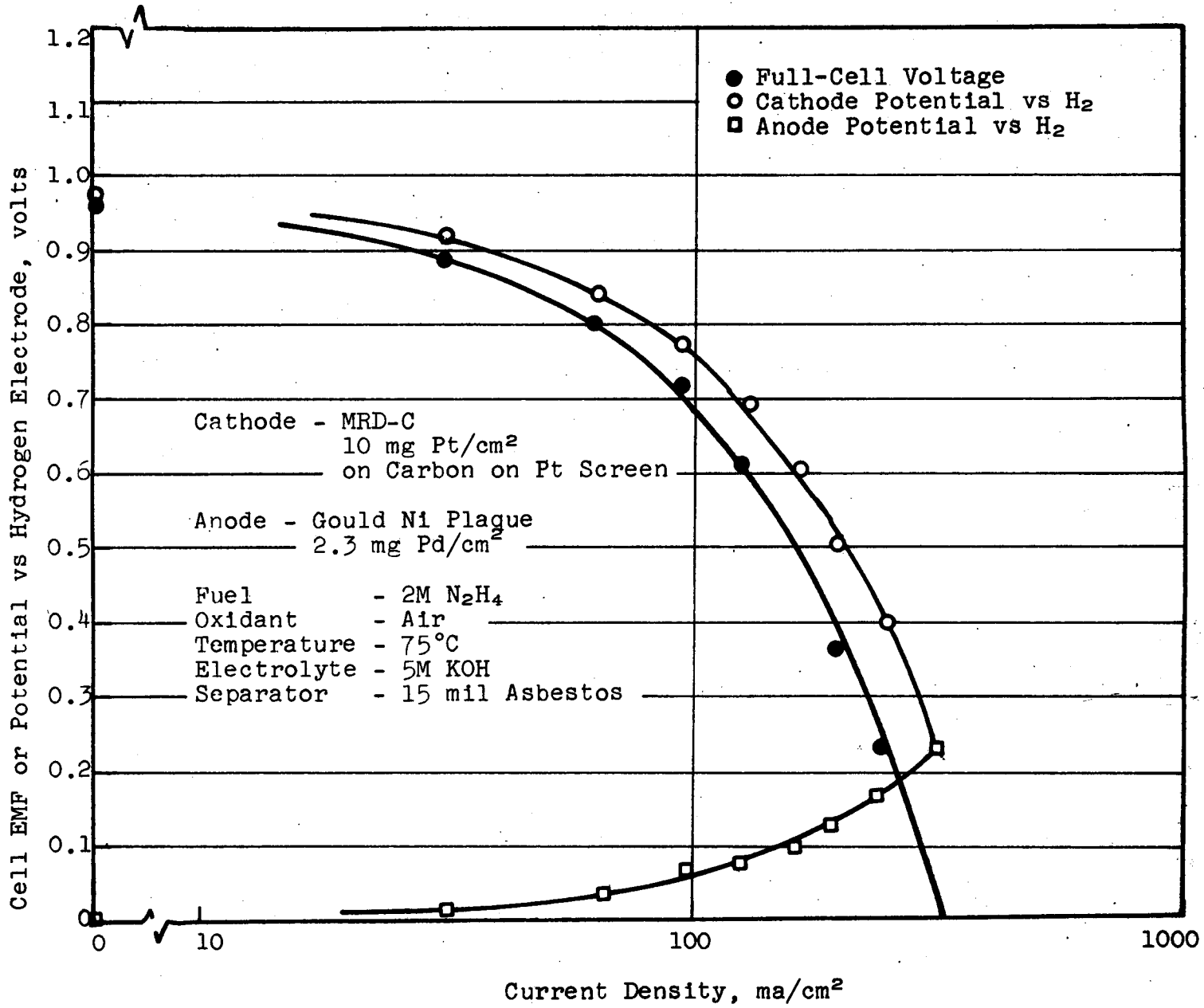

Figure 21. Polarization Curves for Full Cell 65619

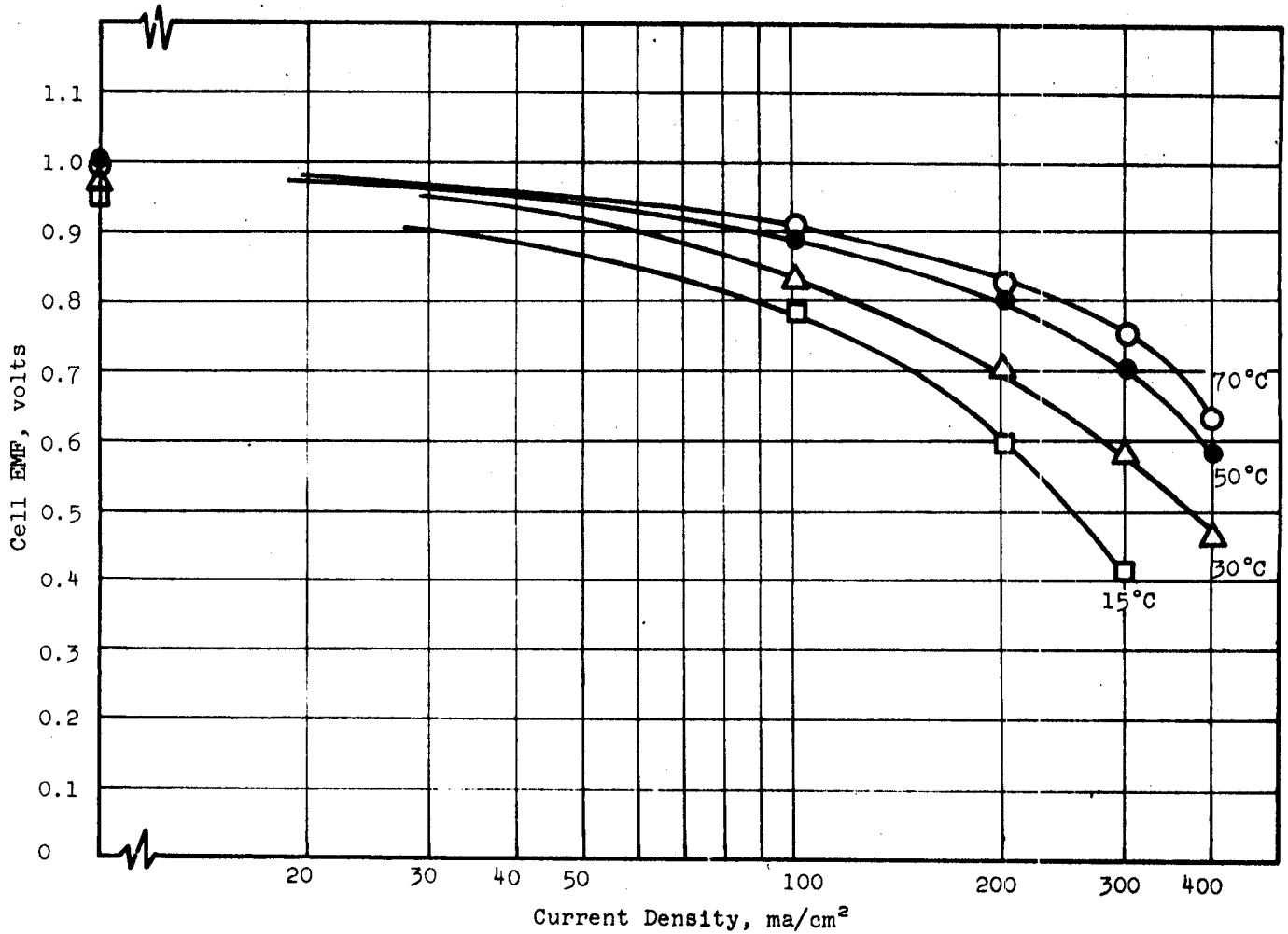

Cathode:	MRD-C 9 in.² 7 mg Pt/cm² on Stainless Steel Screen	Fuel:	2M N_2H_4 in 5M KOH
		Oxidant:	O_2
		Electrolyte:	5M KOH
Anode:	Gould Ni Plaque 25 mils thick, 3 mg Pd/cm²	Separator:	Polypropylene Mat Approx. 5 mils thick

Figure 22. Effect of Temperature on Discharge of Full Cell 67601

The salient characteristics of this cell's performance are:

a. Operation on 0 psig oxygen with only a slight purge (1%) required.

b. Excellent low-temperature characteristics; good performance at room temperature and demonstrated operation at 15°C.

c. Anodic coulombic efficiencies for the oxidation of hydrazine above 90%.

5. Conclusions and Summary

The over-all results of this work are a demonstrated capability for the use of the storable propellants, hydrazine and oxygen or hydrogen peroxide, in an operating fuel cell at high efficiencies with excellent electrical output at low temperatures over an extended period. The development of a hydrogen anode on another contract extends this capability to the hydrogen/oxygen system as well. Cell development has proceeded to the point where a 1-KW NASA system design was submitted, which met all electrical specifications (Appendix IX). The unit measures 1.3 cu ft, weighs 46 lbs, and has 100% overload capability. The system is considered partially optimized, and operating modules for specific missions can be developed.

E. ION EXCHANGE MEMBRANE CELLS - ACID CATHOLYTE AND ANOLYTE

Full cells with cation exchange membranes (CEM) were constructed and characterized to compare various solution electrodes and CEM's.

All cells employed 9-in.^{2} electrodes, incorporated in the cell configurations described previously.

Ion exchange membranes were equilibrated in H_3PO_4 solutions, as specified by the manufacturers, before incorporation into the cells. The membrane was used as the gasket to seal the cell end plates so that in all cases electrode separation was equal to the thickness of the CEM itself.

Electrodes used were as follows:

1. FC-13 Carbon - porous carbon block 1/8-in. thick supplied by Pure Carbon Co., St. Marys, Pa.

2. MRD-A - Monsanto anode containing polytetrafluoroethylene and noble metal blacks; e.g., Pt or Rh. Catalyst loading in all cases 10 mg/cm^2.

3. MRD-C - Monsanto cathode constructed the same as MRD-A.

Ion exchange membranes evaluated were:

1. Permion 1010 (Radiation Applications Co., Long Island City, N.Y.) - a fluorocarbon base membrane of the graft polymer type.

2. AMF C-313 (American Machine and Foundry Co., Springdale, Conn.) - a polystyrene base type cation exchanger.

3. Ionics 61AZ2-183 (Ionics, Inc., Cambridge, Mass.) - a polystyrene-type cation membrane supported on a dynel backing.

Anolyte used for all cells was 1M N_2H_4 in 5.76M H_3PO_4. Catholyte used as 5M HNO_3 in 5.76M H_3PO_4.

All cells were operated for at least 4 hours.

Table 10 is a summary of performance of typical cells constructed in this phase of the work.

With the exception of the Ionics membrane, cell IR losses of about 0.4 volt at 50 ma/cm^2 were experienced with the ion exchange membranes tested. This very high voltage loss, due to the IEM resistance, severely limited the performance of most of the cells and made them unsatisfactory for practical application to the NASA design specifications.

Only Cell No. 61544, incorporating the Ionics membrane, performed at a power level of sufficient magnitude to be of interest. This cell was operated for 30 hours at 100 ma/cm^2 with no appreciable change in electrical characteristics. On disassembly of the cell, no significant HNO_3 attack on the ion exchange membrane or other cell parts was noted. No mixing anolyte and catholyte were observed.

F. ION EXCHANGE MEMBRANE CELL - ACID CATHOLYTE AND ALKALINE ANOLYTE

The advantages of this system have been discussed previously. The work started in the 9 sq in. cell with the idea of protecting a catalyzed palladium foil membrane anode from attack by nitric acid; however, the nickel plaque anode was soon found to work best. Platinum screen solution cathodes were used. Both organic and inorganic ion exchange membranes were used, the inorganic exchanger being zirconium phosphate. Nitric acid (15 M) was used as the oxidant and 1M hydrazine dissolved in 5M potassium hydroxide as the fuel. High voltages and little polarization were found on short-term tests: 1.6 volts at 100 ma/sq cm, 60°C, for an Ionics, Inc. cation exchange membrane. However, life was poor in almost all cases; the best performance was 70 hours at 70°C with the membrane protected by a Teflon felt. Deterioration of the membrane and the

Table 10

ION EXCHANGE MEMBRANE FUEL CELL TESTS

Fuel: 1M N_2H_4 in 5.76M H_3PO_4

Oxidant: 5M HNO_3 in 5.76M H_3PO_4

Electrode Area: 9 $in.^2$

Cell No.	Anode	Cathode	IEM	Temp °C	Electrical Performance -- Cell Potential (volts) at Current Density Listed, ma/cm^2 0	20	40	60	80	100	150	Cell IR Loss, volts at 50 ma/cm^2	Notes
61534	MRD-A Rhodium	FC-13	Permion 1010	90	0.94	0.52	0.23					0.43	Cathode polarized 0.35 volt at 50 ma/cm^2
61538	MRD-A Pt	MRD-C Pt	Permion 1010	43	0.75	0.50	0.28	0.05				0.2	Poor anode performance and low IR loss indicates HNO_3 leakage through IEM
61540	MRD-A Pt	MRD-C Pt	AMF C-313	39	0.90	0.57	0.38	0.22	0.05			0.41	Anode polarized 0.2 volt at 80 ma/cm^2
				90	0.92	0.65	0.44	0.25	0.08			0.38	
61542	MRD-A Rhodium	MRD-C Pt	AMF C-313	69	1.0	0.67	0.39	0.12				0.55	Cathode polarized 0.25 volt at 50 ma/cm^2
61543	MRD-A Rhodium	MRD-C Pt	AMF C-313	69	1.1	0.73	0.50	0.28	0.07			0.48	Anode polarized 0.3 volt at 80 ma/cm^2
61544	MRD-A Rhodium	MRD-C Pt	Ionics *	63	0.95	0.86	0.77	0.68	0.60	0.51	0.28	0.12	Anode polarized 0.3 volt at 160 ma/cm^2

* Ionics, Inc., 61AZ2-183 Cation Exchange Membrane

neutralization reaction that took place across the membrane were the major disadvantages. Further details on this work can be found in Appendix IV.

V. MONOMETHYLHYDRAZINE AND DIMETHYLHYDRAZINE REFORMING

A. BACKGROUND

Monomethylhydrazine (MMH) and unsymmetrical dimethylhydrazine (UDMH) can be utilized as storable rocket propellants. Since no efficient MMH or UDMH fuel cell anode has been found, the materials must first be reformed to hydrogen, nitrogen, and carbon dioxide, and these gaseous products must be fed to a hydrogen-burning fuel cell anode. Kuhn (ref. 3) has described the catalytic reduction of organic nitro compounds with MMH. Using a 5% Pd-charcoal catalyst, the decomposition products contained nitrogen, methane, and ethane. Liquid phase decomposition to nitrogen and hydrogen using platinum black as a catalyst was reported by Tanatar (ref. 4). The complete decomposition of MMH or UDMH to hydrogen, nitrogen and carbon dioxide will require either converting any methane formed to carbon dioxide or inhibiting the formation of the methane in preference to carbon dioxide.

Reformed hydrogen can be used as an anode fuel, either as "dirty" hydrogen (in the presence of other reformed products such as carbon monoxide, carbon dioxide, nitrogen, or ammonia) or as "clean" hydrogen that has been separated from other gases by passing through a palladium diffusion membrane.

B. METHOD

A catalytic reformer, shown schematically in Figure 23, was constructed. The system consisted of a feed tank, pump, vaporizer, preheater, four identical reacting sections, a condenser, and a separator. When the unit was in operation, MMH, or UDMH, and water were fed as liquids, and the effluent was collected as a liquid.

The reactor sections were 6-in. lengths of 304 stainless steel tubing, 5/8-in. O.D. with 0.065-in. walls. The use of tube fittings enabled the easy replacement of a section without removal of all four reacting sections. Catalysts were placed in boats, formed from stainless steel screening, that measured 1-1/2 in. in length and 1/2 in. in diameter. These boats were filled with catalyst and placed in the tube section prior to a run. Sampling lines preceding and following the reactor sections allowed an evaluation of each catalyst tested in a given run.

Heat was supplied by electrical heating tape wrapped around the vaporizer, preheater, and catalyst sections. Thermocouples on all the heated sections plus two in-stream thermocouples enabled close control of temperature throughout the system. Cooling water was uses to condense the product stream, leaving carbon monoxide, ethane, methane, nitrogen, and hydrogen, and

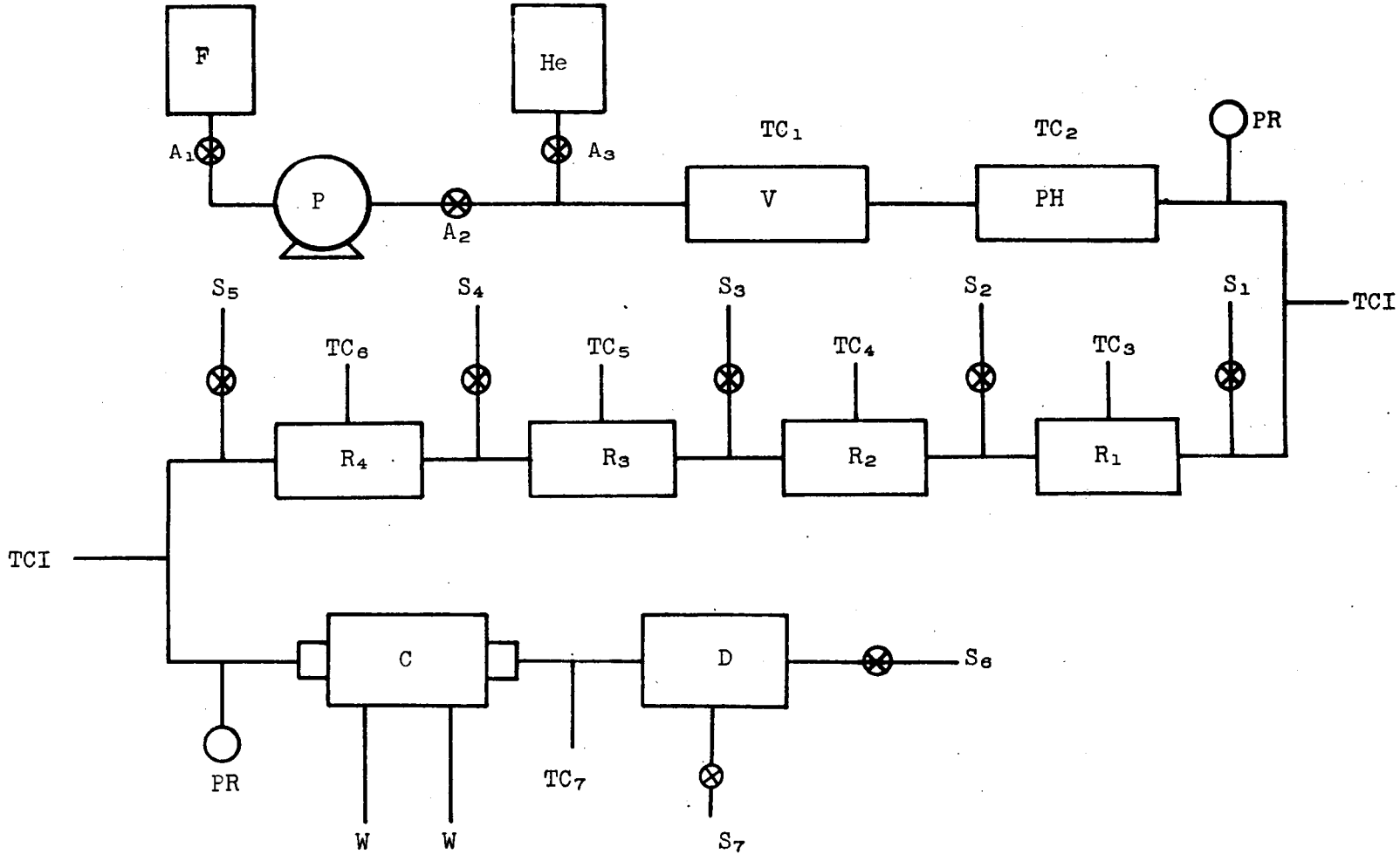

Legend

F = Feed tank
P = Pump
He = Helium cylinder
V = Vaporizer
PH = Preheater

PR = Pressure gage and relief
TCI = In-stream thermocouple
S = Sample line
TC = Thermocouple
R = Reacting section

C = Condenser
D = Separator
A = Feed valves
W = Cooling water

Figure 23. Catalytic Reformer

other product gases for analysis by gas chromatography. Pressure gauges and relief valves were also incorporated in the system.

The feed composition initially tried was 1M MMH in water. Poor results with this concentration led to the use of 1 mole MMH/2 moles water or 1 mole UDMH/4 moles water as the test concentrations.

When making a run the system was first flushed with helium. The MMH or UDMH/water feed tank was filled to the desired level, the heaters were turned on, and the pump was started. Thermocouple readings were recorded and pressure control was maintained by a pressure regulator after the desired temperature had been reached. Effluent liquid was collected and the product gas rate was measured by a wet-test meter.

Gas samples were taken during the run, using gas sample tubes, and were later analyzed by gas chromatography, using a silica gel column. This method gave a direct analysis for hydrogen, nitrogen, carbon monoxide, methane, and ethane.

Reforming conditions for MMH and UDMH and product gas consumption are shown for six runs in Table 11. The product gas, after passing through the four catalyst beds of Run 1, was relatively low in hydrogen (23%) and high in methane and ammonia (27 and 4%). Gas compositions for subsequent runs are given after each catalyst bed.

The higher temperature of Run 2 favored more carbon monoxide formation but also increased the ammonia yield. A material balance for Run 2 is given in Table 12. The hydrogen composition (48.2%) of product gas after passing MMH through catalyst beds of palladium, iridium, and ruthenium/iridium at 297°C was the highest found for any combination of catalyst and temperature, while a single pass through Pd at 263°C was second best. Four beds of palladium catalysts in series were used for Run 5. The hydrogen yields were relatively low, and the ammonia formation was undesirably high. Continued contact with palladium catalyst apparently promoted ammonia formation at the expense of the hydrogen yield.

Lower hydrogen yields resulted from reforming UDMH under the conditions of Run 6 of Table 11 than from reforming MMH under the conditions of Runs 1 to 5.

C. CONCLUSIONS

Reforming of MMH and UDMH appears to be a practical method of obtaining hydrogen-rich fuel cell feed gas. The reforming of MMH with palladium, iridium, and ruthenium/iridium catalysts in series resulted in a high yield of hydrogen. It may be necessary to introduce a gas purifier to effect carbon monoxide,

Table 11

MONOMETHYLHYDRAZINE AND DIMETHYLHYDRAZINE REFORMING

Run No.	1	2				3				4				5				6			
Fuel*	MMH	MMH				MMH				MMH				MMH				UDMH			
Conditions																					
Feed, moles H_2O/ mole Fuel	2	2				2				2				2				4			
Feed Rate, ml/min	1.4	3.85				4.3				2.1				2.3				2.4			
Pressure, psig	16	23				25				24				24				24			
Temperature, °C	150 ± 10	235 ± 5				263 ± 8				297 ± 7				271 ± 19				295 ± 10			
Catalysts	Pd-Pt-Rh-Ru**	Pd	Pt	Rh	Ru	Pd	Pt	Rh		Pd	Ir	Ru/Ir	Ru	Pd	Pd	Pd	Pd	Pd	Pt	Rh	Ru
Product Gas, mole %																					
H_2	23.1†	30.7	38.7	35.1	42.3	43.1	40.0	36.7		38.3	37.1	48.2	40.7	34.8	34.7	35.3	33.0	22.5	17.8	17.2	18.6
N_2	39.1	36.2	27.1	26.5	20.4	28.4	23.2	20.9		42.2	25.7	21.5	24.2	27.4	20.1	19.3	16.6	8.5	13.0	10.2	10.7
CO	6.1	0.8	4.5	9.3	14.4	5.7	8.5	10.9		<2.0	5.2	4.8	7.0	7.5	10.5	12.7	14.1	17.3	9.8	12.2	10.8
CH_4	26.6	29.4	23.4	22.0	10.4	20.2	17.0	15.3		35.6	22.2	18.1	19.3	21.0	16.4	13.9	13.2	10.3	16.0	14.1	15.0
C_2H_6	1.0	1.2	1.9	0.9	0.7	1.5	1.3	1.1		2.0	1.3	1.0	1.0	1.2	0.9	0.8	0.6	0.6	3.6	2.8	3.0
NH_3	4.0	1.8	4.6	6.5	11.7	1.1	10.0	15.2		-	8.6	6.7	8.0	9.2	17.5	18.0	22.7	40.7	39.8	43.5	41.9

* MMH - Monomethylhydrazine
UDMH - Unsymmetrical Dimethylhydrazine

† Analysis after passing through four beds in series.
Other analyses after each catalyst bed.

** Pd - 0.5% Pd on 1/8-in. alumina pellets
Pt - 0.5% Pt on 1/8-in. alumina pellets
Rh - 0.5% Rh on 1/8-in. alumina pellets
Ru - 0.5% Ru on 1/8-in. alumina pellets
Ir - Ir on 8-14 mesh alumina
Ru/Ir - 68% Ru/32% Ir on 8-14 mesh alumina
(All catalysts from Englehard Industries, Inc., Newark, N. J.)

carbon dioxide, and ammonia removal between reformer and fuel cell unless a cell anode is available which is relatively insensitive to poisoning.

Table 12

MASS BALANCE FOR MMH REFORMING

(For Run 2, Table 17)

	MMH		H_2O
Fed	1.64 moles	Fed	3.28 moles
Recovered	0.60	Recovered	2.71
Used	1.04 moles	Used	0.57 moles

Product Gas	Moles
CO	0.57
C_2H_6	0.03
CH_4	0.41
H_2	1.67
N_2	0.81
NH_3	0.46
	3.95 total moles of gas

Recovered: 3.57 moles of gas
plus amount of gas for samples

% Conversion: 1.04/1.64 = 63.5% MMH

H_2 Conversion: 1.67/1.04 = 1.60 moles H_2/mole MMH
1.67/1.61 = 1.04 moles H_2/mole reactants

VI. REPORT AND APPENDIX REFERENCES

1. J. O. Smith, Final Report, "Study of Fuel Cells Using Storable Rocket Propellants," 11 May 1964, Contract No. NAS3-2791.

2. M. C. Deibert, Topical Report, "Fuel Cell Membrane Electrode Configuration," 31 August 1964, Contract DA49-186-AMC-166(X).

3. L. P. Kuhn, J. Am. Chem. Soc., 73, 1510 (1951).

4. Tanatar, Z. physik Chem., 40A, 475 (1907).

5. C. N. Satterfield and T. K. Sherwood, "Role of Diffusion in Catalysis," Addison-Wesley Publishing Co., Inc. (1963) p. 3.

6. D. M. Yost and H. Russell, "Systematic Inorganic Chemistry," Prentice-Hall (1946), p. 78.

7. D. P. Smith, "Hydrogen in Metals," Univ. of Chicago Press, Chicago, 1948.

8. S. Schuldiner and J. P. Hoare, J. Electrochem.Soc. 103, 178 (1956).

9. H. G. Oswin and S. M. Chodash, Fuel Cell Symposium, Division of Fuel Chemistry, American Chemical Society, 7, No. 4, 84-94 (1963).

10. A. S. Darling, Platinum Metals Review, 1, No. 4, 126-129 (1963).

11. O. N. Salmon, D. Randall, E. A. Wilk, "Mechanism of the Diffusion of Hydrogen Through Active and Inactive Palladium," AEC Res. Dev. Report KAPL-1674, Nov. (1956).

12. L. Lederer and N. D. Greene, Electrochimica Acta, 8, 883 (1963).

13. American Soc. for Metals, "Metals Handbook," Vol. 1, p. 1194 (1961).

14. U. R. Evans,"The Corrosion and Oxidation of Metals," Edward Arnold Pub. Ltd., London, p. 108 (1961).

15. J. P. Couglin, "Contributions to the Data on Theoretical Metallurgy," XII Heats and Free Energies of Formation of Inorganic Oxides. Bulletin 542, Bureau of Mines, p. 45 (1954).

16. O. Kubaschewski and B. E. Hopkins, "Oxidation of Metals and Alloys," Academic Press, Inc., New York, p. 24 (1962).

17. Ibid., p. 182.

18. R. W. Crompton and M. T. Elford, J. Sci. Instrum., 39, 480 (1962).

19. W. H. Hatfield, J. Iron and St. Inst., 115, 486 (1927).

20. V. R. Evans, "The Corrosion and Oxidation of Metals," Edward Arnold Pub. Ltd., London, England, pp. 77, 857 (1960).

21. E. M. Wise, "Corrosion Handbook," edited by H. H. Uhlig, John Wiley and Sons, Inc., New York, p. 107 (1958).

22. Ibid., p. 705.

23. Wöhler, L., Z. Elektrochem., 11 839 (1905).

24. J. O. Smith, "Study of Fuel Cells Using Storable Rocket Propellants," Contract NAS3-2791, June 1963 to January 1964.

25. F. Helferick, "Ion Exchange," McGraw Hill, N. Y. 1962.

26. I. J. Gol, and O. S. Gol, "The Ion Exchange of Uranium and Some Fission Products on Titanium and Zirconium Phosphates," Second Geneva Conference (1958). Paper 468, Vol. 28.

27. C. B. Amphlett, L. A. McDonald, and M. J. Redman, J. Inorg. Nucl. Chem., 6, 220 (1958).

28. G. H. Nancollas and R. Paterson, J. Inorg. Nucl. Chem., 22, 259 (1961).

29. C. B. Amphlett, Pat. Apl. No. 17722/56 (1956).

30. D.J.G. Ives and G.J. Janz, "Reference Electrodes," Academic Press (1961).

31. G. G. Koerber and T. DeVries, J. Am. Chem. Soc., 74, 5008 (1962).

32. N. D. Greene and R. B. Leonard, Electrochemica Acta, 9, 45 (1964).

33. R. F. Steigerwald and N. D. Greene, J. Electrochem. Soc., 109, 1026 (1962).

34. H. H. Uhlig, "Corrosion and Corrosion Control," John Wiley and Sons, Inc., New York (1963).

35. Latimer, W. M., "Oxidation Potentials," Prentice-Hall (1952).

36. H. S. Harned and B. B. Owen, "The Physical Chemistry of Electrolytic Solutions," Reinhold (1958).

APPENDIX I

CATHODE DEVELOPMENT

A. BACKGROUND

Vapor diffusion-type porous carbon-Teflon cathodes have been developed for use with nitric acid or dinitrogen tetroxide oxidants. These electrodes provide controlled separation between the oxidants and electrolyte, thus preventing unreacted oxidants from contaminating the electrolyte.

Initial electrodes were made by bonding Teflon and carbon to a porous Teflon sheet. The vapor pressure of nitric acid (Figure A-1) was the driving force to promote diffusion of the vapor through the wet-proofed Teflon sheet to the conducting catalytic surface.

Variables inherent in the use of porous Teflon sheet as a diffusion control medium are pore size, effective pore length, porosity, and character of the carbon-Teflon bonding.

Gas diffusion equations invariably stem from a form of Fick's Law:

$$N = -D_m A \frac{dc}{dL} \qquad \text{(ref. 2)} \qquad (1)$$

where N = moles/unit time
D_m = molal diffusion coefficient
A = diffusion area
L = effective pore length
c = concentration
$\frac{dc}{dL}$ = concentration gradient

Assuming a linear gradient, this integrates to;

$$N = \frac{D_m A (c_1 - c_2)}{L} \qquad (2)$$

If the effective diffusion area A is independent of diffusion path length, the diffusion rate N should be inversely proportional to the thickness of the electrode.

However, for very thin teflon membranes, the surface condition from manufacturing and also from bonding to an electrode support could easily be an important or even limiting factor on the diffusion rate. Thus the diffusion rate N will not be inversely proportional to the thickness.

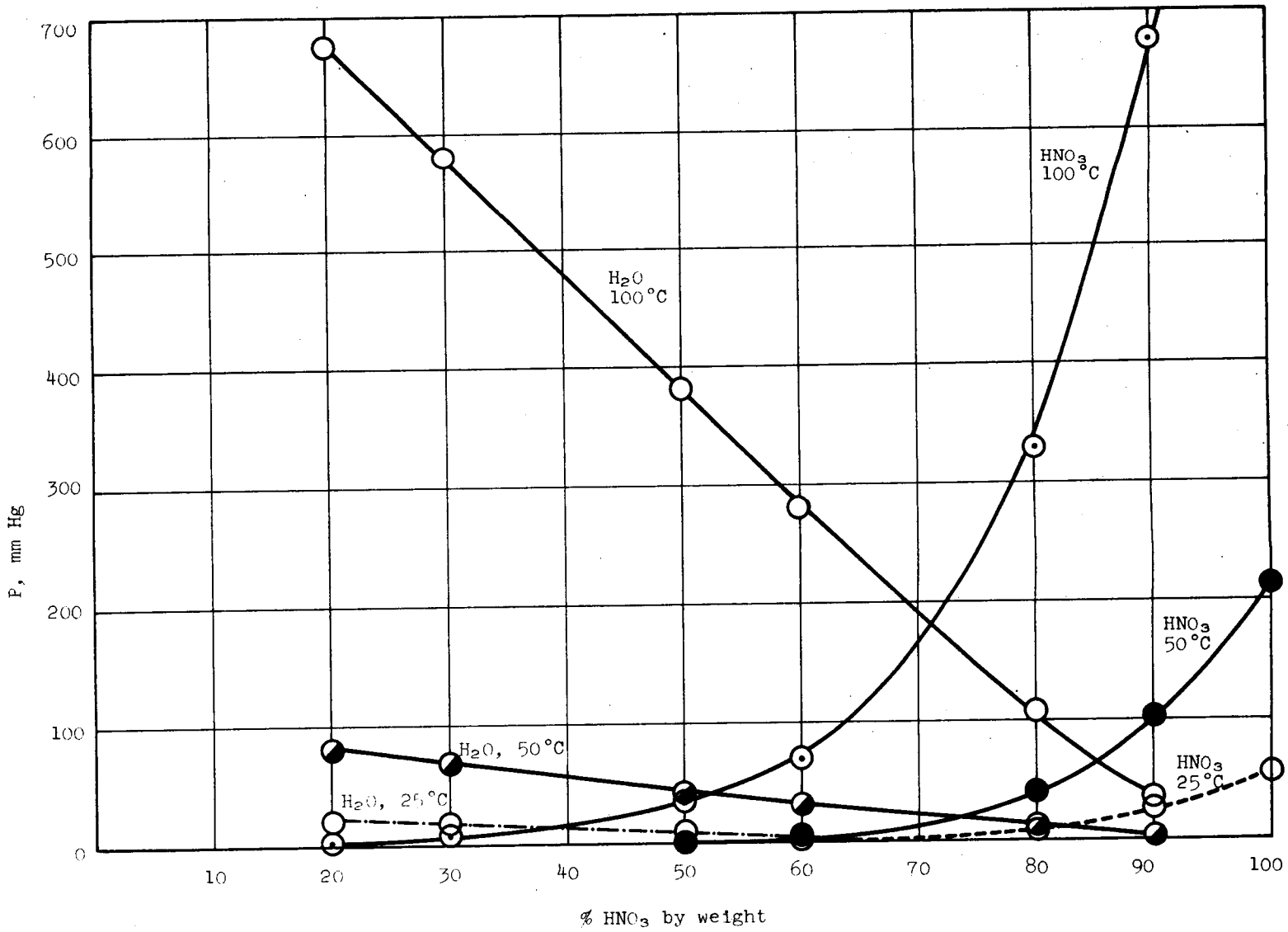

Data from "Systematic Inorganic Chemistry", D. M. Yost and H. Russell. Jr. Pentice-Hall, Inc., 1946.

Figure A-1. Variation of Vapor Pressure of HNO_3-H_2O Mixtures at 25, 50 and 100°C

When using teflon membranes of varying average pore size, the effective path length will vary due to differences in pore structure and thus for the same membrane thickness differences in diffusion rates would be expected.

B. CATHODES UTILIZING POROUS TEFLON DIFFUSION BARRIERS

1. Carbon-Teflon Powder Mixture Pressed into Porous Teflon Sheet

The electrode structure consisted of a tantalum ring holder, a porous Teflon controlling sheet, and the pressed powder mixture of carbon and Teflon powder with a tantalum screen current collector.

a. Variation of Activity with Teflon Loading

The most significant trend noted in the carbon-Teflon powder electrodes is the variation of polarization characteristics with Teflon loading. Voltammetric curves for the reduction of 70% HNO_3 and N_2O_4 (1 atm) with Teflon loadings from 0 to 50 mg/cm^2 are shown in Figure A-2. The lower Teflon loadings resulted in better electrochemical performance.

This effect is due to shorter diffusion path lengths and fewer carbon pores completely sealed off at the lower teflon loadings. Other factors might also be of some importance such as wetting characteristics.

b. Resistance and Reproducibility of Electrode

The carbon-Teflon powder electrodes have been plagued by both erratic and high internal electrode resistance and the difficulty of preventing gross leakage of oxidant around the edges of the electrode. The erratic resistance was attributed to the tantalum screen current collector. Some attempts were made to eliminate this source of resistance by substituting gold plated screens. This proved futile because of a permanent high resistance of the Teflon-carbon mixture.

In most cases, at very low Teflon loadings, lower resistances could be realized. However, the physical stability of the electrodes was poor at low Teflon loadings.

c. Conclusions

Although electrodes fabricated from porous Teflon sheet and

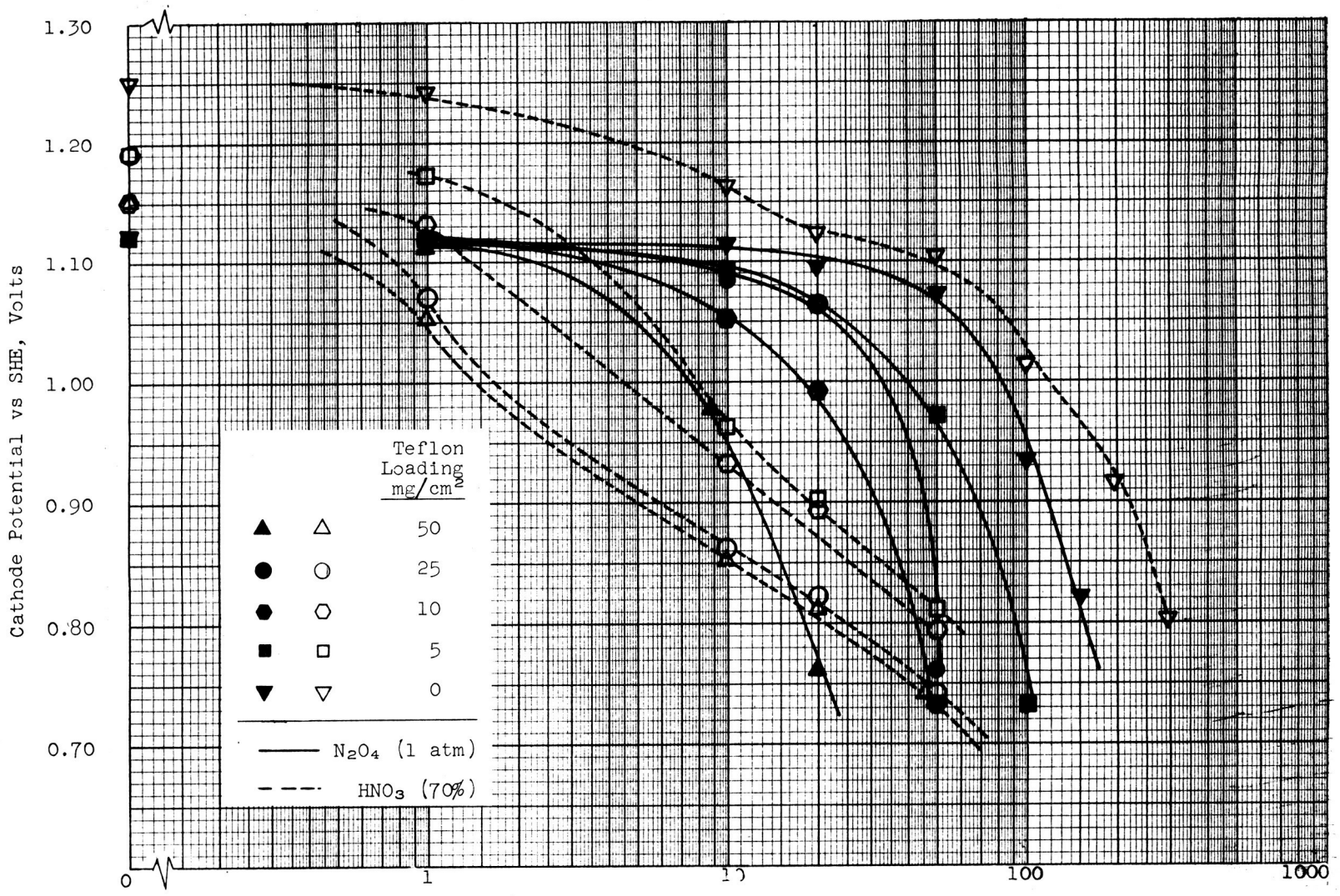

Construction Pressure: 4000 lb/in.²
Construction Temperature: 350°C
Electrolyte: 5M H_2SO_4
Catalyst: Shawinigan Black 25 mg/cm²
Cell Temperature: 90°C. 19 micron 0.015-in. thick porous Teflon

Figure A-2. Effect of Teflon-Carbon Ratio on Cathodic Polarization

carbon powder demonstrated vapor diffusion characteristics, the bonding operation apparently distorted the porous Teflon sufficiently to cause too low diffusion rate of nitric acid vapor, and consequently too low cathodic current density and poor reproducibility. Alternate types of construction were indicated because of the resistance and reproducibility difficulties mentioned above.

2. Porous Carbon Block-Porous Teflon Sheet Cathode

a. Effect of Porosity and Thickness on Limiting Reduction Current

(1) Pore Size

The cathodic polarization characteristics were measured for electrodes that were made by pressing porous Teflon with four different pore sizes against solid FC-14 carbon. The polarization data, presented in Figures A-3 and A-4, show a distinct trend with pore size. The limiting current density (and diffusion rate) of nitric acid increases with increasing pore diameter for electrodes that are normalized for thickness.

(2) Thickness

The dependence of diffusion rate upon thickness is clearly shown by the reversal of the pore size trend by 30-mil thick 34-μ pore diameter Teflon sheet (Figures A-3 and A-4). However, attempts to find a more definitive relation by sanding Teflon samples to 9 to 11 mils thickness showed only small gains in the diffusion rate.

Unsanded Teflon diffusion electrodes with pore sizes of 19μ, 12μ, and 34μ are compared with the respective sanded, thinner electrodes in Figures A-5, A-6, and A-7. The sanded sides of the Teflon sheets were bonded to the carbon for some tests, and the unsanded sides were bonded in other tests. In all cases, the sanded side, when bonded, provided lower diffusion rates than did the same Teflon sheet with the nonsanded side bonded. The diffusion rate of nitric acid remained constant or increased with decreasing thickness of Teflon with the nonsanded side bonded. With 34-μ and 12-μ porous Teflon sheet having thickness of 8 and 20 mils, the sanded samples showed greater diffusion rates than the unsanded samples. The limiting current density was not strictly inversely proportional to the thickness (as Fick's law would indicate). The bonding operation at 350°C [above the melting point (327°C) of Teflon sheet] no doubt caused distortion and plugging of Teflon pores.

(3) Carbon-Teflon Bond

The nature of the Teflon surface when bonded to the carbon substrate had a large and consistent effect on the diffusion rate

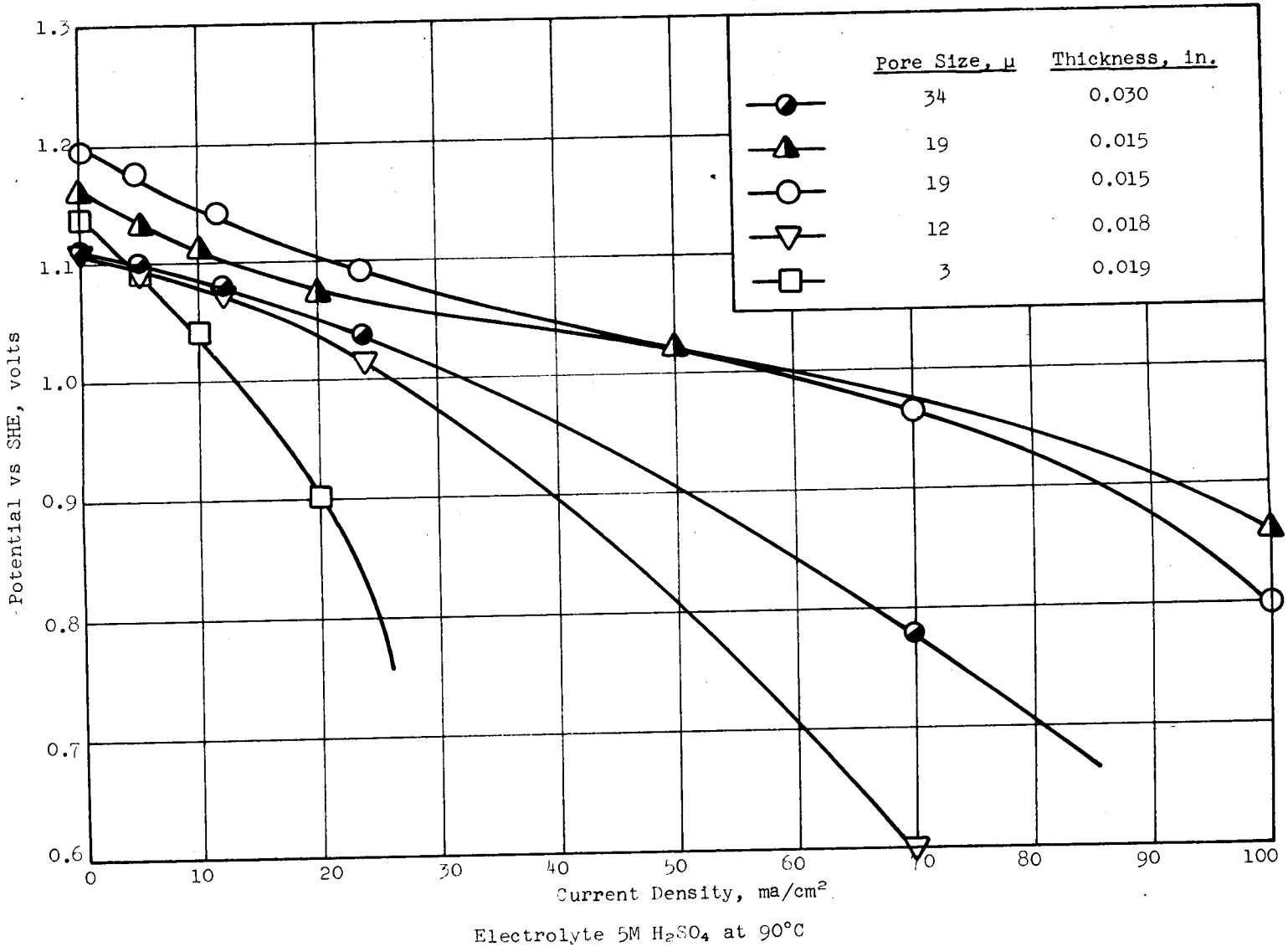

Figure A-3. Variation of N_2O_4 (1 atm) Cathodic Polarization Characteristics with Pore Size of Teflon Diffusion Electrodes

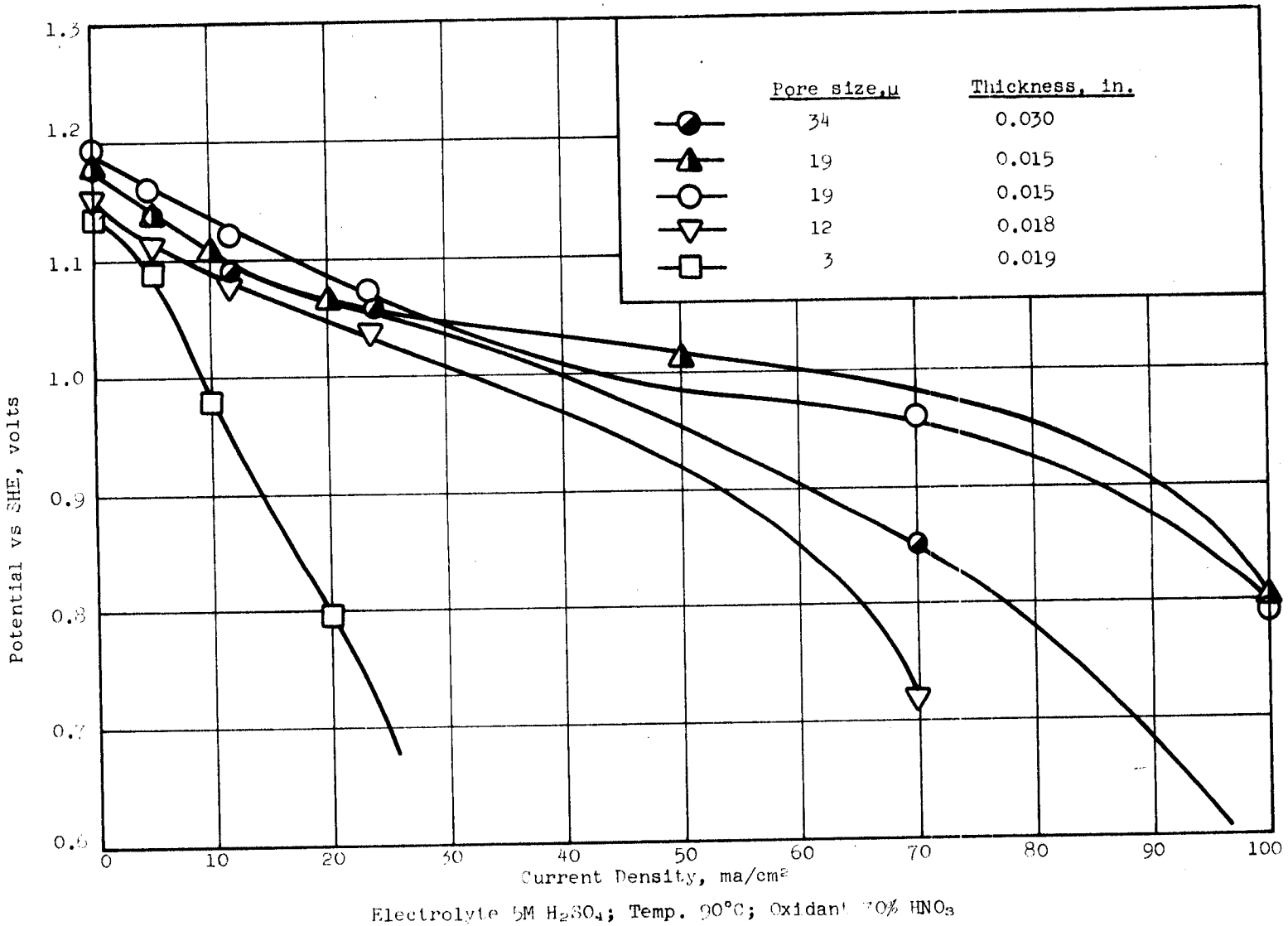

Figure A-4. Variation of HNO_3 Cathodic Polarization Characteristics with Pore Size and Thickness of Teflon Diffusion Electrodes

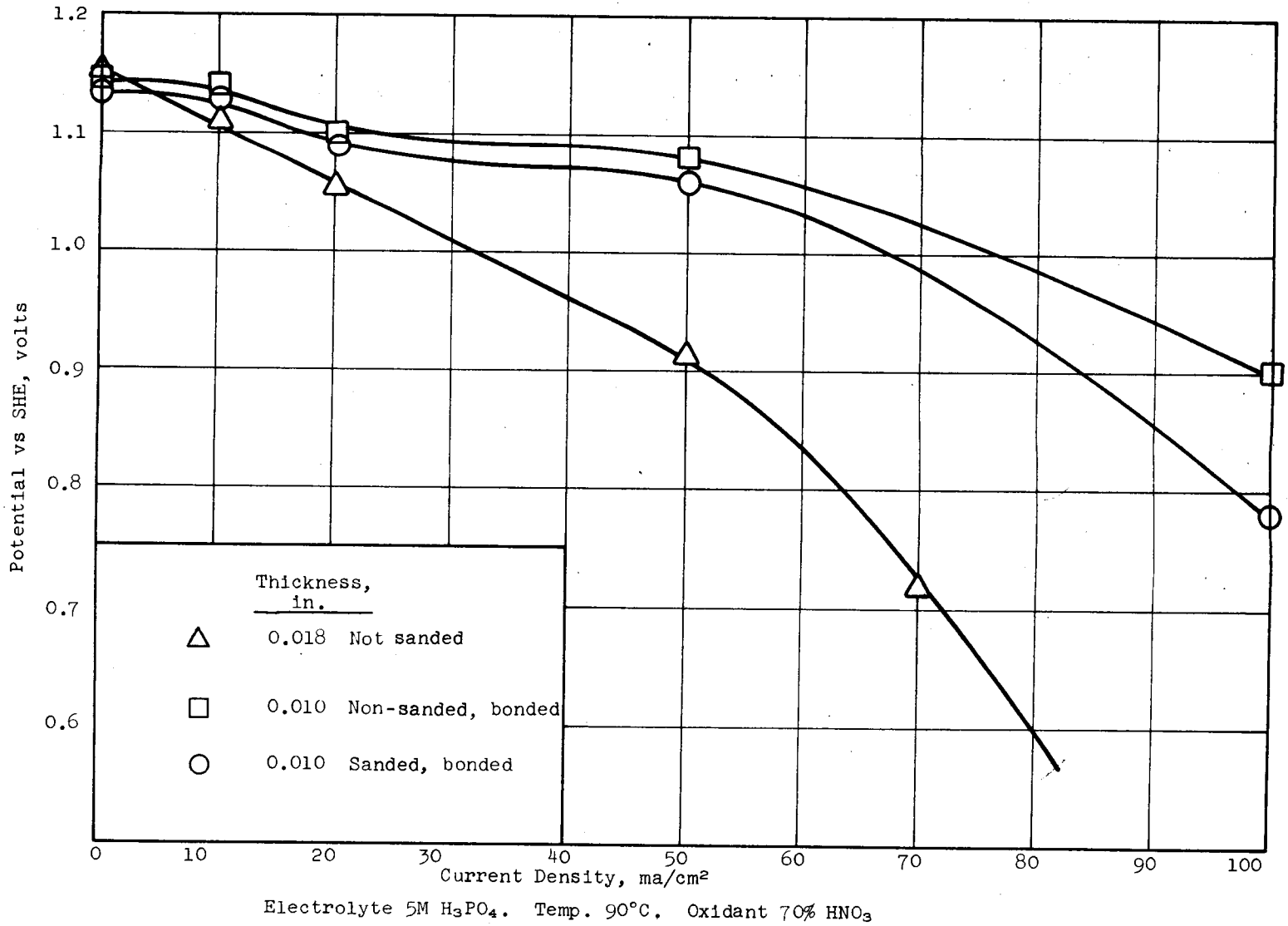

Figure A-5. Effect of Thickness of 12μ Porous Teflon Diffusion Electrodes on HNO_3 Cathodic Polarization Characteristics

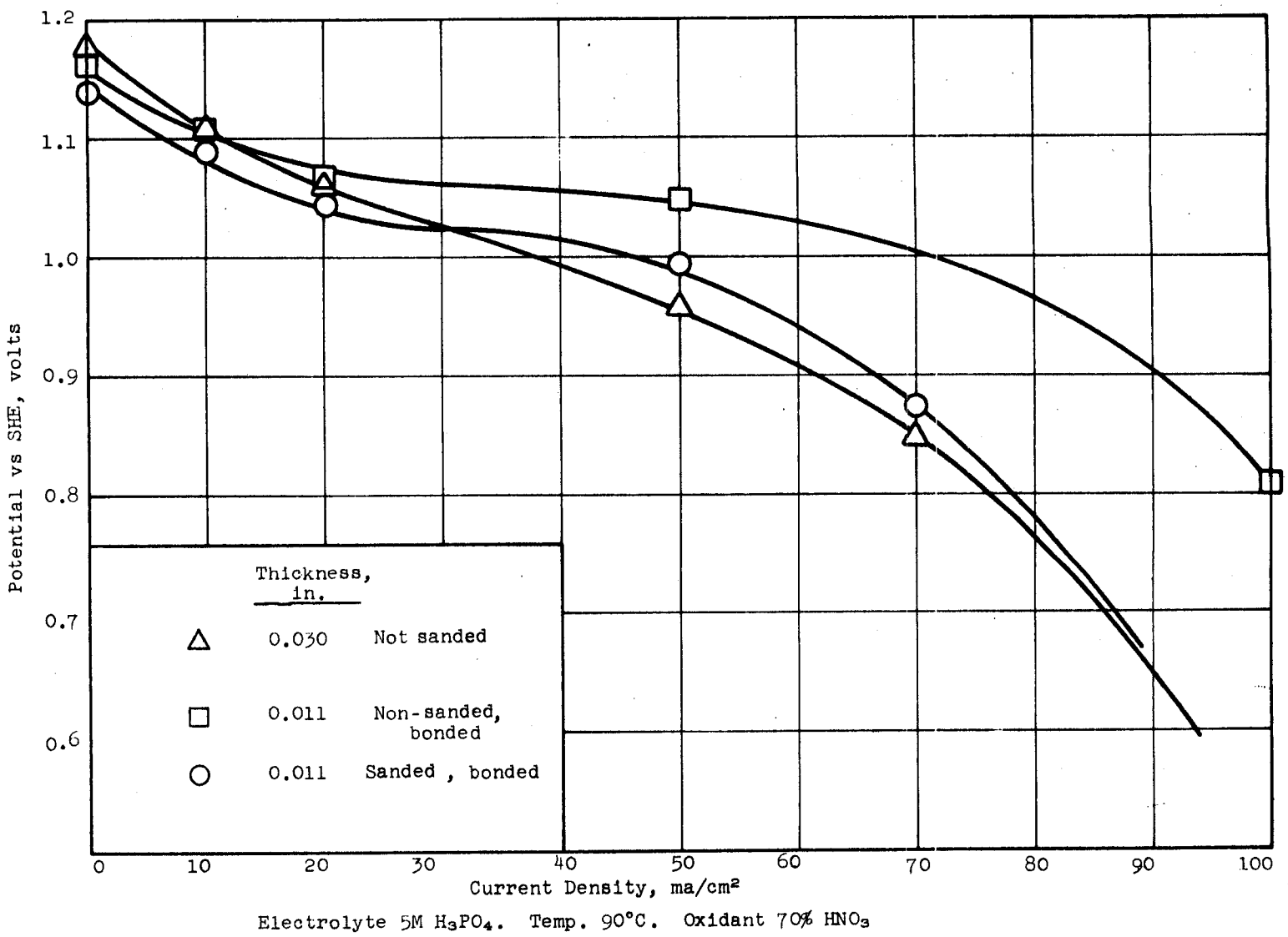

Figure A-6. Effect of Thickness of 34μ Porous Teflon Diffusion Electrodes on HNO_3 Cathodic Polarization Characteristics

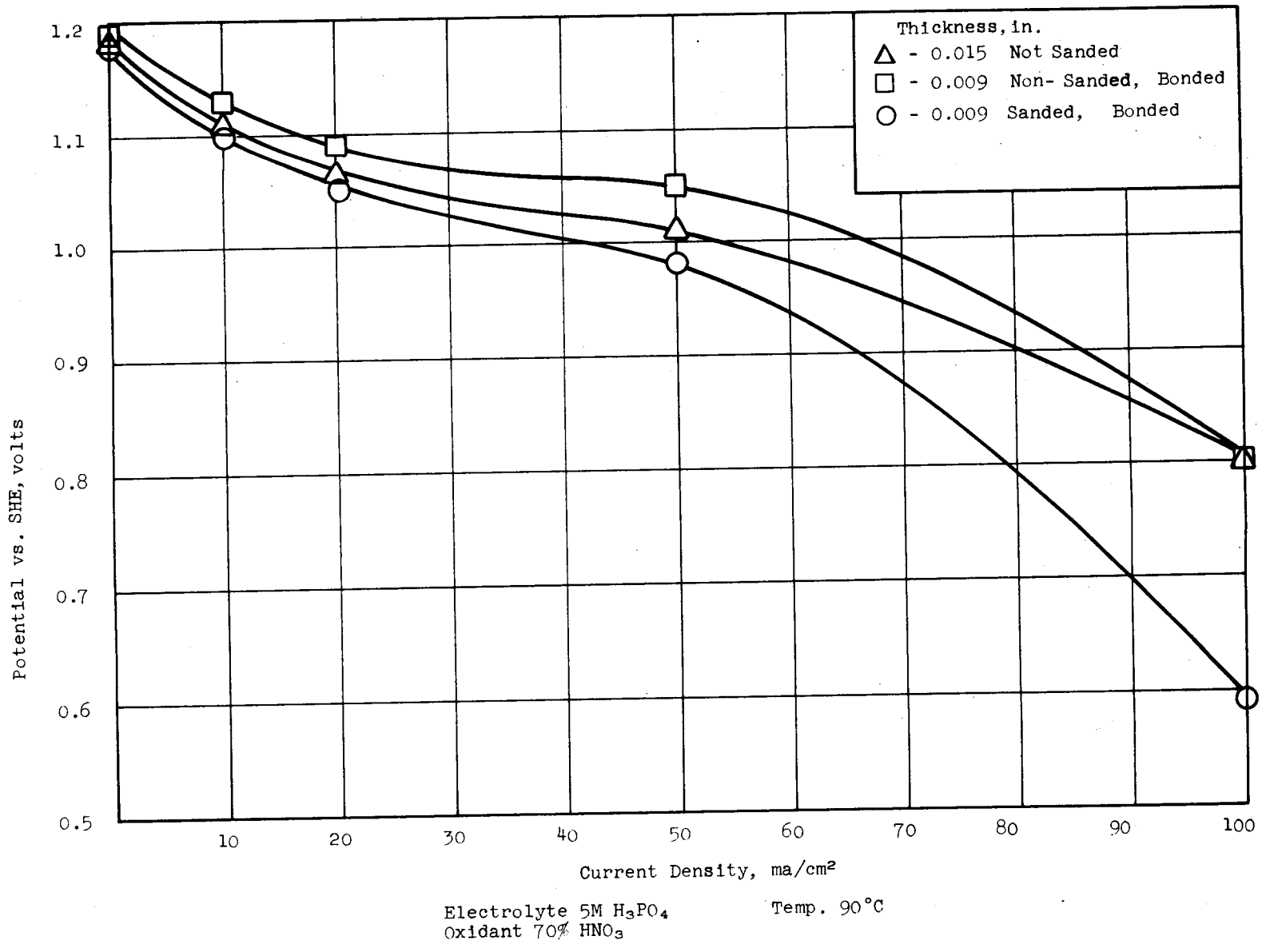

Figure A-7. Effect of Thickness of 19μ Porous Teflon Diffusion Electrodes on HNO_3 Cathodic Polarization Characteristics

of oxidants through the electrode (Figures A-5, A-6, and A-7). The greatest polarization improvement with sanding occurred for 12-μ pore size Teflon sheet that was decreased in thickness by a factor of 2. The 34-μ pore size sheet was decreased in thickness by sanding by a factor of 3. This suggests that either the effect of bonding is less significant in the smaller pore sizes than in the larger pore sizes, or that the sanding process has less effect in plugging smaller pores.

Because of the results of the sanding tests, we felt it was necessary to investigate the effect of both heating and bonding on the diffusion rate of porous Teflon electrodes. A method of measuring the diffusion rate of vapor from 70% HNO_3 through a porous Teflon electrode and into concentrated NaOH was devised. At intervals of 1, 3.25, and 6.5 hours, samples of the NaOH were taken and titrated with standard acid to obtain the amount of diffused HNO_3 vapor. From these data, an equivalent diffusion current for HNO_3 vapor was calculated, assuming the end product of the cathodic reduction to be NO.

At both 30°C and 90°C we tested samples of 25-mil thick, 19-μ pore diameter porous Teflon sheet in the untreated state, heat-treated only at 350°C, and bonded at 350°C (bonded sample obtained by pressing porous sheet on carbon block at 350°C, then stripping from carbon). These data are plotted in Figure A-8. A certain time lag for reaching the maximum diffusion rate is apparent. However, very little change is noted between 3.25 and 6.5 hours.

At 90°C, the equivalent current density with the untreated Teflon sheet is nearly 3 times greater than that with the heat-treated sample and about 20 times greater than that with the bonded sample.

The data obtained at 30°C seem to represent only variations in liquid diffusion through pinholes, since very little vapor diffusion should occur with an HNO_3 vapor pressure of only 2-3 mm. It is fairly certain that the data at 90°C represent mostly vapor diffusion, since even the highest leakage rate at 30°C could not account for the high diffusion rate of the untreated sample at 90°C. (Liquid diffusion is proportional to the square of the absolute temperature.)

It should be pointed out that the 19-μ pore size Teflon sheet used for diffusion tests does not have the same thickness as that in the 19-μ pore size electrodes used for electrochemical test in Section B-2-b. This accounts for the difference in current density of the two testing methods. It was felt that less liquid leakage could be encountered with the thicker Teflon sheet, resulting in more accurate vapor diffusion comparisons for the thicker material.

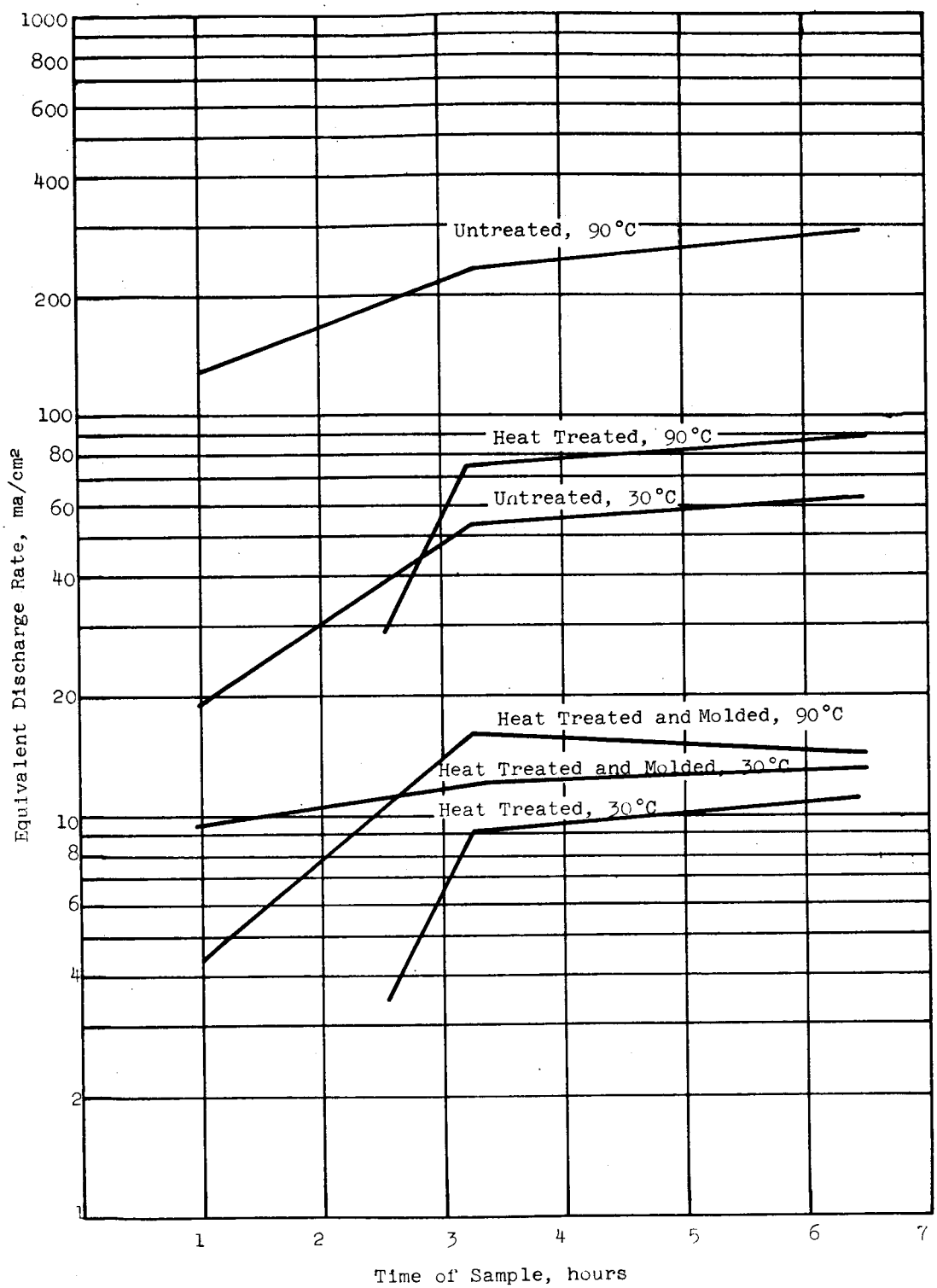

Oxidant, 70% HNO_3. Porous Teflon, 19μ, 0.025 in. thick

Figure A-8. Diffusion Rate of HNO_3 Vapor Through Porous Teflon

(4) Conclusions

All of the data seem to point to the carbon-Teflon bond as being the limiting feature of this type of construction. The factors controlling this bond are numerous; time, temperature, and bonding pressure, as well as the state of the Teflon and carbon surfaces, are critical for deforming and plugging electrode pores. A careful investigation of these variables might lead to a method of providing usable, reproducible diffusion rates, but such a study would be a long and exacting undertaking. Before starting such a line of investigation, a second approach to making Teflon vapor diffusion electrodes was evaluated.

b. Solid Carbon Insert in Tantalum Holder

This type of construction utilized a carbon disc slightly smaller than the opening of a standard tantalum holder. The total assembly (including tantalum mesh to give a tight fit between the holder and the carbon) was pressed at 350°C to bond the Teflon diffusion barrier to the carbon. Erratic electrode resistances resulted, presumably because of a nonreproducible contact between holder, mesh, and carbon. When sufficient pressure was used to insure good contact, mechanical failure of both carbon and Teflon barriers resulted in gross leakage through the electrode.

When construction conditions were well controlled, the performance of the solid carbon insert electrode was quite good. Polarization curves for FC-13 and FC-14 carbons with 70% HNO_3 and N_2O_4 (1 atm) in 5M H_2SO_4 electrolyte are shown in Figure A-9. The polarization is nearly all IR drop up to a current density of 150 ma/cm², where concentration polarization begins to limit the electrode performance. If the IR drop is eliminated from the potentials at 100 ma/cm², the potentials are 1.09 to 1.14 v vs SHE. These excellent IR-free polarization curves indicate that the use of a diffusion barrier bonded to the solid carbon structure has the necessary electrochemical characteristics for the cathodic reduction of nitric acid and dinitrogen tetroxide. Therefore, modified constructions that eliminated the erratic resistance features of the first carbon-Teflon electrode types were designed.

c. Low Resistance Solid Carbon-Teflon Sheet Diffusion Electrodes

(1) One-Piece Carbon Construction with Polystyrene Sealant

To improve the electrical properties of solid carbon-Teflon sheet diffusion electrodes, a one-piece assembly was made. The porous areas outside the "O" ring seal were filled with polystyrene dope. Electrical contact was made through copper clips,

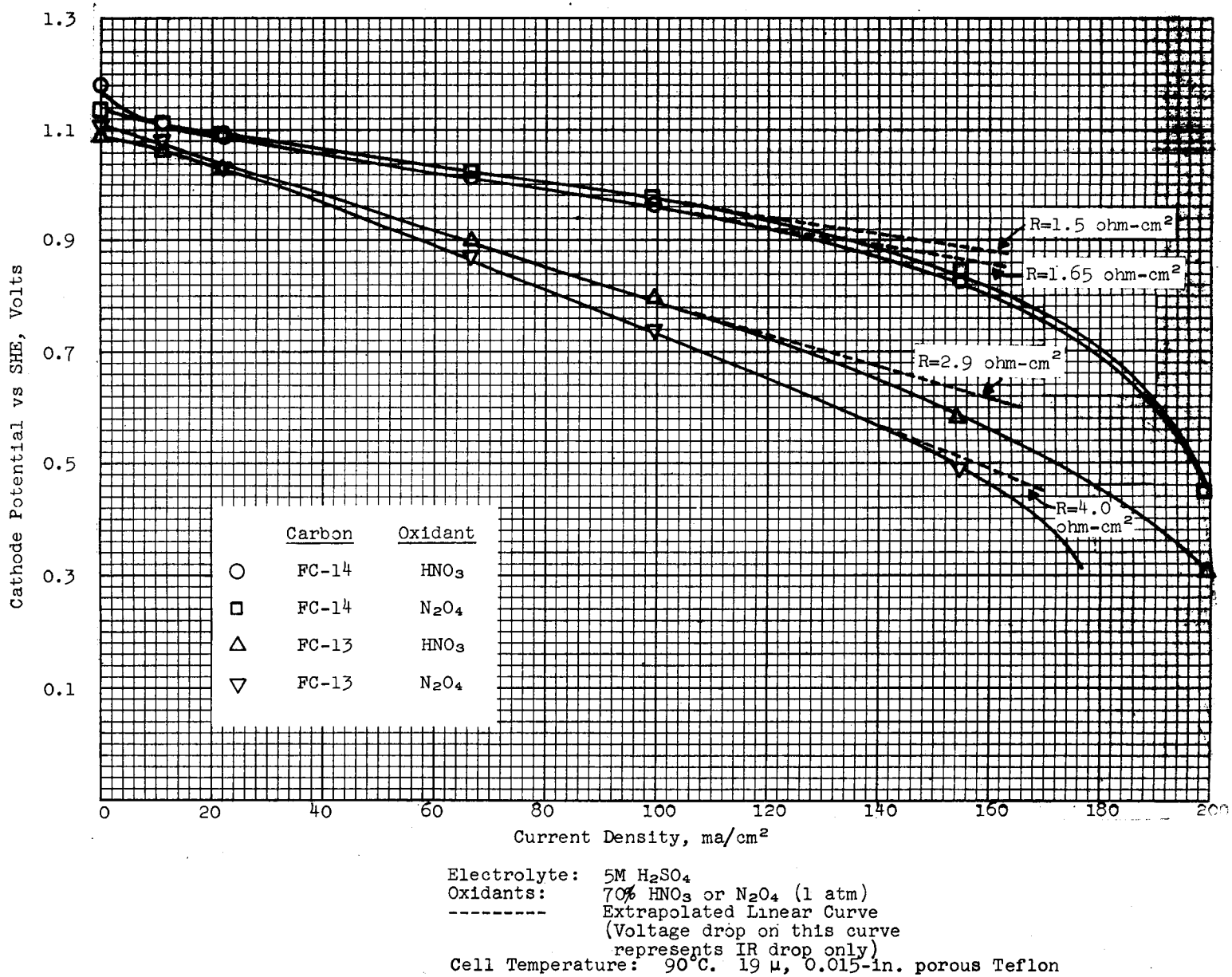

Figure A-9. Cathodic Polarization of Porous Carbon Block and Porous Teflon Sheet Electrodes

attached before doping. This construction gave low electrode resistance on E-I curves (shown in Figure A-10).

(2) Two-Piece Carbon Construction with Shrink-Fit Contacts

Although the one-piece construction mentioned above is satisfactory for preliminary testing, the use of polystyrene as a sealant necessarily adds an impurity to the electrode that is subject to attack by the cell reactants and also results in an ill-defined active electrode area. Thus, while testing with the one-piece construction was underway, the Pure Carbon Company custom-fabricated a two-piece carbon electrode. The construction features, shown in Figure A-11, include a thermally made bond between an active catalytic inner carbon and an impervious outer carbon. This system needs no further waterproofing and insures an exact knowledge of the active electrode area.

3. Teflon Powder Bonded to Solid Carbon

a. Background

Changes in diffusion rates through porous Teflon sheet that are caused by the bonding led to the use of a porous carbon matrix as the diffusion control barrier. If a homogeneous wet-proof surface layer of pores can be formed by melting Teflon powder into the surface of porous carbon, a network of very thin, controlled diffusion paths should occur. The diffusion rate should be controlled by the amount of Teflon powder applied per unit area of the porous carbon.

b. Experimental

(1) Diffusion Control and Cathode Polarization Tests

An initial preparation of Teflon powder-carbon electrodes was made using Teflon powder on FC-14 porous carbon. About 6 mg/cm^2 of Teflon powder was pressed between two 1/16-in. thick rectangles of FC-14 carbon.

The electrode was tested using 70% HNO_3 in the diffusion compartment and 5M H_2SO_4 electrolyte at 90°C. As soon as 70% HNO_3 was added, the electrode was cathodically polarized until a constant potential of 1.0 v vs SHE was attained, corresponding to a current density of 210 ma/cm^2. Product gas (NO) emerged from both sides of the carbon electrode. Qualitatively, more gas was discharged from the diffusion compartment than from the electrolyte side.

The current density of this electrode was lowered to 120 ma/cm^2 for overnight operation. The voltage-time relation for a 26-hour

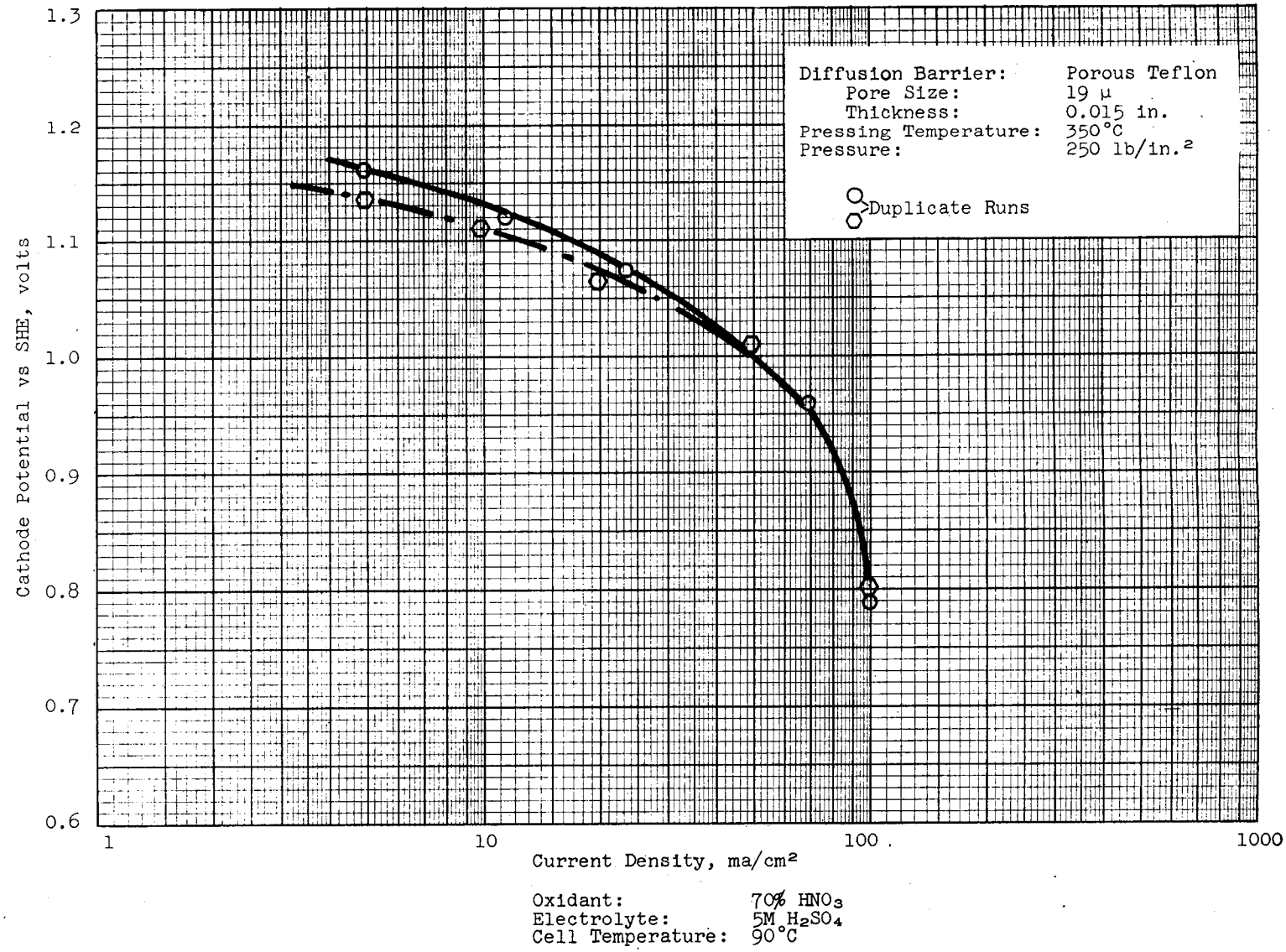

Figure A-10. Cathodic Reduction of HNO_3 at One-Piece Carbon Electrodes

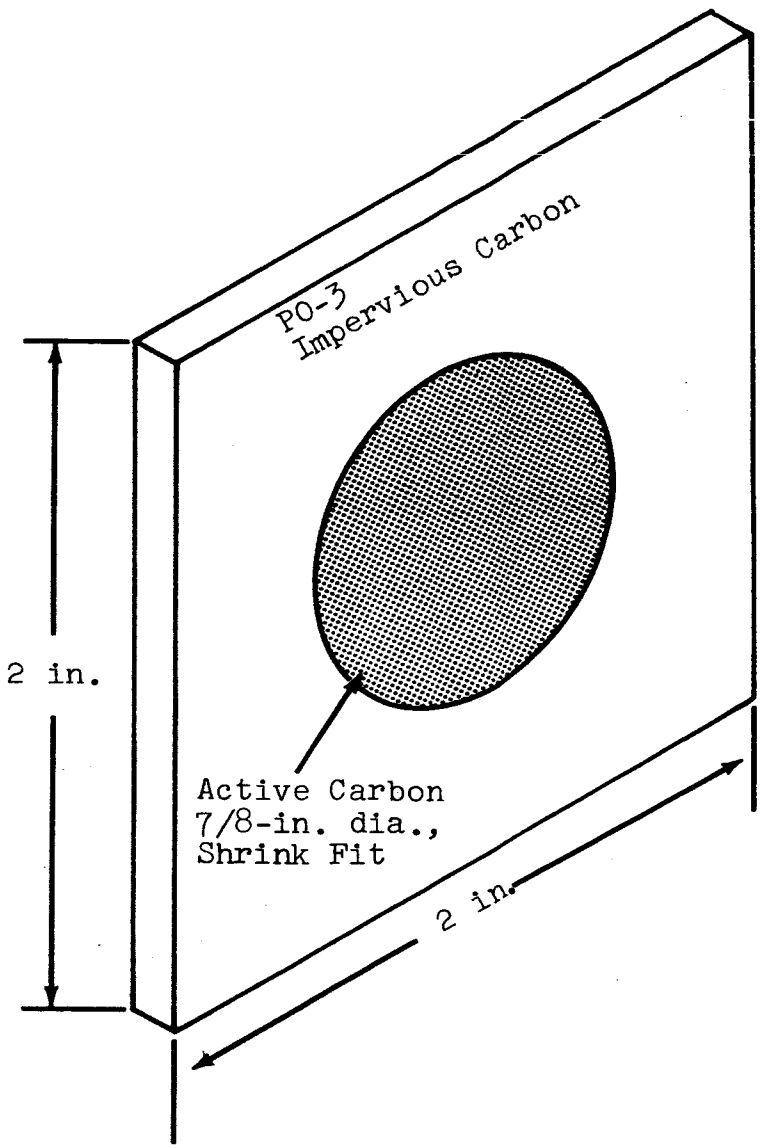

Figure A-11. Dual Carbon Electrode

test (presented in Figure A-12) shows a gradual cathode deterioration of 0.2 v over 18 hours. Adding a fresh solution of nitric acid provided only temporary rejuvenation of the cathode.

After 2 hours and 20 minutes, samples of the electrolyte were tested for contamination and were found to contain 0.01M and 0.03M HNO_3, respectively.

(2) Limiting Current Density Versus Teflon Loading

Control of the limiting current of a vapor diffusion electrode should be determined by the amount of Teflon powder impregnated into the carbon pores.

Experiments were conducted to determine the limitations of diffusion control, electrolyte contamination, and reproducibility. A general problem has been encountered with the dual carbon electrode construction because of a degradation of the shrink fit contact between the active and impervious carbons, resulting in liquid leakage through the electrode. Because of this problem, some tests have been run to distinguish between liquid diffusion and vapor diffusion through the porous electrode. The variation of current density with different Teflon powder loadings is shown in Table A-1.

Table A-1

VARIATION OF CATHODIC CURRENT DENSITY WITH TEFLON LOADING

Oxidant: 70% HNO_3
Electrolyte: 5M H_3PO_4

Carbon	Median Pore Size, μ	BET Surface Area, m^2/g	Teflon Loading mg/cm^2	Current* Density, ma/cm^2	Potential vs SHE, volts	Number of Tests
FC-13	2.1	450	10.0	148 ± 11†	1.01	6
FC-13	2.1	450	12.5	130 ± 2	0.96	2
FC-14	3.5	10	4.0	270	0.96	1
FC-14	3.5	10	8.0	105 ± 5	0.98	2
FC-14	3.5	10	10.5	85	0.96	1

*Currents are not diffusion limited

†Average Deviation $= \sqrt{\frac{\Sigma \Delta s^2}{n-1}} \times \frac{1}{\sqrt{n}}$

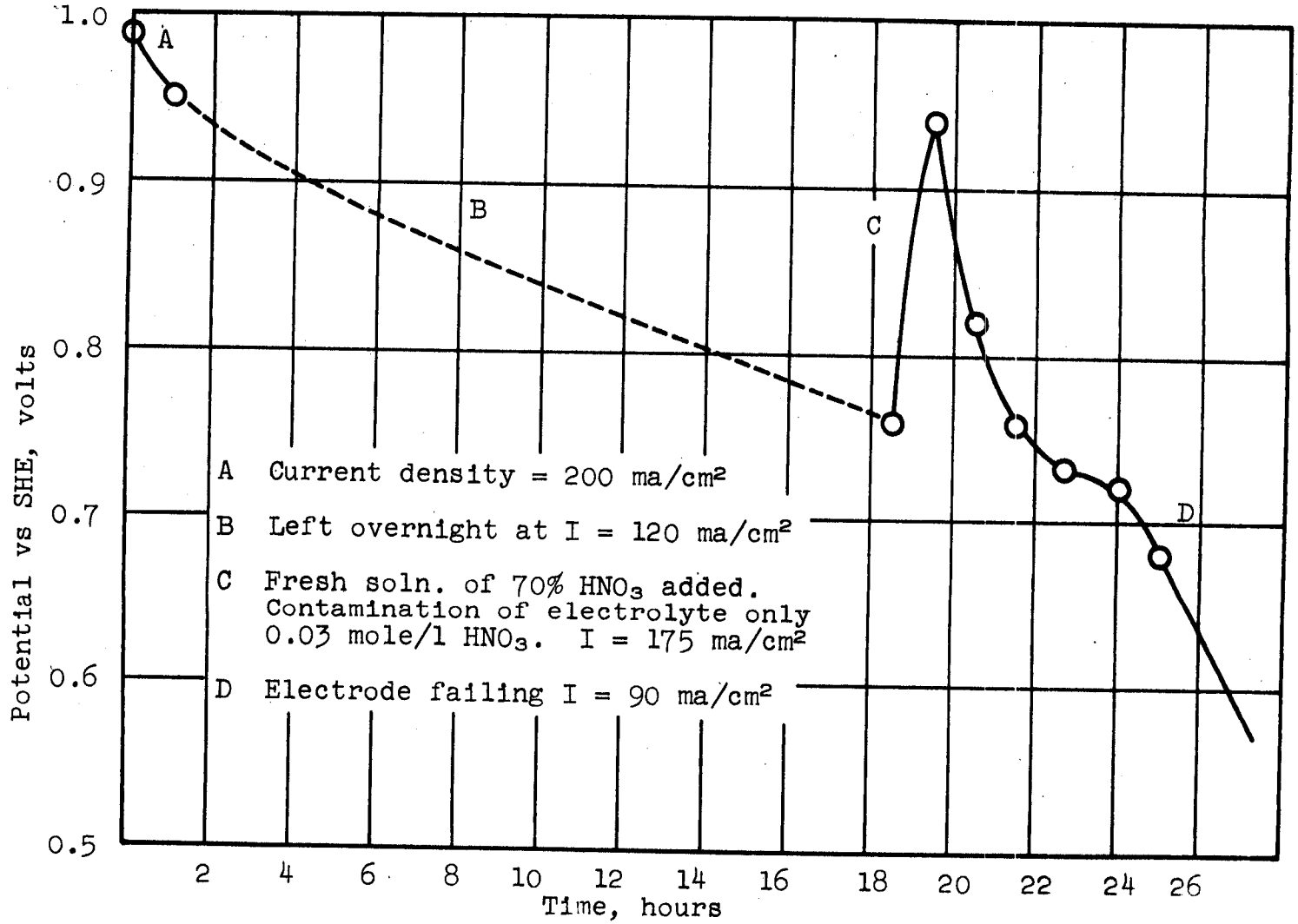

Electrolyte 5M H_2SO_4
Temp. 90°C

6 mg/cm² Teflon Powder
Heat impregnated into
FC-14 carbon electrode.

Figure A-12. Long-Term Cathodic Polarization of HNO_3 Teflon Diffusion Cathode.

The trend of decreasing current density with Teflon loading is expected because of the increasing vapor diffusion thickness and pore blockage during electrode fabrication. The difference between the two types of carbon is somewhat surprising. The carbon with the smaller median pore size (FC-13) supported a larger current density (130 ma/cm^2) than the carbon with the larger pore size (FC-14, 85 ma/cm^2). The much greater surface area of the FC-13 carbon may be associated with an increased surface activity for nitric acid reduction.

(3) Vapor Versus Liquid Diffusion

In many tests liquid leakage apparently occurred around the dual carbon bond. Tests were therefore conducted to determine the extent of liquid leakage.

To be sure that all electrodes were operating chiefly by vapor diffusion, all later tests were conducted first at 30°C, where the vapor pressure of nitric acid from a 70% solution is 2-3 mm, and then at 90°C, where the nitric acid vapor pressure is about 168 mm. Accordingly, most diffusion at 30°C should be due to liquid leakage. In all cases, currents of 10 to 30 ma/cm^2 were found at 30°C in electrodes that did not have gross liquid leakage, while current densities of approximately 100 ma/cm^2 have been attained at 90°C.

The difference in limiting current density between 30 and 90°C indicates that 50 to 80% of diffusion at 90°C is vapor diffusion, since liquid diffusion should increase as the square of the absolute temperature.

(4) Longer-Term Stability Test (Over 8 Hours)

Pertinent details and data of representative longer-term tests performed on Teflon-bonded porous carbon block diffusion cathodes are given in Tables A-2 and A-3, and Figure A-13.

(a) Catalytic Activity

No loss of catalytic activity was notices in any test. Even when a cathode was polarized to the hydrogen potential and allowed to discharge hydrogen, it recovered its activity fully when returned to test conditions. This is well illustrated in the detailed test No. 87, Figure A-13.

(b) Diffusion Rate

(i) Changes in Liquid Leakage Rate

Current density increases frequently occurred before 24 hours. In practically every case this current increase was traced to a breakdown of the dual carbon bond. Other possible causes of

Table A-2

CATHODIC REDUCTION OF HNO_3 AT DUAL CARBON ELECTRODE

Porous Carbon Block - Bonded Teflon Powder

Run No.:	87	Teflon Loading:	10.5 mg/cm²
Carbon:	Dual FC-13	Temperature:	88°C
Electrode Area:	3.8 cm²	Electrolyte:	5M H_3PO_4
Oxidant:	70% HNO_3		

Graph‡‡ No.	Hours	Current Density Ma/cm²	Cathode** Potential, v	Coulombs, Cumulative	HNO_3 Content* Cathode Compartment, moles	HNO_3 Content* Electrolyte Molarity	Coulombic‡ Efficiency, %	Notes
	0.00	59	0.99	0	0.253	0		
	0.79	113	0.96	635				
	1.15	158	0.99	1,312				
1	16.70	158	failed	34,912	0.059	0.30	71	After overnight the concentration of HNO_3 had fallen to ~8M and could not supply enough HNO_3.
	17.20	135	0.97					Fresh HNO_3
	21.82	135	0.97					
2	24.57	125	1.01			0.43		
3	41.02	120	0.61			0.08		Again, potential decreased overnight due to low HNO_3 concentration. Fresh HNO_3
	48.77	105	0.94	0	0.253			
4	65.18	105	0.97	23,600	0.106	0.13	56	
5	72.93	132	1.01			0.08		

* By analysis
** IR-free potentials
‡ Assuming reduction product to be NO
‡‡ Results are plotted in Figure 15

Table A-3

CONDENSED LONG-TERM DATA FROM SELECTED HNO_3 DIFFUSION DUAL CARBON CATHODES

Porous Carbon Block - Bonded Teflon Powder

Cathode Area: 3.8 cm^2
Electrolyte: 5M H_3PO_4
Oxidant: 70% HNO_3

Electrode No.	Running Time, hours	Potential vs SHE, volts	Current Density, ma/cm^2	Contamination, M HNO_3	Temperature °C	Teflon Loading mg/cm^2	Type of Carbon	Remarks
88	0	1.00	110	-	88	8	FC-14	
	2	1.00	120	0.67	"	"	"	
	18	0.81	120	0.19	"	"	"	After overnight HNO_3 below 70%
	19	1.04	120		"	"	"	After fresh HNO_3 added
	26	0.99	130		"	"	"	
	42	0.59	130	0.05	"	"	"	After overnight HNO_3 concentration = 8.2 M in diffusion compartment. Material efficiency overnight was 68%.
	43	0.98	130		"	"	"	Fresh HNO_3
				Testing ended due to O-ring seal failure.				
91	0	1.02	140		88	10	FC-13	
	6	1.02	150	0.44	"	"	"	
	12	0.95	150	0.45	"	"	"	Run ended due to heating bath failure.
		1.07	0					
		1.00	50					Polarization curve taken at termination of test.
		0.98	100					
		0.95	150	Maximum current from supply.				

Table A-3 (Continued)

CONDENSED LONG-TERM DATA FROM SELECTED HNO_3 DIFFUSION DUAL CARBON CATHODES

Electrode No.	Running Time, hours	Potential vs SHE, volts	Current Density, ma/cm^2	Contamination, M HNO_3	Temperature °C	Teflon Loading, mg/cm^2	Type of Carbon	Remarks
102	0	0.96	100		88	8.4	FC-14	Diffusion area used as basis for current density. Diffusion area 1.3 cm^2, catalyst area 3.9 cm^2.
	17	1.01	115	0.48	"	"	"	
		Electrode starting to leak around dual carbon construction. Electrode sealed at cracks with Teflon tape bonded at 280°C, Area still 1.3 cm^2						diffusion side.
	18	0.96	62		88	8.4	FC-14	
	23	0.92	92	0.03	"	"	"	
	41	1.04	95	0.31	"	"	"	Overnight electrode starting to leak as Teflon seal loosens.
		Electrode retaped and sealed at 280°C.						
	42	0.94	85		88	8.4	FC-14	
	61	0.96	170		83	"	"	
	85	1.03	175	0.19	88	"	"	Starting to leak again.
		Resealed with Teflon powder around edges. Added 1 mg/cm^2 Teflon to surface.						
	85	0.96	15		30	9.4	"	
	92	0.97	105	0.06	88	"	"	
	114	0.92	30		30	"	"	Overnight power failure reduced temperature to 30°C.
	122	0.96	115	0.08	88	"	"	
		Started leaking overnight. Run ended.						

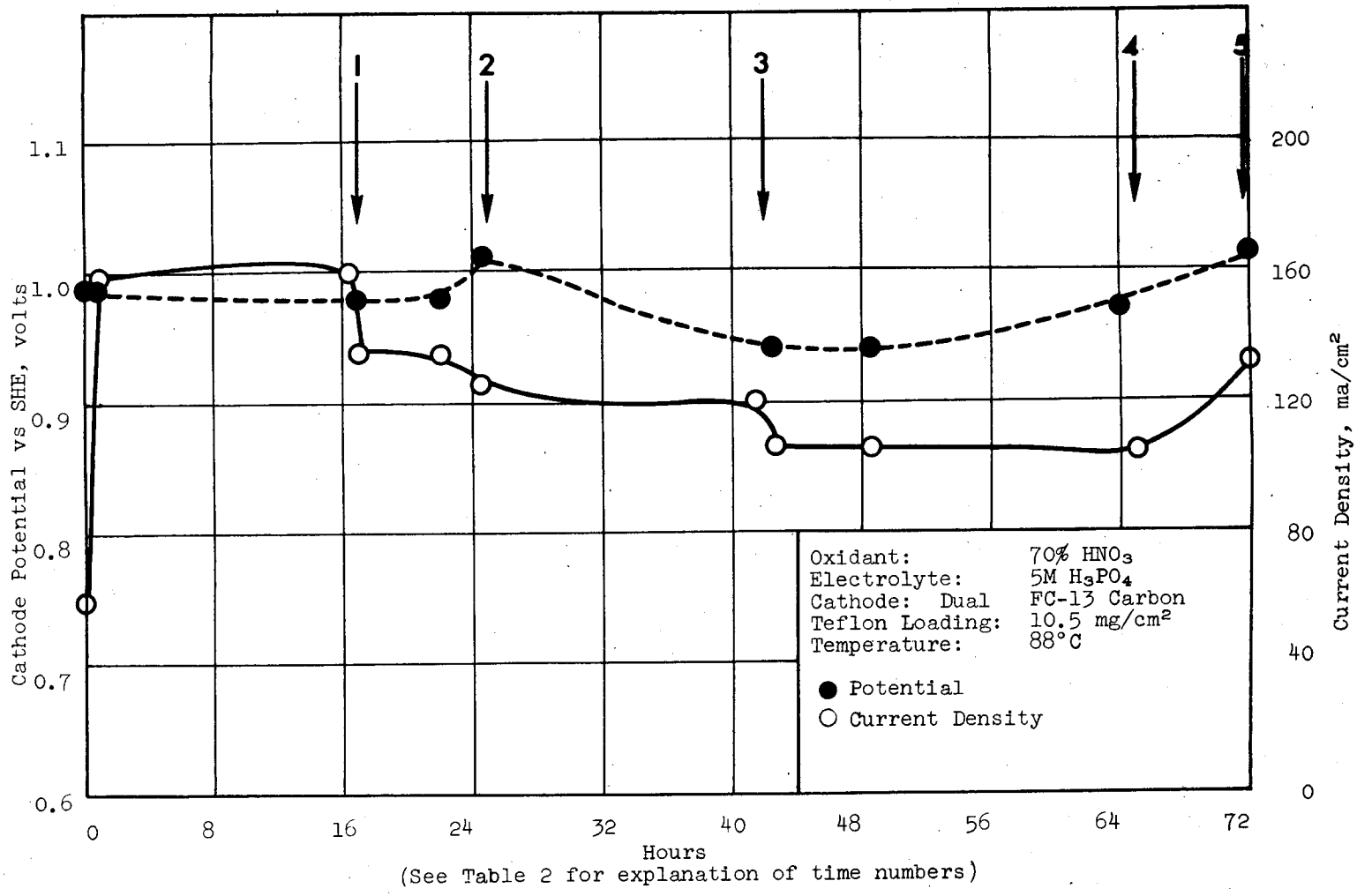

Figure A-13. Long-Term Porous Diffusion Electrode, Test No. 87

liquid leakage may be attack of the carbon-Teflon powder bond or deterioration of the hydrophobic character of the Teflon film over long-time periods. However, Test 87 indicates that the hydrophobic properties of Teflon film are unaffected by 72 hours' contact with concentrated nitric acid.

(ii) Changes in Vapor Diffusion Rate

The data in Tables A-2 and A-3 do not show any obvious trends in diffusion rate with time, except for sudden increases in diffusion rate when the sealing mechanism breaks down at the dual carbon joint. A slight trend towards lower diffusion rate is seen in Test 87, Table A-2. Initially 158 ma/cm^2, and after 48 hours 105 ma/cm^2, was maintained by the electrode. However, at 65 hours the diffusion rate no longer decreased, and at 73 hours the current density had increased to 132 ma/cm^2.

The data do not show any consistent trend, and little change occurs over a 72-hour period.

(5) Contamination Control

Contamination of the electrolyte with traces of oxidant or fuel is easily controllable in long-term tests. However, short-term current and potential changes can cause high fluctuations in contamination level. The half cells used for cathode testing contained 60 ml of liquid, and contamination concentration changed slowly in this large volume. If a full cell has circulating electrolyte, no contamination difficulties should be encountered, but if a small volume of stationary electrolyte is used, short-term surges might cause problems.

Contamination levels for test cell 87 are given in Table A-4. The fact that no continual rise in contamination was found indicates that a steady state was reached. In all cases, the contamination could be held to less than 0.5M HNO_3 by keeping the cathode potential at or more negative that 1.00 volts vs SHE.

Table A-4

CONTAMINATION OF PHOSPHORIC ACID ELECTROLYTE WITH NITRIC ACID

Run No. 87

Hours	HNO_3 Concentration M	Hours	HNO_3 Concentration M
0	0	41	0.08
16	0.30	65	0.13
24	0.43	72	0.08

(6) Material Efficiency of Nitric Acid Cathodic Reduction

Material efficiencies of nitric acid reduction for three overnight tests were from 50 to 65%. The theoretical coulombic capacity was based on reduction to nitric oxide only:

$$HNO_3 + 3H^+ + 3e^- \longrightarrow NO + 2H_2O \qquad (1)$$

It is likely that some nitric acid was lost by evaporation from the bulk container and also (and probably more important) that nitric acid reacted with nitric oxide to form dinitrogen tetroxide, which saturated the solution and then escaped. The brown discoloration of HNO_3 in the storage compartment adjacent to the back side of the cathode indicated that NO had diffused through the electrode into the concentrated HNO_3 storage compartment and had formed N_2O_4 according to the equilibrium:

$$2NO + 4HNO_3 = 3N_2O_4 + 2H_2O \qquad (2)$$

The equilibrium of equation (2) shifts to the right with increase in nitric acid concentration and increase in temperature (ref. 6).

4. Conclusions

(1) Porous Teflon-carbon cathodes can be designed to obtain high diffusion rates with low electrolyte contamination levels.

(2) The Teflon powder-carbon block electrode is preferable to the porous Teflon sheet-carbon cathode because the former is easier to construct.

(3) Decreasing current density with increasing Teflon loading was demonstrated.

(4) Differences in cathodic behavior between carbons may be associated with differences in catalytic properties of the carbons. These catalytic effects may overshadow effects of pore size on electrode processes (other than strictly diffusional effects).

(5) Cathodes deteriorate a maximum of 0.14 v in up to 0.5M N_2H_4 in 5M H_3PO_4.

(6) The electrolyte is only slightly contaminated by leakage of unreacted nitric acid through the cathode.

(7) The cathode can control limiting current densities from 50 to 200 ma/cm^2 at 1.0 v vs SHE.

(8) Electrolyte contamination for diffusion controlled cathodes

increases as the concentration polarization decreases.

(9) Vapor diffusion can be distinguished from gross liquid transfer by the magnitude of the limiting current as well as by the effect of temperature on limiting current.

(10) Because of their excellent electrochemical characteristics, the MRD-C type cathode has replaced the Teflon-carbon diffusion electrode for utilizing storable oxidants.

APPENDIX II

ANODE DEVELOPMENT

A. BACKGROUND

A suitable anode for hydrazine oxidation with a nitric acid or dinitrogen tetroxide cathode should have (1) a suitable catalytic surface that is selective to hydrazine oxidation, (2) provision for control of the fuel-electrolyte interface to prevent contamination of the electrolyte with unreacted fuel, and (3) physical stability and resistance to small concentrations of nitric acid. Although the palladium diffusion membrane (discussed in Section III) meets the first two requirements, its use in fuel cells is not practical because of attack by dilute nitric acid solutions. Since revised contract requirements emphasized the development of the HNO_3 $(N_2O_4)/N_2H_4$ cell, emphasis on development of the palladium membrane work was switched to development of the flow-through and diffusion-controlled types of anode. The operation principles of these two types of anodes have been discussed in Section IIIC in the body of this report.

B. FLOW-THROUGH MRD-A ANODES

1. Method

Depending on the nature of catalyst being tested or on its method of application to the anode structure, several constructions were used in the testing. Of particular interest was the catalyst-Teflon dispersion mixture cured on a metal screen substrate, a technique developed under a concurrent contract (ref. 2). This anode is referred to as the MRD-A type.

This construction was particularly useful to evaluate a series of noble metal blacks. Other tests involved a series of chemiplated and electroplated catalysts for which a porous carbon substrate was used. The outer edges were impregnated with a styrene solution and were heat-cured to provide a sealing area.

2. Catalyst Activity

The best results in uncontaminated hydrazine solutions were repeatedly obtained with platinum and rhodium. Additional tests with the Teflon-catalyst construction described above showed a catalytic activity acceptable for anode use in the cell systems under consideration in this area. The results are shown in Figures A-14 and A-15. Several levels of nitric acid contamination were used, as well as various solution strengths of hydrazine in the phosphoric acid electrolyte. The data show rhodium black to be the superior catalyst when used in "pure" solutions with no nitric acid contamination present. When the latter condition is not true, however, platinum black remains least

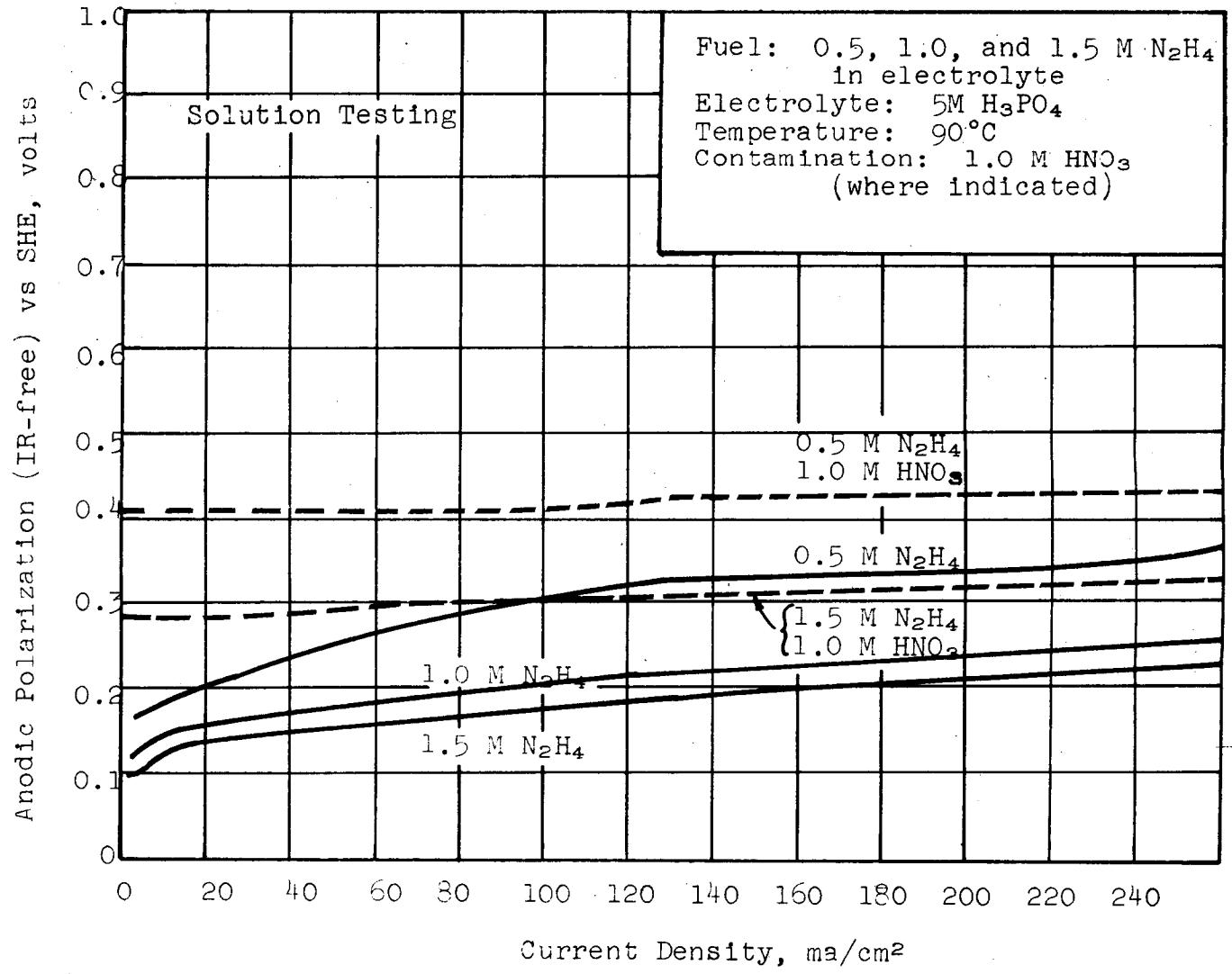

Figure A-14. Anodic Polarization of MRD-A (Pt-Teflon) Electrodes - Fuel in Solution

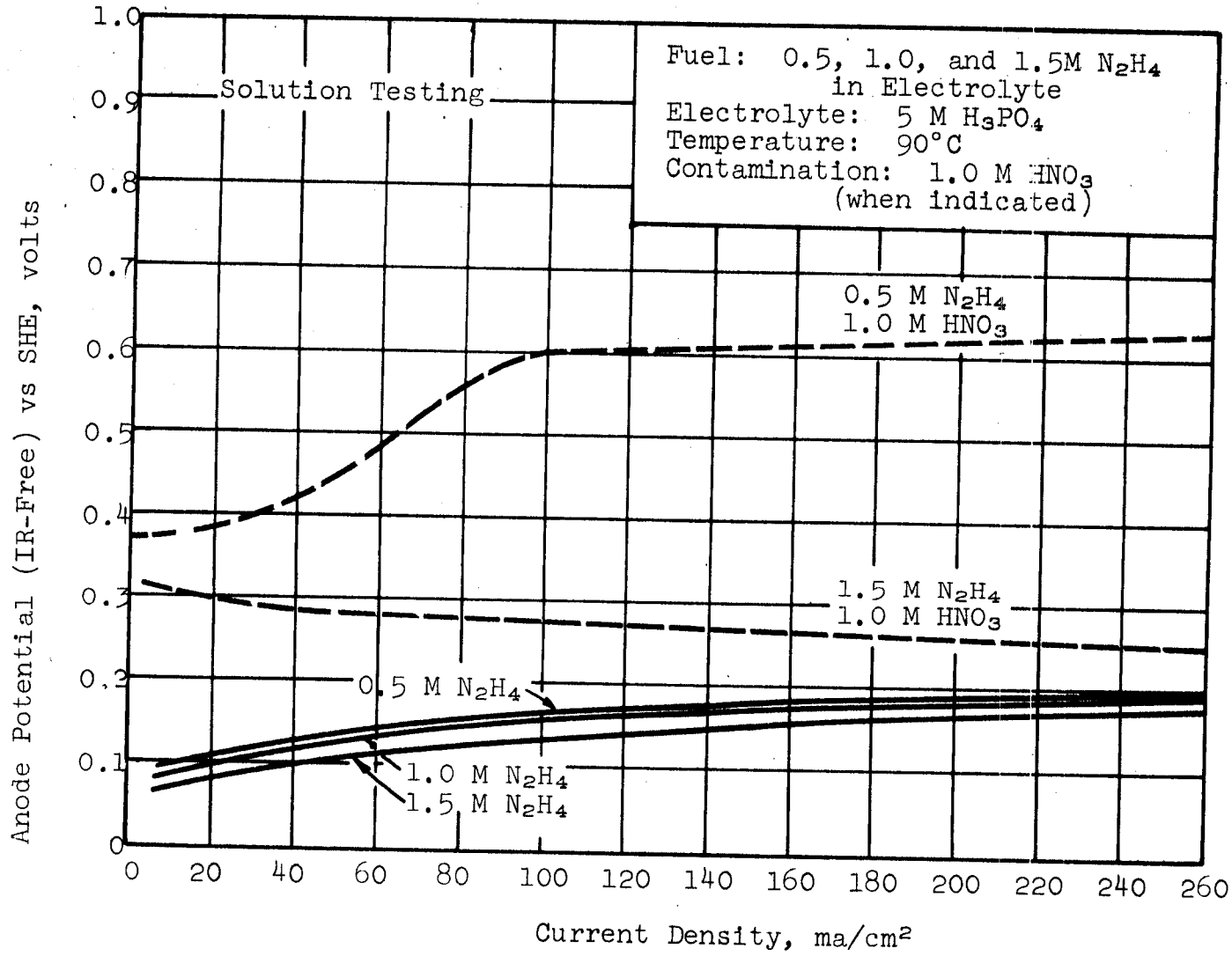

Figure A-15. Anodic Polarization of MRD-A (Rh-Teflon) Electrodes - Fuel in Solution

affected by the contaminant (that is, it is the more selective to hydrazine) and provides the better results.

3. Diffusion Controlled Anodes

a. Diffusion Testing Conditions

The basic difference between the vapor diffusion testing and the solution tests described above is the storage of the concentrated fuel behind the electrode. No hydrazine is dissolved in the electrolyte; fuel feed is determined by the vapor pressure of hydrazine at 90°C, and the physical structure of the porous, wetproofed electrode separating hydrazine from the electrolyte. It is, of course, desirable that no liquid leakage occurs, and that all transport be via the vapor phase only. In this way, fuel flow can be controlled. As before, nitric acid can be added to the electrolyte when testing of its effects is desired.

b. Teflon-Catalyst (MRD-A) Diffusion Structures

Standard MRD electrodes are approximately 4-6 mils thick and do not afford sufficient diffusion control for hydrazine. In an attempt to obtain diffusional limitation, thicker samples were made using both rhodium and platinum blacks. The results are seen in Figures A-16 and A-17. At a thickness of about 20 mils, the rhodium electrode shows some diffusional control, while the platinum electrode shows none.

c. Carbon Catalyst Diffusion Structure

Earlier anode work showed carbon to be a poor carrier for the anode catalyst. This is particularly true in the presence of nitric acid contamination, since the carbon exhibits a distinct tendency to assume a positive potential in the presence of nitric acid. Nevertheless, the use of a porous carbon substrate would be highly desirable from several standpoints, most notably the provision of a low resistance electrode structure and the adaptability to wetproofing for diffusional control.

Accordingly, attempts to utilize these advantages and to minimize the detrimental effects were made. Porous carbon sheets were electroplated from both sides at low current densities for several hours to cover most of the internal surface area. This was followed by 10-30 minute plating step at high current density to form a catalytic black on one surface. The opposite side was then wetproofed with Teflon powder in the manner of our present cathode preparation. A variation of this process involved first wetproofing, then the "slow" and "fast" plating steps from the opposite side only. Anodic polarization data of a platinum electrode prepared by the first method and a rhodium electrode prepared by the second are shown in Figure A-18. The platinum electrode is diffusionally limited at approximately 50 ma/cm^2,

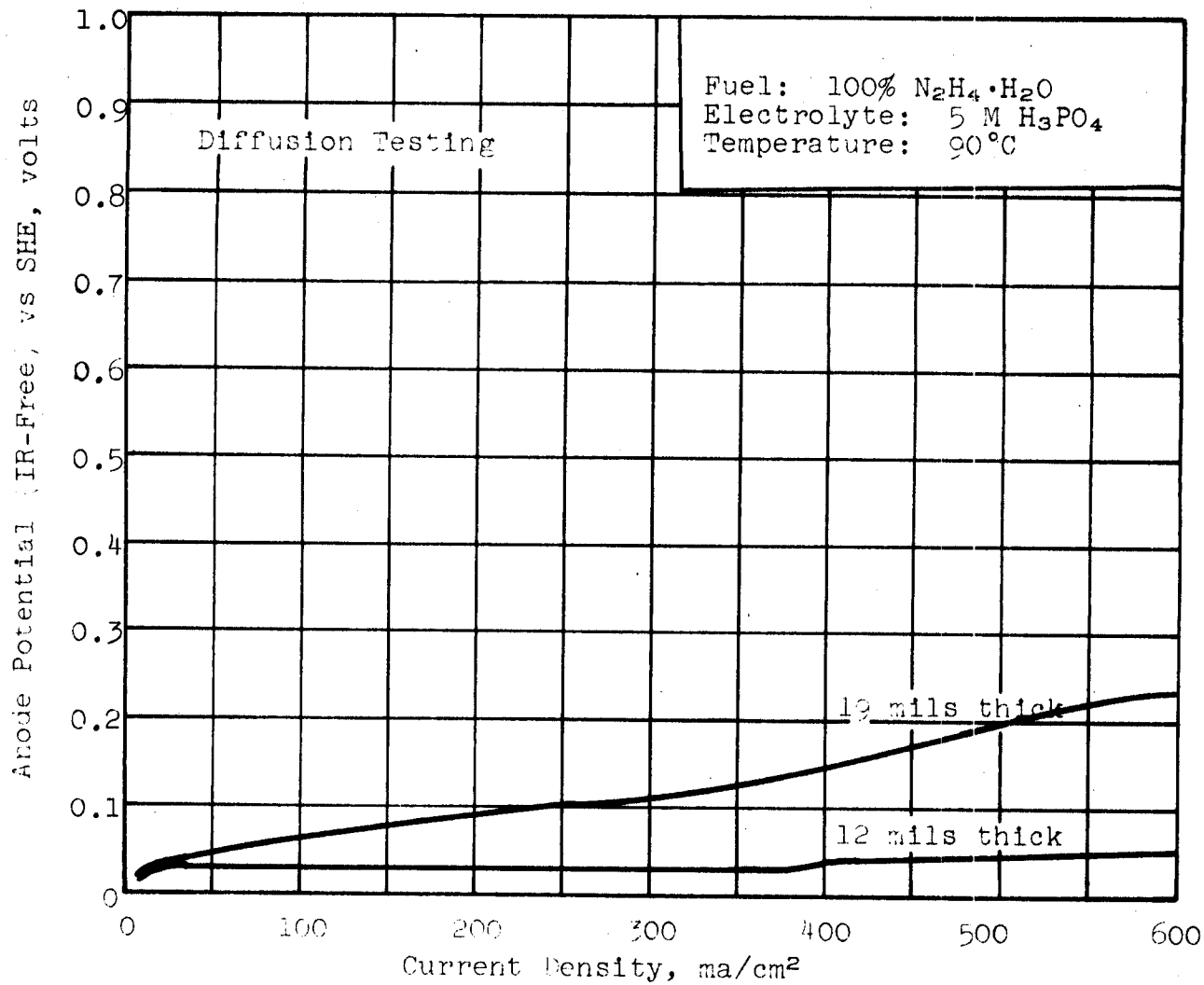

Figure A-15. Anodic Polarization of MRD-A (Pt-Teflon) Electrodes - Vapor Diffusion Testing

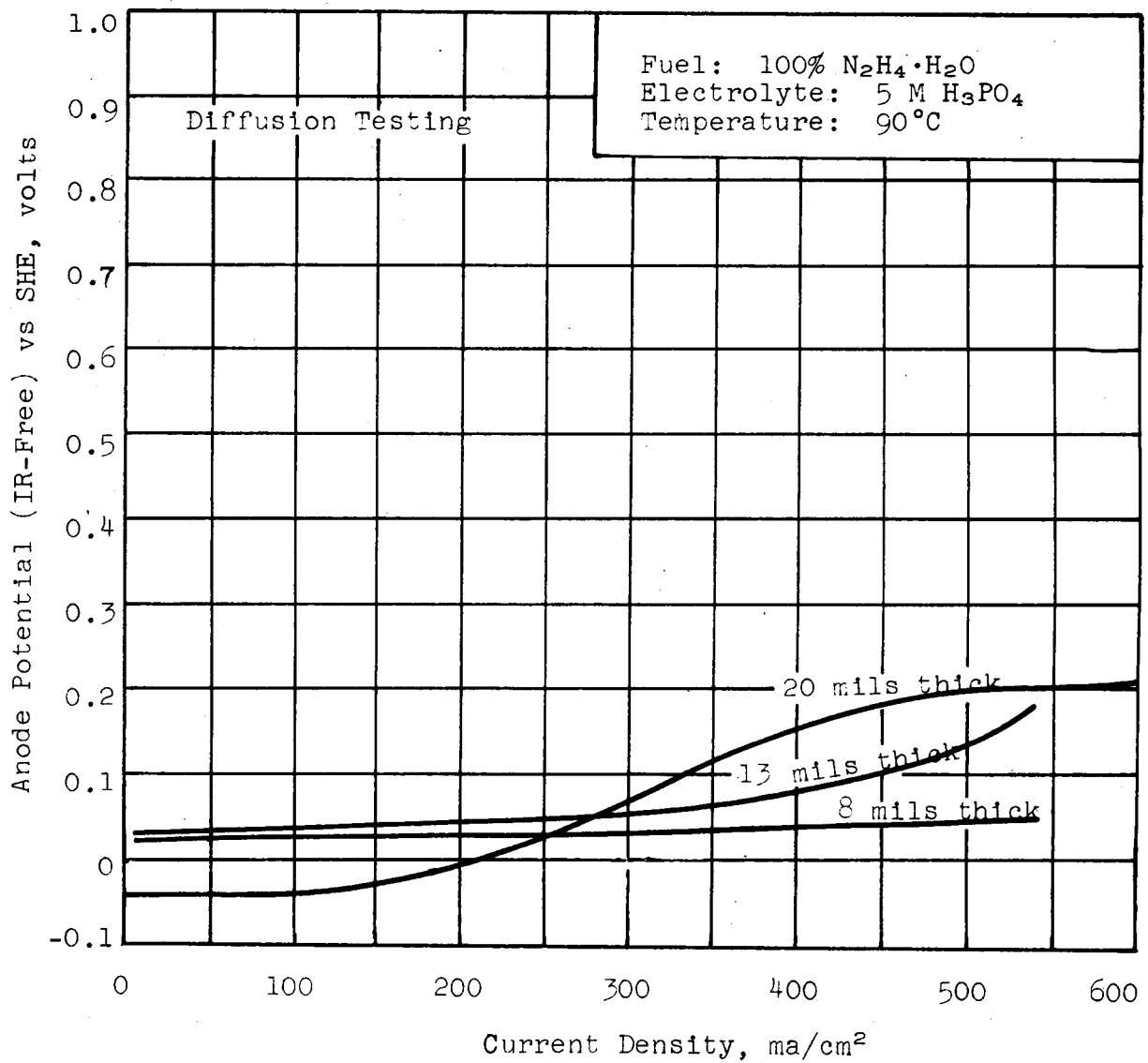

Figure A-17. Anodic Polarization of MRD-A (Rh-Teflon) Electrodes - Vapor Diffusion Testing

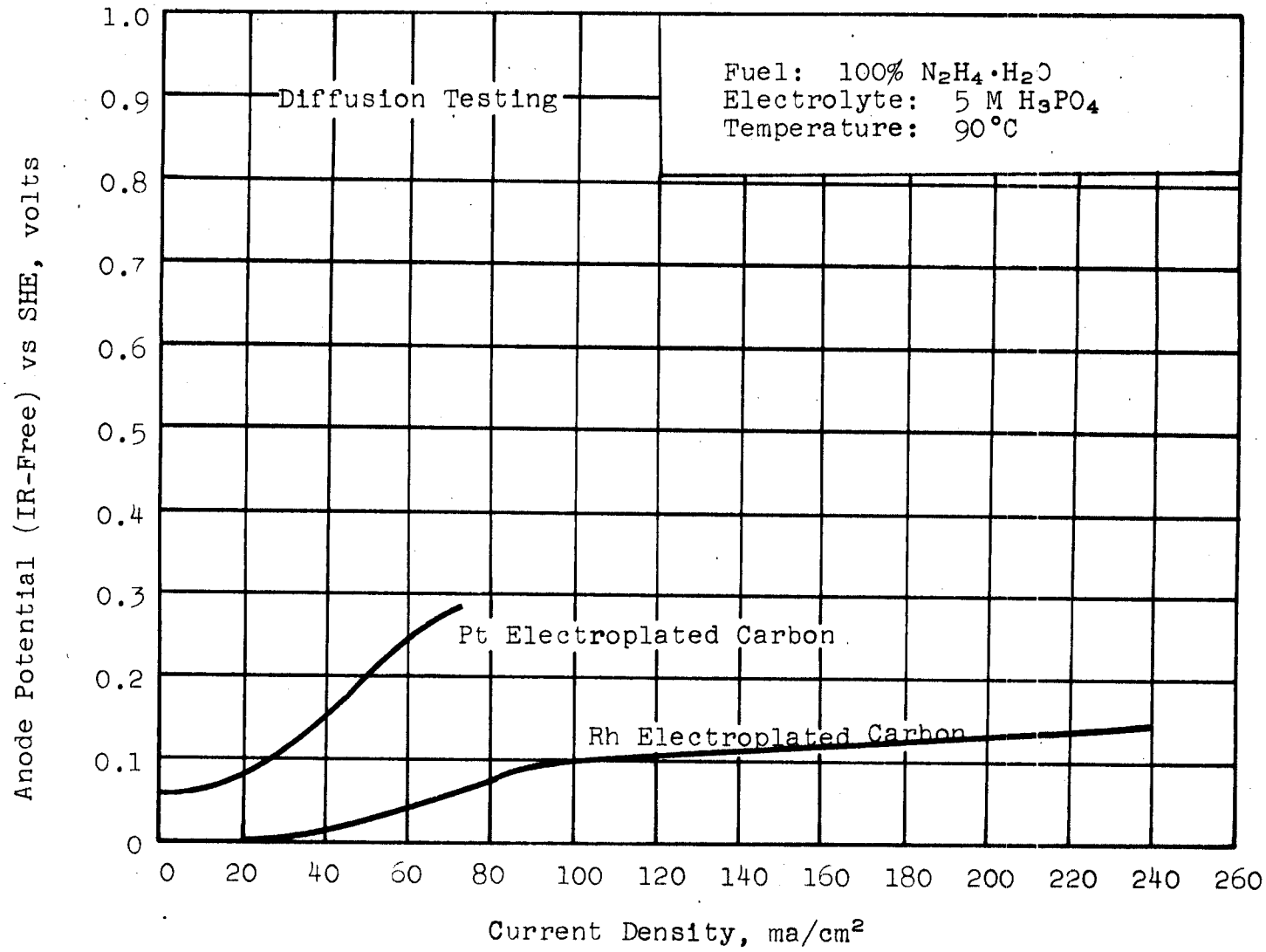

Figure A-18. Anodic Polarization of Electroplated FC-13 Carbon Electrodes - Vapor Diffusion Testing

while the rhodium sample does not exhibit diffusional limitation in the range of current densities covered.

4. Teflon-Catalyst-Carbon Combination

The advantages of each of the above constructions is combined in a third method where a Teflon-catalyst composite is heat-cured to a wetproofed, porous carbon sheet. The effect is to combine excellent catalytic acitivity with diffusion control. Initial results for platinum and rhodium are seen in Figure A-19. In each case diffusional limitation was achieved, although the limiting current density of 50-60 ma/cm^2 is considered too low. The low current densities obtained in the initial tests indicate that excess Teflon is present, and is resulting in pore blockage. This construction then offers most promise for a diffusionally controlled hydrazine anode.

5. Thickened MRD-A (Pt) Electrodes

One of the basic approaches toward diffusional control has centered around the MRD-A (catalyst-Teflon dispersion) construction described previously (ref. 2). On the assumption that thicker membranes would provide greater limitation to vapor transport, a number of samples were previously constructed ranging in thickness from 6 to 20 mils. Since no diffusion limit was reached in these tests (ref. 2) the thickness range was extended to 45 mils. The results are shown in Figure A-20. Again, the current is not limited by vapor transport of hydrazine, and over diffusion occurs. It should be noted also that as membrane thickness (catalyst weight) increases, catalytic decomposition of N_2H_4 becomes more severe. This gassing has a scrubbing effect on the electrode and increases cracking. The 18-mil sample shown in the graph cracked during an all-night run (less than 20 hours) while the heavier membranes (30 and 45 mil) showed evidence of cracking within 2 hours. This approach, therefore, is considered unsatisfactory for diffusional control.

6. Electroplated Porous Carbon

In previous tests, electroplated porous carbon exhibited one of the few true diffusional limitations obtained to date. This method is similar to the cathode approach where the oxidant side of the electrode is wet-proofed with heat cured Teflon powder. For anode usage, the elctrolyte side was then electroplated with the desired catalyst. An additional attempt to use this approach was made, using every effort to improve anode potentials at current densities lower than the diffusion limited values. The electrodes were wet-proofed with controlled amounts of Teflon powder before plating to prevent excessive pore blockage, and the platinum plating time was extended at lower current density in an attempt to achieve total coverage of the carbon

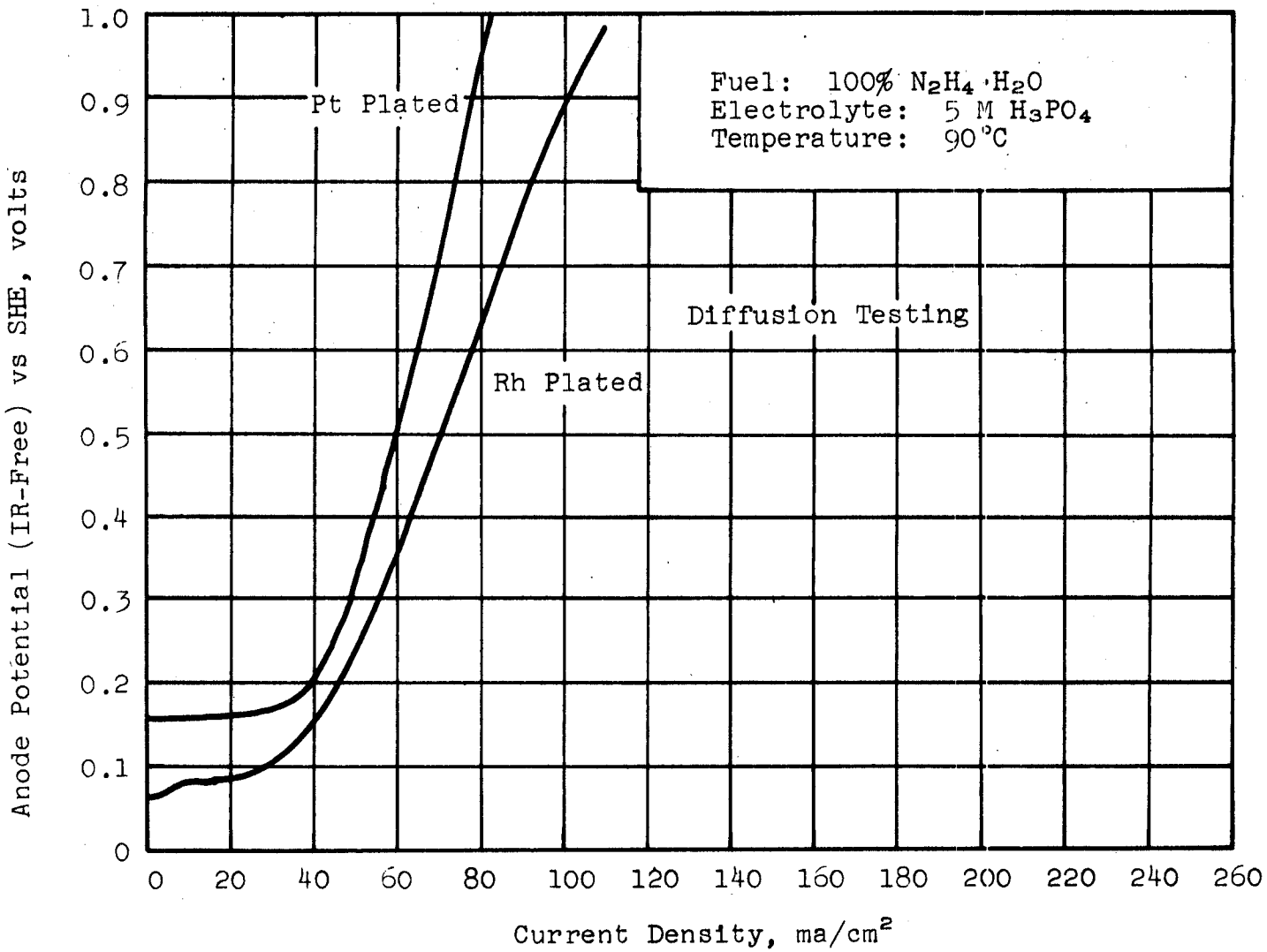

Figure A-19. Anodic Polarization of MRD-A Carbon Composite Electrodes - Vapor Diffusion Testing

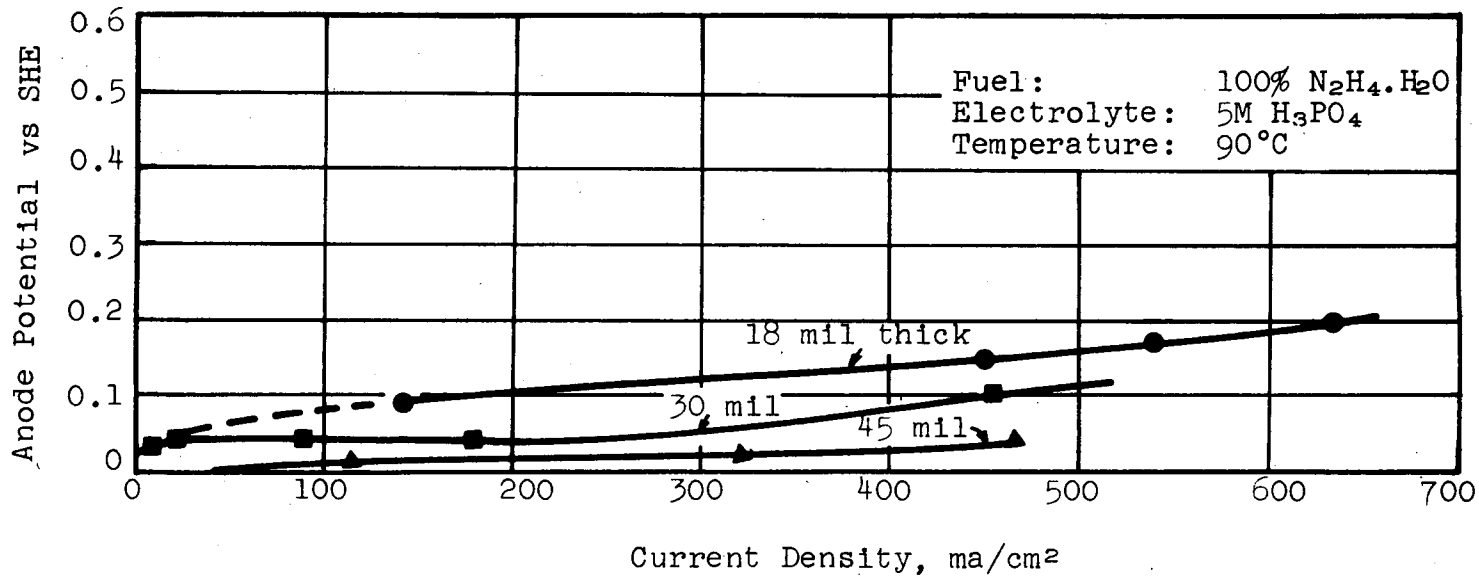

Figure A-20. Anodic Polarization of MRD-A (Pt-Teflon) Electrodes-Vapor Diffusion Testing

surface with platinum. Nevertheless, essentially the same results were obtained as previously reported (ref. 2). In Figure A-21, a series of polarization curves is shown in which a hysteresis loop is traced to assist in defining the mechanism of the (plated) porous carbon operation. Approximately 10 minutes was required to run each leg. As the run begins and the lower current density readings are taken, a local excess of hydrazine accumulates in the carbon pores because of over diffusion. When the current density is increased and the equilibrium point is passed, this excess is consumed. On the retrace immediately following, a slight deficiency of hydrazine exists (compared to the upward run) and this is reflected by the higher polarizations recorded. This condition persists until the current density is low enough to be supported by the rate of hydrazine diffusion. The second upward trace is much like the first, although slightly lower since the run begins with a greater local excess than previously. In support of the local excess phenomenon, it was noted that if current densities beyond the equilibrium point were sustained for a short period, polarization voltages would rise -- reflecting the same consumption of excess hydrazine stored in the carbon pores. When sufficient time was allowed for steady state conditions to be reached, the electrode would support approximately 45 ma/cm^2 at 0.2 v from the H_2 potential. In view of these results, other methods of diffusion control were investigated.

7. Porous Carbon with MRD-A (Pt) Electrodes

In spite of its excellent catalytic activity, the MRD-A type electrode construction has so far not provided sufficient vapor transport control. Although diffusion control is apparently possible for porous carbon cathodes, these electrodes are poor anode catalysts. A combination of the two electrode types, therefore, offers some promise. In this approach, a MRD-A electrode (electrolyte side) is heat-cured to a porous carbon backing (concentrated fuel side). Several samples were tried using various degrees of Teflon powder wet-proofing on the carbon prior to mating with the catalyst-containing MRD-A. The best results were obtained when the carbon was used without prior wet-proofing, allowing the Teflon contained within the MRD-A electrode to perform this function (See Figure A-22). Current densities were somewhat higher and operating potentials were somewhat improved over the values obtained with the plated porous carbon alone. Under steady state conditions (several hours' operation) the electrode would support a diffusion controlled current of 75 ma/cm^2 at .2 v from the hydrogen potential.

Some additional improvement is desirable.

8. Electroplated MRD-A (Carbon) Electrodes

Previous experimental work had shown that the MRD-A (carbon)

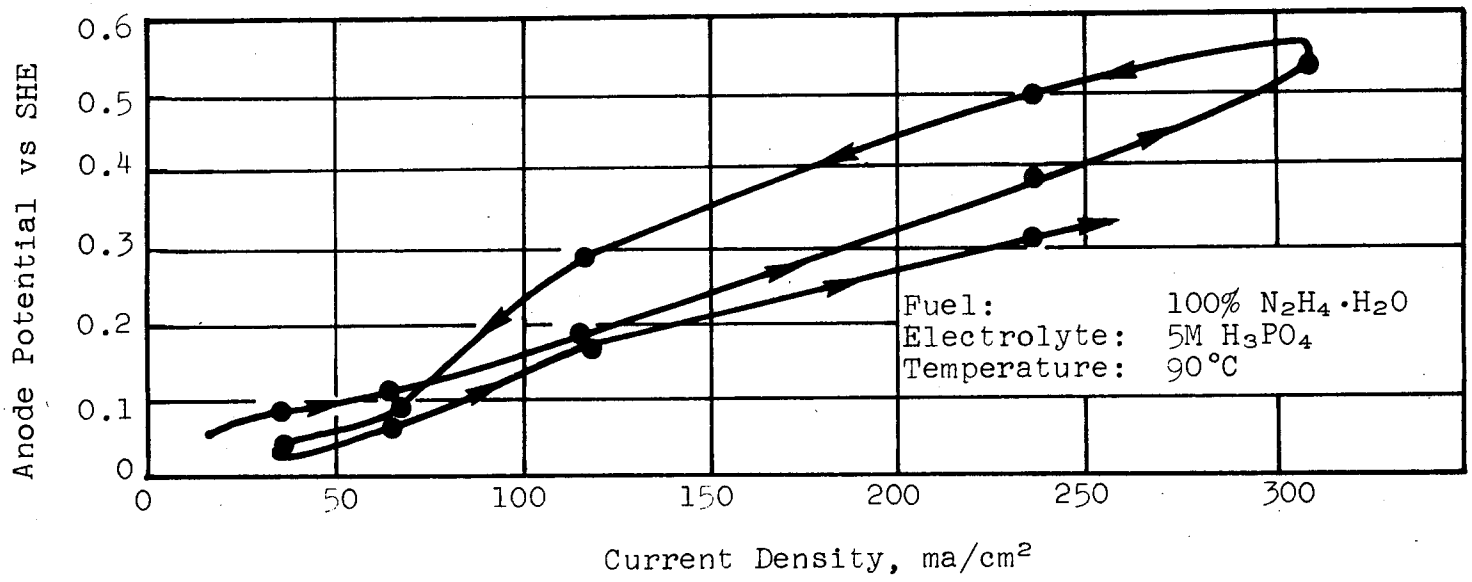

Figure A-21. Anodic Polarization of Pt Plated Porous Carbon Electrodes-Vapor Diffusion Testing

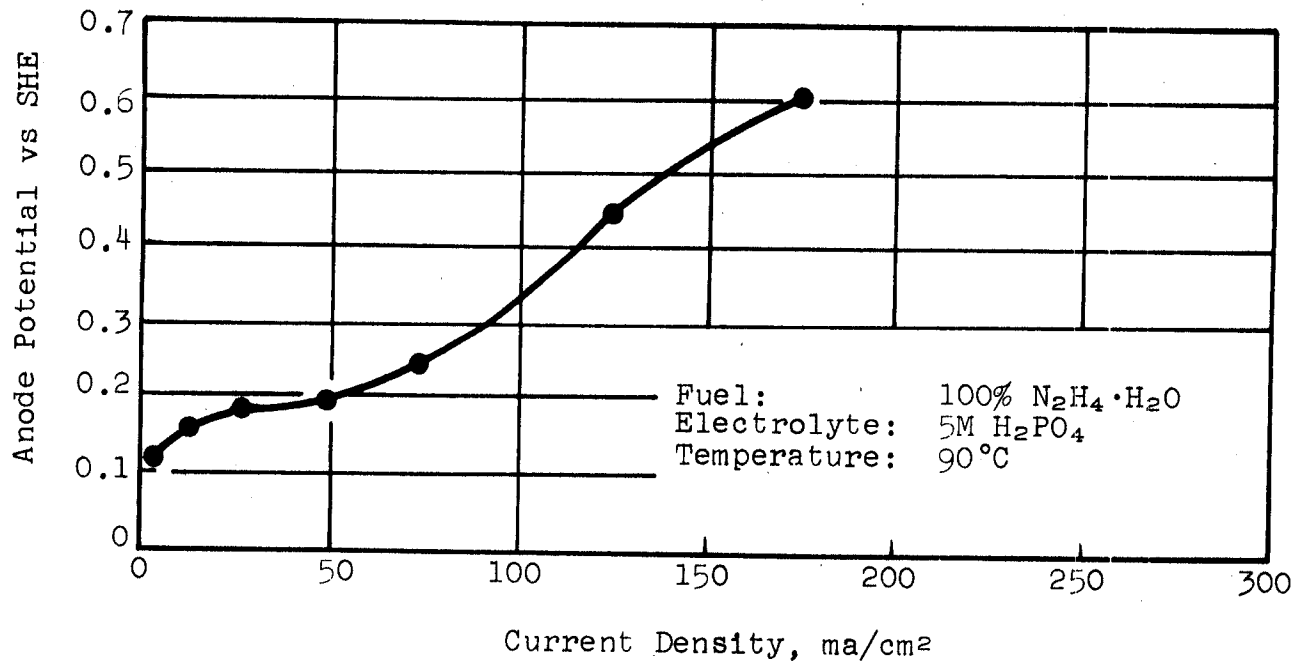

Figure A-22. Anodic Polarization of Porous Carbon-MRD-A (Pt) Composite Electrode-Vapor Diffusion Testing

electrodes differed from their precious metal counterparts in at least one significant way: the resultant electrodes were totally wet-proofed and did not leak or pass any measurable quantity of liquid. At 90°C, however, the diffusion rate of vapor was usually quite high on the normal membranes. With these facts in mind, an MRD-A (carbon) electrode was prepared in the following manner. A 13-mil membrane was heated to 550°F and compressed under 400 lbs/in^2 to a final thickness of 7 mils, a step designed to reduce pore size. Using a 3% solution of H_2PtCl_6, the electrode was then electroplated to give a shiny Pt coating. Testing was performed in the standard diffusional set-up using 100% $N_2H_4 \cdot H_2O$ and 5M H_3PO_4. Since little was known about the resultant electrode, the testing procedure was varied slightly to provide additional information as the run progressed. Some of the data obtained are plotted in Figure A-23. Initially, the electrode was operated at room temperature (28°C) for an extended period to determine if gross leakage was occurring. After approximately 1 hour at 40 ma/cm^2, the electrode potential remained essentially constant and only 0.1M N_2H_4 was found in the electrolyte solution. These data were accepted as equilibrium values for the low temperature condition and represented no measurable electrode leakage. After increasing the temperature to 90°C, the current density was raised to 160 ma/cm^2 and held constant for over an hour. Electrode performance remained essentially stable throughout this period, but titration of the electrolyte revealed 0.5M N_2H_4 in solution. This latter represents over diffusion, although the half molar contamination level is not overly excessive. Nevertheless, the electrode activity (0.1v vs SHE at 160 ma/cm^2) is quite promising. It is possible that the use of heavier membranes, greater compression, or a less concentrated fuel source would help to increase diffusion control.

9. MRD-A (Pt, Rh) Plus MRD-A (Na_2CO_3) Membrane

With the MRD-A (precious metal) construction continually exhibiting excellent catalytic activity, a further attempt to build diffusional control around it was tried. Porous Teflon membranes, used in earlier cathode work, were characterized by the reduction of pore size and excessive pore blockage when heat-bonded to carbon cathodes. This resulted in an appreciable reduction in vapor transport and severe current limitation. The construction of an MRD-A membrane containing a water soluble salt, which is bonded to the precious metal electrode prior to leaching of the salt, offers the possibility of circumventing the pore-sealing difficulties. Several membranes of this type were constructed using sodium carbonate as the contained salt. These were then heat-bonded to three previously characterized platinum and one rhodium MRD-A electrodes. They were then placed in boiling distilled water until tests with barium hydroxide indicated the removal of all of the sodium carbonate. Before polarization studies, all composite electrodes were

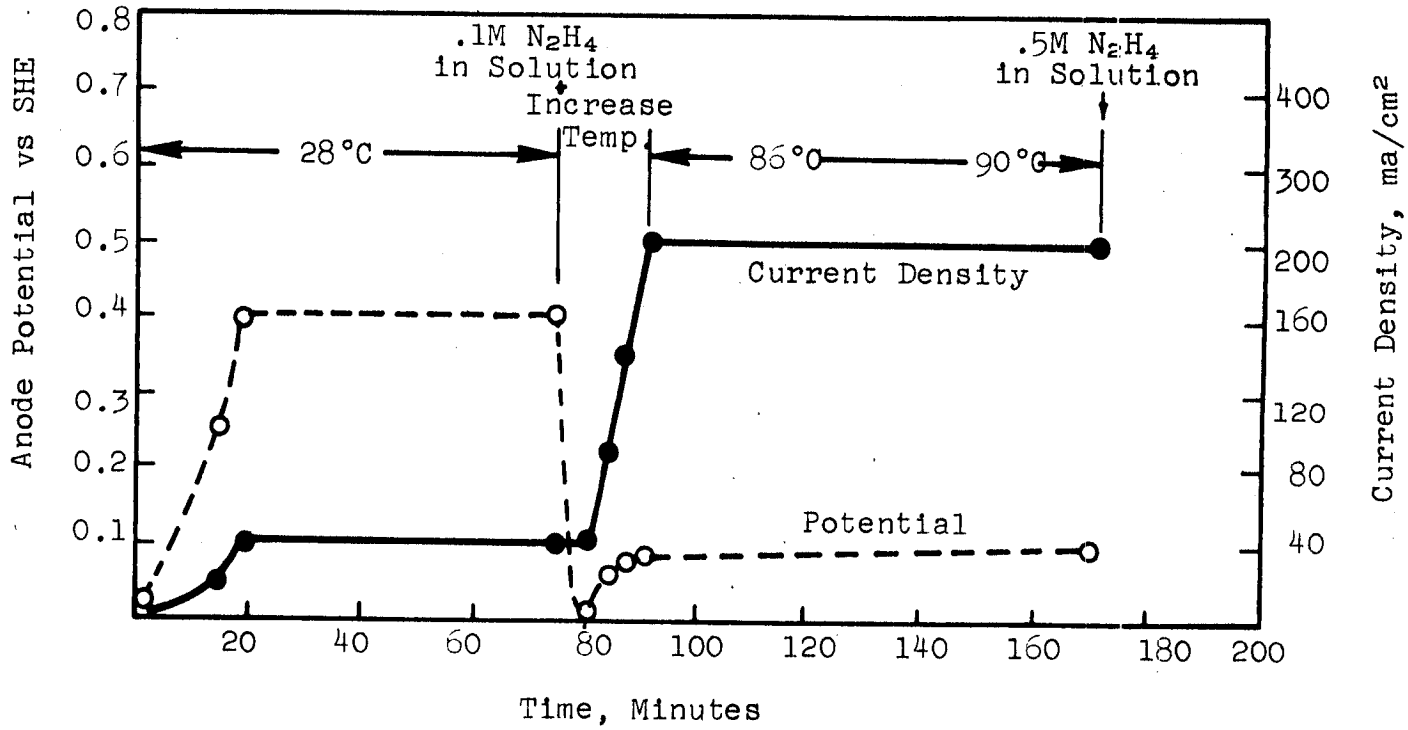

Figure A-23. Anodic Polarization of Pt Plated MRD-A (Carbon) Electrode-Vapor Diffusion Testing

given preliminary testing with water to inspect for leakage. None was able to pass this test; all showed some degree of liquid leakage at room temperature. The method of bonding as well as the effect of boiling in water are possible causes of leakage. In any event, further effort is required to assess the potential of this approach.

10. Conclusions

In view of the number of approaches taken in our anode diffusion work, a reappraisal of our status is appropriate. Several methods offer considerable promise but will, in all probability, require reasonable effort to bring them to an acceptable level of development. On the other hand, diffusion controlled carbon cathodes for acid systems demonstrate remarkable performance even in the presence of 0.5M N_2H_4 contamination in the electrolyte. Such a level of "contamination" provides sufficient strength of dissolved fuel to successfully operate precious metal electrodes of the MRD-A type as solution anodes (See ref. 2). This tends to alleviate the necessity of a diffusion controlled anode structure and to promote the desirability of a circulating anolyte-solution anode-diffusion cathode system.

D. EXTERNALLY REFORMED HYDRAZINE

1. Background

Hydrazine can be catalytically decomposed to hydrogen and nitrogen gases at room temperature. Such external reforming of hydrazine constitutes an alternate procedure to the direct use of aqueous hydrazine at a fuel anode. By externally reforming hydrazine, either a hydrogen-nitrogen gas mixture or pure hydrogen could be supplied to the anode. (Nitrogen could be separated from hydrogen by using a palladium diffusion membrane).

2. Method

The system used to decompose the hydrazine and feed nitrogen and hydrogen gas to the anode is shown in Figure A-24. Rhodium black powder* was used to decompose 85% hydrazine hydrate in an external flask. The rate of hydrogen production was sufficient to support a current of 300 ma/cm², based on the reaction $N_2H_4 \longrightarrow N_2 + 2H_2$.

3. Results

Results of two hydrazine decomposition tests are given in Table A-5. Rates of gas formation were measured for the second run.

*Englehard Industries, Inc., Newark, New Jersey

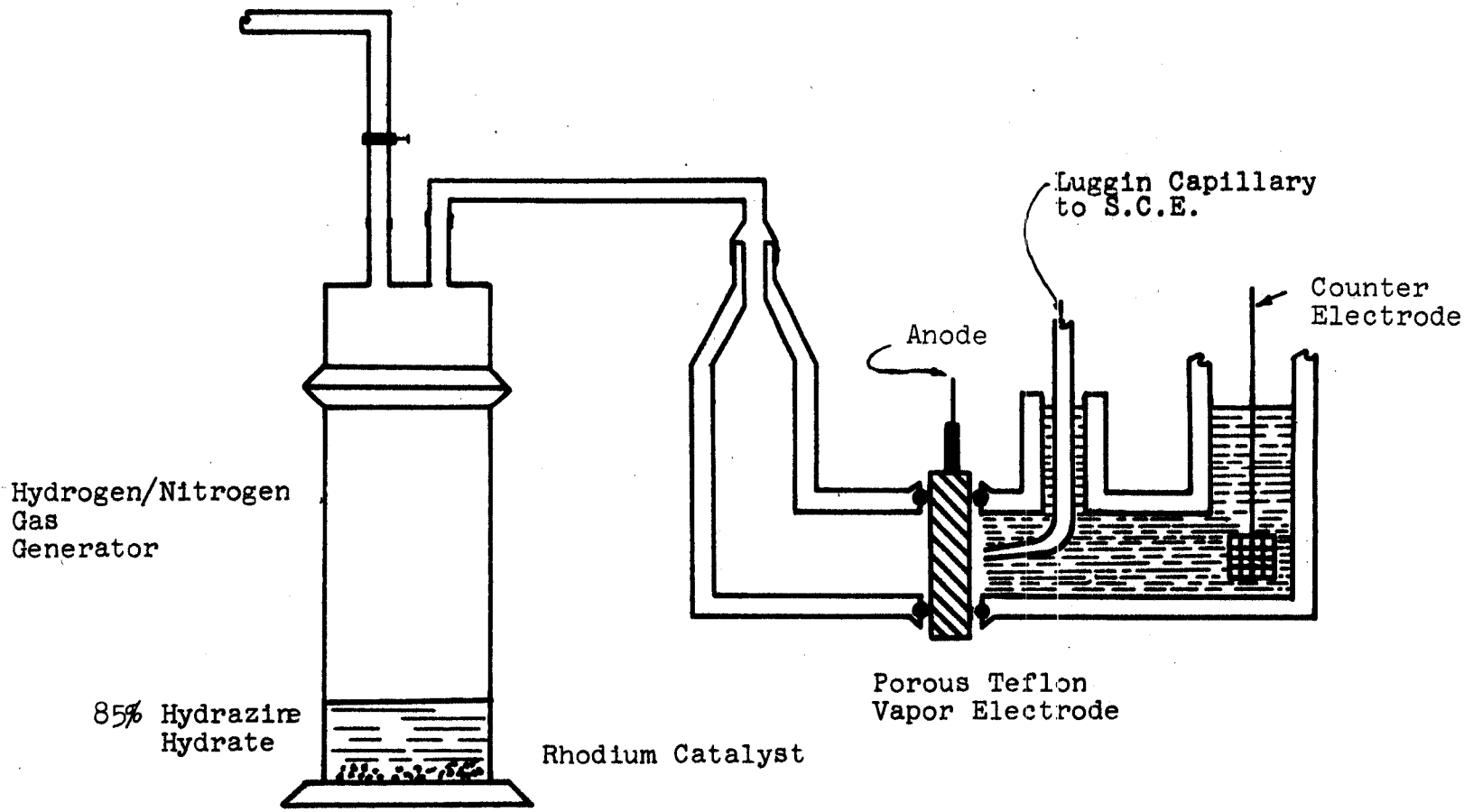

Figure A-24. Apparatus for Externally Decomposing Hydrazine to Hydrogen and Nitrogen and Using the Product Gas at Porous Teflon Anode.

Table A-5

EXTERNAL HYDRAZINE DECOMPOSITION AND UTILIZATION AT POROUS TEFLON ELECTRODE

Electrolyte - 5M H_2SO_4, Anode - PTVDE, 50 mg Pt/cm^2, Temperature - 30°C

Current Density	Potential vs HE at same Temperature and pH	
ma/cm^2	Test I	Test II
0	0.060	0.060
4	0.060	0.075
8	0.060	0.075
20	0.065	0.075
40	0.070	0.080
60	0.070	0.09
80	0.080	0.10
100	0.085	0.11
120	0.09	0.12
200	-----	0.16

Note: For Test II H_2 production rate our feed rate measured assuming $N_2H_4 \rightarrow N_2 + 2H_2$

Total gas evolution rate at 30°C = 9.0 cc/min

H_2 rate = 4.3×10^{-6} moles/sec

Maximum current for H_2 rate = 330 ma/cm^2

Steady currents of 200 ma/cm² could be maintained. At currents higher than 250 ma/cm², the potentials slowly deteriorated. The experimental current efficiency of 70% may be less than theoretical because of insufficient active catalyst surface, or non-homogenous catalyst area, allowing hydrogen to penetrate without contacting the catalyst.

E. SELECTIVITY OF PLATINUM FOR HYDRAZINE OXIDATION

1. Background

Because of the difficulty of preventing some leakage of unreacted nitric acid or dinitrogen tetroxide through a porous cathode, it is desirable to develop an anode catalyst that is selective toward the oxidation of hydrazine in the presence of small concentrations of the oxidants. Platinum is the only known catalyst that is selective to the anodic oxidation of hydrazine in the presence of any reasonable concentration of nitric acid. Since we know that platinum is not the best catalyst for hydrazine oxidation in phosphoric acid solution when no nitric acid is present, a search for other catalytic materials was initiated.

2. Results

a. Non-Contaminated Solutions

Polarization tests for catalytic activity on carbon electrode surfaces are given in Table A-6. Both chemiplated and electroplated precious metals were used when possible. One sample of pure platinum black powder* in a tantalum holder Teflon electrode was used (Run 5, Table A-6). The following trends were noted as a result of tests in uncontaminated solutions:

(1) Tests 2-4, Table A-6, indicate that amount of platinum per unit area is the controlling factor in electrode activity, regardless of type of deposit.

(2) The activity of all chemiplated mixtures is superior to any of the chemiplated metals alone at equal loadings. The best of the mixtures is 60% Pt-20% Ru-20% Au, which has an advantage over any chemiplated pure component at 100 ma/cm².

(3) Electroplated rhodium at very low loading is superior to electroplated platinum at significantly higher loadings and is the best catalyst other than the commercial platinum black electrode listed in Table A-6.

---

*Englehard Industries, Inc., Newark, New Jersey

Table A-6

ANODIC POLARIZATION OF PRECIOUS METAL CATALYSTS FOR N_2H_4 ANODES

Fuel: 0.5M N_2H_4
Electrolyte: 5M H_3PO_4 (Both Uncontaminated and Contaminated with 1M HNO_3)
Temperature: 90°C

Catalyst	Type Deposit ‡	mg/cm²	wt %	Anode Potential (Volts vs SHE)‡‡ Current Density (ma/cm²) 0.5M N_2H_4 OCV	50	100	Current Density (ma/cm²) 0.5M N_2H_4+1M HNO_3 OCV	50	100	Plating Solution
1. FC-13 Carbon (control)	-	-	-	0.54	-	-	0.59	-	-	
2. Platinum	P	13.5	8.2	0.20	0.37	0.49	0.31	0.46	0.58	3% H_2PtCl_6 + 0.3% $Pb(Ac)_2$
3. Platinum	P	12.5	7.7	0.14	0.43	0.53	0.33	0.46	0.56	3% H_2PtCl_6 + 0.3% $Pb(Ac)_2$
4. Platinum	C	4.9	3.3	0.19	0.50	0.60	0.27	0.57	0.79	*
5. Platinum	B	25	-	0.14	0.22	0.25	0.34	0.38	0.40	**
6. Rhodium	P	6.7	4.3	0.14	0.27	0.35	0.30	0.34	0.43	1% $RhCl_3$
7. Rhodium	C	3.7	1.7	0.23	0.48	0.59	0.40	-	-	*
8. Ruthenium	P	25	14.5	0.19	0.29	0.40	0.39	0.55	0.64	1% $RuCl_3$
9. Ruthenium	C	7.9	5.3	0.19	0.38	0.59	0.38	-	-	*
10. Palladium	P	17.3	9.0	0.26	0.45	0.52	0.54	-	-	1% $PdCl_2$
11. Gold	C	2.8	1.9	0.41	0.55	0.64	0.46	0.64	-	*
12. 80%Pt-20%Ru	C	2.9	2.0	0.17	0.335	0.45	0.34	0.55	-	*
13. 67%Ir-33%Ru	C	11.4	7.6	0.19	0.40	0.55	0.36	-	-	*
14. Iridium	C	2.6	1.8	0.27	0.51	0.61	0.40	0.62	-	*
15. 60%Pt-20%Ru-20%Au	C	4.0	2.7	0.16	0.30	0.44	0.32	0.54	0.62	*

* Reduced with $NaBH_4$
** Tantalum diffusion electrode construction (See Section B-1-a)
‡‡ IR-Free

‡ P - Electroplated on FC-13 Carbon (Pure Carbon Company)
C - Chemiplated on FC-13 Carbon
B - Commercial Metallic Black on Pt Screen Grid

b. Contaminated Solutions Containing 1M HNO_3

Only the electroplated rhodium and platinum-containing electrodes showed significant selectivity toward hydrazine oxidation in phosphoric acid solutions containing 1M HNO_3. The rhodium electrode (test no. 6, Table A-6) had less than 0.1 v deterioration of potential in the contaminated solution, as compared with the potential in the uncontaminated solution.

The data of Table A-7 show that platinum-catalyzed FC-14 carbon functions as a fair anode (is hydrazine-selective) with 0.3M N_2H_4 in 5M HNO_3 at 90°C. Ruthenium-catalyzed FC-14 carbon gave a mixed potential and is not selective toward either reactant.

Table A-7

ANODE AND CATHODE POLARIZATION TESTS SHOWING SELECTIVITY OF CATALYSTS TOWARD COMPONENTS OF N_2H_4-HNO_3 SOLUTIONS

Reactants		Current Density	Potential vs SHE*								
			Electrode Material								
			FC-13		FC-14		Pt on FC-14		Ru on FC-14		
N_2H_4	HNO_3	ma/cm²	30°C	90°C	30°C	90°C	30°C	90°C	30°C	90°C	Notes
None	5M	0	1.14	1.13	1.10	--	1.11	--	1.12	--	All tests run as cathode
		10	1.10	1.11	1.08	--	1.08	--	1.07	--	
		20	1.09	1.10	1.07	--	1.07	--	1.06	--	
		50	1.07	1.09	1.05	--	1.05	--	1.05	--	
		100	1.05	1.07	1.02	--	1.03	--	1.04	--	
0.1M	5M	0	1.12	1.14	1.06	--	0.42	--	1.06	--	Pt on FC-14 tested as anode
		10	1.10	1.13	1.04	--	--	--	1.05	--	
		20	1.09	1.12	1.03	--	--	--	1.05	--	
		50	1.07	1.11	1.02	--	--	--	1.04	--	
		100	1.06	1.10	1.00	--	--	--	1.03	--	
0.3M	5M	0	--	--	1.03	1.07	0.34	0.32	0.68	0.67	Ru on FC-14 would not function
		10	--	--	1.02	1.07	0.53	0.36	--	--	as anode or cathode.
		20	--	--	1.01	1.07	--	0.43	--	--	Pt on FC-14 tested as anode
		50	--	--	0.98	1.06	--	0.49	--	--	
		100	--	--	0.95	1.04	--	0.59	--	--	
0.5	5M	0	1.11	1.10							
		10	1.09	1.10							
		20	1.08	1.10							
		50	1.06	1.09							
		100	1.03	1.08							

*SHE - Standard Hydrogen Electrode ($^{a}H^{+}$ = 1) (SCE = 0.24 volt). This reference was used since the exact value of HE (hydrogen electrode at same temperature and pH) cannot be calculated, but should be close to SHE.

APPENDIX III

PALLADIUM DIFFUSION ELECTRODE

A. BACKGROUND

1. General

The solid palladium hydrogen diffusion electrode is attractive for fuel cell systems using hydrogen gas or materials that can be converted to hydrogen gas. The palladium membrane not only provides an electrically conducting electrode but also can absorb and transfer hydrogen (and only hydrogen) from one surface to the opposite surface for use as an anode fuel. Other materials can not penetrate the electrode, so such soluble fuels as hydrazine can be restricted from the electrolyte compartment where they could diffuse to and degrade the cathode.

When dissolved in palladium, hydrogen is said to exist in the ionized state and, under the influence of an electrical field, the proton will be ejected from the metal. Hence, a mechanism is established for emitting a proton in an already ionized state, the essential step, $H = H^+ + e^-$, being produced within the metal (ref. 7). In contact with hydrogen gas at one atmosphere, palladium is known to absorb hydrogen until the ratio of hydrogen to palladium becomes 0.69, after which the electrode is in equilibrium with hydrogen gas at one atmosphere. The potential of this hydrogen-saturated palladium electrode is the same as that of a reversible hydrogen electrode in contact with the same solution. Hoare and Schuldiner (ref. 8) have found that the palladium-hydrogen electrode has a potential plateau that is 50 mv more positive than the reversible hydrogen potential at H/Pd ratios of 0.03 to values approaching the saturation ratio of 0.69 when the reversible hydrogen potential is attained. This could well be attributed to the transformation of hydrogen-palladium solid solution from α-phase to β-phase.

Oswin and Chodosh (ref. 9) have reported the use of nonporous palladium as a hydrogen anode when placed in contact with hydrogen gas on one side and an electrolyte on the reverse side. These authors indicate that some special surface pretreatment is required before high current densities can be drawn from the hydrogen-palladium anode, but they do not disclose the nature of this pretreatment.

Palladium-25% silver foils are preferred to pure palladium for use as active anodes, since the silver alloys do not expand and contract as severely as pure palladium during hydrogen cycling. This expansion and contraction, due to different lattice parameters of

low hydrogen α-phase (3.91 Å) and high hydrogen β-phase (4.02 Å), can cause membrane cracking and failure (ref. 10).

A number of previous workers reported that heat treatment of palladium foil in air at elevated temperature increased the rate of diffusion of hydrogen through the foil (ref. 11) and improved its characteristics as a nonporous anode (ref. 12). The data, however, were rather qualitative, and the optimum condition for the treatment was not given in any of these papers. Also, the mechanism has not yet been clarified.

Although many factors could be related to the palladium heat treatment, the main effects on the characteristics of hydrogen diffusion electrodes are attributed to a change of crystal structure of the alloy and to a change of its surface properties, since heating in air up to 790°C will definitely form an oxide layer on the palladium surface. The effect of plating other elements on the palladium surface also should be considered.

As a nonporous diffusion anode, the palladium membrane is involved in three major reactions: (1) an interfacial reaction with hydrogen fuel involving adsorption and dissociation of hydrogen molecules into atomic hydrogen, or, very likely, protons (for simplicity the term "atomic hydrogen" will be used in this report); (2) diffusion of atomic hydrogen through the membrane; and (3) electrode reaction to release hydrogen atoms into ions at the electrolyte interface. It is most likely that all three reactions will be more or less affected by metallurgical factors resulting from the heat treatment at elevated temperatures.

2. Crystal Structure

Since the very thin foil is severely cold-rolled in the manufacturing process, heating to 600°C (previously recommended, refs. 11, 12) may give some recrystallization and crystal growth in addition to a degree of recovery from the cold work. Heat treatment at 850°C is considered to be an optimum condition for the full annealing of palladium-silver alloys (ref. 13). Different metallurgical structures obtained by various heat treatment probably affect the properties of the membrane through the following mechanisms:

(a) Different rate and amounts of molecular hydrogen may be adsorbed on the surface of cold-rolled palladium and annealed palladium, because a preferred orientation on the surface of severely cold-rolled palladium is possible.

(b) Severe deformation of the alloy crystal structure, such as point defects and dislocations introduced by cold-rolling, will change the rate and amount of absorption and diffusion. Since hydrogen atoms are absorbed into and diffused through interstitial sites of the palladium crystal lattice, these defect sites in the structure may act as traps for the process.

(c) Fine-grained palladium will absorb more atomic hydrogen than coarse-grained material, since grain boundaries are expected to act as a sink for hydrogen atoms.

(d) The diffusion rate of atomic hydrogen in fine-grained palladium will probably be faster than that in coarse-grained palladium, since boundary diffusion is much faster than bulk diffusion.

(e) The effect of cold working and crystal structure on the anodic oxidation of atomic hydrogen to hydrogen ions can not be predicted, although tensile stress in a metal is known to make it anodic to unstressed metal (ref. 14).

3. Oxide Film Formation

Palladium oxidizes readily in an oxygen atmosphere to form a visible oxide layer at 350 to 790°C (ref. 15). In this temperature range only palladium oxide is expected to form on a palladium-silver alloy because of the instability of silver oxide. Palladium monoxide (PdO), the only known oxide of palladium at high temperature, is a p-type semiconductor (cation vacancy type) (ref. 16). Its cation-vacancy structure can be characterized by palladium ion vacancies, $\square Pd^{++}$, and simultaneous electron deficits, $\square e^{-}$, according to the following equation:

$$1/2\ O_2 = PdO + \square Pd^{++} + 2\square e^{-} \qquad (1)$$

Assuming that no other major disorder equilibria are present (i.e., that the concentration of the cation vacancies is one half of the concentration of electron deficits) then the ideal mass action law can be expressed as follows:

$$\frac{c(\square Pd^{++}) \times c(\square e^{-})^2}{(P_{O_2})^{1/2}} = K$$

From the stoichiometric mass balance, $c(\square e^{-}) = 2c(\square Pd^{++})$,

So, $$\frac{c(\square Pd^{++}) \times [2c(\square Pd^{++})]^2}{(P_{O_2})^{1/2}} = \frac{4[c(\square Pd^{++})]^3}{(P_{O_2})^{1/2}} = K$$

or $$c(\square Pd^{++}) = 1/2\ c(\square e^{-}) = \left(\frac{K}{4}\right)^{1/3} (P_{O_2})^{1/6} = K'(P_{O_2})^{1/6}$$

This relation was substantiated by experimental data for the oxidation of copper (ref. 17), and it shows that the concentration of cation vacancies and electron deficits is a function of oxygen pressure. These concentrations are also a function of temperature and the addition of other cations or anions to the oxide.

On the other hand, we may assume that the transfer of hydrogen molecules into hydrogen ions can be represented as follows:

$$H_2 \text{ (gas)} \longrightarrow 2\underline{H}$$

where $\underline{H}$ is absorption as an atom or proton at gas-metal surface.

$$2H \xrightarrow[\text{diffusion in Pd}]{\text{Interstitial}} 2\underline{H} \xrightarrow[\text{surface}]{\text{electrode}}$$

$$2H^+ \text{ (into electrolyte)} + 2e^- \text{ (into metal)} \qquad (3)$$

Consequently, the cation vacancy sites or electron deficits in the palladium oxide layer on either side may increase the reaction as a catalyzer by being an acceptor of protons or free electrons produced by the dissociation process. Further, these sites of crystal defects may supply an easier diffusion path for protons or free electrons in the oxide layer. However, one cannot distinguish between the catalytic effect of cation vacancy sites or of electron deficits at this stage.

4. Controlling Factors on the Concentrations of Cation Vacancies in Palladium Oxide

The concentration of cation vacancies will be increased by: (a) increasing the oxygen pressure according to equation (2), and (b) adding higher valency cations (which will result in decreasing the concentration ratio of electron deficits to cation vacancies, however). The addition of lower valency cations will decrease the concentration of cation vacancies and simultaneously increase the concentration ratio of electron deficits to cation vacancies. The addition of other anions such as sulfur ions also affects the semiconductivity of the oxides.

5. Effect of Alloying Elements

The effect of additional alloying elements in Pd-25%Ag on its performance as a hydrogen diffusion electrode may be attributed to the change of many metallurgical properties including the following.

(a) Change of the lattice parameter by forming solid solutions or intermetallic compounds with main constituents.

(b) Defect crystal structures introduced by alloying such as point defects (lattice vacancies) and dislocations.

(c) Change of the electron configuration of the alloy, particularly vacancy concentration in d-band electrons.

(d) Change of the properties of the surface oxide film, particularly semiconductivity and crystal lattice vacancies.

B. PRELIMINARY EXAMINATIONS OF METALLURGICAL FACTORS INVOLVED IN PALLADIUM-SILVER DIFFUSION ELECTRODE

1. Determination of Impurities in Palladium

An electron microprobe analyzer, Model JxA-3A by Japan Electron-optics Laboratory, Tokyo, Japan, was used to determine impurities in two kinds of Pd-25%Ag foil that were manufactured by two different processes: (a) a "booking" reduction process, and (b) direct rolling by a multiplex cluster rolling mill. A general qualitative analysis showed that the foils contained no appreciable impurities.

A quantitative analysis with the highest sensitivity of the microprobe instrument was performed for specific impurities, particularly those which would presumably affect the palladium-silver electrode performance.

Results of the quantitative analyses are shown in Table A-8. Each value is the average of two samples. The analyses showed that the foil that was reduced by the "booking" process (rolling between copper plates) had three times the copper content of that rolled directly by a cluster rolling mill. Since copper forms a continuous series of solid solutions with palladium and silver, it is reasonable to assume that copper from the supporting plates diffused into the alloy during the rolling process.

Table A-8

IMPURITIES IN PALLADIUM-25% SILVER FOIL

Manufacturing Process	Impurity Content, %			
	Fe	Cu	Ni	Pb
Booking	0.02	0.11	0.00	0.06
Cluster Rolling Mill	0.02	0.04	0.00	0.08

2. Effect of Heat Treatment on Metallographic Structure of the Palladium-25% Silver Foil

The metallographic structure of a cross section of Pd-25%Ag foil as received from the manufacturer (J. Bishop Co.) is shown in

Figure A-25. All crystal grains were thoroughly destroyed during cold-rolling and were severely deformed into an almost laminar structure.

The structures of the foils after heat treatment in air for two hours at 700, 600, and 500°C (without preheating at 850°C) are shown in Figures A-26, A-27, and A-28, respectively. The photographs clearly indicate that some recrystallization occurred at the middle of the foil at 700°C, less at 600°C, and almost none at 500°C. The structure of a foil, after annealing in air for 5 hours at 850°C and quenching in water at room temperature, is shown in Figure A-29. The alloy had not only fully recovered after the heat treatment but also was highly crystalline, probably because of previous severe cold work. However, the grain sizes were extremely small because of a very high rate of nucleation. Since palladium monoxide decomposes at 790°C, no oxide film is formed at 850°C.

Figure A-30 shows the structure of a foil after annealing in air for five hours at 850°C, subsequently oxidizing in air for 2 hours at 700°C, and finally cooling in air. The structure was essentially identical to that of the foil that was annealed only (Figure A-29).

The structure of a foil that was heat-treated in purified hydrogen gas for three hours at 600°C is shown in Figure A-31. The hydrogen gas was purified before being introduced into the furnace by passing over fine copper foil heated at 450°C. The photograph shows that the alloy was recrystallized into a very uniform structure of palladium-silver-hydrogen solid solution as hydrogen diffused into and saturated the foil.

Heating a Pd-25%Ag foil in air for two hours at 600°C and then in purified hydrogen for three hours at 600°C resulted in the structure shown in Figure A-32. The surface of the heat-treated foil appeared very bumpy and blistery. Except for a much smaller grain size in some areas of the foil, the structure was similar to that shown in Figure A-31. The previous heat treatment in air introduced dissolved oxygen into the structure, following the reaction

$$1/2\ O_2\ (\text{gas}) \longrightarrow \underline{O}\ (\text{in alloy})$$

We believe that hydrogen diffused into the alloy and formed water vapor by reacting with the dissolved oxygen. The water vapor eventually escaped from the alloy (explaining the blistered appearance) but hindered somewhat the grain growth of the palladium-silver-hydrogen solid solution, resulting in smaller grain sizes in some areas.

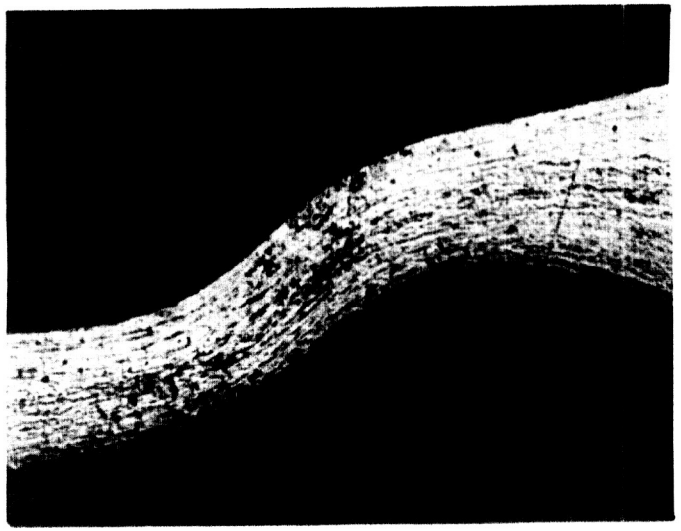

Figure A-25. Pd-25% Ag Foil as Received. 350X

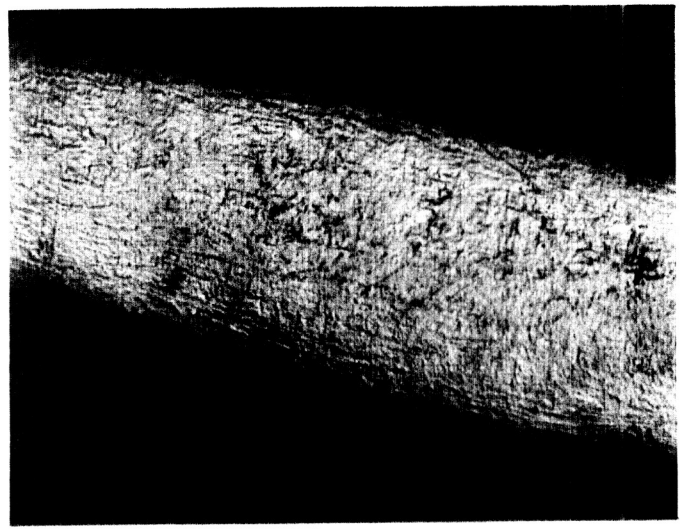

Figure A-26. Pd-25% Ag Foil Heat Treated in Air 2 Hr at 500°C. 350X

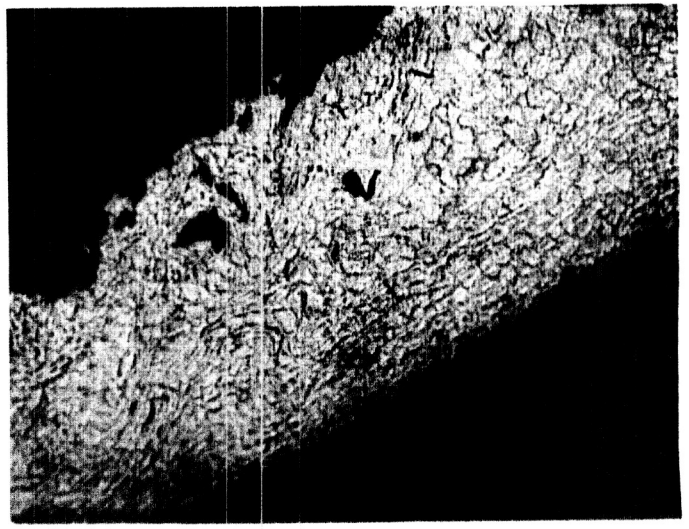

Figure A-27. Pd-25% Ag Foil Heat Treated in Air 2 Hr at 600°C. 350X

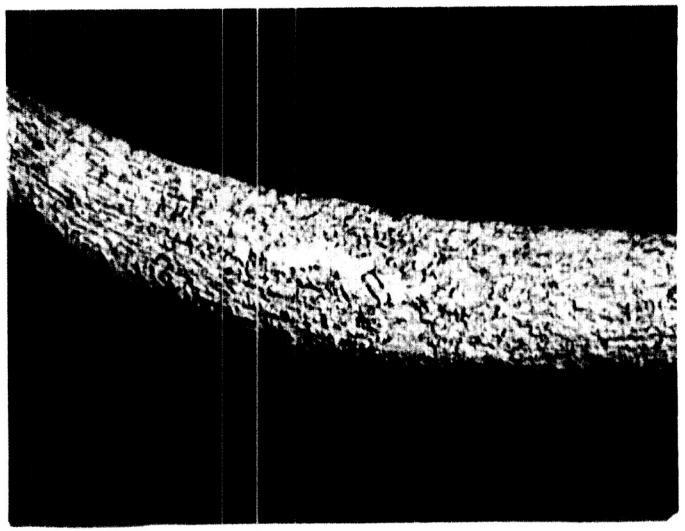

Figure A-28. Pd-25% Ag Foil Heat Treated in Air 2 Hr at 700°C. 350X

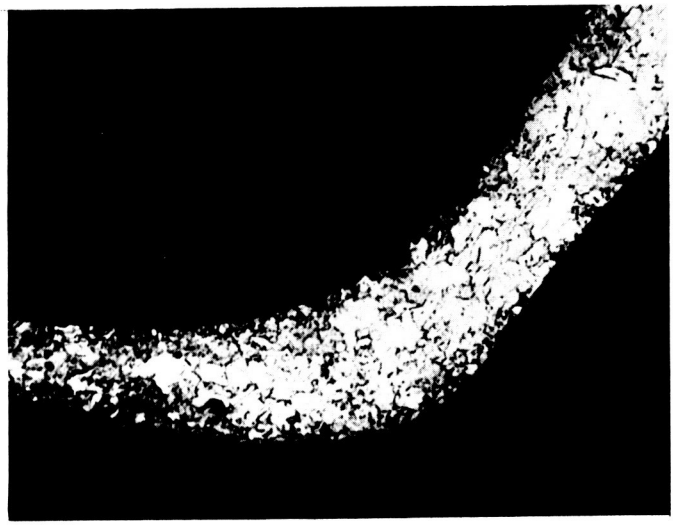

Figure A-29 Pd-25% Ag Foil Heat Treated in Air 5 Hr at 850°C. 350X

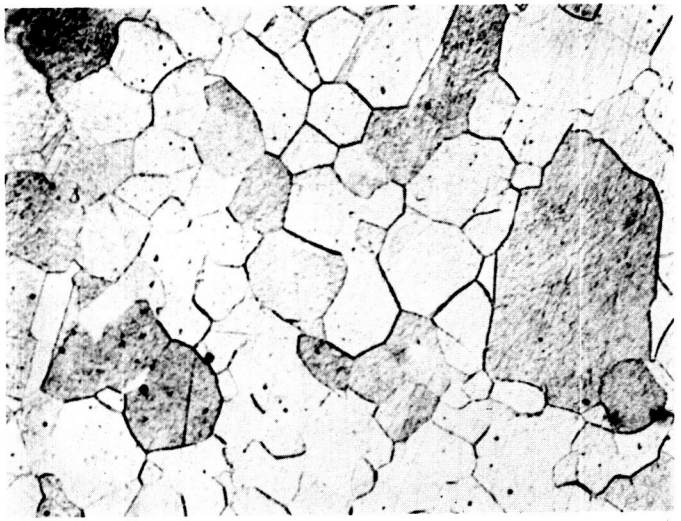

Figure A-31. Pd-25% Ag Foil Heat Treated in H_2 3 Hr at 600°C. 350X

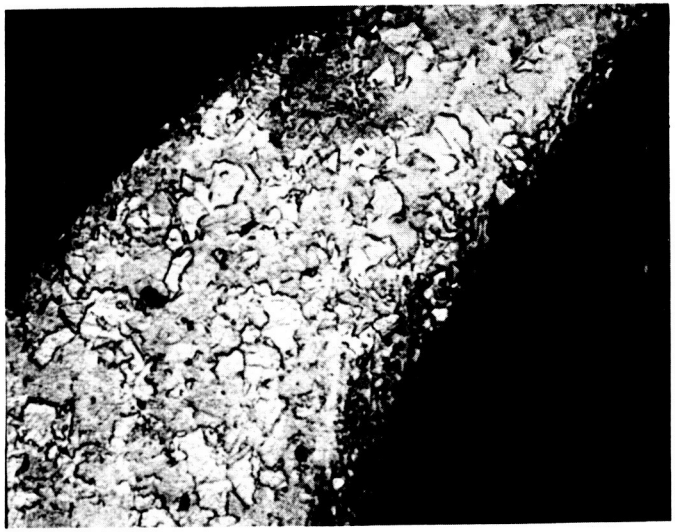

Figure A-30. Pd-25% Ag Foil Heat Treated in Air 5 Hr at 850°C and 2 Hr at

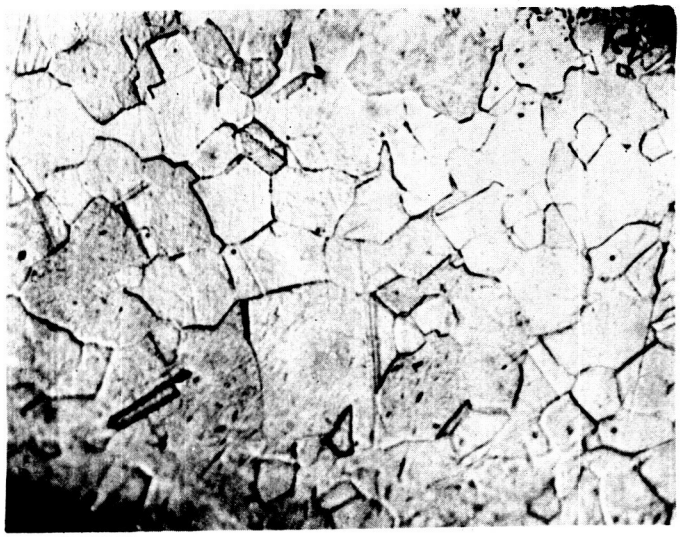

Figure A-32. Pd-25% Ag Foil Heat Treated in Air 2 Hr and in H_2 3 Hr at 600°C. 350X

3. Surface Film Formed by Oxidation

Electron diffraction patterns* were taken by reflection from the surface of Pd-25%Ag foils that had been heat-treated in various manners. The foil that had been annealed at 850°C and quenched in water showed no evidence of an oxide film. Although some palladium oxide film would be expected to form, even during rapid cooling, the film was apparently too thin to be detected by electron diffraction. The foil was shiny in appearance after heating and quenching.

Heating in air between 500°C and 700°C formed a palladium oxide coating of various thicknesses. The film had the crystal pattern of palladium monoxide. The surface of the foil heated at 700°C appeared greyish blue, at 600°C appeared slightly reddish blue, and at 500°C appeared deep blue. No palladium monoxide was detected by electron diffraction examination of a foil that was heat-treated in air at 650°C and that was subsequently used as a hydrogen diffusion electrode until the foil lost its capacity as an anode. The disappearance of the oxide film was attributed to reduction by absorbed hydrogen (either atomic or proton), which is a potent reducing agent.

4. Effect of Heat Treatment and Oxidation on Polarization of Palladium-25% Silver Diffusion Electrode

The effect of the structure of Pd-25%Ag foil on its capacity as an anode was determined by examining anodic polarization characteristics of heat-treated foils. The polarization cell is shown in Figure A-33. All electrodes were cleaned by immersing for 30 minutes in hot concentrated sulfuric acid saturated with chromic acid and washing in distilled water before heat treatment. Electrodes were kept in a desiccator after the cleaning process to avoid surface contamination from the atmosphere.

Full annealing was accomplished by heating the foil in air for five hours at 850°C and quenching in cold water to minimize oxide formation during cooling. The oxide film on the surface was formed by heating the foil in air for two hours at a given temperature and cooling in air.

Hydrogen was generated on the Pd-25%Ag electrode surface in the left compartment by passing a constant current between the electrodes A and B. After saturating the electrode with hydrogen for 45 minutes, the cathodic treatment on the left side was continued at constant current while the right side of B was anodized against counter electrode C. Absorbed hydrogen then diffused through the

---

* Electron microscope model JEM-6C by Japan Electron-optics Laboratory, Tokyo, Japan.

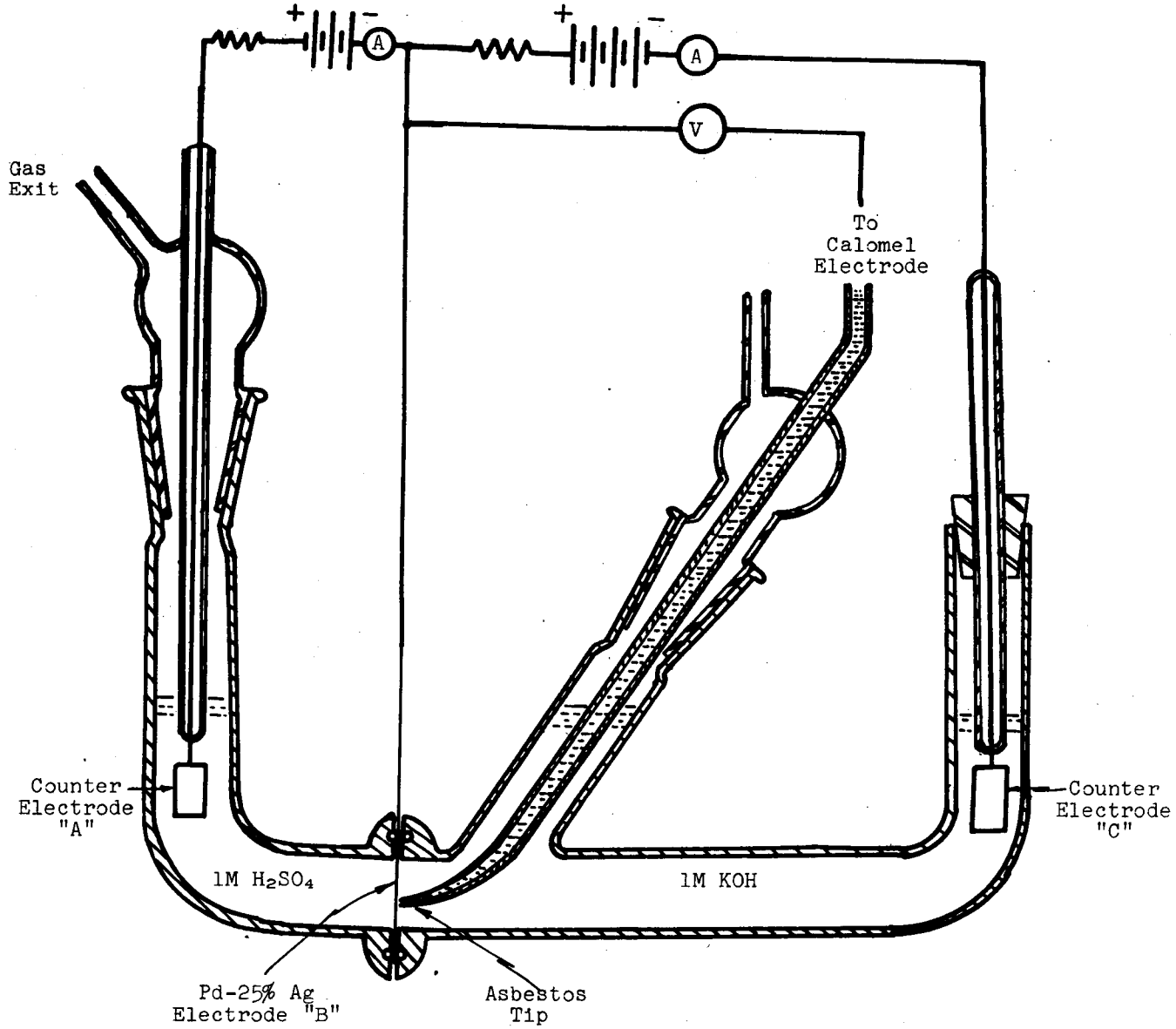

Figure A-33. Polarization Cell Assembly

foil and was discharged from the electrode surface in the right compartment. The anode potential was measured against a saturated calomel electrode (SCE) via a Luggin capillary, which was always placed at the same distance, 1 mm, from the electrode surface so that proper correction could be made for the IR drop between the anode and the tip of the Luggin capillary. At each of three different generating current densities between electrodes A and B, namely, 4, 40, and 250 ma/cm^2, the electrode potentials were measured at various current densities between electrodes B and C to determine the anodic polarization characteristics of the electrode. Potentials were corrected for IR drop by selecting a value of R such that the log I vs potential relation was linear at current densities below the limiting current. All polarization tests were run at 90°C. Potentials in Table A-9 have been calculated in relation to a reversible hydrogen electrode at the same pH and temperature as the test solutions.

The effects of annealing and oxidizing at several temperatures on the anodic polarization characteristics of Pd-25%Ag foils are summarized in the following paragraphs.

a. Effect of Annealing Only

Annealing a Pd-25%Ag foil above the decomposition temperature of palladium monoxide (790°C) and subsequent quenching to prevent oxidation resulted in nonreproducible anodic polarization characteristics (Tests 2a and 2b, Table A-9). Polarization Test 2a was considerably better than that for the untreated foil (Test 1), while Test 2b was not as good as that of the untreated foil. Subsequent experiments showed that controlled oxidation of the annealed foil is required for reproducibly good anodic polarization characteristics. Slightly different amounts of oxide film formed on electrodes 2a and 2b probably account for the considerable difference in discharge behavior.

b. Effect of Annealing and Oxidizing

Annealing at 850°C followed by oxidation in air at 700, 650, 600, and 500°C were the heat treatments for Pd-25%Ag foils in Tests 3 through 6, Table A-9. All in this series showed better anodic polarization characteristics than Tests 1, 2a, or 2b, involving the foil as received or with annealing only and no oxidation. The foil that was oxidized at the highest temperature (700°C) (Test 3), showed the best anodic properties, particularly at higher current densities. This may be attributed to the higher number of cation vacancies in the oxide film formed by oxidation at the higher temperature. The other foils of this series (Tests 4 through 6) were oxidized at lower temperatures down to 500°C and were all strong anodes although somewhat less effective than the foil oxidized at the highest temperature (Test 3).

Table A-9

EFFECT OF HEAT TREATMENT ON PALLADIUM-25% SILVER ELECTRODE

Electrode Potential vs Hydrogen Electrode at same pH and Temperature
Electrolyte - 1M KOH; Fuel - Hydrogen Cathodically Generated in 1M H_2SO_4; Temperature - 90°C

Test No.	Fuel Generation ma/cm²	4						40						200					
	Fuel Consumption ma/cm²	0	0.4	0.8	2.0	3.2	4.0	0	4	8	20	32	40	0	40	80	120	160	200
	min. / Heat Treatment	45	5	5	5	10	10	10	5	5	5	10	10	10	5	5	5	5	5
1	None (as received)	0.17	0.41	0.46	0.57	0.93	-	0.11	0.43	0.49	0.61	1.13	-	0.03	0.60	-	-	-	-
2a	850°C, 5 hr and	0.15	0.26	0.30	0.32	0.41	0.46	0.10	0.41	0.42	0.51	0.62	-	0.08	0.56	0.67	-	-	-
b	Water Quench	0.19	0.33	0.38	0.48	0.80	-	0.19	1.13	-	-	-	-	0.15	1.10	-	-	-	-
3a	850°C, 5 hr and	0.16	0.16	0.16	0.16	0.17	0.18	0.06	0.08	0.08	0.12	0.17	0.20	0.03	0.11	0.15	0.19	0.21	0.30
b	700°C, 2 hr	0.17	0.17	0.16	0.16	0.16	0.19	0.08	0.08	0.11	0.14	0.18	0.24	0.15	0.15	0.19	0.20	0.22	-
4	850°C, 5 hr, and 650°C, 2 hr	0.15	0.14	0.13	0.14	0.16	0.17	0.06	0.11	0.13	0.23	0.31	0.44	0.03	0.22	0.24	0.33	0.46	0.66
5	850°C, 5 hr and 600°C, 2 hr	0.15	0.14	0.14	0.14	0.16	0.16	0.04	0.12	0.15	0.22	0.28	0.36	0.03	0.21	0.24	0.52	0.68	-
6	850°C, 5 hr and 500°C, 2 hr	0.10	0.14	0.16	0.21	0.25	0.28	0.06	0.15	0.15	0.20	0.26	0.47	0.02	0.24	0.30	0.36	0.66	-
7	700°C, 2 hr	0.15	0.15	0.15	0.15	0.16	0.17	0.06	0.10	0.15	0.21	0.28	0.35	0.05	0.23	0.32	0.40	0.49	0.68
8a	650°C, 2 hr	0.15	0.16	0.16	0.15	0.17	0.19	0.05	0.11	0.18	0.23	0.28	0.53	0.04	0.25	0.32	0.48	0.63	-
b		0.10	0.10	0.10	0.12	0.15	0.20	0.05	0.08	0.12	0.23	0.33	0.47	0.02	0.25	0.39	0.50	0.59	-
9	600°C, 2 hr	0.14	0.13	0.12	0.13	0.14	0.15	0.07	0.09	0.11	0.16	0.20	0.23	0.04	0.18	0.26	0.32	0.41	0.48
10	500°C, 2 hr	0.13	0.18	0.21	0.26	0.35	0.76	0.06	0.19	0.22	0.28	0.45	-	0.04	0.35	1.03	-	-	-
11	650°C, 1 hr and Quench in Liquid Air 3 Cycles	0.13	0.13	0.12	0.14	0.15	0.16	0.07	0.12	0.16	0.24	0.32	0.43	0.05	0.35	0.47	0.58	-	-

c. Effect of Oxidizing Only

Palladium-silver foils were oxidized at temperatures below the decomposition temperature of palladium monoxide in Tests 7 through 10, Table A-9.

Of the oxidation temperatures chosen (700, 650, 600, and 500°C) the best anode was oxidized at 600°C. The reason for this maximum performance at an intermediate temperature with the anodic properties decreasing as the temperature rises or falls is not clear. It is noted, however, that the electrodes, fully annealed before oxidation (Tests 3 through 6), had, in general, better polarization curves than those without previous full annealing (Tests 7 through 10). The Tests 3 and 6 were repeated to check reproducibility. The results indicated good reproducibility between two tests (a) and (b) as shown in the table.

d. Effect of Temperature Cycling

The electrode for Test 11 (Table A-9) was repeatedly heated for one hour at 650°C and cooled in liquid air. After the third heating, the foil was cooled in air to room temperature. No scaling was observed during the operation, and the electrode surface was greyish, indicating that a much thicker oxide film was formed than for the previous electrodes. The anodic polarization test for Test 11 was not as good as that for Test 8 (a single heating at 650°C for 2 hours), particularly at higher current densities. This result indicated that the electrode activity was controlled not by the quantity of the oxide formed on the surface but by the nature of the oxide which appeared dependent on the oxidation temperature and that the excess oxide instead prevented passage of high current.

e. Effect of Heat Treatment in Hydrogen Atmosphere

A set of tests was made on electrodes preheated in a hydrogen atmosphere to determine the effect of presaturation of hydrogen in connection with the surface oxide. Three foils were tested in the following ways: (1) heating in air for one hour at 600°C; (2) heating in hydrogen for three hours at 600°C; and (3) heating in air for one hour and subsequently in hydrogen for three hours at 600°C. The cell used for the tests is shown in Figure A-33, but hydrogen gas was purged directly into the left side compartment instead of being generated by electrolysis. The results shown in Table A-10 indicate again that palladium oxide is a fundamental catalyst for hydrogen transfer and oxidation, and that reduction of the oxide with hydrogen deactivates the electrode.

Table A-10

EFFECT OF HEAT TREATMENT IN HYDROGEN ATMOSPHERE ON PALLADIUM-HYDROGEN ELECTRODE

Electrode Potential vs Hydrogen Electrode at same pH and temperature

Electrolyte: 5M KOH Fuel: Hydrogen gas
Temperature: room temperature

Test No.	Electrode Preparation	Current Density, ma/cm^2							
		0	8	16	32	80	160	240	320
1	1 hr in air at 600°C	0.00	0.30	0.40	0.47	0.58	0.65	0.70	0.73
2	3 hr in H_2 at 600°C	0.11	-	(No current was drawn before the potential reached that of oxygen evolution.)					
3	1 hr in air at 600°C 3 hr in H_2 at 600°C	0.08	0.58	(Maximum current density, 14 ma/cm^2, reached at 0.72 volt.)					

C. EFFECT OF RHODIUM PLATING ON PALLADIUM-SILVER ELECTRODES

Since previous work in this laboratory showed that rhodium plating improved the performance of untreated Pd-25%Ag diffusion electrodes, a series of experiments was performed to determine more definitely the effect of rhodium plating. The cell used was similar to that shown in Figure A-33 except that pure hydrogen gas was directly supplied as a fuel to the left compartment, and 5M KOH was used as an electrolyte in the right compartment. The hydrogen gas was purified by passing through a cylinder filled with palladium pellets* for conversion of traces of oxygen to water.

The gas was then passed through an Ascarite tower to remove water vapor and carbon dioxide. The gas entrance tube into the cell was arranged so that the gas impinged directly on the Pd-25%Ag foil and a fresh supply of purified hydrogen continually swept the electrode surface (ref. 18).

The electrode was first saturated with hydrogen by purging the fuel compartment with the gas until the electrode potential became constant for at least 10 minutes. The right-hand side of the foil (Figure A-33) was then anodically polarized by a potentiostat** for one minute each in potential increments of 100 mv until either a current density of 400 ma/cm^2 or the oxygen gassing potential was attained.

The Pd-25%Ag foil was heat-treated in air for one hour at 600°C before plating with rhodium black. Rhodium was plated first for 15 minutes at 10 ma/cm^2 and then for 35 minutes at 40 ma/cm^2 in 0.005M $RhCl_3$ adjusted to pH 1 with hydrochloric acid. All tests were made at room temperature. However, the temperature of the electrolyte increased slowly during the tests. Results are plotted as log I vs E by adjusting IR drop between the Pd-Ag electrode and a Luggin capillary until a straight Tafel relation was obtained for a range of current densities. Potentials at various current densities on the adjusted curve are given in Table A-11, including the results shown in Table A-10 for a comparison.

1. Effect of Rhodium Plating on Pre-Oxidized Foil

Rhodium plating on oxidized foil with no further treatment was deleterious to the anodic polarization characteristics as shown by a comparison of Tests 1 and 2, Table A-11. The oxide film formed by preliminary heat treatment at 600°C (previously shown to be required for good anodic properties) was probably reduced by evolved hydrogen during the rhodium plating in the low pH solution.

---

* A commercial unit supplied by Engelhard Ind., Inc., N. J.

** Wenking (West Germany) Model 6376TR.

Table A-11

EFFECT OF RHODIUM PLATING ON ANODIC POLARIZATION OF PALLADIUM-25% SILVER DIFFUSION ELECTRODES

Electrode Potential vs HE at Same pH and Temperature (volts)
Electrolyte: 5M KOH; Fuel: Hydrogen Gas; Temperature: Room Temperature

Test No.	Electrode Preparation	Current Density ma/cm² 0	8	16	32	80	160	240	320	400	Remarks
1*	1 hr in air at 600°C	0.00	0.30	0.40	0.47	0.58	0.65	0.70	0.73	-	
2	1 hr in air at 600°C Rh plating on elect. side	0.00	-	0.11	0.19	-	-	-	-	-	Max. Current Density 55 ma/cm² at 0.29 v vs HE
3a	1 hr in air at 600°C Rh plating on elect. side 1 hr in air at 650°C	0.03	0.11	0.12	0.16	0.29	0.41	0.49	0.54	0.63	
3b	(duplicate runs)	0.00	0.01	0.11	0.15	0.26	0.37	0.44	0.49	0.58	Electrolysis continued at 400 ma/cm². Best potential of 0.48 volt attained as temperature gradually increased. Current diminished to almost zero overnight.
4	1 hr in air at 600°C Rh plating on fuel side 1 hr in air at 650°C	0.00	0.31	0.39	0.48	0.59	-	-	-	-	Limiting current density, 120 ma/cm², reached at 0.64 volt
5	1 hr in air at 600°C Rh plating on both sides 1 hr in air at 650°C	0.00	0.11	0.12	0.16	0.30	0.42	0.49	0.55	0.63	Electrolysis continued at 400 ma/cm². Max. potential was 0.57 volt. Current started to drop after 10 hours.
6*	3 hr in H_2 at 600°C	0.11	-	-	-	-	-	-	-	-	No current was drawn until the potential reached that of oxygen evolution.
7*	1 hr in air at 600°C 3 hr in H_2 at 600°C	0.08	0.58	-	-	-	-	-	-	-	Max. current density 14 ma/cm², reached at 0.72 volt.
8	1 hr in air at 600°C 3 hr in H_2 at 600°C Rh plating on electrolyte side	0.05	0.25	0.50	-	-	-	-	-	-	Max. current density 19 ma/cm², reached at 0.62 volt.
9	1 hr in air at 600°C 3 hr in H_2 at 600°C Rh plating on electrolyte side 1 hr in air at 650°C	0.08	0.34	0.40	0.46	0.55	0.61	0.65	0.70	-	Limiting current density 330 ma/cm² at 0.70 volt.

* Results are also shown in Table A-10.

2. Effect of Oxidizing after Rhodium Plating

Good current density relations (0.38 v polarization at 100 ma/cm^2) were obtained by polarizing foils that had been rhodium plated and then oxidized at 650°C (Test 3a and 3b). By this heating, some alloy formation at boundaries by diffusion as well as oxidation was expected. Much better results were obtained than those for the control electrode (Test 1) which was oxidized only without plating. Duplicate experiments, a and b for Test 3, were in good agreement.

Palladium oxide, then, is an effective catalyst for the oxidation of hydrogen from the molecular to the ionic state, resulting in improvement of overall utilization of hydrogen fuel. The addition of rhodium improves the catalytic action of palladium oxide. Mechanisms involved in the effect of rhodium plating are assumed as follows:

Rhodium is oxidized in air at 650°C to form Rh_2O_3 and RhO.

The addition of Rh_2O_3 to PdO increases the concentration of cation vacancies and decreases the ratio of the concentration of electron deficits to the concentration of cation vacancies according to the following equation:

$$Rh_2O_3 = 2Rh^{+++}(Pd) + 3\square Pd^{++} + 3PdO \qquad (4)$$

where $Rh^{+++}(Pd)$ denotes Rh^{+++} ions on Pd^{++} vacant sites. The increase in the concentration of cation vacancies would then benefit the electrode performance.

3. Effect of Location of Rhodium Plating

Rhodium plating was effective only at the electrolyte surface and was ineffective at the gas surface, as is shown by a comparison of Tests 3 and 4 (Table A-11). Electrode 3, plated on the electrolyte side only, had excellent anodic polarization characteristics, while electrode 4, plated on the gas side only, polarized severely at low current densities. A Pd-25%Ag foil, plated with rhodium on both sides, showed the same good anodic behavior as foils plated on the electrolyte side only (Test 5).

4. Effect of Heat Treatment in Hydrogen Atmosphere

Rhodium plating on the electrode pretreated in hydrogen (Test 8) showed some improvement over one without rhodium plating (Test 7). When this electrode was further oxidized in air at 650°C (Test 9), the anodic properties of the electrode were greatly improved, compared with Tests 6, 7 and 8, but the polarization curve was not as good as that of Tests 3 and 5 without high temperature hydrogen treatment.

5. Duration of Palladium-Silver Electrode Activation

The rhodium-plated Pd-25%Ag foils of the type used in Tests 3 and 5 were polarized for 10 hours at constant potential before current failure occurred. The reduction of palladium oxide by hydrogen at room temperature, which is thermodynamically favorable, is probably the cause of the electrode degradation.

D. EFFECT OF ALLOYING ELEMENTS

Since rhodium plating showed such a significantly favorable effect on anode activity of Pd-25%Ag electrodes, the effect of other alloy elements and of the oxides of these elements on the performance of the diffusion electrodes was further studied. Metallographic examination and electron microprobe analyses on the cross sections of these foils were made to determine the structure of the electrodes, particularly of the diffusion layer between the plating and the substrate. Results of those examinations will be discussed later in a separate section.

1. Constitution of Alloys

Elements selected for alloying with Pd-25%Ag foil were classified into the following categories:

a. Valencies of the Most Stable Metal Ions

High valency metals	Fe, Ir, Ru, Th, Ti, Zr, Rh
Low valency metals	Ag, Cu, Li
Bivalency metals	Co, Mg, Ni, Pt
Alloys	Zr-Ni, Ni-Cr

b. Types of Oxides Formed by These Metals

n-type semiconductor	Fe(Fe_2O_3), Mg(MgO), Th(ThO_2), Ti(TiO_2), Zr(ZrO_2)
p-type semiconductor	Ag(Ag_2O), Co(CoO), Cu(Cu_2O), Fe(FeO), Ni(NiO), Rh(RhO, Rh_2O_3), Pt(PtO, PtO_2)
Amphoteric type semiconductors	Ir(IrO_2), Ru(RuO_2), Ti(TiO, Ti_2O_3)

c. Thermal Characteristics of Hydrogen Occlusion

Exothermic	Th, Ti, Zr (Ir, Rh)*
Endothermic	Ag, Co, Cu, Fe, Ni, Pt

* Uncertain about thermal characteristics and practically are not hydrogen occluders.

2. Phase Diagrams of Alloying Metals with Palladium

Ag, Cu, Ni, Fe, Co, Pt, Ir, and Rh, with Pd: A continuous series of solid solutions is formed (Ir-Pd has not yet been studied; however, they likely make an unbroken series of solid solutions since both have face centered cubic structure and very similar lattice parameters). Cu and Fe have ordered structures at lower temperatures in some concentration ranges.

Pd-Li, Pd-Th: Not known

Pd-Mg: The c/a ratio of the Mg hexagonal lattice is slightly decreased by adding Pd because of an increment of the a parameter of Mg, although the atomic radius of Pd is smaller than that of Mg.

Pd-Sn: Several intermetallic compounds, including a partially filled As-Ni structure at around 40 atomic-% Sn. The solid solubility of Sn in Pd (α phase) was estimated to be about 9.5 atomic-% Sn.

Pd-Ru: Cannot form a continuous series of solid solutions because of different lattice structure. Otherwise, not well known.

Pd-Al: Not very well investigated. However, three intermetallic compounds are known. There is almost no solubility of Pd in the Al-rich range, and Pd forms a solid solution at about 25 atomic-% Pd.

Pd-Ti: Form several intermediate phases.

Pd-Zr: Preliminary experiments showed that the lattice of Pd is expanded by Zr.

3. Preparation of Alloy Foils

Since we are primarily interested in the surface composition of the Pd-25%Ag foil, alloying elements were diffused into the surface after application of the alloying metal by electroplating, vacuum evaporation, or compound decomposition techniques.

Three electrodes were prepared for each alloying element. One electrode was plated on both surfaces, and the other two were plated on only one side. The alloying of all elements, except lithium with palladium foils, consisted of the following steps:

(a) Degreasing with trichloroethylene and acetone.

(b) Chemical cleaning with warm chromic acid cleaning solution.

(c) Plating of alloying metal by electrolysis or by vacuum evaporation.

(d) Diffusing into the palladium surface by heating for two hours at 850°C in an argon atmosphere.

(e) Oxidizing in air for two hours at 650°C.

Plating conditions for metal deposition are summarized in Table A-12. The plating time was sufficient to deposit approximately 5 mg/cm^2 of metal in each case, so that if all metal diffused into the surface, the foil contained approximately 10% of the metal.

Lithium was deposited as lithium oxide by heating the foil in argon for two hours at 850°C, then in air for one hour at 700°C. The foil was then dipped into saturated lithium carbonate solution, dried in air, and heated in air for ten minutes at 700°C. The treatment with lithium carbonate solution was repeated three times.

Other metals, magnesium, titanium, zirconium, thorium, zirconium-nickel, and nickel-chromium, are being deposited on palladium foil by vacuum evaporation*. Because of the nature of the evaporation method, the amount of these metals and alloys was very small. After four to ten cycles of metal evaporation, the weight increase of the foil was 0.01 to 0.1 mg/cm^2.

4. Anodic Polarization Characteristics of Alloyed Palladium-Silver Electrodes

Polarization measurements were made by the same procedure described in Section C.2. Hydrogen gas was the fuel and 5M KOH the electrolyte.

a. Plating on Both Sides of the Electrode

Current density-potential data for electrodes alloyed on both sides determined potentiostatically at 25, 60, and 90°C are given in Table A-13. Elements in Table A-13 are arranged as follows:

From No. 1 to No. 3: The foil was alloyed almost uniformly across the thickness.

No. 4 and No. 5: Not uniform alloying across the thickness, but sufficiently deep diffusion layer and considerable amount of alloying element near the surface of the foil.

From No. 6 to No. 9: Large amounts of the alloying element were deposited, but a deep diffusion layer was not formed.

---

* Model JEE-4V Vacuum Evaporator, Japan Electron-optics Laboratory, Tokyo, Japan.

Table A-12

CONDITIONS FOR ELECTRO-PLATING PALLADIUM-SILVER ELECTRODES

Metal	Solution	Approximate pH	Current Density ma/cm^2	Temperature
Ag	$AgNO_3$: 40 g/ℓ HNO_3: 4 g/ℓ, $NaNO_3$: 75 g/ℓ		15	40°C
Cu	$CuSO_4.5H_2O$: 80 g/ℓ H_2SO_4: 150 g/ℓ		90	R.T.+
Ni	$NiCl_2$: 13 g/ℓ, NH_4Cl: 20 g/ℓ, NaCl: 10 g/ℓ	6.0	45	R.T.
Fe	$FeCl_2.4H_2O$: 24 g/ℓ KCl: 180 g/ℓ	5.5	25	R.T.
Co	$Co(NH_4)_2.(SO_4)_2.6H_2O$: 175 g/ℓ, As_2O_3: 0.1 mg/ℓ	5.5	50	R.T.
Su	$SnCl_2.2H_2O$: 3 g/ℓ NaOH: 100 g/ℓ		50	R.T.
Pt	H_2PtCl_6: 25 g/ℓ $Pb(C_2H_3O_2)_2$: 0.3 g/ℓ	1 (HCl)	30	R.T.
Ir*	H_2IrCl_6: 4.1 g/ℓ	1 (HCl)	50	R.T.
Rh	$RhCl_3$: 2.1 g/ℓ	1 (HCl)	300	R.T.
Ru	$RuCl_3$: 2.1 g/ℓ	1 (HCl)	300	R.T.

*Before electroplating, the Pd-25% Ag foil was treated to obtain an adherent Ir black plating. The foil was dipped into saturated iridium chloride solution and heated in a gas flame to yellow heat. This treatment was repeated three times. + RT = Room Temperature

Table A-13

ANODIC CURRENT DENSITIES, ma/cm^2, FOR Pd-25% Ag ELECTRODES WITH DIFFUSED ALLOYING ELEMENTS

Electrode: 0.001-in. Pd-25%Ag foil diffused with an alloying element on both sides.
Electrolyte: 5M KOH
Fuel: H_2 gas

Metal	Temp °C	OCP* v	Overpotential (η) vs HE** 0.1	0.2	0.3	0.4	0.5
Fe	25	0.09	0.1	0.25	0.6	1.3	2.6
	60	0.03	0.25	0.95	2.4	4.6	8.8
	90	0.03	0.4	1.3	3.2	5.8	10.0
Cu	25	0.74	None				
	60	0.74	None				
	90	0.68	None				
Ag	25	0.24	-	≈0.3	0.8	1.7	2.5
	60	0.13	-	4.5	6.2	7.4	8.2
	90	0.16	-	8.0	11.0	13.0	14.5
Co	25	0.00	1.1	9.5	27.5	52	72
	60	0.00	1.5	8.0	23.0	40	58
	90	0.00	6.6	19.0	26.0	51	70
Ni	25	0.06	<1.0	<1.0	1.5	4.0	9.0
	60	0.09	-	0.9	2.6	6.8	15.0
	90	0.04	-	2.0	6.5	14.0	32.0
Ru (a)	25	0.06	-	0.8	1.6	3.1	5.0
	60	0.04	-	1.3	2.6	4.0	5.6
	90	0.12	0.8	1.3	2.3	3.6	5.5
Ru (b)	25	0.00	0.4	1.8	5.6	10.0	16.5
Rh	25	0.00	10	24	40	63	100
	60	0.00	22	52	90	140	225
	90	0.00	40	100	180	330	(400 at η=0.43v)
Ir	25	0.00	18	50	93	145	200
	60	0.03	13	40	80	120	170
	90	0.03	20	50	93	130	200

Table A-13 (Continued)

ANODIC CURRENT DENSITIES, ma/cm^2, FOR Pd-25%Ag ELECTRODES WITH DIFFUSED ALLOYING ELEMENTS

Metal	Temp °C	OCP* v	Overpotential (η) vs HE** 0.1	0.2	0.3	0.4	0.5
Pt	25	0.00	42	96	170	210	250
	60	0.00	90	160	270	340	370
	90	0.00	140	370	(400 at η=0.23v)		
Mg	25	0.00	1.4	5.0	9.8	15.0	21.5
	60	0.00	0.8	1.6	-	-	-
	90	-	-	-	-	-	-
Ti	25	0.01	4	14	42	82	155
	60	0.01	7	22	49	102	205
	90	0.02	15	52	100	195	350
Zr	25	0.02	0.45	4.8	8.4	13.5	26
	60	0.00	2.7	16.5	21.0	26.5	46
	90	0.02	11.2	26.5	28.5	40	90
Th	25	0.00	1.5	7.6	23	61	140
	60	0.00	1.8	12.5	44	78	170
	90	0.00	8.2	43	88	135	250
Zr-Ni	25	0.05	1.65	5.1	15	45	120
	60	0.02	2.9	14	42	120	235
	90	0.02	8	31	60	120	270
Ni-Cr (80-20)	25	0.03	-	0.12	0.28	0.55	1.1
	60	0.03	0.13	0.54	1.18	1.6	2.4
	90	0.03	0.52	1.7	3.1	3.7	5.1
None	25	0.02	1.3	3.2	8.0	16.0	40.0
	60	0.02	1.0	4.0	9.4	19.0	49.0
	90	0.02	3.8	14.5	23.5	44.0	115.0

* Open Circuit Potential vs HE.

** Hydrogen electrode potential in the same electrolyte and at the same temperature.

From No. 10 to No. 13: Smaller amounts of alloying element were deposited by vacuum evaporation.

No. 14 and 15: Alloy deposition by vacuum evaporation.

Within each group above, the elements were arranged according to the periodicity of elements.

b. Plating on One Side of the Electrode

Anode current density of the foils plated on one side at the overpotential of 0.5 v vs HE are given in Table A-14.

A kind of oversaturation during continuous polarization of some electrodes was noted at higher temperatures following low temperature polarization. This phenomenon was more significant for those electrodes that showed better performance at room temperature. Such electrodes carried very high current densities at elevated temperatures, and, as the current density was further increased, the current dropped significantly and then increased again as the polarization increased. This phenomenon was more noticeable for electrodes that were plated on their fuel sides. A typical curve for an electrode that was plated with rhodium on the fuel side is shown in Figure A-34. One of the electrodes showing oversaturation was immediately polarized downward (from high to low current) after the upward polarization curve was recorded. The continuous downward curve is shown as curve D in Figure A-34. The oversaturation was perhaps due to a slow recovery of a severe concentration gradient of hydrogen caused by high current polarization at lower temperature. Before attaining equilibrium with hydrogen at the higher temperature, the electrode could carry higher current densities than those under the equilibrium.

5. Discussion

Our original plan for this study was to alloy Pd-25%Ag with metals that could be plated on the surface of the foil and heated to promote alloy formation by diffusion. These electrodes would then be used to determine the effect of alloying with a third component upon the polarization characteristics of the electrode when used as a hydrogen anode. Some elements, such as silver, copper, iron, cobalt, and nickel, diffused rapidly enough into the Pd-25%Ag foil to form a definite alloy layer, although some of the unalloyed element was left on the surface of the electrodes. Such elements as platinum, ruthenium, and rhodium, however, diffused so slowly that a comparatively thin diffusion layer was formed on the foil, and the majority of the elements remained on the foil surface. A considerable amount of palladium actually diffused into the deposited layer. Other groups of elements, magnesium, titanium, zirconium, and thorium, were deposited in small quantities on the surface of the foil, but they were oxidized by traces of oxygen in

Table A-14

EFFECT OF ALLOYING ON ONE SIDE OF THE
Pd-25% Ag DIFFUSION ELECTRODE

(Anodic current densities ma/cm^2 at 0.5 volt vs HE)

Electrode: 0.001-in. Pd-25% Ag foil alloyed
Electrolyte: 5M KOH
Fuel: H_2 gas
Temp: 25°C

Metal	Plating	
	Fuel Side	Electrolyte Side
None	40.0	40.0
Fe	11.0	65.0
Cu	2.6	0.1
Ag	3.9	3.3
Co	140.0	8.0
Ni	110.0	34.0
Ru	110.0	44.0
Rh	25.0	>400.0
Ir	180.0	240.0
Pt	210.0	38.0
Mg	110.0	66.0
Ti	80.0	125.0
Zr	36.0	43.0
Th	115.0	155.0
Ni-Zr	27.0	170.0
Ni-Cr	17.0	3.3

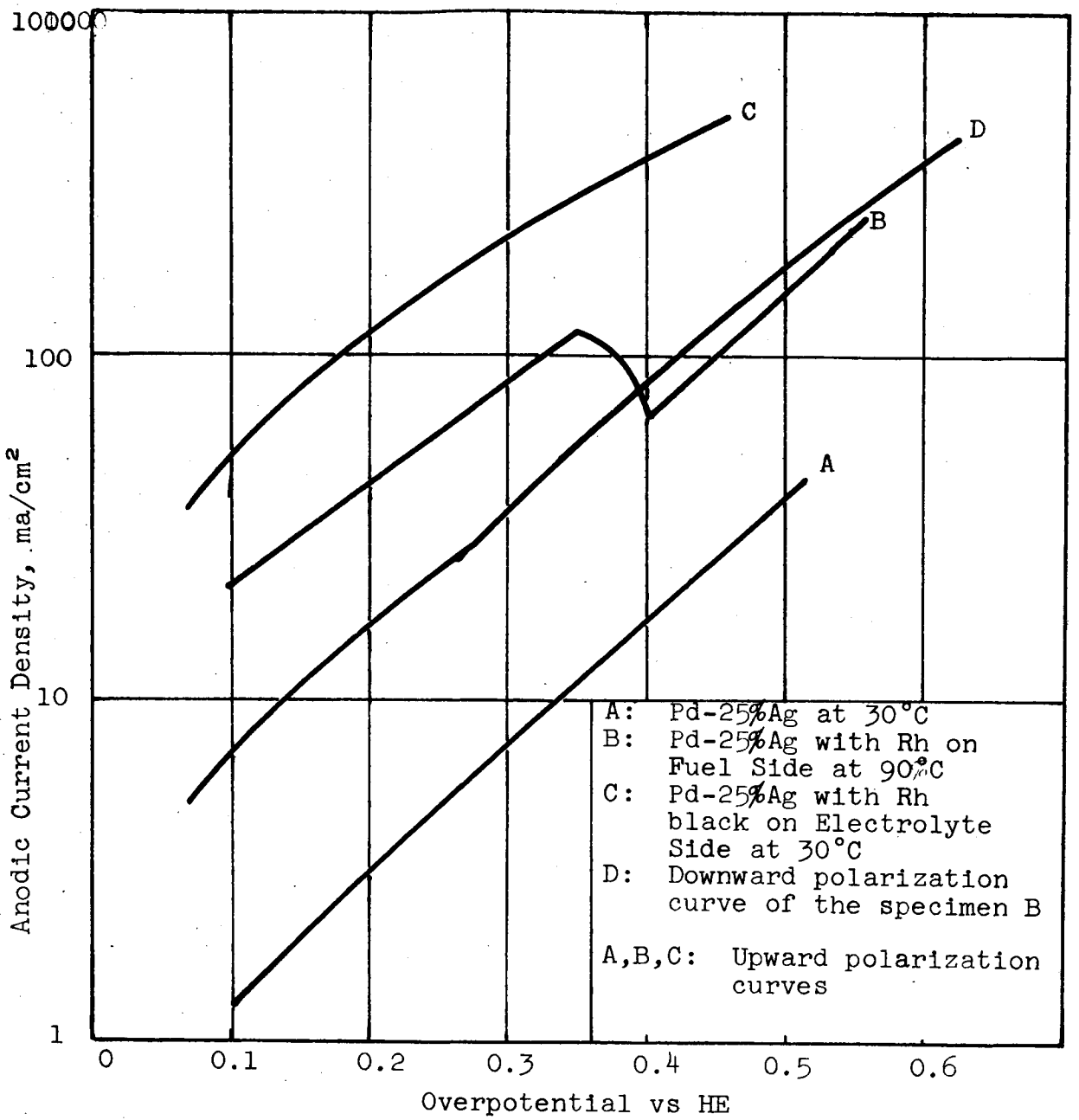

Figure A-34. Effect of Alloying Pd-25%Ag Electrode With Rh on Anodic Polarization

argon before sufficient diffusion occurred since these elements were good oxygen getters. With the above considerations in mind, certain generalizations regarding the effect of added elements on polarization behavior of the Pd-25%Ag system can be made:

(a) Alloying with low valency metals (silver and copper) is unfavorable to anodic polarization characteristics.

(b) Improvement of polarization characteristics is obtained by alloying with high valency metals (iridium, ruthenium, platinum, titanium, and rhodium).

(c) Alloying of exothermic hydrogen occluders improved the electrode performance.

(d) An increase in temperature decreased polarization.

(e) The effect of alloying on the fuel side is independent of the effect on the electrolyte side.

(f) Alloying on the fuel side of the electrode does not significantly change the slope of the straight portion of the polarization curve of the Pd-25%Ag foil with no plating, and curves are approximately parallel. Alloying on the electrolyte side changed both slope and height of the polarization curves of Pd-25%Ag electrode, as shown in Figure A-34.

(g) Some of the best elements to improve the anodic polarization of the Pd-25%Ag diffusion electrode were:

Fuel side:	platinum, iridium, and cobalt
Electrolyte side:	rhodium, iridium, and nickel-zirconium
Both sides together:	platinum, rhodium, and iridium

E. EFFECT OF MIXED OXIDES ON SURFACE CATALYSIS

1. Background

The original plan for Pd-25%Ag electrode catalytic treatment was to test the effect on electrode performance of adding a third metal to the palladium oxide layer, according to the concepts that cation vacancy sites in the palladium oxide layer act catalytically, and a change of concentration of vacancies caused by the presence of a foreign metal should affect the electrode performance. However, since the amount of palladium oxide is so small, it is almost impossible to control the amount of added element to the palladium oxide surface. Consequently, an improved technique would be to plate much more of the added metal than the final amount of palladium oxide surface coating. The plated surface would then be heated to form mixed oxides of palladium and the added metal, without appreciable diffusion of the metal into the Pd-25%Ag foil. The oxides selected for the tests were of those elements that were studied in the previous section.

2. Electrode Preparation

Pd-25%Ag foil was annealed in an argon atmosphere for two hours at 850°C and then oxidized in air for two hours at 700°C. A third metal was then deposited, either by electroplating or by vacuum deposition. Finally, the foil was again oxidized in air for two hours at 700°C. It was hoped that the last temperature for the final oxidation was not high enough to allow substantial diffusion of the deposited metal into the foil, since the palladium oxide layer formed in the first oxidation before plating could act as a diffusion barrier.

The exact condition of the surface was determined by metallographic and microprobe analyses. The amount of metal deposited was approximately 0.1 mg/cm^2 by electroplating and 0.01 mg/cm^2 by vacuum evaporation.

3. Polarization Characteristics

Table A-15 gives anodic polarization characteristics of the electrodes plated on both sides with third metals and oxidized, together with data on a control electrode with no plating. Elements in Table A-15 were arranged according to their chemical periodicity. Elements that belong to the same periodic group were arranged according to their molecular weights.

Table A-16 gives anodic polarization characteristics of the electrodes plated either on the fuel side or on the electrolyte side alone in terms of current density at an overpotential 0.5 v vs HE at 30°C.

During this series of tests, the oversaturation phenomenon discussed in the previous section was observed on anodic polarization curves of almost all electrodes except the electrodes coated with magnesium. The phenomenon was particularly significant on the electrodes coated on the fuel side.

4. Discussion

Data for the effect of mixed oxides as surface catalysts were more consistent than those for the alloyed electrodes. The reason is perhaps that approximately the same amount of metal was on the electrode surface regardless of whether metals were oxidized or not, since no diffusion took place during the heat treatment. However, the surface concentration of these metal oxides varied because of different rates of oxidation of some metals. Those elements that were electroplated might be present in too great concentrations on the surfaces, since it is believed that a catalyst coating should be very thin. An excess of oxide inhibits good polarization characteristics because of poor electrical conductance and possibly slow diffusion of hydrogen through the oxide layer.

Table A-15

ANODIC CURRENT DENSITIES, ma/cm², FOR Pd-25%Ag ELECTRODES COATED WITH OTHER METAL OXIDES

Electrode: 0.001-in. Pd-25%Ag foil with another metal oxide on both sides.
Electrolyte: 5M KOH
Fuel: H_2 gas

Metal	Temp °C	OCP* v	Overpotential (η) vs HE** 0.1	0.2	0.3	0.4	0.5
Li	25	0.64	none	-	-	-	-
	60	0.03	3.1	11.5	30	54	57
	90	0.01	10.0	29.0	60	60	60
Mg	30	0.00	1.9	6.0	12.0	19.5	28
	60	0.00	3.3	11.2	17.0	27.0	37
	90	0.00	5.7	14.5	24.5	37.5	48
Ti	30	0.00	0.9	5.7	18.5	32	57
	60	0.00	10	32	36.5	34	56
	90	0.00	34	82	68	60	42
Zr	30	0.03	0.46	2.8	9.3	25	58
	60	0.03	4	10	16	18.5	60
	90	0.03	13	32.5	34	47	105
Th	30	0.00	0.9	5.6	16	29	50
	60	0.00	2.0	5.0	11.0	18.0	40
	90	0.00	2.4	7.6	13.5	18.5	29
Co	30	0.06	2.0	18.5	37	62	83
	60	0.06	1.7	10.5	30	48	67
	90	0.06	3.3	24	38	62	86
Ni	30	0.00	4.2	17	54	210	(400 at η=0.45v)
	60	0.00	8.4	40	160	(400 at η=0.38v)	
	90	0.03	17	82	260	(400 at η=0.33v)	
Ru	30	0.00	11.5	38	94	195	380
	60	0.00	16.5	60	125	280	(400 at η=0.46v)
	90	0.00	42	155	390	(400 at η=0.31v)	

Table A-15 (Continued)

ANODIC CURRENT DENSITIES, ma/cm^2, FOR Pd-25%Ag ELECTRODES COATED WITH OTHER METAL OXIDES

Metal	Temp °C	OCP* v	Overpotential (η) vs HE** 0.1	0.2	0.3	0.4	0.5
Rh	30	0.00	38	83	155	210	300
	60	0.00	74	130	195	260	360
	90	0.00			(400 at η=0.08 v)		
Pt	30	0.02	22	68	200	(400 at η=0.37v)	
	60	0.03	26	100	300	(400 at η=0.37v)	
	90	0.03	43	140	310	(400 at η=0.33v)	
Cu	30	0.24	-	-	2.3	4.3	10.5
	60	0.11	-	-	3.7	9.0	18.5
	90	0.17	0.9	2.6	7.8	12.5	19.0
Zr-Ni	30	0.00	1.3	7.7	24	56	100
	60	0.00	2.0	10	28	64	115
	90	0.03	11	40	83	130	220
Ni-Cr	30	0.06	0.13	0.63	1.8	3.8	8.0
	60	0.06	0.9	2.4	4.0	5.5	10.0
	90	0.06	7.6	15.5	11.0	12.0	22.5
None	25	0.02	1.3	3.2	8.0	16.0	40.0
	30	0.02	0.5	2.8	8.4	19.0	42.0
	60	0.02	1.1	4.0	9.4	19.0	49.0
	90	0.02	3.8	14.5	23.5	44.0	115.0

* Open Circuit Potential

** Hydrogen electrode potential in the same solution and at the same temperature.

Table A-16

EFFECT OF FOREIGN METAL OXIDE ON ONE SIDE
OF PD-25%Ag DIFFUSION ELECTRODE
(Anodic Current Densities ma/cm² at 0.5 Volts vs HE)

Electrode: 0.001-in. Pd-25%Ag foil covered with foreign metal oxide (or mixed with PdO)

Electrolyte: 5M KOH

Fuel: H_2 gas

Temperature: Room temperature (25°C)

Plating	Li	Mg	Ti	Zr	Th	Co	Ni	Ru	Rh	Pt	Cu	Zr-Ni	Ni-Cr
Fuel side	93	120	40	48	220	35	70	115	95	82	120	60	20
Electrolyte side	120	100	175	10	92	110	>400	140	>400	>400	6.8	13	3.2

Because of various amounts of oxides of the individual metals, the true mechanism of the catalytic activity of these metal oxides is not clearly understood. However, there are some indications of correlation of the catalytic activity with the fundamental nature of the elements, that is, the "periodicity" of the elements, as shown in Figure A-35, although this was more significantly shown on the results in the previous section (see Tables A-15 and A-16).

The following empirical observations of general effects of mixed oxides on electrode performance were made after examining the data in Tables A-15 and A-16, although there are a small number of exceptions.

(a) Elements that strongly activate the electrolyte side are the best catalysts when plated on both sides of the electrode, although they were not the best activators on the fuel side (nickel, platinum, rhodium, and ruthenium).

(b) Oxides of the p-type semiconductors were better activators than those of n-type semiconductors when the metals were plated on both sides of the electrode or on the electrolyte side only.

p-type semiconductor group: nickel, cobalt, platinum, rhodium, and ruthenium (Amphoteric RuO_2 could act as a cation vacancy type oxide).

n-type semiconductor group: magnesium, zirconium, titanium, thorium, and chromium.

(c) Some n-type semiconductor oxides improved the anodic polarization of Pd-25%Ag electrodes when they were plated on one side of the electrode, only one particular side (titanium on electrolyte side) or even both sides individually (magnesium and thorium). However, when the electrodes were plated with these metals on both sides, negative or no effects resulted.

(d) Thermal characteristics of hydrogen occlusion have no effects, since metals plated did not diffuse into the foil and stayed on the surface either as the oxides or as a powdery deposit.

(e) Some of the best oxides to improve the anodic polarization of Pd-25%Ag diffusion electrodes were:

Fuel side:	thorium, copper, ruthenium, and magnesium
Electrolyte side:	nickel, platinum, and ruthenium
Both sides together:	platinum, rhodium, ruthenium, and nickel

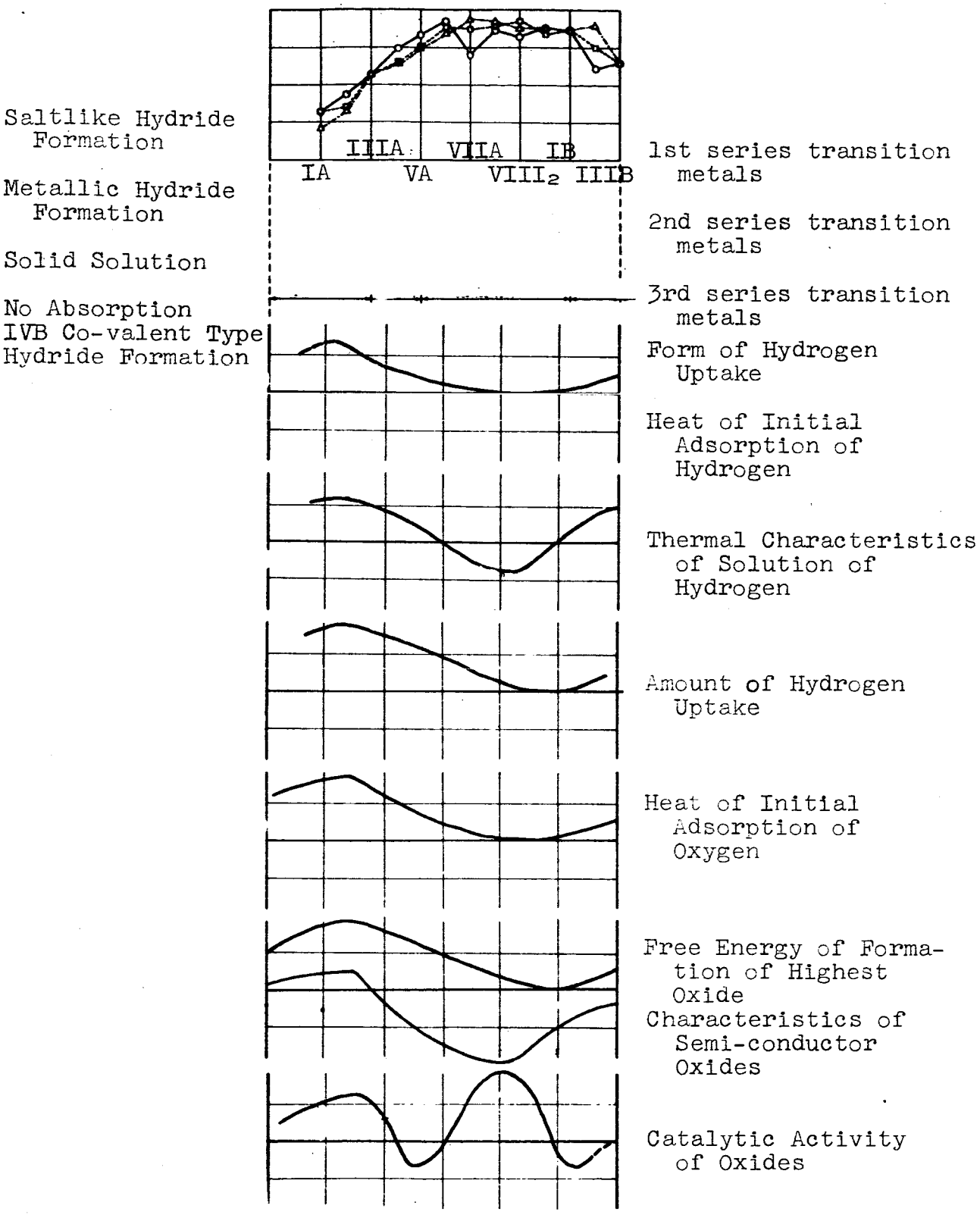

Figure A-35. Periodic Characteristics of Transition Metal Elements Related with Hydrogen Diffusion Electrodes.

F. METALLOGRAPHIC STUDIES AND DETERMINATION OF THICKNESS OF THE DIFFUSION LAYER

Metallographic examinations and electron microprobe analyses were made on cross sections of Pd-25%Ag electrodes that were plated on either one side or both sides with other elements.

One set of foils was diffusion treated in argon for 2 hours at 850°C before oxidation treatment in air for 2 hours at 700°C. The other set of foils was annealed at 850°C and then oxidized in air for 2 hours at 700°C before plating, and again oxidized in air for 2 hours at 700°C after plating. Metallographic examination and electron microprobe analyses were made after those foils were tested for anodic polarization.

1. Metallography

Metallographic examinations showed a drastic change of structure on those electrodes that were plated and diffused with rapid diffusing elements such as iron, copper, and cobalt. These materials showed finely divided intermetallic crystal structures. The foil plated and diffused with nickel also showed a significant change. On the other hand, the foils plated and diffused with slow diffusing elements showed almost the same structure as that of Pd-25%Ag. Plated silver diffused into the foil rapidly but did not significantly change the structure, since palladium and silver form a continuous series of solid solutions. The foils plated by vacuum evaporation also showed no visible change on the structure.

The foils plated and oxidized without diffusion treatment did not change the structure of the foil, indicating that metals and alloys plated were oxidized without significant diffusion.

The foil plated and diffused with rhodium showed numerous microcracks across the foil. Typical metallographic photographs are shown in Figures A-36 to A-41.

2. Electron Microprobe Analyses*

Some recording chart records of electron microprobe analyses of particular interest for characterizing alloyed and heat treated palladium foils are shown in Figures A-42 to A-49. Since the thin foils were mounted in the sample holders at various angles with the face of the holder, the cross sectional true distance of the foil is shown on the charts as a micron (μ) scale. The digit "0" at the bottom of an arrow indicating the concentration of each element indicates the ground level for each measurement. The concentration of palladium can be read downward from the top edge,

---

* Electron microprobe analyzer Model JxA-3A, Japan Electron-optics Laboratory, Tokyo, Japan.

Figure A-36. Pd-25%Ag Foil Plated on Both Sides with Rh, Diffused in Argon and Oxidized in Air. After Electrochemical Tests. x500

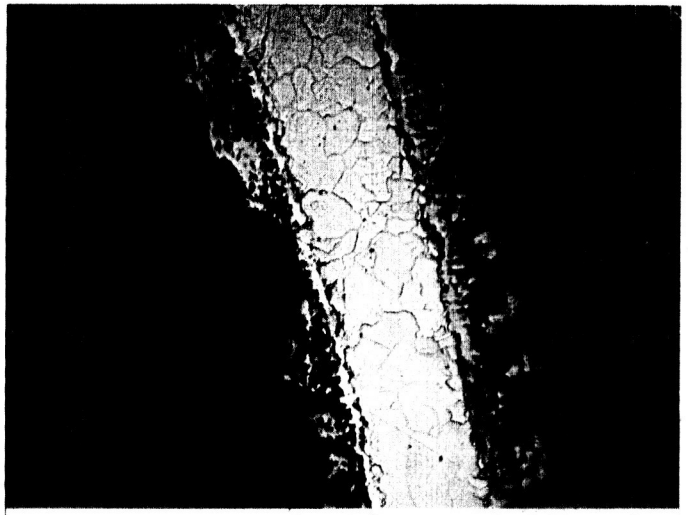

Figure A-37. Pd-25%Ag Foil Plated on Both Sides with Pt, Diffused in Argon and Oxidized in Air. After Electrochemical Tests. x500

Figure A-38. Pd-25%Ag Foil Plated on Both Sides with Ni, Diffused in Argon and Oxidized in Air. After Electrochemical Tests. x500

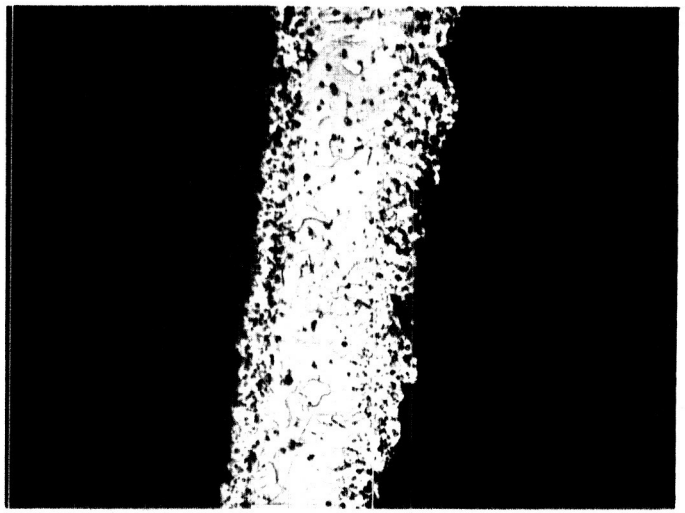

Figure A-39. Pd-25%Ag Foil Plated on Both Sides with Cu, Diffused in Argon and Oxidized in Air. After Electrochemical Tests. x500

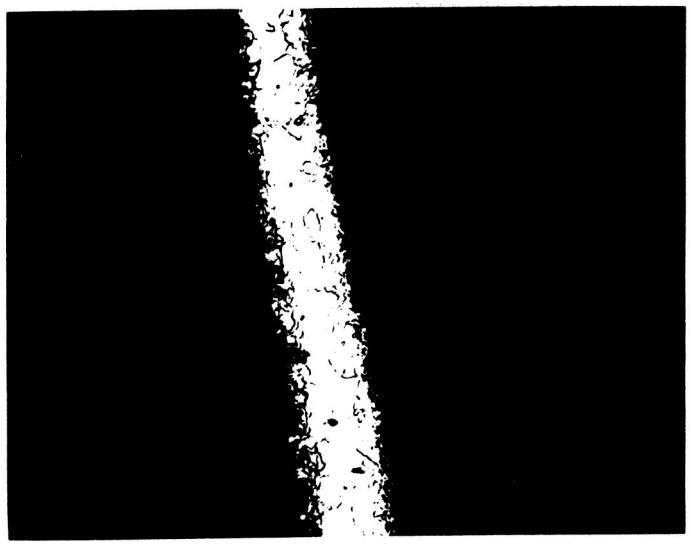

Figure A-40. Pd-25%Ag Foil Plated on Both Sides with Ag, Diffused in Argon and Oxidized in Air. After Electrochemical Tests. x500

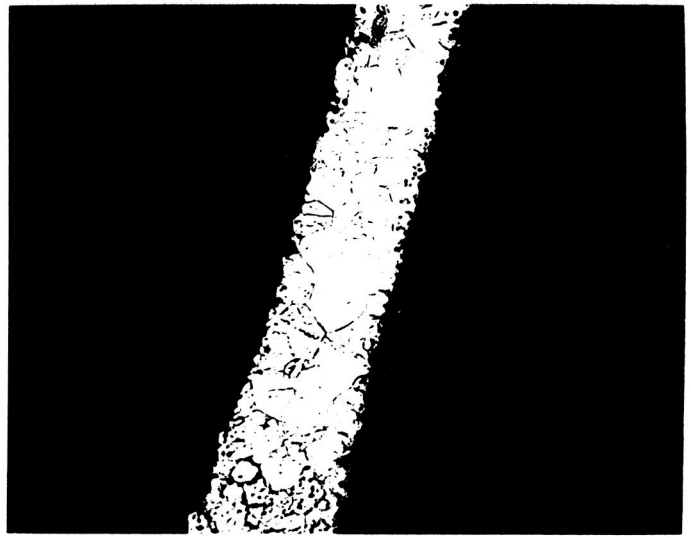

Figure A-41. Pd-25%Ag Foil Coated on Both Sides with Ir by $IrCl_3$ Decomposition, Diffused in Argon and Oxidized in Air. After Electrochemical Tests. x500

Etchant for all specimens: Mixture of 5% KCN and 5% $(NH_4)_2SO_4$ with trace of KI crystals at room temperature.

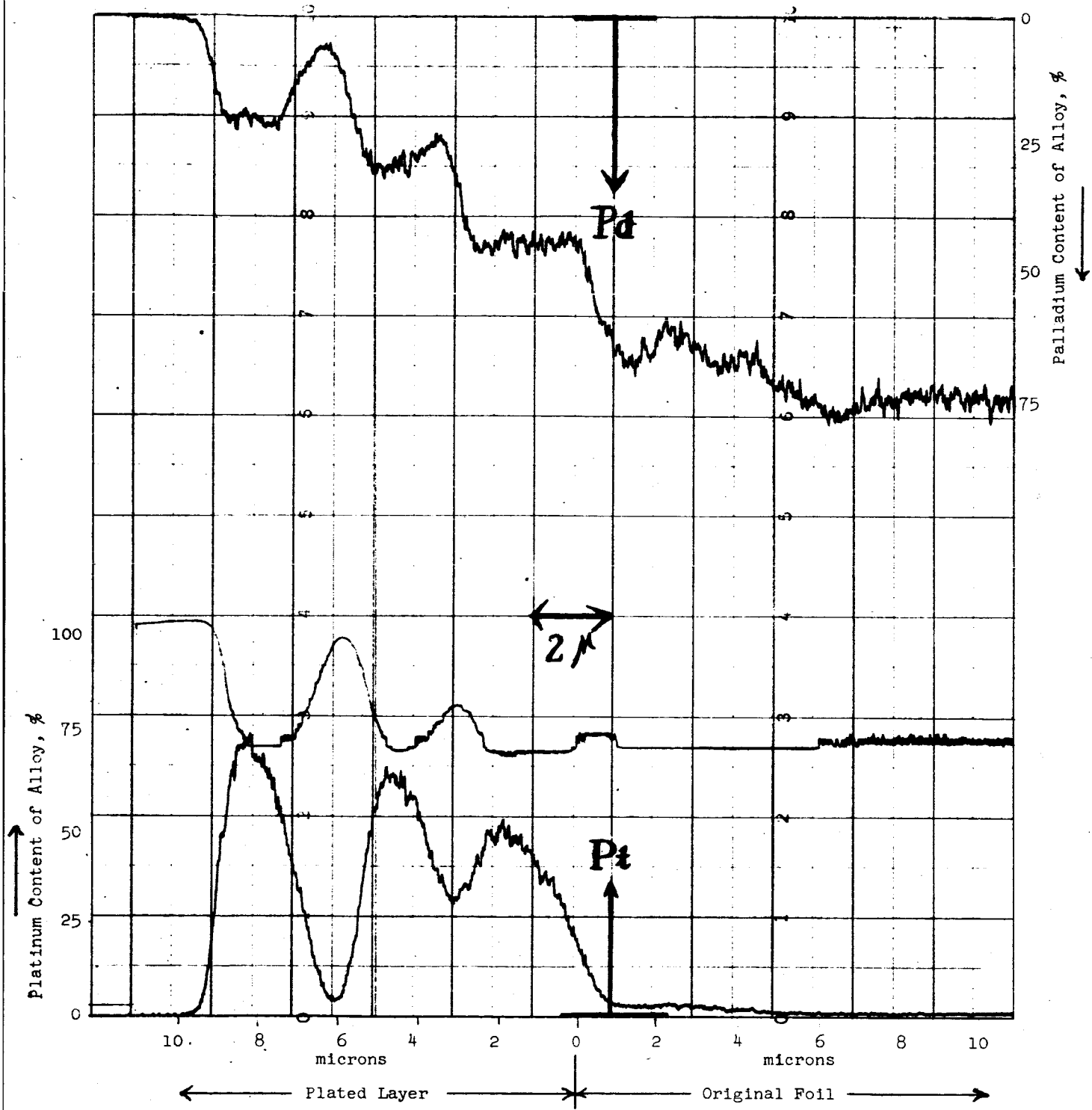

Figure A-42. Cross section of the diffusion layer of Pt into Pd-25%Ag (diffusion treatment in argon for two hours at 850°C). Maximum points on both concentrations indicate the powdery Pt deposit.

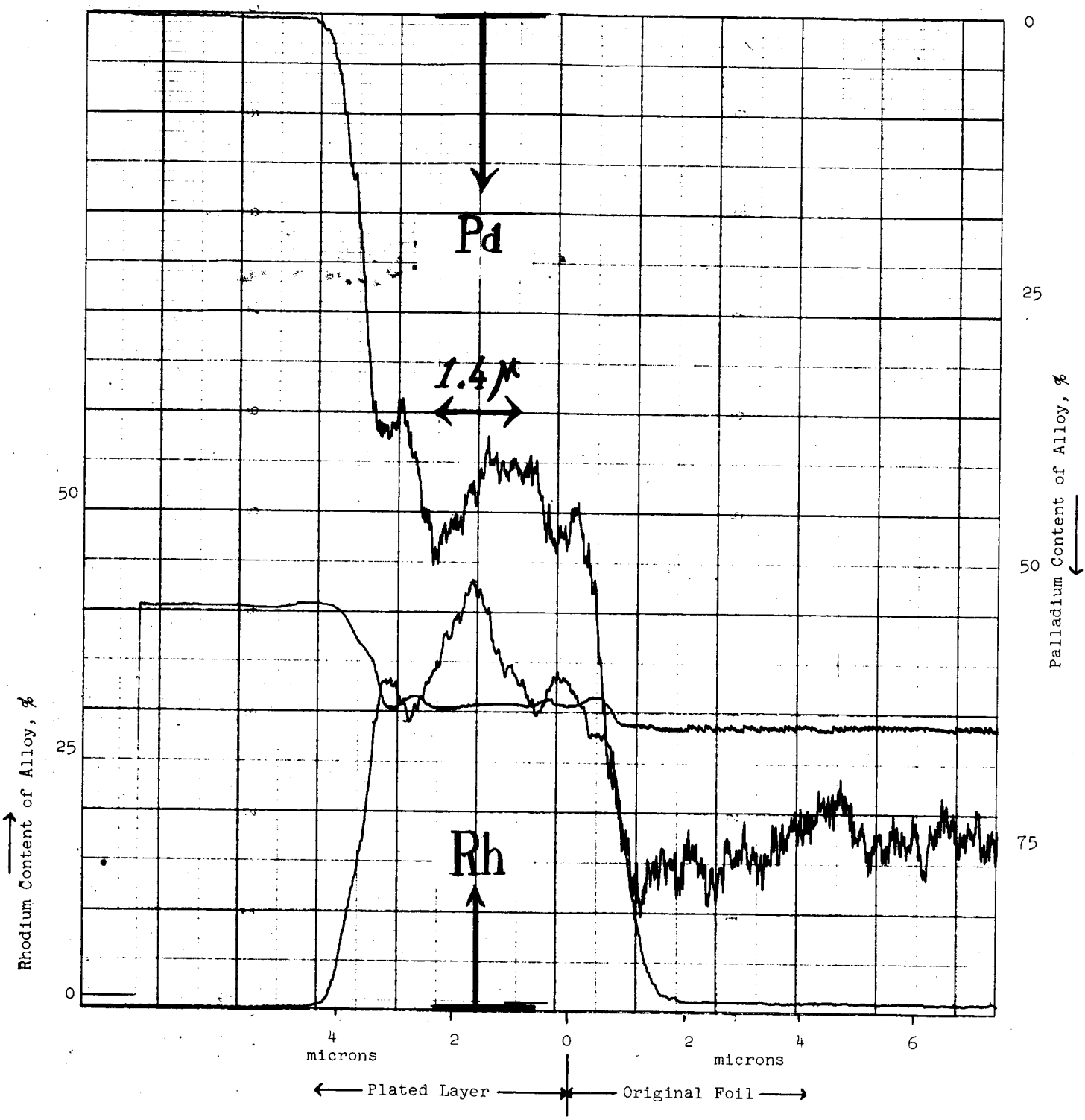

Figure A-43. Cross section of the diffusion layer of Rh into Pd-25%Ag (diffusion treatment in argon for two hours at 850°C).

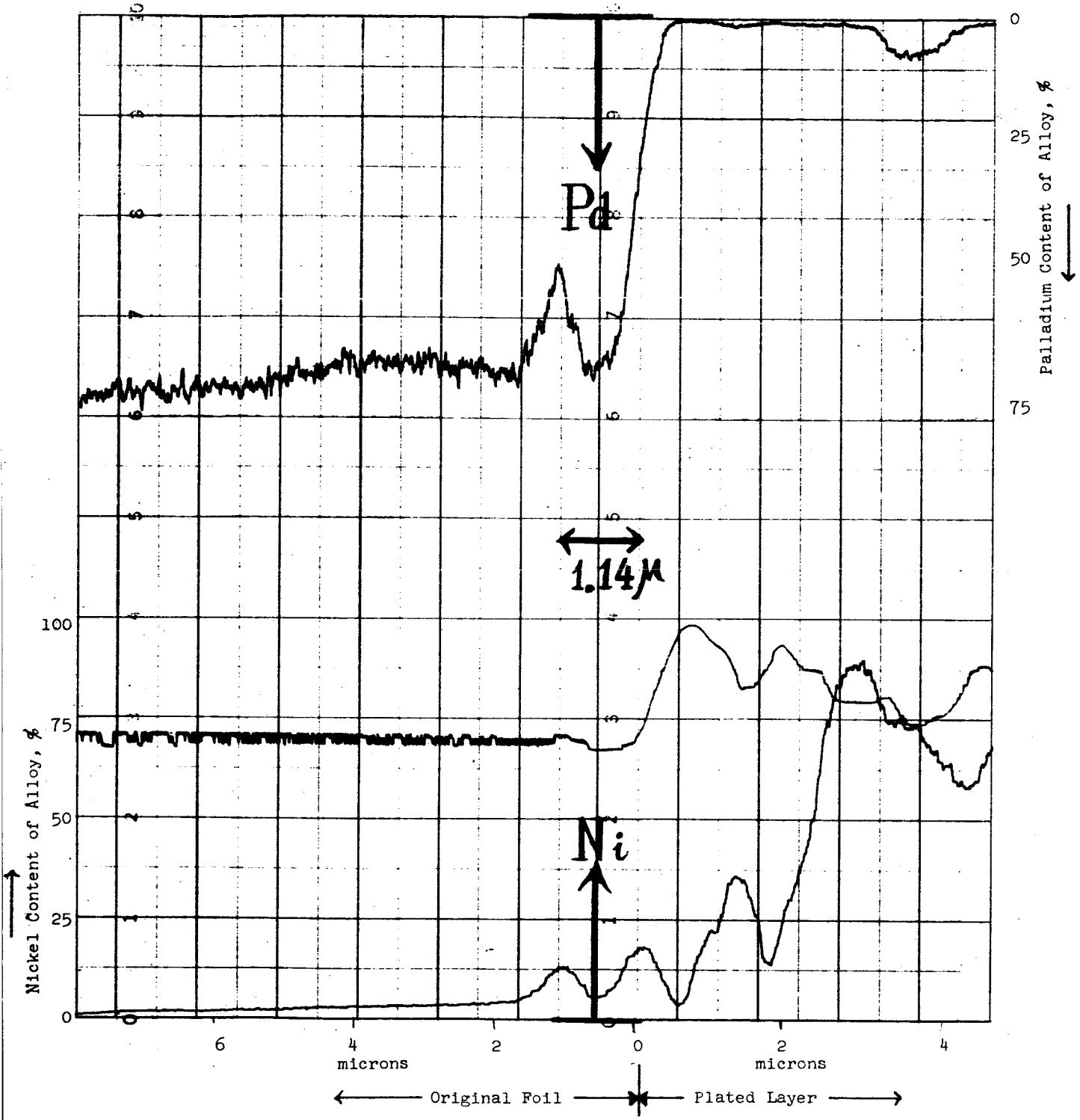

Figure A-44. Cross section of diffusion layer of Ni into Pd-25%Ag (diffusion treatment in argon for two hours at 850°C). A small valley on the Pd curve indicates a heavy diffusion of nickel at the palladium grain boundary.

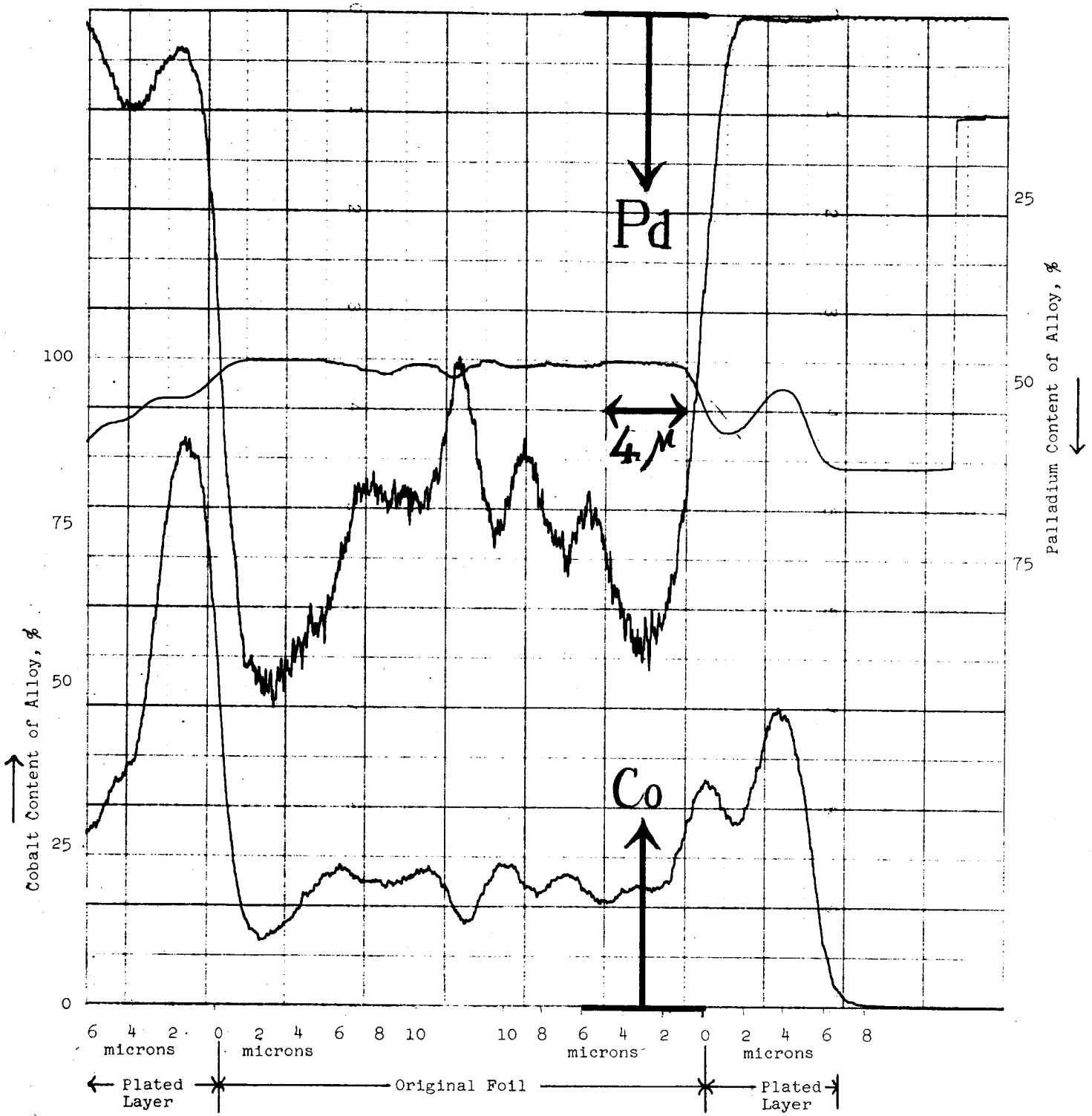

Figure A-45. Cross section of Pd-25%Ag foil alloyed with Co by diffusion treatment in argon for two hours at 850°C

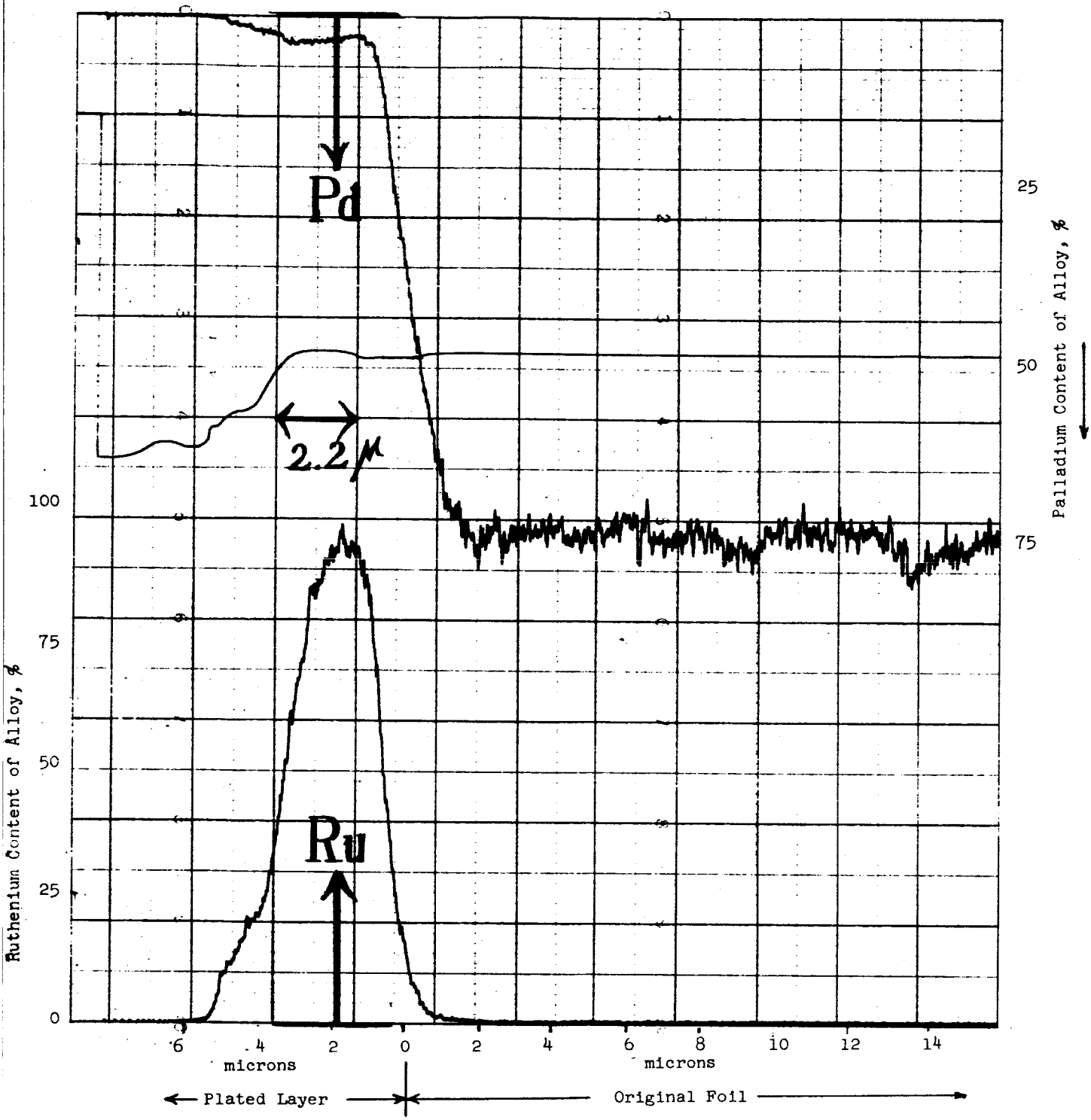

Figure A-46. Cross section of the diffusion layer between Ru and Pd-25%Ag (diffusion treatment in argon for two hours at 850°C).

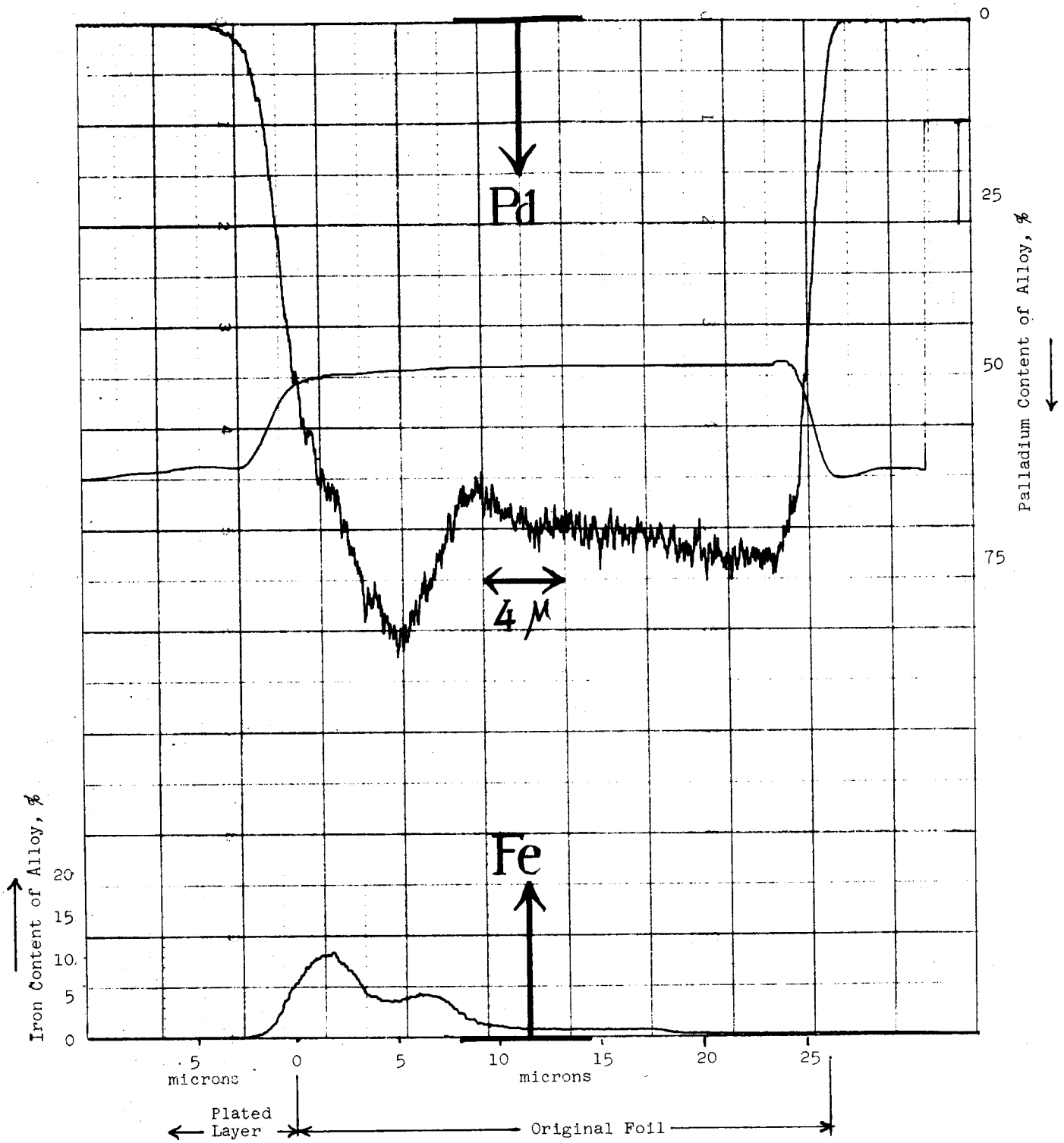

Figure A-47. Cross section of Pd-25%Ag foil diffused through with Fe plated on one side (diffusion treatment in argon for two hours at 850°C).

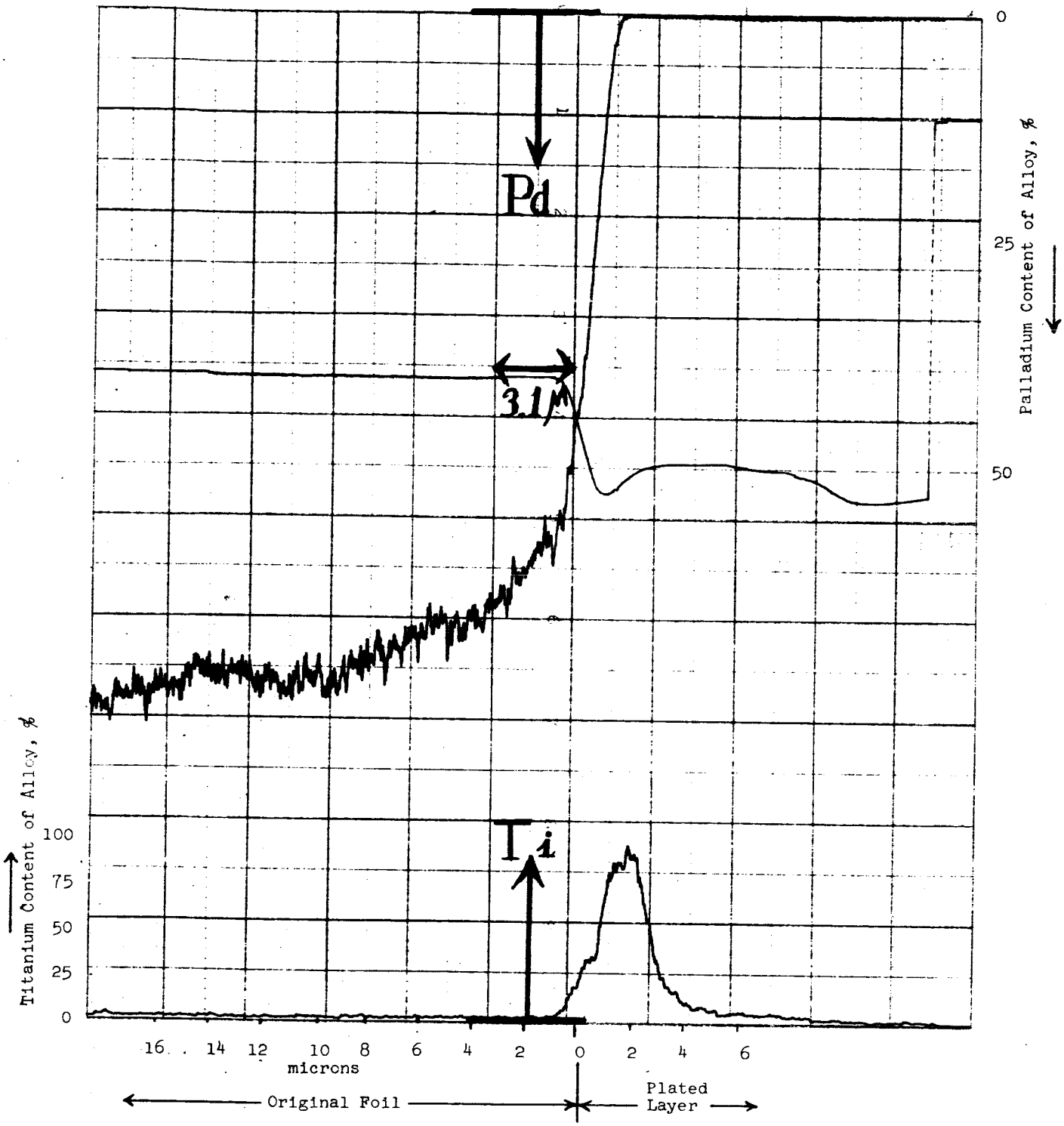

Figure A-48. Cross section of diffusion layer between Ti and Pd-25%Ag (diffusion treatment in Argon for two hours at 850°C).

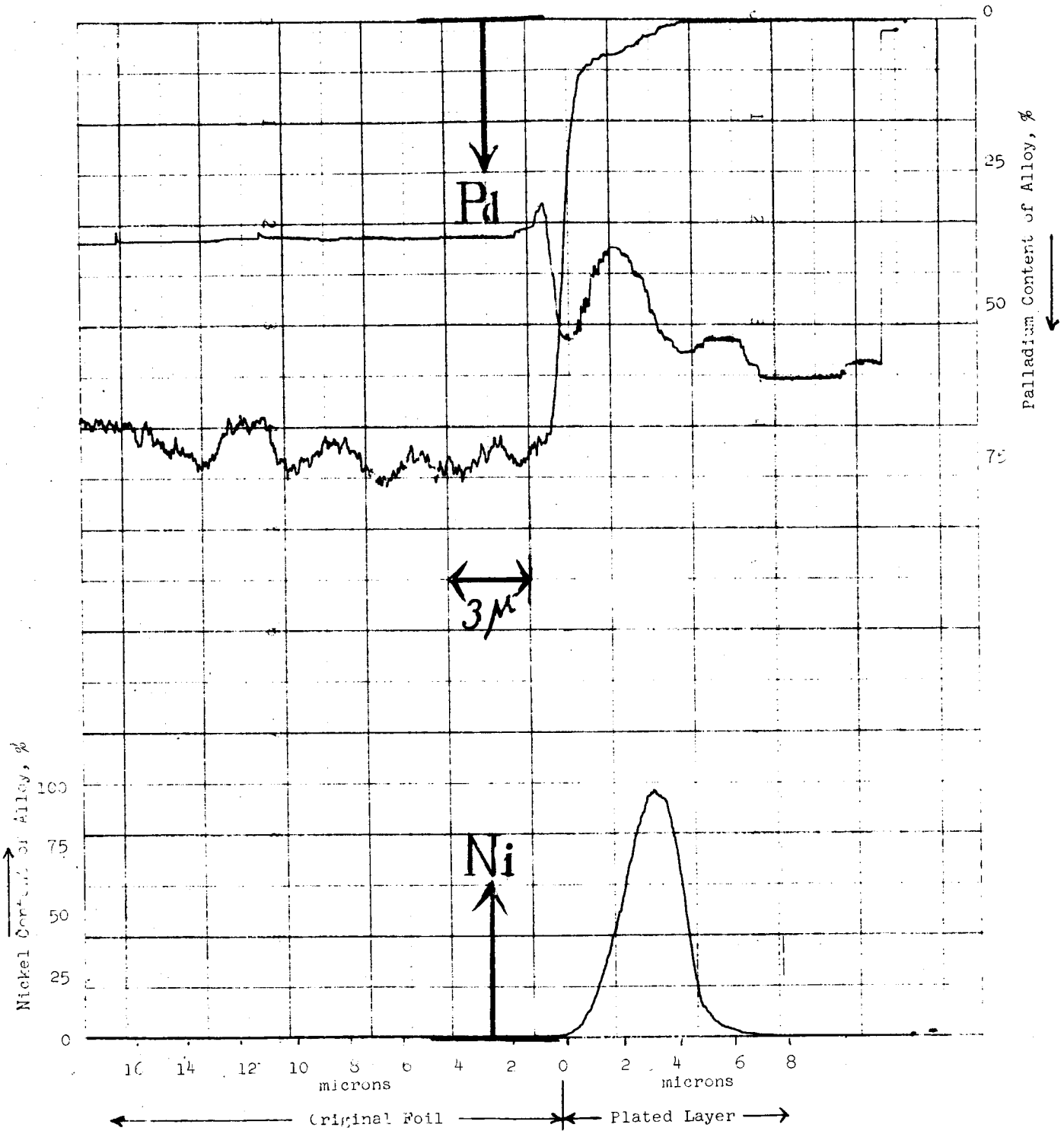

Figure A-49. Cross section of Pd-25%Ag foil plated with Ni (no diffusion treatment, oxidation in air for two hours at 700°C).

and the concentrations of plated metals can be read upward from the bottom edge in these figures. The middle lines in the figures indicate the total intensity of the counting. Since various analyzing crystals were used for the analyses, and since the curves were recorded on various counting scales, metal concentrations as indicated by these curves cannot be directly compared. On each figure, the approximate scale for the concentration of each element and the original interface between the foil and the plated layer are indicated.

The following analyzing crystals were used for each element:

Mica:	palladium, rhodium, and ruthenium
LiF:	platinum
Quartz:	nickel, cobalt, and iron

Microprobe examination of Pd-25%Ag foils that were plated and diffused with other metals indicated that the rates of diffusion were very different from one element to another, resulting in various thicknesses in the diffusion layers. Diffusion rates for copper, cobalt, and iron were very fast, resulting in uniform alloying of approximately 10% of the foil thickness. A small amount of excess copper, cobalt, and iron remained on the surface, which is believed to be oxidizing during the heat treatment. The thickness of the diffusion layer of palladium into the excess metal layer was about 2μ (1μ = 10^{-4} cm) for copper, 1μ for cobalt, and about 0.5μ for iron.

Diffusion of nickel was somewhat slower than that of copper, iron, or palladium. The thickness of the diffusion layer was about 10μ, and the highest concentration of nickel in the foil was about 5%, resulting in a considerable amount of unalloyed nickel on the electrode surface. The thickness of the diffusion layer of palladium into the excess nickel layer was about 1μ.

Diffusion of rhodium, platinum, or iridium was much slower than that of copper, iron, or nickel, but the diffusion of palladium into rhodium, platinum, or iridium was much faster; every particle of powdery deposits of rhodium, platinum, or iridium contained a significant amount of palladium. The thickness of the diffusion layer at the surface of the foil was approximately 8μ, 6μ, and 2μ, respectively, for platinum, rhodium, and iridium. Among these three elements, only rhodium showed some indication of further diffusion into the bulk of the foil. However, the concentration of rhodium in the bulk was so small that data were not conclusive by the method used.

Almost no diffusion was observed on ruthenium, titanium, and zirconium.

Foils plated and diffused on only one side with silver, copper, iron, and cobalt showed that these elements diffused so rapidly

that even the unplated side contained some of these elements diffused from the other side during the treatment. Foils plated and diffused with other elements on one side showed that alloying was limited to the plated side.

Foils plated and oxidized without the diffusion process showed no diffusion on those elements that are readily oxidized. However, elements that cannot be readily oxidized, such as platinum, diffused to some extent into the foil, and some palladium diffused into the plated layer. Diffusion of palladium into the plated layer took place to a small extent also in the case of nickel plate.

G. PLATINUM-PALLADIUM-SILVER ALLOY ELECTRODE

A special alloy, prepared by adding 10% platinum to the Pd-25%Ag alloy and rolling to 0.001 in. foil*, is reported** to have higher corrosion resistance to nitric acid attack than either Pd-25%Ag or pure palladium. The special alloy was tested, therefore, to determine its feasibility for use as a hydrogen diffusion electrode in conjunction with a nitric acid cathode. Foils of the special alloy were cleaned in the same manner as for the Pd-25%Ag electrodes, plated on both sides with rhodium black, and oxidized for two hours in air at 600°C. Tests under four sets of conditions (Table A-17) showed that the material is not a promising anode under the conditions of the tests. The reasons for the poor performances were probably low occlusion or low permeability of hydrogen, since low limiting currents were obtained at small overpotentials.

Foils of the same alloy were then tested as a hydrogen diffusion electrode in 5M KOH electrolyte. A foil was heated in air for 2 hours at 850°C. The open-circuit potential (OCP) of the electrode vs the hydrogen electrode potential was 0.9 volt after purging with hydrogen gas for 150 minutes. This inactive electrode was then reheated in air for two hours at 700°C. The electrode then had an OCP of 0.02 v (vs HE) and withstood 62 ma/cm^2 anodic polarization at an overpotential of 0.5 v (vs HE).

A foil treated for 2 hours in air at 700°C and then for 2 hours in air at 500°C withstood 38 ma/cm^2 at an overpotential of 0.5 v. Another foil treated for 2 hours in air at 700°C and then for 2 hours in air at 400°C, where platinum oxide can be formed, withstood 82 ma/cm^2 at the same overpotential.

This series of tests indicated that the palladium-silver-platinum alloy has a similar capability for occlusion and diffusion of hydrogen as Pd-25%Ag. Since the palladium-silver-platinum alloy has

---

* J. Bishop Co., Malvern, Pennsylvania.

** Wise, E. A., U. S. Patent 2,129,721.

Table A-17

ANODIC POLARIZATION OF THE PLATINUM-PALLADIUM-SILVER DIFFUSION ELECTRODE IN ACID ELECTROLYTE

Test No.	Electrolyte	Fuel	OCP vs SCE	Temperature °C	Results
1	5M H_3PO_4	N_2H_4	-0.30	Room Temp. 50	No current up to 0.24 v vs OCP. A limiting current 1.6 ma/cm² at 1.1 v vs OCP.
2	5M H_3PO_4	H_2 gas	-0.23	Room Temp. 60	Max. current 72 ma/cm² at 0.58 v vs OCP. Max. current 80 ma/cm² at 0.78 v vs OCP.
3	5M H_3PO_4 + 0.2M HNO_3	H_2 gas	-0.18	Room Temp.	A limiting current 22 ma/cm² at 0.28 v vs OCP. No improvement with temperature increase.
4	5M H_2SO_4 + 0.2M HNO_3	H_2 gas	-0.09	Room Temp.	A max. current 10 ma/cm² at 0.19 v vs OCP.

a better resistance to acid than Pd-25%Ag, utilization of the palladium-silver-platinum alloy as a hydrogen diffusion electrode in acid systems cannot be overlooked if a nitric acid-resistant foil is required for fuel cell application.

H. EFFECT OF SULFUR DIOXIDE GAS IN OXIDATION ATMOSPHERE

1. Background

Hatfield (ref. 19) reported a 10% increase in the oxidation rate of mild steel and a 50% increase in the oxidation rate of 18-8 stainless steel by adding 2% sulfur dioxide to the air. Hatfield also found that the sulfur dioxide increased the oxidation rates even more if water vapor was also added to the air. Evans (ref. 20) attributed this effect to the introduction of excess cation vacancies in the oxide film by sulfur ions. Wise (ref. 21) reported that palladium was severely attacked by hydrogen sulfide gas above 600°C and, more moderately, by sulfur dioxide gas up to 1000°C.

In the present program, sulfur dioxide was chosen to attempt a moderate increase of the oxidation rate of palladium with the object of improving the palladium-hydrogen anode.

2. Electrode Preparation

Two Pd-25%Ag foils were annealed for two hours in argon at 800°C, plated with rhodium black, and then oxidized in air containing about 15.5% (by volume) of sulfur dioxide for two hours, one at 600°C and another at 700°C (Specimen No. 1 and 2). Three other foils were prepared by heating in a sulfur dioxide atmosphere and plated with rhodium as indicated in the footnote of Table A-18.

3. Anodic Polarization Tests

Anodic polarization data of control Pd-25%Ag electrodes are compared in Table A-18 with those of electrodes that were rhodium plated and heated in sulfur dioxide.

4. Discussion and Conclusions

Specimens 1, 2, and 3 (Table A-18) showed formation of heavy greyish black film when treated in air containing sulfur dioxide gas or in pure sulfur dioxide gas, showing the formation of oxide, sulfide, or most likely a mixture of both. Both palladium and silver were probably attacked by sulfur dioxide gas.

Although the increase of oxidation rate might suggest the increase of cation vacancy sites or excess anions in the oxide (with sulfide) film, according to the Wagner mechanism, the polarization data indicated a definite poisoning of hydrogen uptake to the foil and the electrode reaction by treatment with sulfur dioxide gas.

Table A-18

ANODIC CURRENT DENSITIES, ma/cm², FOR Pd-25%Ag ELECTRODES HEAT TREATED IN SULFUR DIOXIDE GAS OR IN AIR CONTAINING 15.5% SULFUR DIOXIDE GAS

Electrode: 0.001-in. Pd-25%Ag oxidized in SO_2 containing air.
Electrolyte: 5M KOH
Fuel: H_2 gas
Temperature: 25°C

Specimen No.§§	OCP* v	Anodic Current Densities ma/cm² at Various Overpotentials vs HE**, volts 0.1	0.2	0.3	0.4	0.5
1	0.20	-	0.7	0.3	--	--
2	0.02	13	20	29	41	31
3a	0.83	-	-	-	-	-
3b‡	0.00	9	14.5	19	21.5	26
4‡‡	0.00	3.8	8.0	12.8	17.5	23
5§	0.00	3.3	4.5	6	8.6	13

---

* Open Circuit Potential vs HE.

** Hydrogen electrode potential in the same solution and at the same temperature.

‡ The current increased sharply after 0.6 volt vs HE and the electrode withstood 400 ma/cm² at 1.24 volts vs HE.

‡‡ Reached the limiting current, 96 ma/cm², at 0.87 volt vs HE.

§ The current increased sharply beyond 0.5 volt and the electrode withstood 400 ma/cm² at 0.94 volt vs HE.

§§ Specimen 3a: Heated in pure SO_2 for two hours at 850°C.
Specimen 3b: Rh black plated on both sides of the foil and heated in pure SO_2 gas for two hours at 850°C. (Specimen 3a was used again after the polarization test.)
Specimen 4: Rh black plated on both sides of the annealed foil and heated in pure SO_2 gas for 2 hours at 850°C.
Specimen 5: Rh black plated on both sides of the annealed foil and heated in pure SO_2 gas for two hours at 850°C and subsequently for two hours at 700°C.

It was also observed that the surface film (rhodium plating on specimens no. 4 and 5) fell off during the polarization tests, indicating the poor bonding between the foil and the film.

I. SUBSTITUTION OF MORE STABLE OXIDES FOR PALLADIUM OXIDE AS A HYDROGEN TRANSFER CATALYST IN PALLADIUM FOIL

1. Background

Although palladium oxide itself has been shown to be a relatively active catalyst for the transfer of hydrogen in Pd-25%Ag foil, the oxide is rather rapidly reduced by the hydrogen and the capacity of the foil as an anode is destroyed. Platinum and rhodium were found to be the most active catalysts (Section C and D), but they also form very little or no stable oxide at the temperatures used to form palladium oxide. The electrodes plated with rhodium black and oxidized at 650°C afterwards lost their activity by approximately 10 hours (section C-e). Consequently, it is necessary to substitute the readily reducible palladium oxide by a more stable catalytically active oxide. Rhodium oxide, which is more stable than palladium oxide, can be formed most rapidly at about 800°C on finely divided rhodium (ref. 22). On the other hand, palladium oxide decomposes above 790°C (ref. 23). Consequently, if a Pd-25%Ag foil plated with rhodium is heated above 790°C, the rhodium, but not the palladium or silver, would be oxidized.

2. Electrode Preparation

A Pd-25%Ag electrode was pretreated by (a) annealing in argon at 850°C, (b) rhodium-plating on both sides by the conditions of Table A-37(Appendix V), (c) oxidation in air at 850°C, and (d) rapid cooling in air.

3. Anodic Polarization Tests

The anodic polarization data are shown below.

After the polarization data were collected, the current was kept constant at 400 ma/cm^2, and the electrode potential was recorded. The temperature of the electrolyte increased to 49°C within 30 minutes, reached 55°C after about 4 hours, and then stayed approximately constant. The electrode potential gradually shifted overnight to less noble values and became constant at 0.57 v ± 0.04 v vs HE. The electrolysis was discontinued after 104 hours without any degradation of the electrode. However, the electrode failed to resume the same good performance after it was exposed to air for about four hours during the interruption of electrolysis. The electrode carried 9 ma/cm^2 at 0.12 v and reached a limiting current of 20 ma/cm^2 at 0.31 v, although the OCP was 0.03 v.

ANODIC POLARIZATION OF RHODIUM PLATED
Pd-25%Ag FOIL, OXIDIZED AT 850°C

Electrolyte: 5M KOH
Temperature: 25°C
Fuel: H_2 gas

Current Density, ma/cm²	Potential vs HE*, volt	Current Density, ma/cm²	Potential vs HE*, volt
0	0.02	175	0.40
23.5	0.10	240	0.50
56.0	0.20	300	0.60
110	0.30	400	0.69

* HE = Reversible hydrogen potential at same pH and temperature.

4. Thermal Reactivation of Electrode

A thermal reactivation of the above electrode by heating for two hours in air at 850°C fully rejuvenated the electrode. The electrode showed the similar polarization curve as that by the previous active condition up to 400 ma/cm². The electrode was tested again for longevity at 250 ma/cm² at 60°C. The potential was 0.35 v in the beginning, leveled off to about 0.5 v after 3 hours until about 300 hours were reached, and then very gradually decreased to 0.66 v until the test was stopped at 336 hours (14 days). A duplicate electrode was made and was operated at 60°C at 400 ma/cm² for 18 hours. The potential shifted from 0.80 v to 0.65 v. The operation was continued further at 250 ma/cm² for 120 hours, and the potential shifted from 0.62 v to 0.82 v. Those potentials of the duplicate were somewhat larger than that of the first one.

5. Electrode Improvement

Further improvement was made in two ways:

(a) Oxidation in air by two steps after rhodium black plating, 2 hours at 850°C, and 2 hours at 700°C. This process introduces not only rhodium oxide but also palladium oxide, which has better polarization characteristics. [The (d log I)/dE slope is steeper.]

(b) Oxidation in oxygen instead of air to increase the activity. Cation vacancy concentration is proportional to the 1/6 power of the oxygen partial pressure.

Anodic polarization data on these electrodes (Table A-19) showed better characteristics than that of an electrode oxidized only at 850°C in air. The specimen with treatment (a) above was tested at 60°C at 250 ma/cm^2. The potential was 0.39 v in the beginning, leveled off to about 0.6 v for over 200 hours, and gradually increased to 0.8 v at the end of the test (336 hours). The second specimen with treatment (b) was tested at 250 ma/cm^2 at 90°C. The potential leveled off quickly to 0.56 v and showed no further change during the test for 336 hours.

6. Discussion

The life of an activated Pd-25%Ag diffusion electrode was prolonged from ten to more than 336 hours by using rhodium oxide as a principal catalyst instead of palladium oxide, although the polarization was somewhat greater than that of electrodes activated by palladium oxide, particularly at higher current densities. This improvement may be due to a slower reduction rate of rhodium oxide than palladium oxide by hydrogen. Furthermore, higher and more prolonged activity was introduced by oxidizing in pure oxygen instead of in air. This result suggested the further possibility that many p-type oxide films might be active as catalysts for the diffusion electrode.

Interruption of the test and exposure of the electrode to air destroyed the hydrogen permeability of the electrode. This result might be attributed to the following reasons: (a) hydrogen existing as a screening proton while the electrode was active changed to a more stable form such as a type of hydride and prevented further hydrogen transport, (b) oxygen from air diffused into the palladium lattice, formed a water molecule, and prevented further activity as a diffusion electrode. However, the true reason for this destruction by interruption is not understood.

Thermal reactivation restored the hydrogen permeability and the activity retained during the test for 336 hours.

These series of tests were most encouraging for the development of a palladium-hydrogen diffusion electrode that will operate continuously with high current drain and good potential.

J. EFFECT OF CONDITIONS OF RHODIUM PLATING ON ANODIC POLARIZATION OF DIFFUSION ELECTRODE

Since rhodium black plating was very promising as the electrode catalyst on Pd-25%Ag diffusion electrodes, a series of experiments was conducted to optimize the condition for the most active rhodium plating.

Table A-19

ANODIC POLARIZATION OF Pd-25%Ag ELECTRODE
WITH RHODIUM OXIDE

Electrode: 0.001-in. Pd-25%Ag foil plated with rhodium, about 1 mg/cm^2, and oxidized.

Electrolyte: 5M KOH

Temperature: 25°C

Heat Treatment	OCP* v	Current Densities ma/cm^2 at Various Overpotentials vs HE**, volts 0.1	0.2	0.3	0.4	0.5
2 hours at 850°C and 2 hours at 700°C in air	0.00	29	64	140	220	310
2 hours at 850°C in oxygen gas	0.00	44	73	125	195	270

* Open Circuit Potential vs HE.

** Hydrogen electrode potential in the same solution and at the same temperature.

1. Electrolyte

Two types of electrolyte were tested. One was a commercial rhodium plating solution* giving a shiny deposit and the other was 0.01M $RhCl_3$ solution of pH 1 giving a rhodium black deposit.

Approximately 1 mg/cm^2 of rhodium was plated on both sides of a foil that was previously annealed at 850°C in an argon atmosphere. The foil plated with rhodium was then oxidized (activated) at 850°C for 2 hours in air. Two plating cathode current densities, 10 ma/cm^2 and 125 ma/cm^2, were tested for each electrolyte.

Table A-20 shows the anodic current densities of Pd-25%Ag diffusion electrodes at various overpotentials vs the standard hydrogen electrode. Results indicate that the electrodes with rhodium black plated from 0.01M $RhCl_3$ solution supported a current at least ten times higher than that of an electrode with shiny rhodium plated from Rhodex solution, although all electrodes gave the same open-circuit potential.

Results also indicated that the foils plated at the higher current density gave higher anodic current at the same overpotentials than did foils plated at the lower current density.

2. Cathode Current Density for Plating

Approximately 1 mg/cm^2 of rhodium black was plated on both sides of Pd-25%Ag foils under various cathode current densities from 0.01M $RhCl_3$ solution of pH 1, and anodic polarization characteristics of these foils were determined.

Heat treatment of the foils was the same as those in the previous section; i.e., annealing at 850°C before plating and oxidation at 850°C after plating. However, during this series of tests (tabulated in Table A-21) a few electrodes, particularly those plated at 250 ma/cm^2, showed poor activity. One of those electrodes (Test No. 5 in Table A-19) was then reheated to 700°C and run again for the anodic polarization tests. Results indicated a slight improvement in the anodic current density at an overpotential of 0.1 v and more significant improvement at higher overpotentials. This improvement in dI/dE slope perhaps suggests that the palladium oxide is a better catalyst than rhodium oxide for the process.

3. Effect of Amount of Plated Rhodium on Electrode Performance

Palladium-25% silver foils were plated with various amounts of rhodium black from 0.01M $RhCl_3$ solution at the same current density, 125 ma/cm^2, which gave one of the best results among the

---

* Rhodex by Sel-Rex Co.

Table A-20

ANODIC CURRENT DENSITIES, ma/cm^2, OF Pd-25%Ag DIFFUSION ELECTRODE WITH RHODIUM PLATING FROM DIFFERENT PLATING BATHS

Electrolyte: 5M KOH

Fuel: H_2 gas

Temperature: Room Temperature

Test No.	Plating Bath	Cathode Current Density for Plating ma/cm^2	Weight of Rh Deposit mg/cm^2	OCP* v	Anodic Current Densities, ma/cm^2 at Overpotentials vs HE**, volts				
					0.1	0.2	0.3	0.4	0.5
1	Rhodex	10	1.2	0.00	1.4	3.8	7.4	11.0	13.2
2	Rhodex	125	0.9	0.00	5.2	9.8	17.0	25.0	36.0
3	.01M $RhCl_3$	10	1.1	0.00	52	92	124	158	175
4	.01M $RhCl_3$	125	1.0	0.00	56	112	178	221	270

* Open Circuit Potential vs HE.

** Hydrogen electrode in the same solution and at the same temperature.

Table A-21

ANODIC CURRENT DENSITIES, MA/CM^2, OF Pd-25%Ag DIFFUSION ELECTRODE WITH RHODIUM BLACK PLATED AT VARIOUS CURRENT DENSITIES, AT VARIOUS OVERPOTENTIALS

Electrolyte: 5M KOH
Fuel: H_2 gas
Temperature: Room Temperature
Plating Bath for Rh Black: 0.01M $RhCl_3$

Test No.	Cathode Current Density for Plating ma/cm^2	Weight of Rh Plated mg/cm^2	OCP* v	Anodic Current Densities, ma/cm^2, at Various Overpotentials (η)**				
				0.1	0.2	0.3	0.4	0.5
1	10	1.2	0.00	52	92	124	158	175
2	30‡	0.6	0.00	29	59	103	165	240
3	50	1.0	0.00	60	112	170	210	240
4	125	1.0	0.00	56	112	178	221	270
5a	250	0.8	0.00	26	44	56	70	82
5b	250	1.0	0.00	22	40	58	75	86
5c	250‡	1.0	0.00	25	55	110	176	250
5d	250‡‡	4.3	0.00	39	77	120	175	215

* Open Circuit Potential vs Hydrogen Electrode in the same solution and at the same temperature, HE.
** Hydrogen Overpotential vs HE.
‡ 5c: The electrode for the tests 5b was reheated to 700°C in air for 2 hours.
‡‡ Oxidized at 850°C and further at 600°C in air.

previous tests on the effect of current density for plating. The pH of the plating solution was adjusted to 1 with HCl except for one foil, which was plated from a solution that had been adjusted to pH 2 (Test No. 3 in Table A-22).

Foils were annealed in argon at 850°C before plating and oxidized in air at 850°C for two hours and further in air at 700°C for two hours. Results on anodic polarization of these foils are given in Table A-22.

Results indicate no significant effect as a result of different amounts of rhodium deposit. Current densities on the electrode plated from the pH 2 electrolyte were somewhat lower than those plated from pH 1 electrolyte.

Since the electron-probe analysis showed that sufficient diffusion of palladium into rhodium takes place during oxidation, even at 700°C, the insignificant effect of the amount of rhodium deposit is believed reasonable.

K. LIFE TEST OF THE Pd-25%Ag DIFFUSION ELECTRODE WITH HYDROGEN FUEL

1. Electrodes with Various Coatings

Continuous polarization tests of several Pd-25%Ag electrodes were conducted for periods up to two weeks to test the durability of electrode activity. For these tests, the anodic current was kept constant, and the electrode potential was intermittently measured. The cell temperature was kept constant within ±5°C by controlling current through a heating tape that was wrapped around the cell. The results, summarized in Table A-23, indicate that the most stable electrode is one plated with rhodium and heat treated in air or oxygen at a temperature high enough to form rhodium oxide. However, the better potential value was obtained from the electrode that was also treated at the lower temperature where palladium oxide could be formed.

The electrodes plated with thin nickel or platinum and oxidized showed excellent polarization characteristics in the beginning of the test, but died out before the end of the two-week period. The reason for a short life of the electrodes with platinum may be attributed to reduction of palladium oxide and platinum oxide by hydrogen, but the failure of the electrode with nickel oxide must be caused by some other factor, such as plugging of nickel ion vacancy sites by stable hydrogen ions, since nickel oxide is believed to be very stable.

Table A-22

ANODIC CURRENT DENSITIES, ma/cm², ON Pd-25%Ag ELECTRODES WITH VARIOUS AMOUNTS OF RHODIUM BLACK

Electrode: 1-mil Pd-25%Ag foil rhodium plated

Fuel: H_2 gas

Electrolyte: 5M KOH

Temperature: Room Temperature

Test No.	Amount of Rh Black mg/cm²	OCP* v	Current Densities, ma/cm² at Overpotentials (η) vs HE**, volts			
			0.1	0.2	0.3	0.4
1	0.26	0.00	44	108	215	308
2	0.50	0.00	52	110	210	315
3	0.53‡	0.00	33	76	152	260
4	1.00‡‡	0.00	56	112	178	221
5	1.60	0.00	57	126	222	315
6	3.76	0.00	57	138	240	315

* Open Circuit Potential vs HE.

** Hydrogen electrode potential.

‡ pH of $RhCl_3$ solution was adjusted to 2.

‡‡ Oxidized only at 850°C, listed previously in Table A-21.

Table A-23

DURABILITY OF ELECTRODE ACTIVITY

Electrolyte: 5M KOH
Fuel: H_2 gas

Specimen No.	Electrode Preparation	Temp. °C	Current Density ma/cm^2	Time hr	Overpotential vs HE*, volts		
					Start	Level	End
1	Rh plating on both sides. Heat in air for 2 hr at 850°C	60	250	336	0.35	0.50 ±0.05	0.66
2a	Same as 1.	60	400	18	0.65	0.65	0.82
2b	Continuation of 2a.	60	250	120	0.62	±0.05	0.82
3	Rh plating on both sides. Heat in air for 2 hr at 850°C, for 2 hr at 700°C.	60	250	336	0.39	0.65 ±0.05	0.82
4	Same as 3.	90	250	284	0.18	0.60 ±0.05	0.80
5	Same as 3	90	250	336	0.52	0.50 ±0.05	0.62
6	Rh plating on both sides. Heat in O_2 for 2 hr at 850°C.	90	250	336	0.56	0.50 ±0.05	0.55
7‡	Pt plating on both sides. Heat in Ar for 2 hr at 850°C, for 2 hr at 700°C.	90	250	48	0.35	0.50 ±0.05	-

Notes at end of table

Table A-23 (Continued)

DURABILITY OF ELECTRODE ACTIVITY

Specimen No.	Electrode Preparation	Temp. °C	Current Density ma/cm²	Time hr	Overpotential vs HE*, volts		
					Start	Level	End
8‡	Pt plating on both sides. Heat in air for 2 hr each at 850, 700 and 400°C.	90	250	<24	0.50	-	-
9‡‡	Pt plating on fuel side and Rh plating on electrolyte side. Heat in air 2 hr each at 850, 700 and 400°C.	90	250	146	0.41	0.40 ±0.10	0.43
10‡	Zr-Ni plating on both sides. Heat in Ar for 2 hr at 850°C, in air for 2 hr at 700°C.	90	250	48	0.73	0.70	-
11‡‡‡	Ni plating on both sides. Heat in Ar for 2 hr at 850°C, in air for 2 hr at 700°C.	90	250	240	0.51	0.65 ±0.10	0.57
12‡‡‡	Ru plating on both sides. Heat in Ar for 2 hr at 850°C, in air for 2 hr at 700°C.	90	250	175	0.75	0.80 ±0.05	0.80

Notes at end of table

Table A-23 (Continued)

DURABILITY OF ELECTRODE ACTIVITY

Specimen No.	Electrode Preparation	Temp. °C	Current Density ma/cm²	Time hr	Overpotential vs H_3*, volts		
					Start	Level	End
13‡	Heat in Ar for 2 hr at 850°C, in air for 2 hr at 700°C. Then Ru plating on both sides. Heat again in air for 2 hr at 700°C.	90	250	48	0.58	0.50 ±0.05	0.54

---

* Hydrogen electrode potential in the same solution and at the same temperature.

‡ Died out during the night.

‡‡ Died out as Rh plating dropped off.

‡‡‡ Died out by suddenly evolving oxygen. The potential turned instantaneously to the oxygen evolution potential, about 1.7 volts vs HE.

2. Optimization of Heat Treatment of the Electrodes Plated With Rhodium Black

Various tests conducted up to this point definitely indicated that the electrodes plated with rhodium black and with a suitable heat treatment were the most promising hydrogen electrodes, and were practically the only electrodes to be considered for both activity and electrode life. Consequently, as the final stage of the work, optimization of heat treatment of the electrodes plated with rhodium black under the optimum condition (1 mg/cm^2 of Rh at 125 ma/cm^2 in 0.01M $RhCl_3$ adjusted to pH 1, see section J) was carried out.

Palladium-25% silver electrodes, rhodium plated on both sides and heat treated in various manners, were tested as anodes using gaseous hydrogen as a fuel. All foils were annealed in argon for 30 minutes at 850°C, plated with rhodium black, heated for diffusion bonding in argon for 30 minutes at 850°C, and then oxidized according to the following schedule:

Foil	Oxidation Treatment (for a 2-hour period)
1	in O_2 at 600°C
2	in O_2 at 700°C
3	in O_2 at 850°C
4	in O_2 at 850°C, then in O_2 at 700°C
5	in air at 850°C, then in air at 700°C

Anodic polarization curves of these electrodes at room temperature are shown in Figure A-50, and those at 90°C are shown in Figure A-51. The following trends can be seen upon examining Figures A-50 and A-51.

(a) Oxidation of foils in pure oxygen below 790°C: Oxidation at 700°C produced more active anodes than oxidation at 600°C. (Foils 1 and 2)

(b) Oxidation of foils in pure oxygen at 850°C or with subsequent additional oxidation at 700°C: The electrodes oxidized at 850°C showed activity intermediate between that of electrodes oxidized at 700°C or 600°C. (Compare curves 1, 2, and 3.) Subsequent additional oxidation at 700°C did not improve the polarization characteristics.

(c) Oxidation in air for 2 hours each at 850°C and, subsequently, at 700°C: The electrode oxidized in air (Foil 5) was far superior to that oxidized in pure O_2.

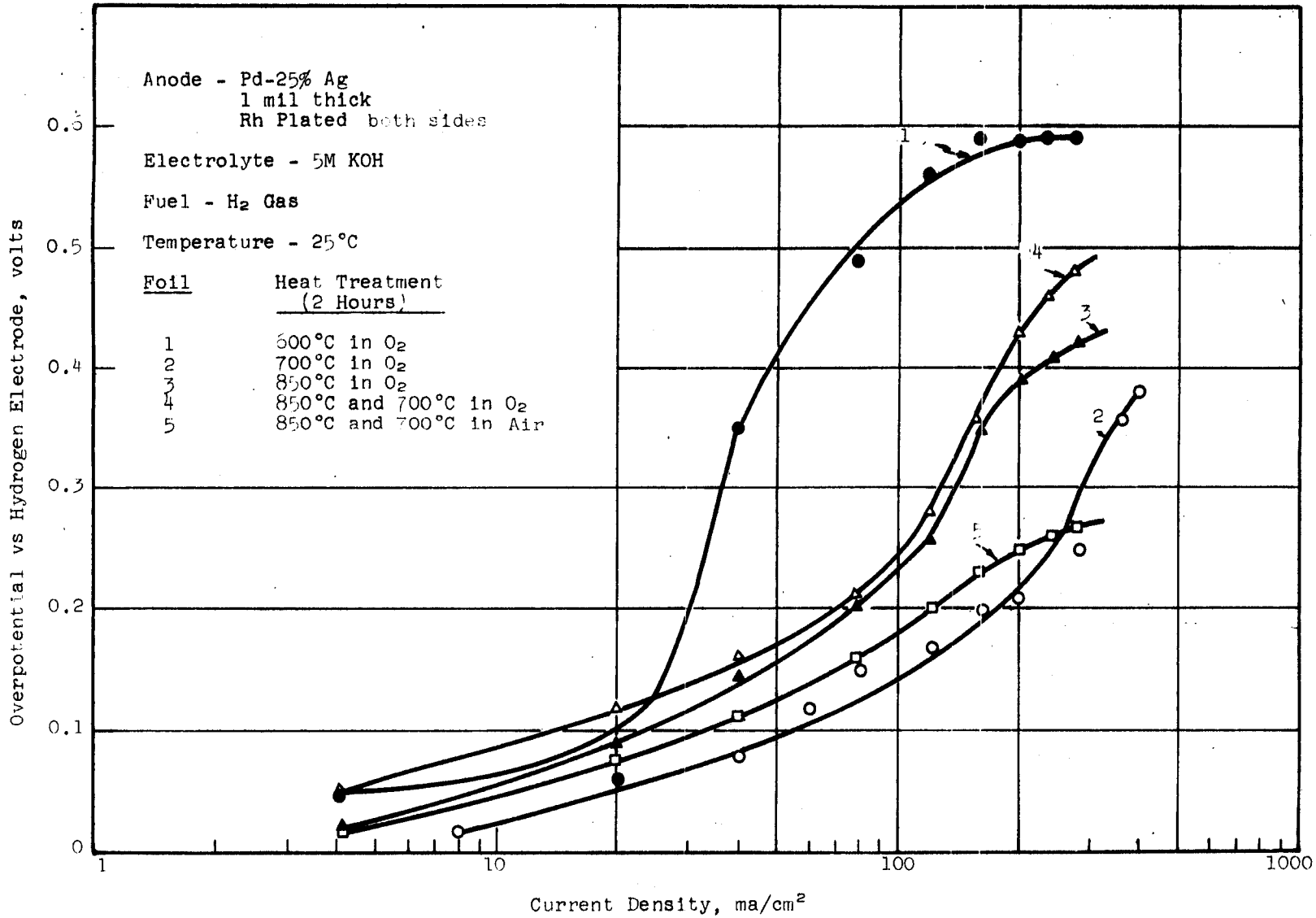

Figure A-50. Anodic Polarization Curves of Pd-25%Ag Hydrogen Diffusion Electrodes at 25°C Plated with Rh Black and Oxidized in Various Manners

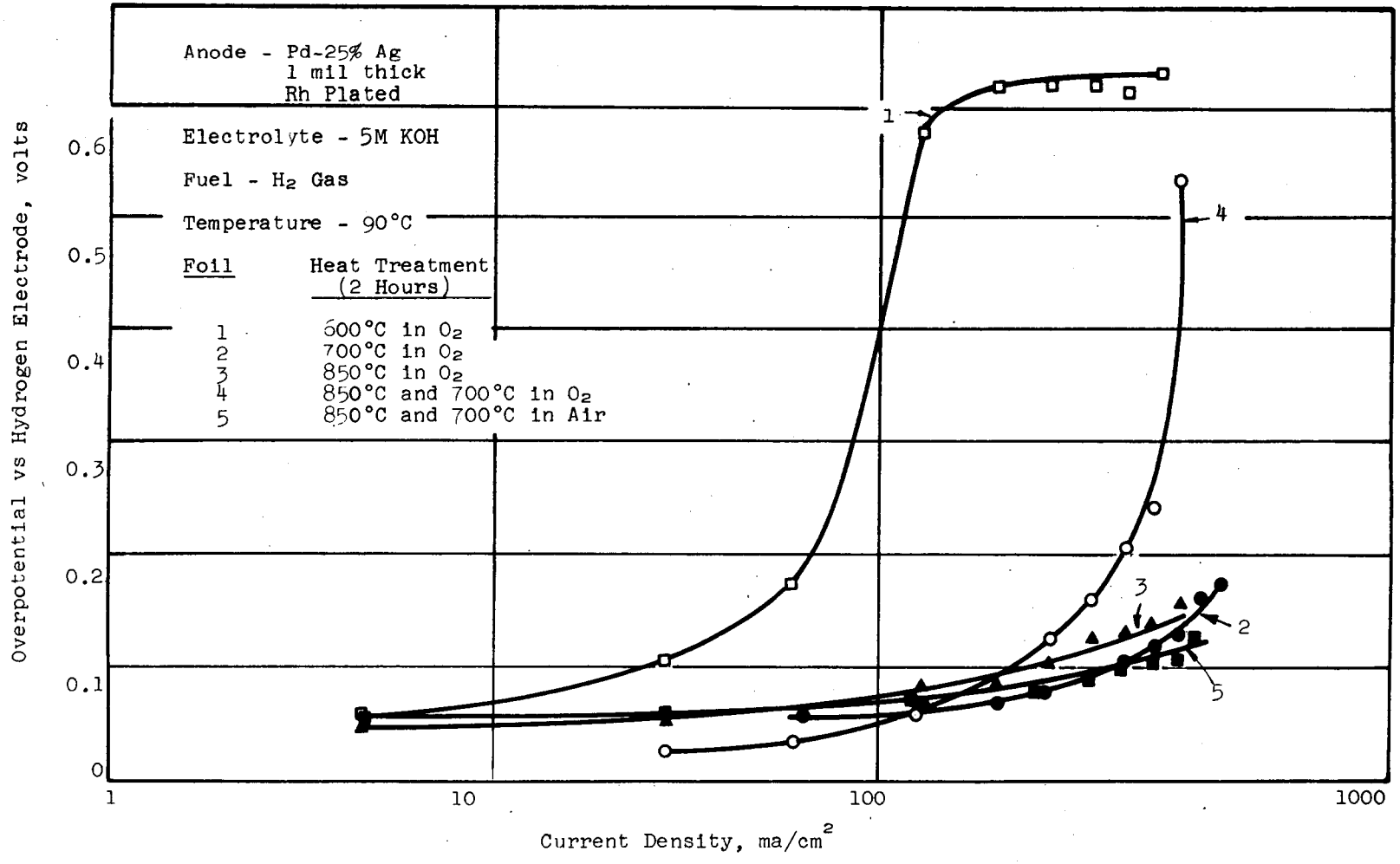

Figure A-51. Anodic Polarization Curves of Pd-25%Ag Hydrogen Diffusion Electrodes at 90°C Plated with Rh Black and Oxidized in Various Manners

Life tests were conducted by passing a constant anodic current of 250 ma/cm^2 through the electrode and measuring the anode potential from time to time. All of the five electrodes tested showed a rapid overpotential increase to 0.6 v vs H_2 during the first 50 hours. Afterwards, the potentials remained nearly constant until the end of the test. A summary of the life test data is given in Table A-24.

The data in Table A-24 indicate that:

(a) Initial high catalytic activity diminished down to the steady state activity after approximately 50 hours of polarization at 250 ma/cm^2.

(b) The steady state activity was independent of the oxidation temperature for one-step oxidation in oxygen, although the initial activity varied with the temperature of the oxidation. (Foil 1, 2, and 3)

(c) The highest steady state activity was obtained by the double step oxidation in oxygen (Foil 4).

(d) The steady state activities of those electrodes oxidized in oxygen (Foil 1, 2, 3, and 4) were higher than that oxidized in air (Foil 5), although the highest initial activity was obtained by Foil 5.

L. ANODIC OXIDATION OF HYDRAZINE WITH PALLADIUM-SILVER-HYDROGEN DIFFUSION ANODE

1. Background

To meet the objectives of the present contract, storable hydrogen-containing fuels such as hydrazine were anodically oxidized at the palladium diffusion electrode. Two phases of the program included (a) evaluation of the effect of different metal oxide surface coatings on the decomposition rate of hydrazine to hydrogen and nitrogen, and (b) evaluation of the catalytic activity of metal oxide coatings on the Pd-25%Ag electrodes by determining anodic polarization characteristics of the electrodes.

Life tests were also made for electrodes that were coated with rhodium black on the electrolyte side and with either rhodium black or cobalt black on the fuel side. The latter electrodes showed the best activity among those tested in the above screening experiments.

Electrodes were prepared by coating both sides of a Pd-25%Ag foil with rhodium black and heat treating in various manners. These anodes were tested for the oxidation of hydrogen fuel.

Table A-24

LIFE TEST OF PALLADIUM HYDROGEN DIFFUSION ELECTRODE PLATED WITH RHODIUM BLACK AND OXIDIZED IN VARIOUS MANNERS

Electrode: Pd-25%Ag, 1 mil thick, prepared as specified

Electrolyte: 5M KOH

Fuel: H_2

Temperature: 90°C

Foil No.	OCP*	Anode Current Density, ma/cm²	Testing Period, hr	Initial† Potential, volts	Leveled-off** Potential, volts
1	0.05	250	304	0.53	≈0.65
2	0.02	250	196	0.10	≈0.65
3	0.04	250	304	0.11	≈0.65
4	0.04	250	210	0.19	≈0.60
5	0.02	250	304	0.09	≈0.75

* Open-circuit potential vs hydrogen electrode in the same solution.

† Over-potentials vs hydrogen electrode in the same solution. Initial potential is the potential observed during the polarization study.

** Over-potentials vs hydrogen electrode in the same solution. Leveled-off potentials indicate the electrode potentials when those reached the nearly stable values after approximately 50 hours of tests.

2. Effect of Metal Oxide Surface on Decomposition Rate of Hydrazine

The use of the solid Pd-25%Ag hydrogen diffusion membrane for the anodic oxidation of hydrazine depends on at least three processes: (a) catalytic reforming of hydrazine to atomic or molecular hydrogen, (b) diffusion of hydrogen through the membrane, and (c) anodic oxidation of hydrogen on the electrolyte side of the membrane. Since the reforming of hydrazine to hydrogen and nitrogen is required for the operation of the anode, a series of tests was conducted to evaluate the catalytic activity of different surface coatings for hydrogen formation.

A 5-ml precision buret was filled with 100% hydrazine hydrate and placed upside down in a small beaker of the same solution. A 5 x 5 mm piece of Pd-25%Ag foil, coated with various metal oxides, was placed under the middle of a funnel, which was connected to the bottom of the buret. Foils were cut from specimens previously used for experiments involving the transfer and anodic oxidation of hydrogen. The amount of gas evolved by decomposition of hydrazine was then measured from time to time.

Total volumes of gas evolved at 25°C are shown as a function of time in Figure A-52. The curves indicate that the decomposition rate of hydrazine was increased approximately 10 to 20% by those metal oxides that previously showed promise as diffusion electrode catalysts when using hydrogen gas as a fuel.

3. Anodic Polarization of Pd-25%Ag Diffusion Electrodes with Hydrazine Fuel

During the operation of an anode using hydrazine fuel with a palladium diffusion electrode, hydrogen will probably be directly absorbed as a proton in the palladium electrode without forming molecular hydrogen gas:

$$N_2H_4 \longrightarrow N_2\ (g) + 4\underline{H}\ (\text{in Pd}) \qquad (3)$$

Consequently, determining the decomposition rate of hydrogen by measuring the amounts of nitrogen and hydrogen reformed in contact with the electrode without passing an anodic current through the electrode may not be a direct indication of surface activity, although results gave a certain suggestion of a catalytic action of transition metal oxides for reforming hydrazine. For this reason, a second series of screening tests was conducted to evaluate Pd-25%Ag electrode catalytic treatment in terms of anodic polarization and life tests.

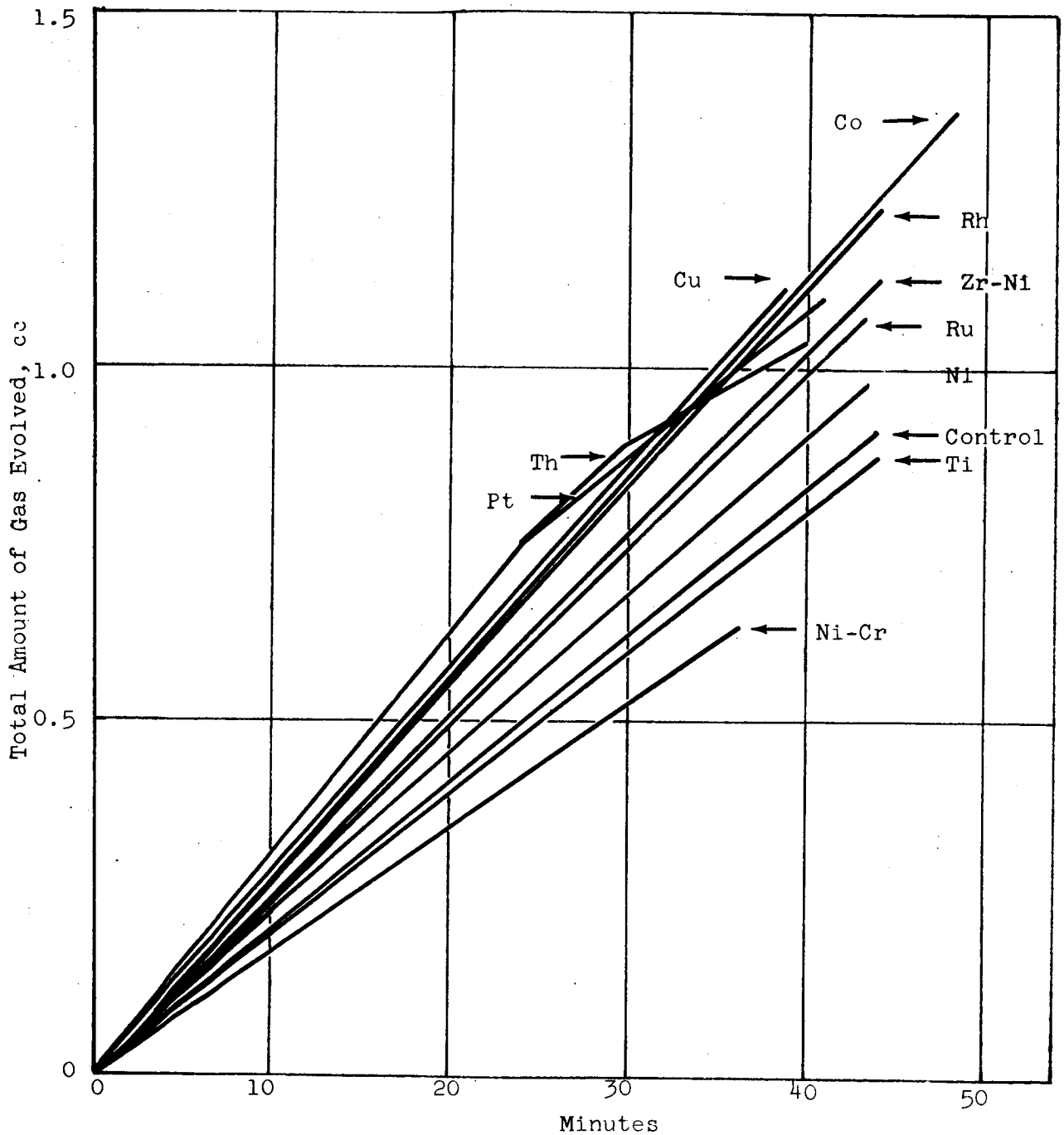

Figure A-52. Gas Evolution of Surface-Treated Pd-25%Ag Foils Immersed in 100% N_2H_4

a. Screening Test for Catalytic Activity of Metal Oxides

Anodic polarization curves of Pd-25%Ag electrodes in contact with hydrazine as a fuel were determined galvanostatically, using a K-M bridge to eliminate IR drop in the voltage measurement. Since the previous work with hydrogen gas indicated that rhodium plating with the proper heat treatment gave the most reliable activity on the electrolyte side, all electrodes tested were plated with 1 mg/cm^2 of rhodium black on the electrolyte side at a current density of 125 ma/cm^2 in 0.01M $RhCl_3$ solutions, adjusted to pH 1 with hydrochloric acid.

The fuel side of these electrodes was then plated with various metals and heat treated to form the desired metal oxide catalysts. For comparisons, one additional electrode (Foil 12) was coated with cobalt black on both sides. All foils were annealed before plating by heating in argon for 30 minutes at 850°C. Methods of preparation of the test electrodes are listed in Table A-25.

The test cell was heated to 90°C to obtain more rapid decomposition of hydrazine than at 25°C. The overpotential of the hydrazine electrode vs the hydrogen electrode in the same solution at various anodic current densities is shown in Table A-26.

Results in Table A-26 show the following:

(1) On the electrolyte side, rhodium oxide was more active than cobalt oxide.

(2) On the hydrazine side, rhodium oxide and cobalt oxide were far better catalysts among those oxides tested. Iridium oxide showed some activity.

(3) Teflon coating did not change the polarization characteristics of the electrode, but also did not show any improvement.

After determining the polarization curves, the electrolysis of Foils 2 and 3 was continued at constant current for a life test. The overpotential of Foil 2 decreased from 0.56 to 0.46 v during 12 minutes of electrolysis at 340 ma/cm^2 but increased to 0.71 v one hour after adding pure hydrazine and a small amount of potassium hydroxide solution. After decreasing the current to 160 ma/cm^2, the overpotential remained constant for more than five hours although cold hydrazine was added twice during this period. However, when a small amount of potassium hydroxide solution was added again to the fuel, the potential changed very rapidly in a positive direction, and oxygen evolution was observed on the electrode surface.

Foil 3 was continuously anodically polarized at 160 ma/cm^2. The overpotential increased to 0.24 v during the first two hours and remained constant for more than 24 hours. During this period, a

Table A-25

CATALYTIC TREATMENT OF Pd-25%Ag ANODES FOR N_2H_4 OXIDATION

Foil No.	Electrolyte Side	N_2H_4 Fuel Side	Heat Treatment
1	Rh black plating	Rh black plating	30 min in argon at 850°C, then oxidation for 2 hr in pure O_2 at 850°C.
2	Foil 1 (re-use)		Reactivation by heating in air for 1 hr at 700°C.
3	Rh black plating	Rh black plating	30 min in argon at 850°C, then oxidation in pure O_2 for 2 hr each at 850°C and 700°C.
4	Rh black plating	Li_2O by decomposition of Li_2CO_3	Oxidation for 1 hr in air at 700°C.
5	Rh black plating	Ir black plating (0.4 mg/cm²)	Same as Foil 3
6	Rh black plating	Co black plating (0.9 mg/cm²)	Same as Foil 3
7	Rh black plating	Fe black plating (0.9 mg/cm²)	Same as Foil 3
8	Rh black plating	Ni black plating (1.0 mg/cm²)	Same as Foil 3
9	Rh black plating	Pt black plating (1.0 mg/cm²)	Additional oxidation in pure O_2 for 2 hr at 350°C after treating as Foil 3
10	Rh black plating	Pt black plating	After treating as Foil 9, electrode was coated with Teflon suspension‡ and cured in air for 1 hr each at 100°C and 300°C.
11	Rh black plating	Ru black plating (1.0 mg/cm²)	Same as Foil 3
12	Co black plating	Co black plating	Same as Foil 3

‡ 50% Teflon suspension, E.I. DuPont de Nemours and Co., Inc.

Table A-26

ANODIC POLARIZATION OF Pd-25%Ag ELECTRODES USING N_2H_4 FUEL

Electrode: Pd-25%Ag foil, 1 mil thick, coated with Rh black on the electrolyte side and the other metal oxide on the fuel side
Electrolyte: 5M KOH
Fuel: 100% N_2H_4
Temperature: 90°C

Foil No.	OCP*	Anode Current Density, ma/cm²														
		4	8	20	40	60	80	100	120	140	160	180	200	240	300	340
1 (Rh-Rh)	0.00	-	-	0.05	0.06		0.11				0.10		>1.13**			
2 (Rh-Rh)	0.02			0.02	0.03	0.03	0.03	0.04		0.03	0.04	0.04	0.35		0.39	0.56
3 (Rh-Rh)	0.01				0.06	0.06	0.05	0.06	0.06	0.09	0.10					
4 (Li-Rh)	0.13	0.14		0.25	>1.13**											
5 (Ir-Rh)	0.10	0.09	0.08	0.10	0.13	0.15	0.17		0.20	0.25	0.53	1.3**				
6 (Co-Rh)	0.01			0.03	0.04			0.09	0.11	0.11	0.13	0.14	0.18	0.55		
7 (Fe-Rh)	0.11	0.11	0.11	0.12	0.14	0.19	0.78									
8 (Ni-Rh)	0.11		0.12	0.15	0.19	0.27	0.83									
9 (Pt-Rh)	0.08				0.14		0.18	0.35	(1.38)†							
10 (Pt-Rh)‡	0.08				0.11		0.16	0.38	(1.38)†							
11 (Ru-Rh)	0.13				(1.52)**											
12 (Co-Co)	0.04	0.04		0.10	0.12		0.18		(1.63)**							

* Open circuit potential vs hydrogen electrode potential in the same solution.

** The potential changed very rapidly to the positive direction, and oxygen evolution started.

† As the electrolysis was continued at 100 ma/cm², the potential gradually shifted positively, and finally reached the value in parentheses when oxygen evolution started.

‡ After treating as Foil 9, electrode was coated with Teflon suspension as described in Table A-25.

small amount of gas evolution was observed at the electrolyte surface, starting at approximately two hours after the start of electrolysis and gradually increasing with time. After about 24 hours electrolysis, the overpotential suddenly dropped to almost zero while hydrazine and potassium hydroxide solution apparently flowed freely through the membrane. The electrolysis was continued for one more day without changing the overpotential, even when the temperature of the cell was dropped to room temperature. The overpotential of the electrode was 0.03 v at 320 ma/cm^2, showing that the electrode was electrochemically very active. A number of visible cracks were observed on the electrode surface after the tests. The cause of these cracks, although not definitely determined, may be the high pressure of water vapor formed at grain boundaries by reduction of oxides with hydrogen. Since the electrode was oxidized in pure oxygen, it is likely that a considerable amount of oxide was formed or an excess amount of dissolved oxygen was present at the grain boundaries.

b. Life Test of Diffusion Electrodes Using Hydrazine Fuel

Since the above screening tests indicated that the most promising catalysts were rhodium or cobalt oxides on the hydrazine side and rhodium on the electrolyte side of the foil, electrodes for life tests were prepared as shown in Table A-27.

Anodic polarization curves were also determined for some of those electrodes before the life tests were started.

The results of anodic polarization tests of electrodes 13 to 20 are given in Table A-28. Overpotentials of the electrodes are given versus the hydrogen electrode in the same solution. Life test results for these electrodes are summarized in Table A-29.

The data presented in Tables A-28 and A-29 indicate that:

(1) Oxidation at 850°C and subsequently at 700°C gave higher activity than that by oxidation only at 700°C, on the electrodes coated with rhodium black on both sides.

(2) Pre-oxidation at 700°C before plating caused severe shedding of rhodium plate during the electrode process with hydrazine as fuel (Foil 18), although this also happened to some extent to the electrodes without pre-oxidation.

(3) Teflon coating over the electrode surface to protect the oxide layer sacrificed slightly the electrode activity (Foil 19), but did not improve the life of the electrode.

(4) The highest activity was obtained by the electrode coated with rhodium black on the electrolyte side and with cobalt black on the fuel side.

Table A-27

CATALYTIC TREATMENT OF Pd-25%Ag ANODES FOR LIFE TESTS

Foil No.	Electrolyte Side	N_2H_4 Fuel Side	Heat Treatment
13,14,15, 16	Rh black plating	Rh black plating	30 min in argon at 850°C, then oxidation in O_2 for 2 hr each at 850°C and 700°C
17	Rh black plating‡	Rh black plating‡	Diffusion treatment in argon, then oxidation in air for 2 hr at 700°C
18	Foil 17 (re-use)		Re-oxidation of Foil 17 in pure O_2 for 1 hr each at 850°C and 700°C
19	Rh black plating‡	Rh black plating‡	Diffusion treatment in argon, then oxidation in air for 2 hr at 700°C†
20	Rh black plating	Co black plating	10 min in argon at 850°C, then oxidation in O_2 for 10 min each at 850°C and 700°C

‡ Oxidation for 2 hr in air at 700°C before plating.

† Teflon coating after final oxidation; Teflon cured 1 hr in air at 300°C.

Table A-28

ANODIC POLARIZATION OF PALLADIUM ELECTRODE USING N_2H_4 FUEL‡‡

(Overpotentials at Various Current Densities)

Electrode: Pd-25%Ag Foil, 1 mil thick, prepared as specified in Table 12

Electrolyte: 5M KOH

Fuel: 100% N_2H_4

Temperature: 90°C

Foil No.	OCP*	Anode Current Densities, ma/cm²													
		4	8	20	40	60	80	100	120	140	160	200	240	280	310
13	0.03	0.03	0.04	0.06	0.10	0.13	0.16	0.19	0.24	0.30	0.69				
17	0.02							1.63‡							
19	0.05	0.13		0.46	1.31										
20	0.00	0.02		0.02	0.04		0.06		0.09		0.11	0.12	0.13	0.13	0.14

‡‡ Kordesch-Marko Bridge, IR-free potentials.

* Open-circuit potential vs the hydrogen electrode in the same solution.

‡ O_2 evolution.

Table A-29

LIFE TESTS OF PALLADIUM HYDROGEN DIFFUSION ELECTRODES USING N_2H_4 FUEL

Electrode: Pd-25%Ag Foil, 1 mil thick, prepared as specified in Table 12

Electrolyte: 5M KOH

Fuel: 100% N_2H_4

Temperature: 90°C

Foil No.	Anode Current Density, ma/cm^2	Testing Period, hr	Initial* Potential, volts	Final* Potential, volts
13†	250	18	0.30	1.65‡
14	40	43	0.09	0.28
	100(a)	69	0.31	0.13
15	40(b)	46	0.15	0.15
16	40	48	0.02	0.00
	100(c)	69	0.01	0.01
18	40(d)	30	0.59	1.51‡
20	250	54	0.15	0.35

* Over-potential of the electrode vs the hydrogen electrode in the same solution.

† Rh black was plated again after the determination of polarization curve, because a large part of Rh black came off from the fuel side.

‡ O_2 evolution during the night.

(a) The current was increased to 100 ma/cm^2, immediately after the test at 40 ma/cm^2 was ended. The over-potential dropped to 0.14 volt after 4 hours and stayed constant thereafter.

(b) Rh plating came off at about 48 hours and O_2 evolution started.

(c) 100 ma/cm^2 was passed immediately after the end of the 40 ma/cm^2 test.

(d) Rh plating completely fell off from the electrode during the night.

After the tests, the electrodes were examined under an optical microscope. Some of the electrodes that were tested for a long time and that still showed very active potentials at the end of the test period showed microcrack formation along the Teflon O-ring seal. The cracks penetrated intergranularly toward the middle of the electrode. Some unsuccessful attempts were made to eliminate the crack formation by decreasing the pressure at the contact with a thin elastic washer underneath the O-ring, by using a larger O-ring, or by using a synthetic rubber O-ring. A very small amount of stress apparently was sufficient to cause this stress corrosion cracking, because saturation of the electrode with hydrogen probably accentuated crack formation. In other words, the phenomenon can be interpreted as hydrogen cracking under stressed condition.

4. Conclusions

(a) Among those tested, the most promising Pd-25%Ag electrodes using hydrazine as a fuel included those coated with rhodium black on the electrolyte side and with either rhodium or cobalt black on the fuel side. The steps for preparing these electrodes were: full annealing, plating, diffusion, and oxidation in pure oxygen at 850°C and subsequently at 700°C for two hours each for rhodium or 10 minutes each for cobalt.

(b) The life of the hydrazine electrode is limited to approximately two to three days at 100 ma/cm^2 because of stress cracking beneath the O-ring gasket, in conjunction with hydrogen saturation; in other words, hydrogen cracking under stressed condition. This limitation is imposed by the test half-cell construction and it is expected that the problem will not be encountered when the foils are installed in the 3 x 3 in. full-cell design.

M. GENERAL CONCLUSIONS

(1) For both fuels, hydrogen gas and hydrazine, the best electrode, both in terms of life and anodic polarization characteristics, found to date is prepared by the following process: full annealing, rhodium black plating, and oxidation in pure oxygen at 850°C (perhaps followed by the further oxidation at 700°C in oxygen). This electrode can carry a substantial current density with hydrogen gas fuel for more than two weeks.

(2) The electrodes tested with hydrazine showed severe cracking after a certain period of polarization. This behavior was apparently a kind of hydrogen cracking under an external stress, mainly due to the configuration of the cell assemblies.

(3) The optimum condition for rhodium black plating is the cathodic current density of 125 ma/cm^2 in 0.01M $RhCl_3$ adjusted to pH 1.

(4) The amount of rhodium has no restriction in the range of 0.5 to 3.5 mg/cm^2.

(5) Alloying Pd-25%Ag foils with high valency metals (iridium, ruthenium, platinum, titanium, and rhodium) improves anodic polarization characteristics. Alloying with low valency metals (silver and copper) is deleterious to anodic polarization characteristics.

(6) Alloying Pd-25%Ag foils with exothermic hydrogen occluders improves the electrode performance.

(7) The effect of alloying the Pd-25%Ag foil on the fuel side is independent of the effect of alloying on the electrolyte side.

(8) Alloying elements that improved the electrode performance most significantly include:

Fuel side:	platinum, iridium, and cobalt
Electrolyte side:	rhodium, iridium, and nickel-zirconium
Both sides together:	platinum, rhodium, and iridium

(9) The structure type of an oxide (whether the n- or p-type) is the property that most strongly affects the anodic polarization characteristics of a Pd-25%Ag foil when the oxide is applied to the surface of the foil

Some of the best oxides to improve the electrode are:

Fuel side:	thorium, copper, ruthenium, and magnesium
Electrolyte side:	nickel, platinum, and rhodium
Both sides together:	platinum, rhodium, ruthenium, and nickel

(10) Heat treating foils in a hydrogen atmosphere degrades the electrodes by reducing the palladium oxide catalytic film.

(11) Substitution of palladium oxide by rhodium oxide (perhaps Rh_2O_3) as a catalyst prolongs the life of the Pd-25%Ag electrode more than 30 fold.

(12) Palladium-25% silver electrodes oxidized in pure oxygen show better performance than those oxidized in air, although there is some sacrifice in the polarization characteristics for a short period.

(13) Metallographic examination and electron microprobe analyses indicate that the diffusion rates of alloying elements vary widely so that alloys of some elements are satisfactorily prepared while other elements fail to alloy.

(14) Thick oxide films formed by temperature cycling do not improve electrode characteristics. Polarization was actually more severe at high current densities for the thick oxide electrodes.

(15) Palladium-25% silver, alloyed with 10% platinum, showed the similar capability for occlusion and diffusion of hydrogen as Pd-25%Ag, so the platinum alloy can be used in a proper acid electrolyte system containing nitric acid because of its resistance to oxidizing acids.

Sulfur dioxide gas in an oxidizing atmosphere poisons the Pd-25%Ag electrode.

APPENDIX IV

FULL CELL TESTING

A. CONTAINED ACID FULL CELL TESTING AND CHARACTERIZATION

This appendix presents the details of the contained acid electrolyte full cell testing. The specifications for each individual cell have been summarized in Table 8 in the body of the report.

1. Cell 61896 (N_2O_4/N_2H_4)

This cell had discharged at 0.62-0.70 v, 100 ma/cm^2, 60-90°C, for approximately 150 hours (to 13 November 1964) when Kel-F oil from the N_2O_4 flow meter destroyed the cathode activity by pore blockage. The electrical performance had been uniform over the life of the cell (see Figure A-53). Catalytic activity of the electrodes was essentially no different after 129 hours at 100 ma/cm^2 (see Figure A-54).

2. Cell 65113 (N_2H_4/N_2O_4 Acid)

This cell had been operated for 110 hours (to 1 December 1964) at 60-90°C, 100 ma/cm^2, with terminal voltage between 0.61 and 0.68 v. At that time relatively large accumulations of electrolyte in the cathode water trap indicated leakage through the electrodes. The cell was disassembled and examined. The leakage was caused by cracks and blisters in the electrodes, which corresponded exactly with the manifold slots in the cell electrode holder. We developed a two-screen electrode structure that gave sufficient support to the electrode to prevent similar accidents in later cells. A polarization curve for this cell is shown in Figure A-55. The operating characteristics of this cell were thoroughly characterized before the cathode leak occurred.

The objective of this investigation was to discover and optimize the factors controlling cell performance, and to obtain data for the NASA 1-kw N_2H_4/HNO_3-N_2O_4 system design.

a. Temperature

The effect of temperature on cell performance is shown in Figure A-56. In general, the best results were obtained at 90°C. Both the anode and the cathode improved with increasing temperature. It should be noted that these results refer only to short-term tests. For longer operation, the effects of high temperature on materials of construction and electrode degradation should be considered.

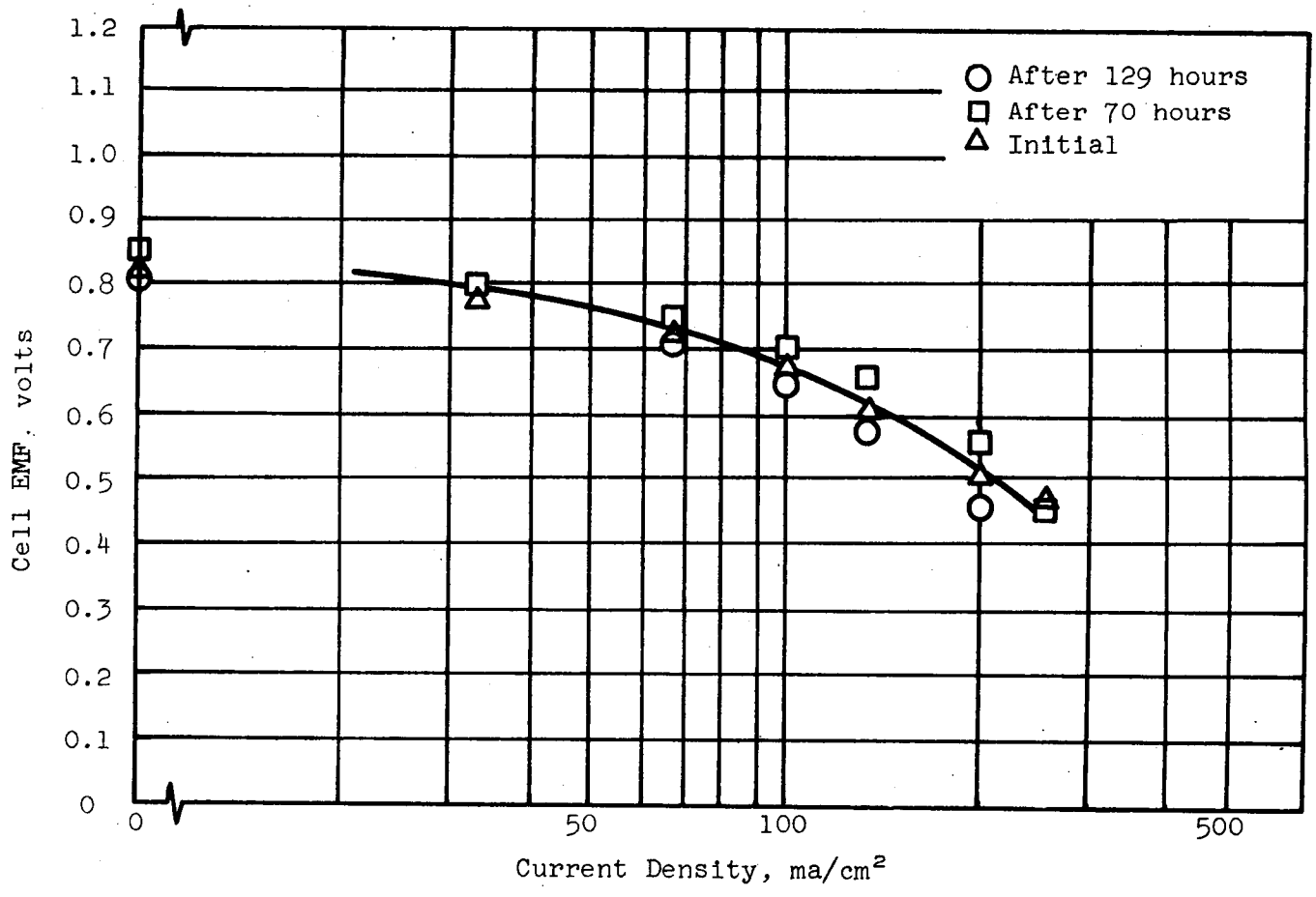

Anode:	20 mg Pt/cm² on 80 mesh Stainless Steel screen	Oxidant:	N_2O_4 gas
Cathode:	20 mil Carbon on 30 mesh Stainless Steel screen	Separator:	Santocel FRC-H_3PO_4 Gel
Fuel:	3M N_2H_4 in 5M H_3PO_4	Electrolyte:	5M H_3PO_4
		Temperature:	90°C

Figure A-53. Polarization vs Cell Life for Full Cell 61896 (N_2O_4/N_2H_4)

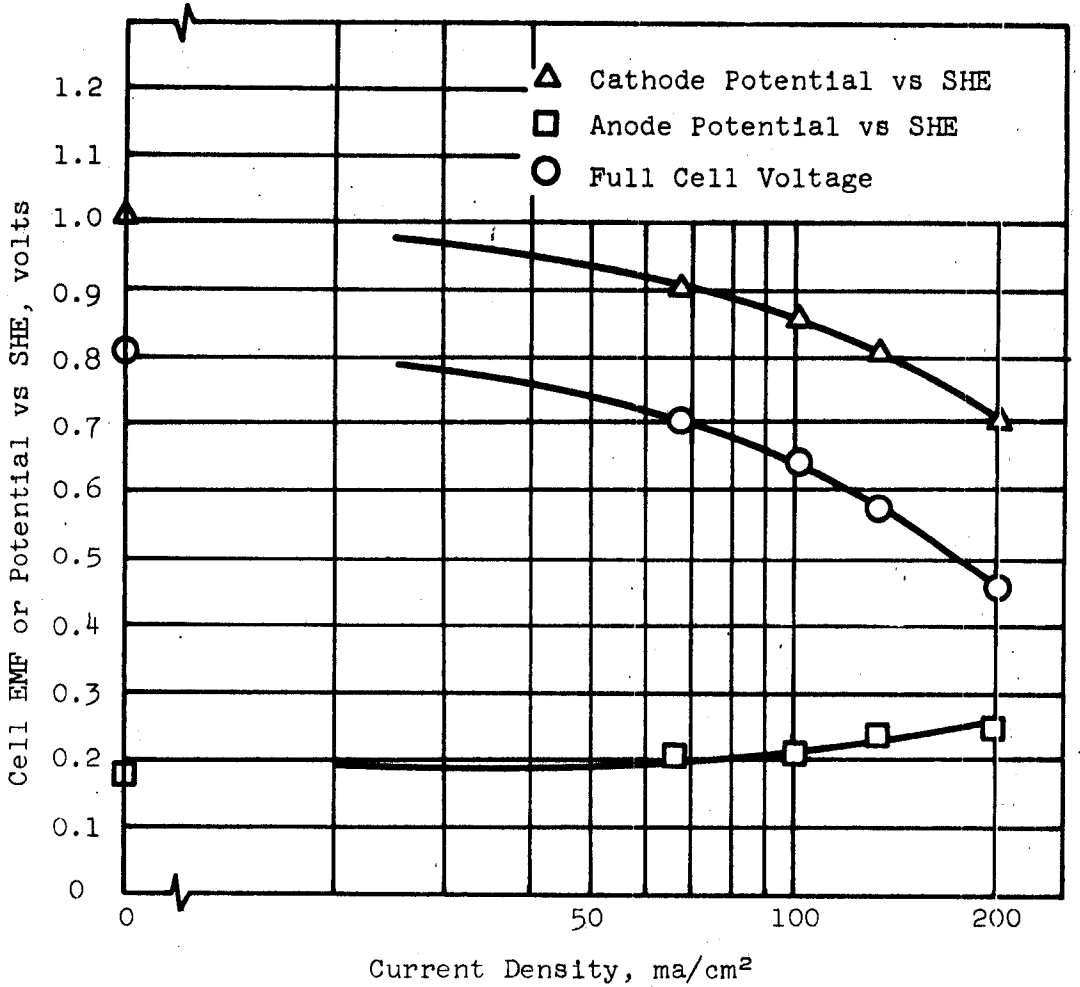

Anode: 20 mg Pt/cm² on 80 mesh Stainless Steel screen
Cathode: 20 mil Carbon on 30 mesh Stainless Steel screen
Fuel: 3M N_2H_4 in 5M H_3PO_4
Temperature: 90°C

Oxidant: N_2O_4 gas
Separator: Santocel FRC-H_3PO_4 Gel
Electrolyte: 5M H_3PO_4
Time: After 129 hours at 60-90°C and 100 ma/cm²

Figure A-54. Polarization Characteristics of Full Cell 61896 (N_2O_4/N_2H_4)

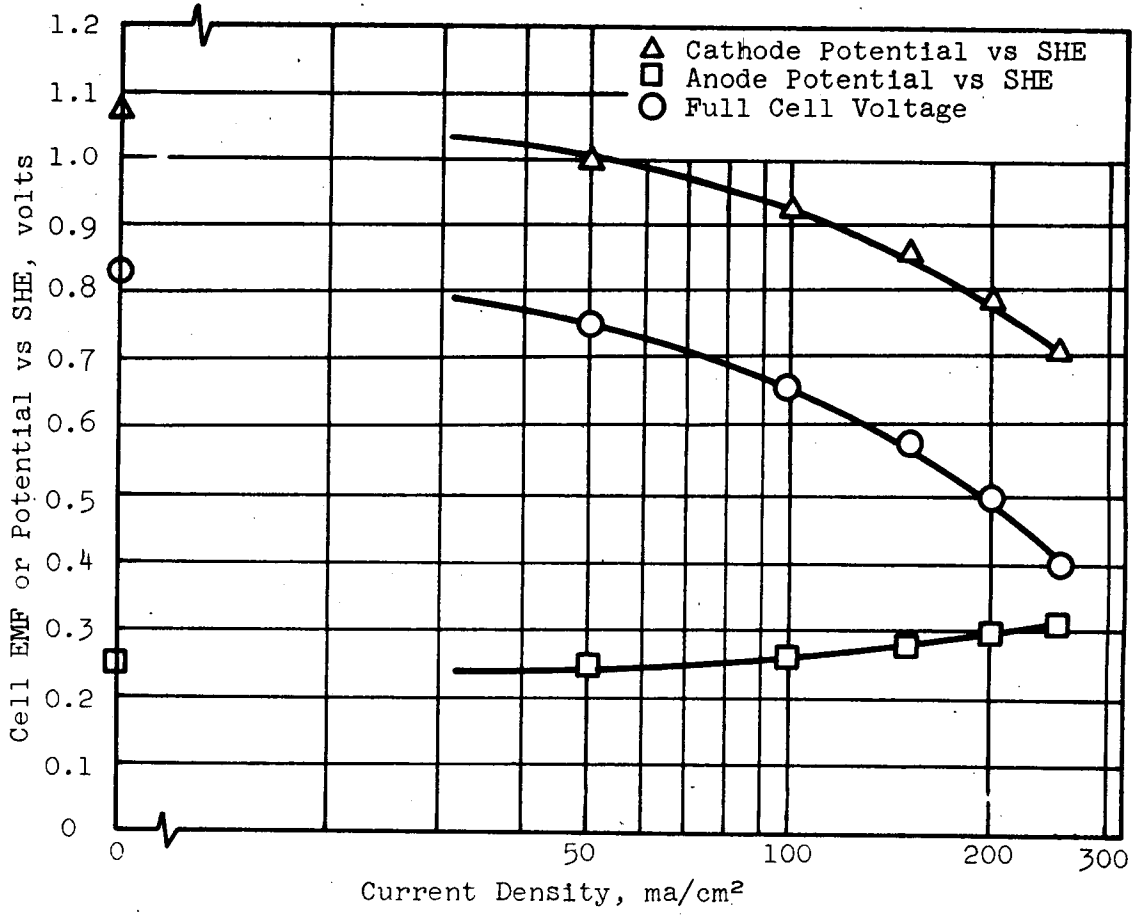

Cathode: 20 mil Carbon on 30 mesh Stainless Steel screen
Anode: 20 mg Pt/cm² on 80 mesh Stainless Steel screen
Fuel: 3M N_2H_4 in 5M H_3PO_4

Oxidant: N_2O_4 gas
Separator: Santocel FRC-H_3PO_4 Gel
Electrolyte: 5M H_3PO_4
Temperature: 90°C
Time: After 30 hours at 70-90°C, 100 ma/cm²

Figure A-55. Polarization Curve, Full Cell 65113 (N_2O_4/N_2H_4)

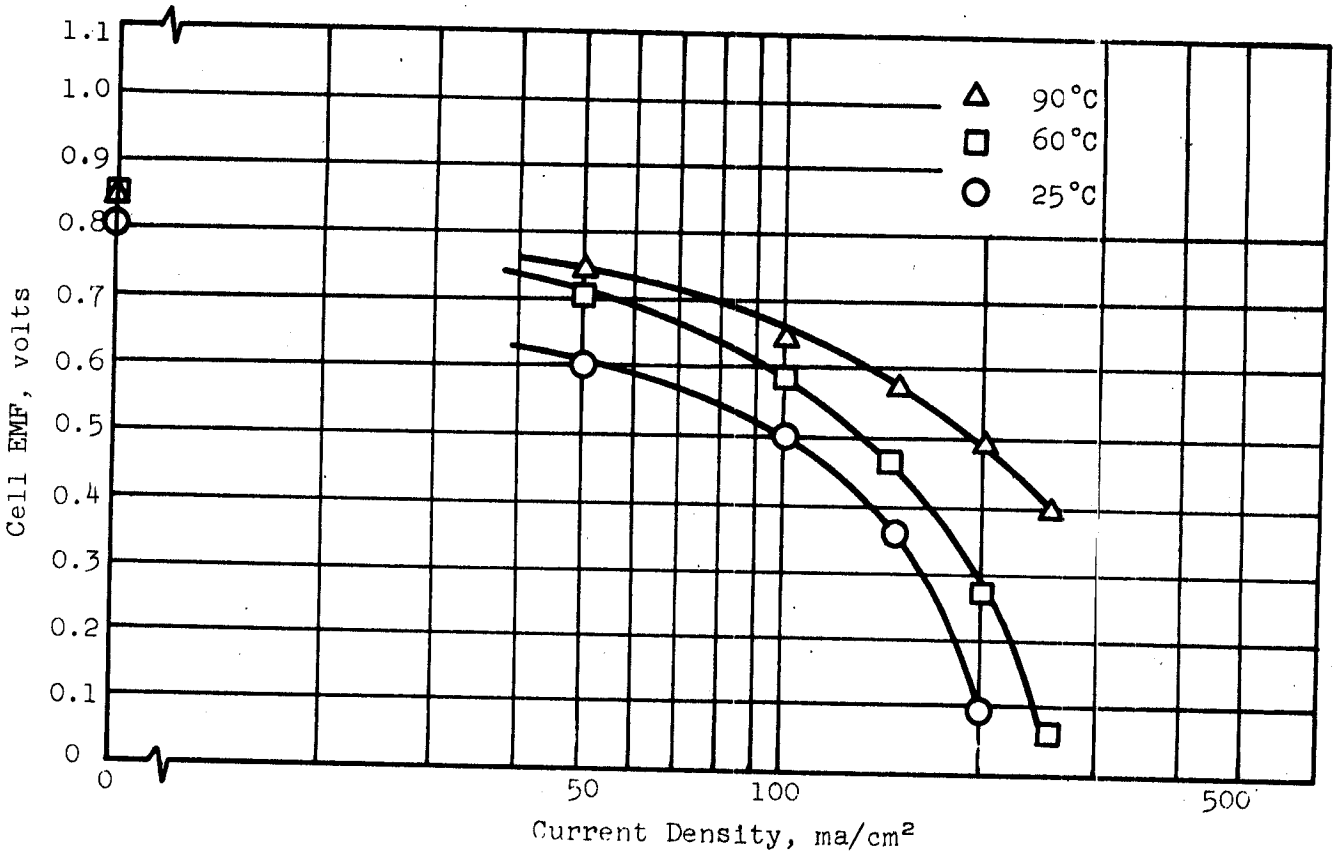

Cathode: MRD-C No. 9(2)
20 mil Carbon on 30 mesh
Stainless Steel screen
Anode: MRD-A No. 22-101464
20 mg Pt/cm² on 80 mesh
Stainless Steel screen
Anolyte Flow Rate: 132 ml/min

Oxidant: N_2O_4 gas
N_2O_4 Flow Rate: 34 mg/cm²-min
N_2O_4 Pressure: 5.4 in. H_2O
Separator: Santocel FRC-H_3PO_4 Gel
Electrolyte: 5M H_3PO_4
Fuel: 3M N_2H_4 in 5M H_3PO_4

Figure A-56. Polarization as a Function of Temperature, Full Cell 65113 (N_2O_4/N_2H_4)

b. N_2O_4 Flow Rate and Pressure

Figure A-57 presents evidence that high N_2O_4 flow rates are essential for high current operation. Removal of product water and NO is believed to be the important function. The results of a designed experiment, given in Table A-30, show that: (1) flow rates greater than 8.6 mg N_2O_4/cm^2-min are required at a current density of 100 ma/cm^2 (all cathode potentials are too low); (2) pressures up to 16.1 in. of water do not improve performance. The effect of higher flow rates is shown in Figure A-57. The data indicate a minimum rate of 34 mg N_2O_4/cm^2-min at current densities above 100 ma/cm^2. Product removal is undoubtedly the function of the N_2O_4 purge. Therefore, proper design of cell manifolds and electrodes to give high local gas velocities should greatly reduce the minimum flow rate required.

c. N_2H_4 Concentration and Anolyte Flow Rate

The effect of N_2H_4 concentration is illustrated in Figure A-58. Optimum performance is obtained with 3M N_2H_4, and this concentration has been used for all life tests to date. The higher anolyte pumping rate improved performance (see Figure A-59). The "gas lift" rate refers to an unpumped natural convection due to escape of nitrogen gas and thermal convection. The principal effect is undoubtedly removal of reaction products, so redesigning manifolds and electrodes will probably improve the gas lift rate.

d. Material Balance

The material efficiencies were calculated by assuming the following reactions:

$$\text{Overall} - N_2O_4 + N_2H_4 = 2NO + N_2 + 2H_2O$$

$$\text{Cathode} - N_2O_4 + 4H^+ + 4e^- = 2NO + 2H_2O$$

$$\text{Anode} - N_2H_4 = N_2 + 4H^+ + 4e^-$$

The electrochemical equivalents for the reactants are 0.85 g N_2O_4/amp-hr and 0.299 g N_2H_4/amp-hr.

At a flow rate of 2.0 g N_2O_4/min (34 mg N_2O_4/cm^2-min) the N_2O_4 material efficiency is 4.3%.

For N_2H_4 utilization, two duplicate runs of about 6 hours at 100 ma/cm^2 were made and N_2H_4 concentrations were analyzed. The N_2H_4 material efficiency averaged 35.4%. We believe the loss in calculated efficiency was caused by:

(1) Catalytic decomposition of N_2H_4 at the electrode. Lower operating temperatures and further optimization of electrodes should reduce this effect.

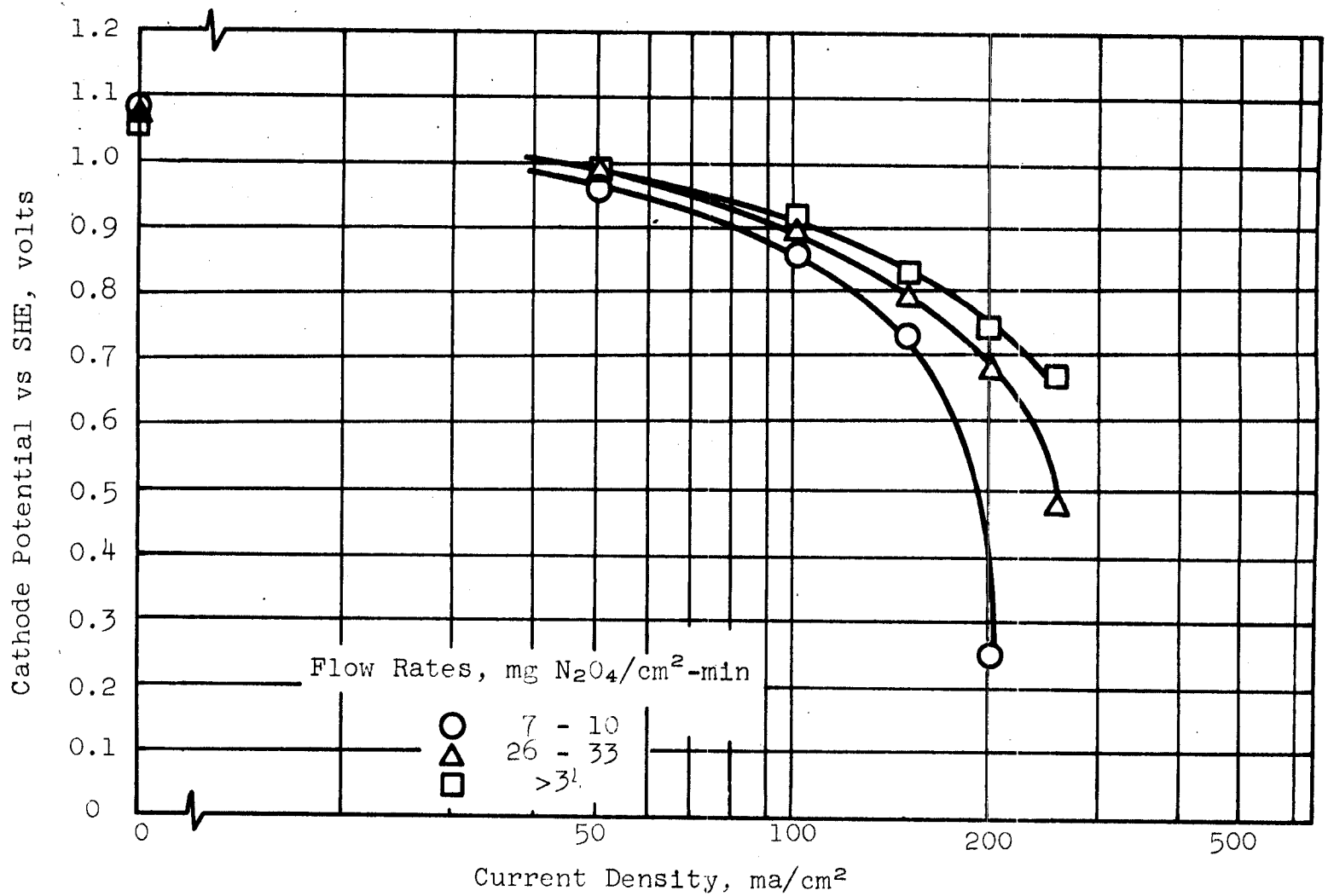

Fuel: 3M N_2H_4 in 5M H_3PO_4
Oxidant: N_2O_4 gas
N_2O_4 Pressure: 5.4 in. H_2O

Temperature: 90°C
Flow Rates determined by adsorption of gas into KOH

Figure A-57. Effect of N_2O_4 Flow Rate on Cathode Polarization, Full Cell 65113

Table A-30

EFFECT OF N_2O_4 PRESSURE AND FLOW RATE

Full Cell No. 65113 described previously

Fuel: 3M N_2H_4 in 5M H_3PO_4
Oxidant: N_2O_4 gas
Temperature: 90°C
Flow Rates - measured by calibrated Kel-F Oil Flowmeter
Pressure - varied by Kel-F Oil Manostats

Data are cathode potentials vs SHE in volts after 5 min at 100 ma/cm^2.

Flow Rate, mg N_2O_4/cm^2-min	N_2O_4 Pressure, in. of H_2O 5.4	10.7	16.1	Flow Rate Averages
1.7	0.75	0.80	0.74	0.76
5.2	0.81	0.81	0.81	0.81
8.6	0.85	0.84	0.76	0.82
Pressure Averages	0.80	0.82	0.77	

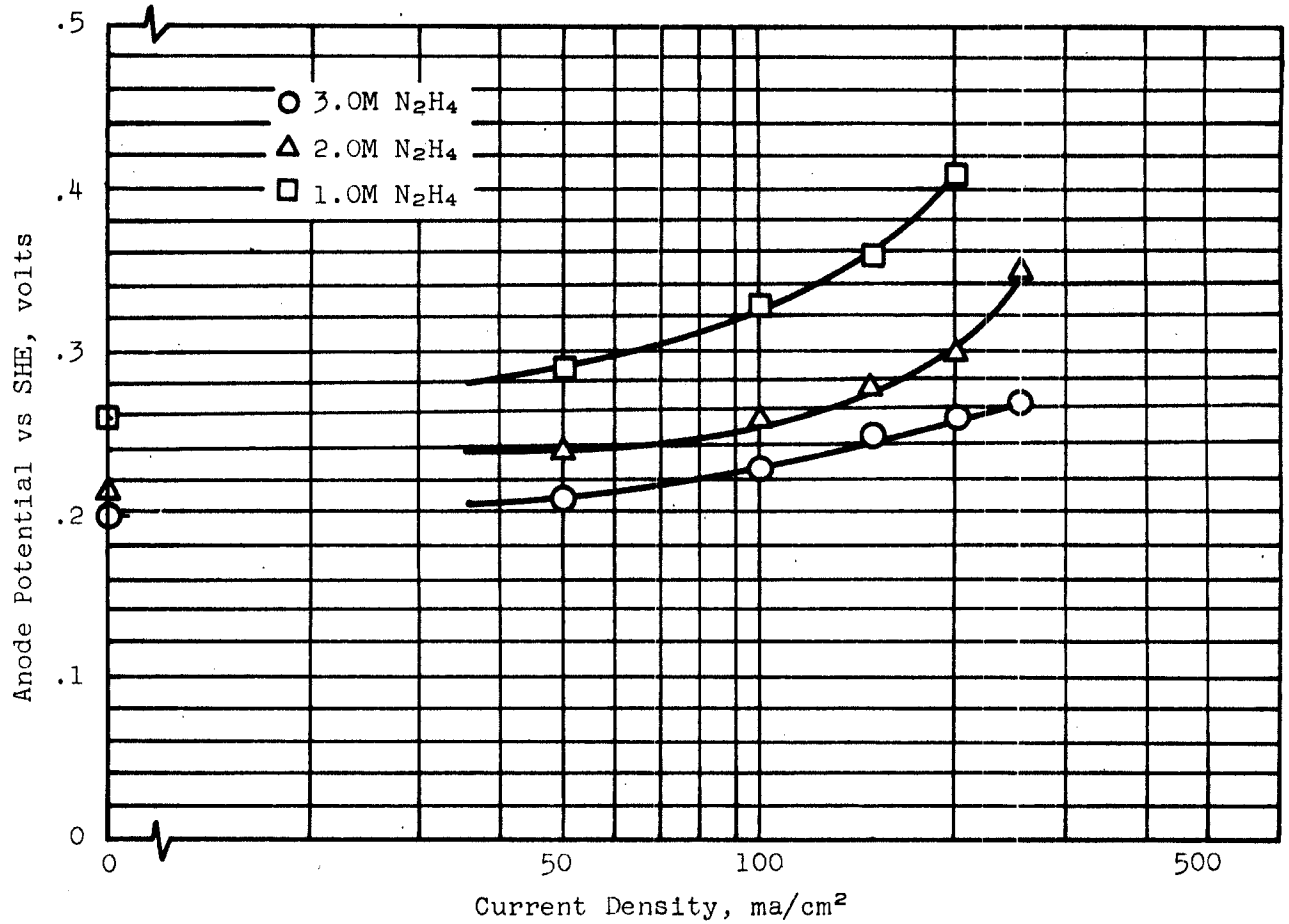

Fuel: 1-3M N_2H_4 in 5M H_3PO_4
Anolyte Flow Rate: 250 ml/min
Temperature: 90°C

Oxidant: N_2O_4 gas
N_2O_4 Flow Rate above 34 mg/cm²-min

Figure A-58. Effect of N_2H_4 Concentration on Anode Polarization, Full Cell 65113

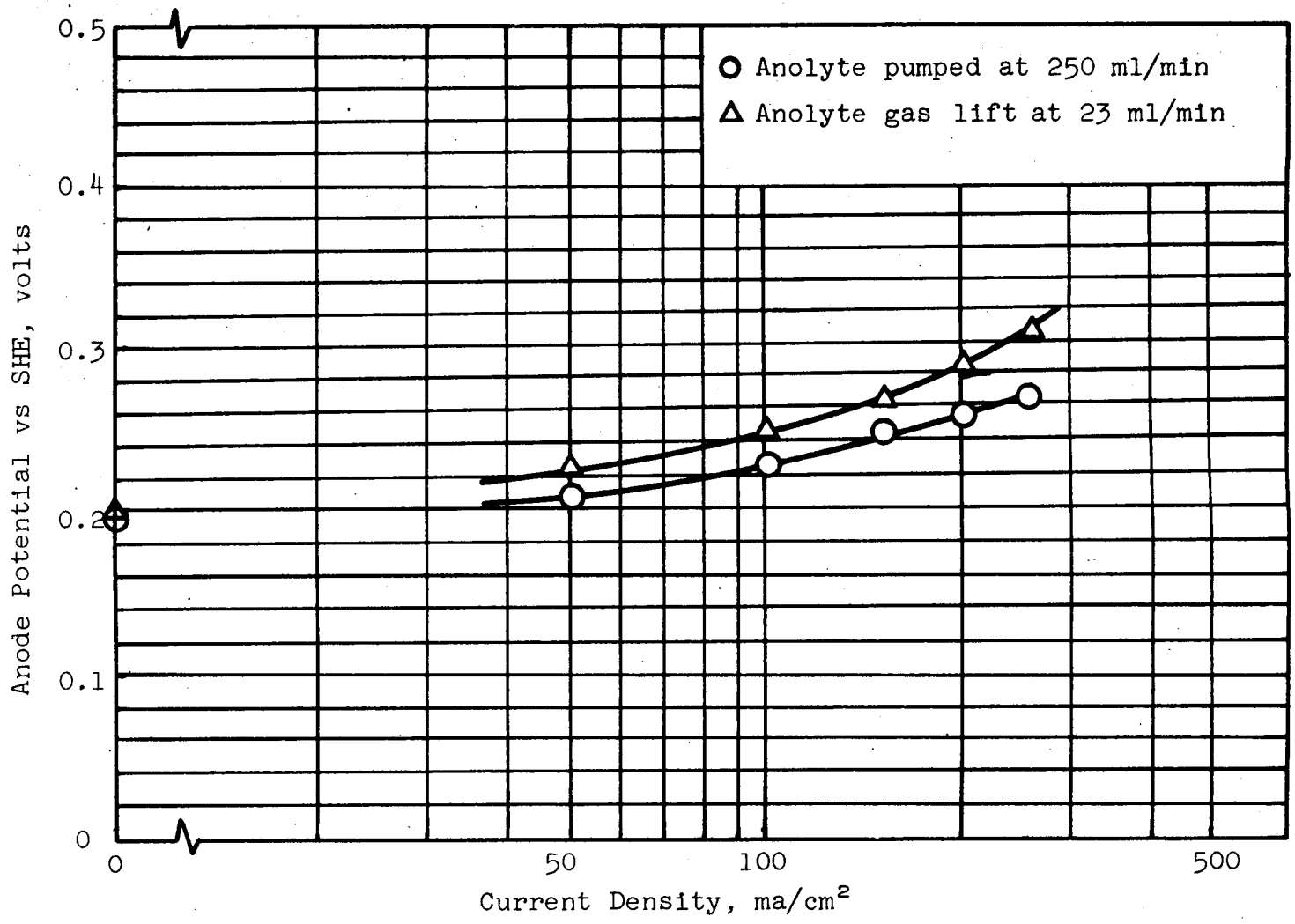

Fuel: 3M N_2H_4 in 5M H_3PO_4 Oxidant: N_2O_4 gas
Temperature: 90°C N_2O_4 Flow Rate above 34 mg/cm²-min

Figure A-59. Effect of Anolyte Pumping Rate on Anode Polarization, Full Cell 65113

(2) Dilution of anolyte by product water. No correction was made for this effect in the calculations.

(3) Cross contamination and in situ reaction of N_2O_4 and N_2H_4. Better diffusional control would reduce this effect.

(4) Evaporation losses despite the condenser. More efficient condenser design would eliminate this effect.

3. Cell 65105 (N_2O_4/N_2H_4)

We constructed cell 65105 to test a rhodium-catalyzed anode. Earlier half-cell work (Table A-6) indicated rhodium to be a better anode catalyst than platinum in electrolytes uncontaminated with nitric acid.

The polarization curve for this cell at 60°C has been given in Figure 15 in the body of the report. Although the cathode polarized more than expected, the anode potential is at least 0.10 v better than the platinum-catalyzed anodes have been at this temperature. The cell was operated for one hour at 90°C, 100 ma/cm^2, 0.76-0.70 v. The cell failed because of separator wash-out caused by anolyte leaks through cracks in the anode. The subsequent high N_2H_4 concentration caused deterioration of the cathode potential. The rhodium-catalyzed electrode had a greater tendency to crack during fabrication than similar platinum electrodes; however, the problem is mechanical and can be worked out with improvements in formulations and techniques.

4. Cell 65129

This cell was constructed mainly to run short-term tests on Aerozine-50 and a new cathode configuration. The results of the Aerozine-50 testing have been given in Figure 14 in the body of the report.

Improved cathode performance has resulted from electrodes made by pressing two single layer carbon MRD-C electrodes (3 x 3 in.) together at 2660 lb/in.^{2} This type cathode has been partially characterized. The results are given below.

a. Effect of N_2O_4 Flow Rate on Cathode Polarization

Although quantitative measurements have not been completed, this type electrode appears to operate satisfactorily with lower N_2O_4 flow rates than unpressed double carbon electrodes. Preliminary measurements indicate a rate of 22 mg N_2O_4/min-cm^2 is satisfactory for operation above 100 ma/cm^2. This represents a cathode current efficiency of 7.7%, compared to 4.3% found with unpressed double carbon cathodes (see Fig. A-57).

b. Effect of NO Concentration on Cathode Polarization

To operate efficiently a cathode gas recirculation system is probably necessary (Appendix X). Product NO will gradually accumulate in such a system and the cathode must tolerate relatively large NO concentrations if the system is to be feasible. The effects of NO concentration are shown in Figure 12 in the body of the report. Volume concentrations up to 50% NO can be tolerated with little reduction in performance.

c. Effect of Temperature on Cathode Polarization

Figure A-60 illustrates the performance of the pressed double carbon cathodes at different temperatures. The relatively good performance at the lower temperatures appears to be one of the desirable characteristics of this electrode; consequently an extended capability is possible at lower temperatures. It should be noted that all anodes tested to date steadily improve with increasing temperature.

5. Cell 65121 (N_2H_4/N_2O_4 Acid)

This cell has operated for 645 hours (to 1 February 1965) at 60°C, 100 ma/cm^2, with terminal voltage between 0.66 and 0.74 v. The cell was constructed with a cathode made by pressing two single carbon MDC electrodes (3 x 3 in.) together at 2660 lb/in.^{2} The pressing operation gave better diffusion control and resulted in more efficient cathode performance. Polarization characteristics have been shown in Figure 11 in the body of the report. Full cell polarization as a function of temperature has been given in Figure 13.

B. CONTAINED BASIC ELECTROLYTE FULL CELLS (EARLY WORK)

1. Hydrogen Peroxide-Hydrogen Cell

A complete cell using a PTVDE cathode with hydrogen peroxide and a rhodium-catalyzed palladium anode with 85% hydrazine hydrate is shown in Figure 3 . The electrolyte compartment was made by combining three silicone rubber gaskets with a gas vent in the middle. The separation between electrodes was about 3 mm. The electrolyte was 5M potassium hydroxide. Data for two such cells are listed in Table A-31. The cell resistance in ohm-cm^2 was determined by dividing the IR drop across the cell by the current density. The IR drop was taken as the difference between the cell voltage and the Kordesch-Marko bridge voltage (IR-free). The cell resistance values of 2 to 3 ohm-cm^2 are larger than the calculated resistance for 3 mm of 5M potassium hydroxide at 30 and 50°C (0.4 ohm-cm^2 and 0.3 ohm-cm^2, respectively)*, so our measured values may include contact resistances.

* Lange's Handbook of Chemistry; Calculated from data listed at 15°C using a 2% per degree temperature correction.

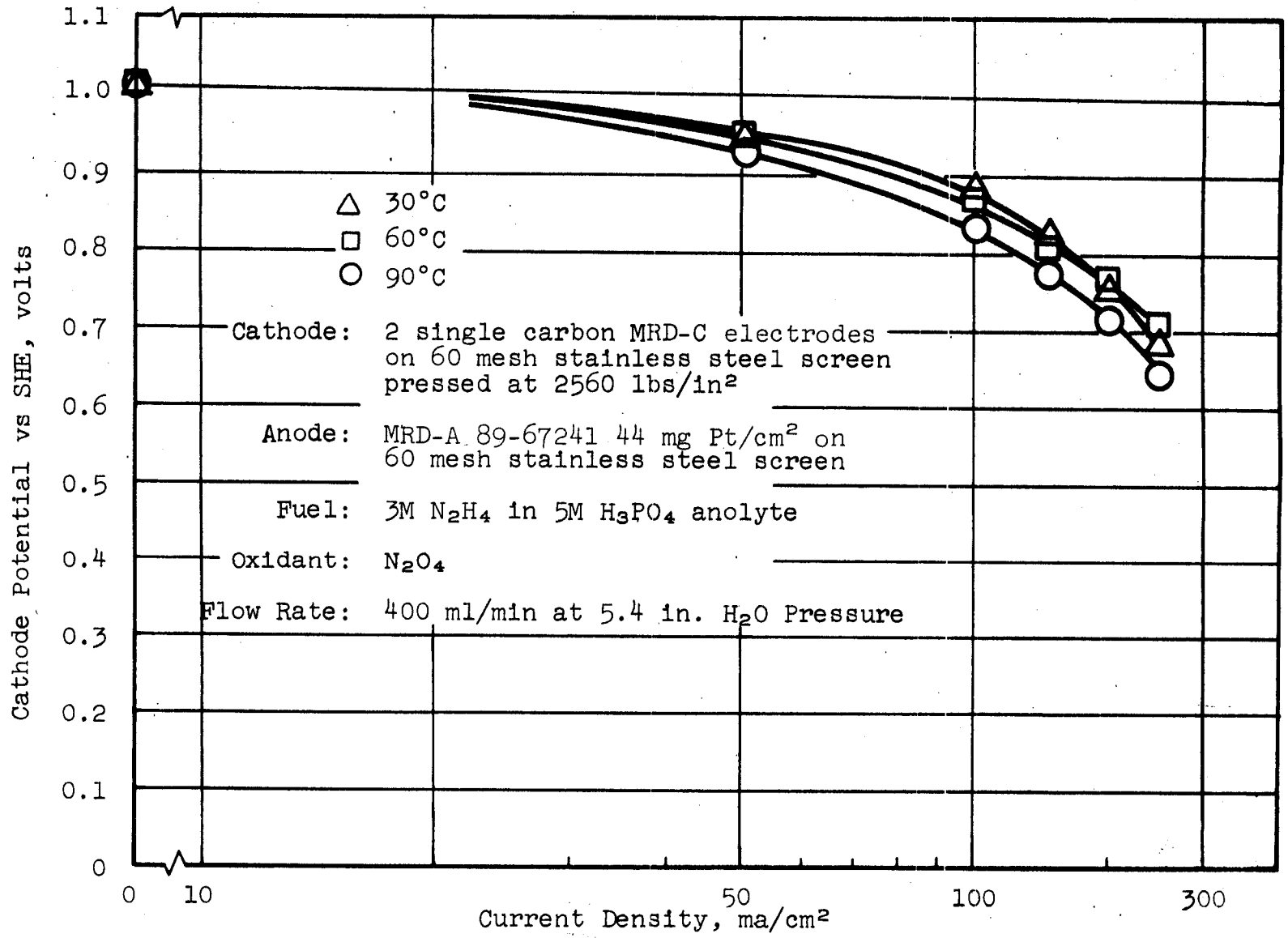

Figure A-60. Effect of Temperature on Cathode Polarization Full Cell 65129 (N_2H_4/N_2O_4)

Table A-31

HYDRAZINE-HYDROGEN PEROXIDE FULL CELL PERFORMANCE

Fuel: 85% Hydrazine Hydrate
Anode: Palladium Membrane
Cathode: PTVDE, 50 mg Pt/cm²
Oxidant: 30% H_2O_2
Temperature: 35°C - 50°C
Electrolyte: 5M KOH

	Cell I				Cell II			
Current Density ma/cm²	V_{k-m}	V_{IR}	IR drop	Resistance ohms-cm²	V_{k-m}	V_{IR}	IR drop	Resistance ohms-cm²
0	---	0.99	---	-------	----	1.00	----	-----
2	0.93	0.91	0.02		0.975	0.96	0.015	7.5
4	0.92	0.91	0.01		0.96	0.945	0.015	3.75
8	0.89	0.865	0.025	3.1	0.92	0.89	0.030	3.75
12	0.88	0.85	0.03	2.5	0.915	0.89	0.025	2.1
20	0.85	0.81	0.04	2.0	0.875	0.845	0.03	1.5
30	0.73	0.67	0.06	2.0	0.76			
40					0.70			
100(max current)					0.15			

No longer using KM Bridge, but loading external resistor.

V_{k-m} is IR free voltage measured on Kordesch-Marko bridge.
V_{IR} is voltage, including IR component, measured directly.

The best cell output, 0.70 volt at 40 ma/cm^2 represented a promising start in full-cell development. Each cell ran for about three hours before severe deterioration. At the time of voltage failure, the peroxide concentration had dropped from 10M to about 2M in the bulk feed solution. Rejuvenation of the peroxide concentration improved the cell performance to close to the original conditions.

2. Oxygen-Hydrogen (or Hydrazine) Cell (3 x 3 in. Electrodes)

Work was started on the construction and testing of fuel cell units with an electrode area of 9 in.^{2} Hydrogen and hydrazine were tested as fuels, and oxygen and hydrogen peroxide were tested as oxidants.

Construction details for the fuel cell have been given in the body of this report. The end plates were made of nickel plated stainless steel. The corrugated structure of the end plate allows uniform reactant distribution while making good electrical contact with the conducting electrode surface. The anode consisted of a solid palladium hydrogen diffusion membrane, 0.001 in. thick, supported on the back side by 0.030 in. thick nickel plaque*. The nickel plaque had a porosity of approximately 75% and so did not seriously affect the ease of fuel transport to the back side of the palladium anode. Both sides of the palladium foil were catalyzed with rhodium by electroplating from a 1% rhodium chloride ($RhCl_3$) solution, adjusted to pH 1 by adding hydrochloric acid. A black coating of rhodium was deposited on the 3 x 3 in. foil by passing a current of 200 to 500 ma between a 1 cm^2 platinum anode and the surface of the palladium foil. The anode was moved manually to different positions close to the foil until the surface was completely darkened. After plating, the palladium was heat treated at 700°C for 1 hour. The palladium foil was reactivated after use by heat treating at 700°C for 2 to 4 hours.

The cathode was made from the same nickel plaque, catalyzed with either platinum or platinum-palladium. Both metals were spontaneously chemiplated on the porous nickel surface from dilute chloride salt solutions. A precious metal loading of 25 mg/in.^{2} was used.

The electrolyte, 5M potassium hydroxide, saturated a 0.030-in. thick asbestos mat which also served to electrically insulate the anode from the cathode. The outside edges of the asbestos mat were sealed with a 100°C melting point wax. The back of one end plate was drilled and fitted with Teflon tubing stuffed with highly compressed asbestos as a Luggin capillary between the back side of the porous electrode and a reference electrode outside of the fuel cell. This reference electrode was used to determine which electrode was polarized after voltage failure during discharge.

---

* Gould National Batteries, Inc., St. Paul, Minnesota.

Results of initial experiments with the palladium membrane fuel cell using oxygen as the oxidizer and hydrogen or hydrazine as the fuel are given in Table A-32. The best power output for the cell was 2.1 watts or 37 mw/cm^2 at 90°C with oxygen and hydrazine. At the end of the test, half-cell measurements showed that the cathode only was appreciably polarized.

An alternate method of preparing the palladium membrane consisted of first heat treating the foil and then electroplating with rhodium. Palladium membranes prepared in this manner were not as good anodes as those made by first plating and then heat treating.

Hydrogen peroxide could be used as an oxidant for only short periods because of the rapid evolution of oxygen when heated in contact with the catalyzed electrodes. For a five minute period, 105 ma/cm^2 was drawn at 0.40 volts. Hydrogen peroxide thus offered a good possibility as an oxidant if spontaneous oxygen release could be controlled.

C. ION EXCHANGE MEMBRANE FULL CELLS - ACID/BASE

1. Background

a. Organic Ion Exchange Membranes

The use of ion exchange membranes (IEM) as so-called "solid electrolytes" is of considerable interest in this program because of the IEM's theoretical ability to isolate noncompatible fuel-oxidizer combinations.

Solid palladium membrane hydrogen diffusion electrodes are not currently available with resistance to the corrosive action of nitric acid oxidant. Therefore, the possibility of using a palladium membrane anode in conjunction with a nitric acid cathode depends on physical separation of anolyte and catholyte. An ion exchange membrane electrolyte with suitable properties could effect this physical separation.

Additionally, the extremely high voltages and low polarization afforded by the acid-base cell (nitric acid catholyte-separator-hydrazine in 5-10M KOH) make this construction of considerable interest. Again, an ion exchange membrane provides the most convenient route to such a construction.

The principal properties required of an IEM for this duty are:

(1) Long-term resistance to nitric acid, and strong base,

(2) Low internal electrical resistance,

(3) Good mechanical strength, and

(4) Moderate heat resistance.

Table A-32

OXYGEN AND HYDROGEN (OR HYDRAZINE) FULL CELL*

Electrolyte - 5M KOH

Temp. °C	Fuel	Current Density ma/cm²	Voltage IR-free volts	Cell Voltage IR-included volts	R ohms-cm²	Cumulative Time hr	Notes
67	H_2	0	--	1.02	--	0	
68	"	1	0.965	0.965			
68	"	1.7	0.965	0.945		0.25	
69	"	3.4	0.92	0.91	2.9		
69	"	6.8	0.865	0.84	3.9	0.50	
70	"	12.1	0.78	0.74	3.3		
73	"	16.6	0.62	0.55	4.2	0.75	P_{O_2} = 10 psig P_{H_2} = 10 psig
74	"	16.6	0.65	0.60	3.0	1.0	Purging H_2 increased output
78	"	16.6	0.78	0.76	1.2	2.0	
83	"	29.6	--	0.60		2.5	Slow H_2 Purge
84	"	36.2	--	0.45		3.0	
80	100% $N_2H_4 \cdot H_2O$	16.6	--	0.78		5.0	
90	"	55	--	0.60		6.0	
90	H_2	43	--	0.50		8.0	Purging H_2
90	"	52	--	0.60		9.5	
30	100% $N_2H_4 \cdot H_2O$	0	--	0.99			
30	"	16.8	0.50	0.38	6.9	10.5	
90	"	57	--	0.65	--	13.0	Cathode** Limiting Cell

*Anode Pd-Ag membrane 3 x 3 x 0.001 inches
Rh plated and heat treated at 600°C

Cathode Ni plaque (Gould) 3 x 3 x 0.030 inches
Pt deposited (25 mg/sq. in.)

Separator Iron-Free Asbestos 0.030 inch thick

**Anode potential was 0.08 vs HE at same pH and Temperature
Cathode potential was 0.71 vs HE at same pH and temperature

Previous work in this laboratory (ref. 24) indicated that some available anion and cation exchange membranes possessed these properties to a limited extent.

The operation of the HNO_3-N_2H_4 cell with an IEM involves transfer of potassium ions from the KOH fuel carrier through the membrane and into the cathode compartment in addition to the cathodic reduction of HNO_3 and the anodic oxidation of N_2H_4. The cell reactions are summarized as follows:

$$\text{Cathode:} \quad 4HNO_3 + 12H^+ + 12e^- \longrightarrow 4NO + 8H_2O \qquad (1)$$

$$\text{Anode:} \quad 3N_2H_4 + 12OH^- \longrightarrow 3N_2 + 12e^- + 12H_2O \qquad (2)$$

$$\text{Cell:} \quad 4HNO_3 + 3N_2H_4 + 12H_2O \longrightarrow 4NO + 20H_2O + 3N_2 \qquad (3)$$

To transfer 12 Faradays of current across the cation exchange membrane (CEM), 12 potassium equivalents must migrate from the anolyte through the cation membrane and into the catholyte:

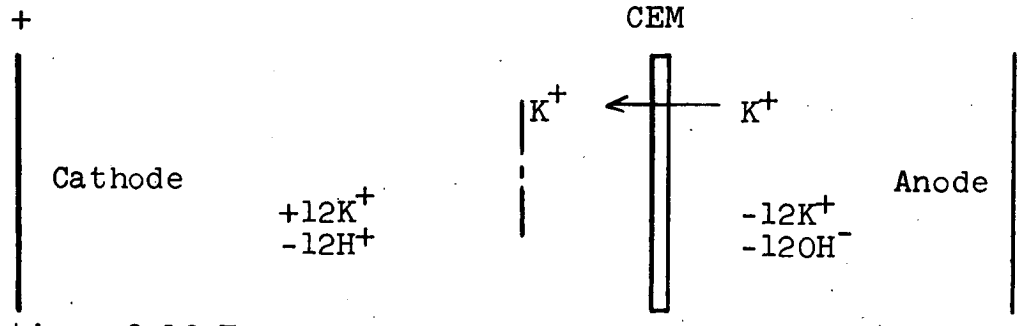

The generation of 12 Faradays of current by reaction (3) by the membrane cell will then require the gain of 12 K^+ and the loss of 12 H^+ in the catholyte and the loss of 12 K^+ and 12 OH^- in the anolyte. This is equivalent to the overall neutralization reaction:

$$12KOH + 12HNO_3 \longrightarrow 12H_2O + 12KNO_3 \qquad (4)$$

Adding equation (4) to equation (3) gives an equation for the complete oxidation, reduction, and neutralization reactions required for cell operation:

$$16HNO_3 + 3N_2H_4 + 12KOH \longrightarrow 4NO + 3N_2 + 12KNO_3 + 20H_2O \qquad (5)$$

$$\Delta F^\circ = -494 \text{ Kcal/g-mole}; \quad E^\circ = 1.78 \text{ v}$$

It is obvious from reaction (5) that large quantities of KOH and HNO_3 are consumed and large amounts of KNO_3 are formed. These factors make it impractical to base a fuel cell system on this reaction. It is obvious that the voltage calculated from ΔF cannot be sustained in a practical cell by using the presently available ion exchange membranes.

b. Zirconium Phosphate Separators

Organic ion exchange membranes have limited life in concentrated acids, bases, or oxidizing agents (ref. 25). Inorganic ion exchangers incorporated in an inert binding fabric may be more durable than organic membranes in contact with corrosive reactants such as HNO_3. Zirconium phosphate has been studied as a cation exchanger (ref. 26, 27, and 28), and several methods of preparing the compound have been described (ref. 26, 27, and 29).

Zirconium phosphate crystals exhibit cation exchange properties and are reported to be stable in strong acid (13M HNO_3) and also in base up to a pH of at least 13 (ref. 26).

2. Method

a. Cell Description

Full cell evaluation of cation exchange membranes was conducted using an adaptation of the 3 x 3 in. cell construction described previously.

All membranes were obtained from commercial sources. Ion exchange membranes were cut to 5 x 5 in. dimensions and punched to accommodate the end plate bolts. Each membrane served as its own gasket to seal the cell.

The palladized nickel anode was selected because of its high activity and relative economy. Furthermore, failure of the IEM would be readily apparent from appearance of nickel nitrate byproduct resulting from HNO_3 attack on the anode.

In all cases, the fuel/potassium hydroxide (KOH) mixture was pumped through the anode cavity at a rate of approximately 200 cc/min.

Cell temperature was maintained by heating the fuel/base mixture in the fuel tank, with anolyte recirculation providing adequate heat transfer to the cell. Nitric acid was circulated either by pumping or by a gas lift energized by byproduct NO. Concentration of the HNO_3 stream was allowed to decrease from 15M to a minimum of 5M, at which point the entire oxidizer charge was replaced.

Because both anode and cathode characteristics were well defined, complete polarization data on each cell were not taken. Runs were made at the maximum current density consistent with voltage stability. Load for the cell was provided either by a resistor or dc power supply.

The full cell reactant handling system has been shown schematically in Figure A-61 for the case where oxidant is circulated by gas lift.

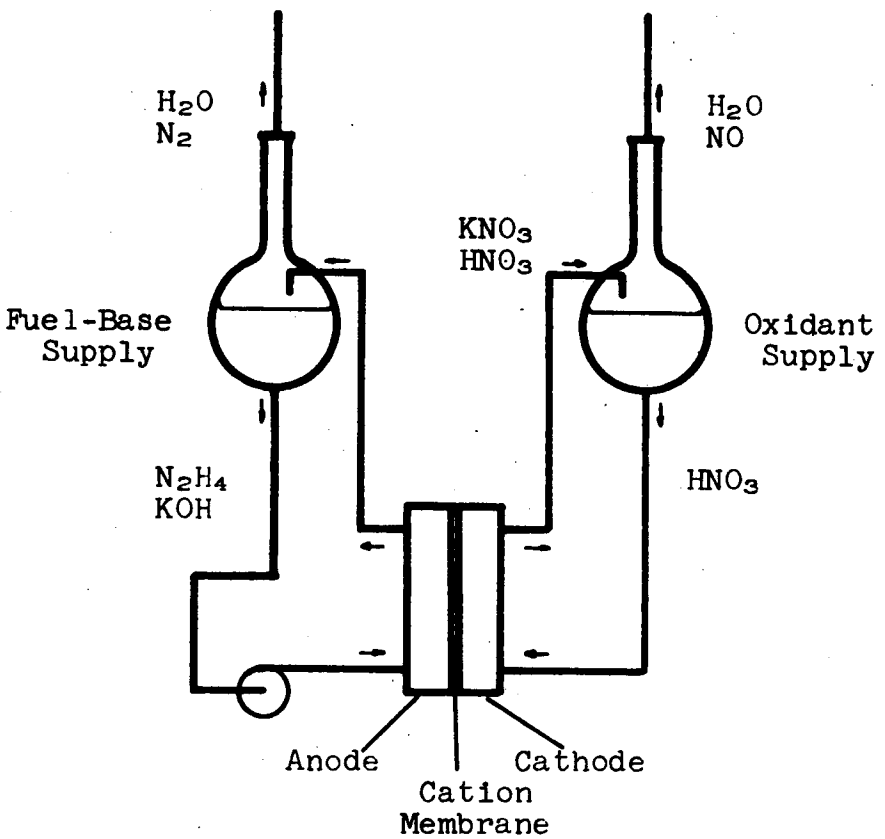

Figure A-61. Fuel Cell and Pumping System

b. Zirconium Phosphate Separators

Zirconium phosphate was prepared by mixing either zirconium sulfate or zirconyl chloride with H_3PO_4. The washed precipitate was pressed between two sheets of Teflon felt at 800 psig, 220°F, for 1 hour. A flexible, integral cation exchange separator resulted. This separator was incorporated into Cell 61507, listed in Table A-33.

3. Results and Discussion

Table A-33 summarizes construction and operation of the types of ion exchange membrane cells studied during this quarter.

a. N_2H_4 | Pd(Rh) | CEM | Pt | HNO_3 (Cell 54905)

The rapid deterioration of the palladium membrane anode by HNO_3 attack indicates the need for an IEM completely inpervious to acid back leakage. This leakage occurred with relatively dilute HNO_3 catholyte (5M).

Despite the failure, the good initial open circuit voltage (OCV) and total polarization of only 0.2 volt from actual OCV at 70 ma/cm^2 and 30°C are indicative of reasonable performance to be expected from suitably protected palladium membrane anodes.

b. N_2H_4 (in KOH) | Ni(Pd) | CEM | Pt | HNO_3 (Cell 54906 and 54918)

This cell is characteristic of the performance of the Ionics 61AZ2-183 cation exchange membrane. Figure A-62 illustrates the degree of polarization and power density with increasing current density. Electrical performance is adequate, but the membrane's poor resistance to HNO_3 limits the effective life of the cell to 7-12 hours.

The fresh membrane material used in Cell 54918 performed similarly to the older material used in Cell 54906.

c. Porous Fiber Mat

To protect the cation exchange membrane from direct contact with HNO_3, a series of cells was constructed incorporating a porous fiber mat between the cathode and IEM. Hopefully, potassium ions migrating through the membrane would react with NO_3^- ions to form a layer of KNO_3, which would be retained in the porous mat material. This salt layer would effectively limit access of HNO_3 to the IEM surface. A decrease in electrical performance was expected because of the increased IR drop resulting from the extra distance between electrodes and the higher resistance of the KNO_3 solution.

Table A-33

SUMMARY OF ION EXCHANGE MEMBRANE FULL CELLS

Electrode Area: 9 in.^{2}

Cell No.	Anode	Cathode	Membrane	Fuel	Oxidant	Performance Summary	Notes
54905	1.0 mil thick Pd foil Rhodium plated, heated to 650°C	Platinized 100-mesh 5 mil Platinum screen supported on 22 mil thick 304SS expanded metal.	Ionics, Inc.*, 61AZ2-183 cation exchange membrane	85% $N_2H_4 \cdot H_2O$	5M HNO_3	OCV = 1.0 volt Life = 10 min Temperature = 30°C E_{cell} = 0.8 volt	Acid penetrated pinholes in IEM and attacked Pd anode.
54906	25 mil thick Gould** nickel plaque, 20 mg/in.^{2} Pd catalyst	Duplicate of 54905	Duplicate of 54905	1M N_2H_4 in 5M KOH (pumped)	10M HNO_3 (circulated by gas lift)	See Figure 15. Life = 8 hours Run at 120 ma/cm^2, 1.55 v. Temperature = 60°C	IEM badly attacked by HNO_3. Numerous holes in membrane.
54918	Duplicate of 54906	Duplicate of 54905	Duplicate of 54905 Membrane from fresh supply	1M N_2H_4 in 5M KOH (pumped)	15M HNO_3 (pumped)	OCV = 2.1 volts Run at 120 ma/cm^2, 1.4 v Temperature = 70°C Life = 9 hours	Failure same as 54906
61508	Duplicate of 54906	Duplicate of 54905	Duplicate of 54918 10 mil thick woven glass cloth between cathode and membrane	1M N_2H_4 in 5M KOH (pumped)	15M HNO_3 (circulated by gas lift)	OCV = 2.2 volts Run at 100 ma/cm^2, 1.1 v for 8 hours Temperature = 70°C Life = 8 hours	Glass cloth deteriorated exposing IEM to direct HNO_3 attack.
54911	Duplicate of 54906	Duplicate of 54905	Duplicate of 54918‡ 15 mil thick asbestos between cathode and membrane.	1M N_2H_4 in 5M KOH (pumped)	15M HNO_3 (pumped)	OCV = 1.9 volts Run at 70 ma/cm^2, 1.0 v Temperature = 70°C Life = 32 hours	Fragile asbestos paper finally ripped, exposing IEM to HNO_3 attack.
54916	Duplicate of 54906	Duplicate of 54905	Duplicate of 54918 25 mil thick Teflon felt between cathode and IEM	1M N_2H_4 in 5M KOH (pumped)	15M HNO_3 (circulated by gas lift for first 58 hours; pumped to end)	OCV = 1.9 volts Run at 70 ma/cm^2, 1.1 v Temperature = 70°C Life = 70 hours	IEM showed attack and pinhole leaks in area of acid inlet and outlet manifolds, indicating deleterious effect of rapid pumping.

Table A-33 (Continued)

SUMMARY OF ION EXCHANGE MEMBRANE FULL CELLS

Cell No.	Anode	Cathode	Membrane	Fuel	Oxidant	Performance Summary	Notes
61509	Duplicate of 54906	Duplicate of 54905	AMF cation exchange membrane C-313	1M N_2H_4 in 5M KOH (pumped)	15M HNO_3 (pumped)	OCV = 2.1 volts Run at 50 ma/cm², 1.5 v Temperature = 70°C Life = 2-1/2 hours	Cell gradually fell off to negligible output. IEM very brittle from action of caustic.
61510	Duplicate of 54906	Duplicate of 54905	Duplicate of 61509 25 mil thick Teflon felt between cathode and IEM	1M N_2H_4 in 5M KOH (pumped)	15M HNO_3 (pumped)	Performance same as 61509. Life = 3 hours	No change in performance with time-developed serious leak in Teflon felt seal which required shutdown. IEM again showed caustic embrittlement.
61512	Duplicate of 54906	Duplicate of 54905	Permion 1010‡‡ cation exchange membrane	1M N_2H_4 in 5M KOH (pumped)	15M HNO_3 (pumped)	OCV = 2.2 volts Immediate deterioration No life	Anolyte stream showed immediate HNO_3 attack on nickel anode. IEM was sample and apparently contained pinhole leaks.
61507	Duplicate 54906	Duplicate 54905	Monsanto Research zirconium phosphate separator	1M N_2H_4 in 5M KOH (pumped)	15M HNO_3 (pumped)	OCV = 2.1 volts Run at 70 ma/cm², 0.94 v Temperature = 70°C Life = 3 hours	Failed due to HNO_3 attack on anode. Zirconium phosphate deteriorated by caustic and washed out of separator, permitting mixing of acid and base.

* Ionics, Inc., Cambridge, Massachusetts.
** Gould National Batteries, St. Paul, Minnesota.
‡ Johns-Manville Corp., Fuel Cell Paper, Tilton, New Hampshire.
‡‡ Radiation Applications Company, Long Island, New York.
§ TE2050 - American Felt Company, Glenville, Connecticut.

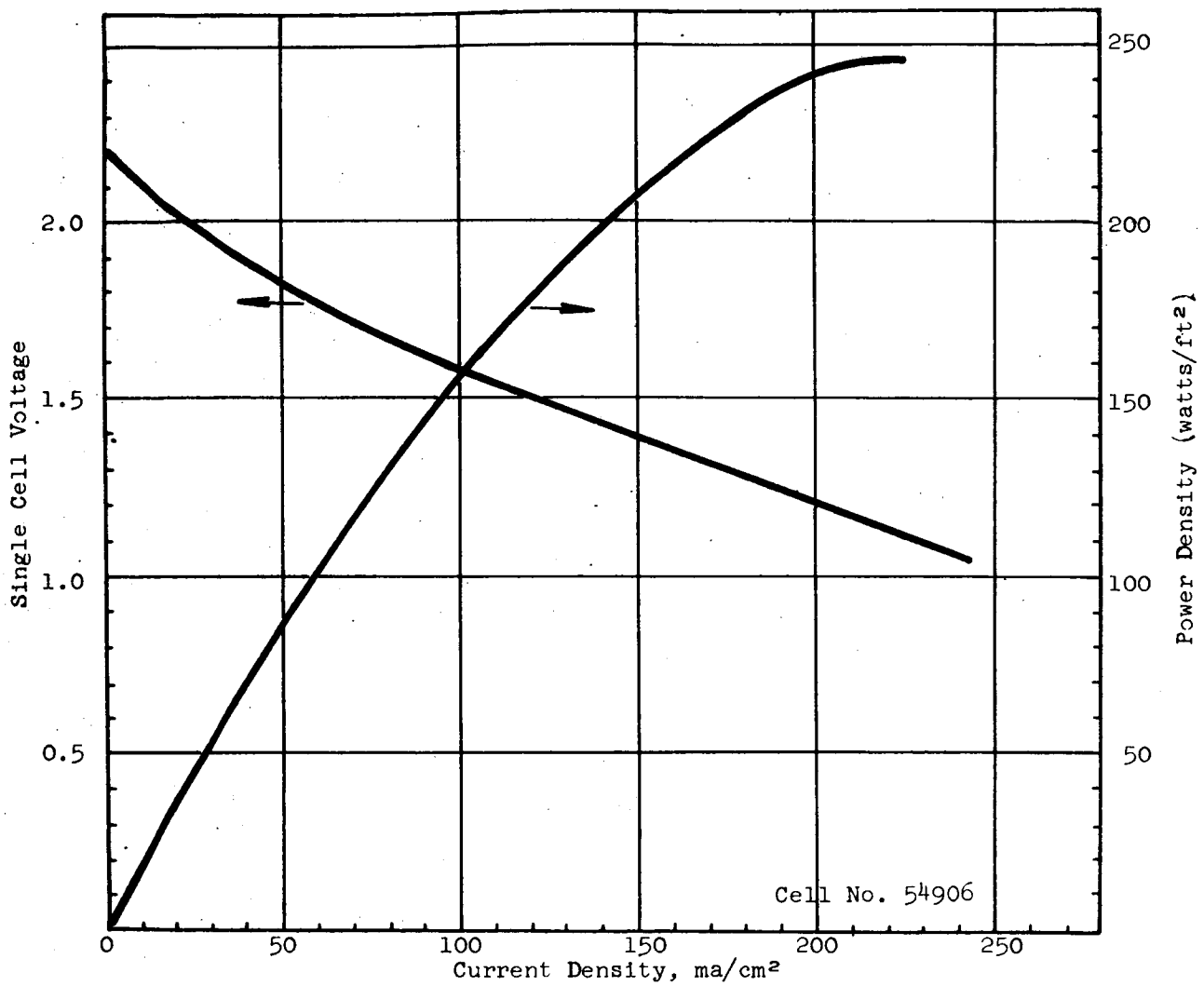

1M N_2H_4 / 5M KOH - Cation Exchange Membrane - 10M HNO_3
Operating Temperature: 60°C
Electrode Area: 9 in²

Figure A-62. Voltage and Power Density Characteristics of N_2H_4 - HNO_3 Fuel Cell with Cation Exchange Membrane

d. N_2H_4 (in KOH)|Ni(Pd)|CEM|Glass Fiber|Pt|HNO_3 (Cell 61508)

This cell employed a layer of woven glass cloth as the porous mat. At 100 ma/cm^2 a decrease in voltage performance of about 30% was noted. Life was only 8 hours. Disassembly of the cell showed that the glass cloth was torn in several places and had lost its flexibility. Apparently binders used in the cloth had been attacked by the strong acid, causing failure to structural integrity and rapid attack on the exposed IEM.

e. N_2H_4 (in KOH)|Ni(Pd)|CEM|Asbestos Mat|Pt|HNO_3 (Cell 54911)

Cell 54911 incorporated a 15 mil thick asbestos paper as the porous layer. Voltage performance at 70 ma/cm^2 was about 40% poorer than that of Cell 54906, but an effective life of 32 hours was obtained. Inspection of the failed cell components showed that the fragile asbestos sheet had torn, probably as a result of high catholyte liquid velocities.

f. N_2H_4 (in KOH)|Ni(Pd)|CEM|Teflon Felt|Pt|HNO_3

Cell 54916 was operated at 70 ma/cm^2, 1.1 volt, and 70°C for 70 hours before IEM failure. Protective buffer material between cathode and IEM was 25 mil thick Teflon felt. The failed membrane showed appreciable HNO_3 attack only in the catholyte manifold areas, suggesting again that rapid pumping of acid tends to wash out the protective KNO_3 layer where liquid velocities are highest. This could be modified with design changes.

g. N_2H_4 (in KOH)|Ni(Pd)|CEM|Pt|HNO_3 (Cell 61509)

Cell 61509 and 61510 tested a commercial cation exchange membrane (AMF-C-313) from another source. Electrical performance was only moderate, the cell being unable to stably carry current densities higher than about 50 ma/cm^2. Cell 61509 probably leaked HNO_3 slowly through the IEM to gradually polarize the anode and ultimately attack it.

h. N_2H_4 (in KOH)|Ni(Pd)|CEM|Teflon Felt|Pt|HNO_3 (Cell 61510)

Cell 61510 used the Teflon felt buffer with the AMF-C-313 membrane. Electrical performance was approximately the same as that of Cell 61509, the increased internal resistance caused by the Teflon felt probably being nearly equivalent to Cell 61509's poisoned anode effect. Difficulty in sealing the cell forced a shut down after 3 hours when HNO_3 leakage out of the cell became excessive. There was no fall-off in electrical output with time.

The AMF-C-313 membrane showed good resistance to HNO_3 but became quite brittle when exposed to the strongly basic anolyte stream. Testing was therefore discontinued with this membrane in the acid/base cell, though it could have application in a nitric acid/hydrazine (in pH 6-12 solution) cell.

i. N_2H_4 (in KOH)|Ni(Pd)|CEM|Pt|HNO_3 (Cell 61512)

The Permion 1010 cation exchange membrane was also evaluated. This is a very thin membrane and the small sample available either contained pinhole leaks when supplied or was punctured during cell assembly. No performance data were obtained because of immediate leakage of HNO_3 to the anode compartment. A new sample is on order and suitable precautions will be taken to insure its undamaged installation in a cell.

j. N_2H_4 (in KOH)|Ni(Pd)|CEM|Zr Phosphate|Pt|HNO_3 (Cell 61507)

The zirconium phosphate separator was incorporated into Cell 61507. An OCV of 2.1 volts was obtained, and the cell was run at 70 ma/cm² and 0.94 volt at 70°C before gradual decrease in electrical performance. After 3 hours, leakage of HNO_3 to the anode was observed and the cell was shut down. Examination showed deterioration of the zirconium phosphate layer in the separator probably by basic attack. This material should have better application in cells with hydrazine in pH 6-12 solution.

Other zirconium phosphate separators were prepared by forming the precipitate in asbestos sheet or loose fibers. Subsequent processing included washing out of excess acid, drying, shredding, and pressing into sheet form. The resulting separators although integral, were judged too fragile for fuel cell use.

D. CONCLUSIONS

The acid/base fuel cell possesses attractive electrical output performance if a suitable ion-exchange membrane can be found to provide effective solution separation over a long period of time.

The life of commercial IEM's presently available can be extended from about 8 hours to at least 70 hours for the HNO_3/N_2H_4-in-base system. This improvement in life is obtained by employing a buffer layer of porous material between the cathode and IEM. The porous layer apparently becomes loaded with neutralization products that shield the IEM from direct acid attack. This is considered new technology.

Of the several commercial IEM's tested for HNO_3/N_2H_4-in-base fuel cell systems, none exhibit completely satisfactory qualities. Further tests are needed to characterize the Permion 1010 membrane.

Zirconium phosphate ion exchange separators for fuel cell use have been fabricated and tested. Results are still inconclusive but specialized applications appear likely. The method of fabrication and the form of zirconium phosphate separators are considered new technology.

APPENDIX V

BENZENESULFONIC ACID AS AN ELECTROLYTE

A. BACKGROUND

The attainment of high battery discharge rates with minimum voltage loss because of internal resistance requires the use of a high conductance electrolyte. Strong acids such as sulfuric acid or strong bases such as potassium hydroxide are commonly used in battery systems to attain low internal resistance. Potassium hydroxide is an excellent anolyte for the hydrazine anode, but an acid anolyte is required if the hydrazine anode is to be paired with a nitric acid cathode. The combination of a basic anolyte with an acidic catholyte, even with a separator or ion exchange membrane between the two compartments, eventually results in direct reaction between the acid and base, undesirable salt formation, and heating. No conducting separator or ion exchange membrane has yet been found which will effectively separate acidic and basic solutions without eventually plugging or disintegrating. Sulfuric acid cannot be used as the anolyte for a hydrazine anode because of the formation of insoluble hydrazine sulfate. Phosphoric acid has been used as an acidic anolyte for the hydrazine electrode, but since phosphoric acid is weak, the IR drop is large compared with the IR drop through a strong acid. For this reason, benzenesulfonic acid (BSA) has been screened as an anolyte for use with the hydrazine anode. Benzenesulfonic acid, a relatively strong acid, has an ionization constant of 2×10^{-1} compared with 7.5×10^{-3} for phosphoric acid at 25°C. Within certain concentration and temperature limits, BSA does not form insoluble precipitates when mixed with hydrazine.

B. CONDUCTANCE OF BENZENESULFONIC ACID SOLUTIONS

The relative conductance of solutions of BSA, phosphoric acid, and mixtures of hydrazine and BSA are tabulated in Table A-34. Conductances are expressed as ratios of the conductance of given solutions to that of 5M H_3PO_4 at 25°C (0.23 mho/cm).*

The greater conductance of BSA compared with that of phosphoric acid is shown by the data of Table A-34. The conductance of 2M BSA is 50% greater than that of 5M H_3PO_4, so the IR drop in a full cell would be 2/3 as great when using BSA as the electrolyte. The maximum conductance for BSA solutions is at approximately 2M. Solutions that are 0.5M and 1M in N_2H_4 are soluble in 2M BSA at 55-60°C but not at 25°C. The low conductance of a mixture of 0.5M N_2H_4 and 1M BSA at 25°C was due to partial neutralization of BSA with hydrazine (a base).

---

* Lange's Handbook of Chemistry and Physics:
A temperature correction of 2% per degree was used.

Table A-34

CONDUCTANCE OF BENZENESULFONIC ACID SOLUTIONS

Solution	Temperature, °C	Ratio Conductivity of Solution to Conductivity of 5M H_3PO_4 at 25°C
1M BSA	25	1.18
2M BSA	25	1.51
4M BSA	25	1.22
1M H_2SO_4	25	1.85
0.5M N_2H_4 + 1M BSA	25	0.70
1M BSA	55-60	1.95
2M BSA	55-60	2.23
4M BSA	55-60	1.73
0.5M N_2H_4 + 1M BSA	55-60	1.05
0.5M N_2H_4 + 2M BSA	55-60	2.14
1M N_2H_4 + 2M BSA	55-60	1.63
0.5M N_2H_4 + 0.5M HNO_3 + 2M BSA	55-60	2.23

C. COMPARISON OF BENZENESULFONIC AND PHOSPHORIC ACIDS AS ELECTROLYTES FOR THE NITRIC ACID CATHODE

Polarization curves for three concentrations of nitric acid in 4M BSA and for 3M HNO_3 in 5M H_3PO_4 are shown in Figure A-63. At 200 ma/cm^2 potentials of 1.00, 1.06, and 1.09 volts were attained by FC-13 porous carbon electrodes in contact with 0.5M, 1M, and 3M HNO_3, respectively. All three of the cathodes with BSA electrolyte were less polarized than the cathode with phosphoric acid electrolyte.

D. COMPARISON OF BENZENESULFONIC AND PHOSPHORIC ACIDS AS ELECTROLYTES FOR THE HYDRAZINE ANODE

Anodic polarization curves for the oxidation of hydrazine in both phosphoric acid and BSA electrolytes are given in Figure A-64. Little difference between the two electrolytes was found. Anodes in contact with 1M N_2H_4 polarized less than those in contact with 0.5M N_2H_4. Contamination of the anolyte with 0.5M HNO_3 did not cause severe deterioration of the anode potential. Since this anode was a different electrode than that used with the uncontaminated electrolytes, the results in contaminated and uncontaminated electrolytes cannot be compared directly.

E. CORROSION OF 316 STAINLESS STEEL IN BENZENESULFONIC ACID

Very slight discoloration of 2M BSA occurred after 10 days' contact at 90°C with 316 stainless steel. The steel showed no appreciable corrosion.

F. CONCLUSION

Benzenesulfonic acid could probably be substituted for phosphoric acid as an acid electrolyte for the nitric acid-hydrazine system. The conductance of BSA solutions has been shown to be better than that of phosphoric acid solutions, and the IR-free potentials of the HNO_3 cathodes and the hydrazine anodes are at least as good with BSA as with phosphoric acid electrolyte.

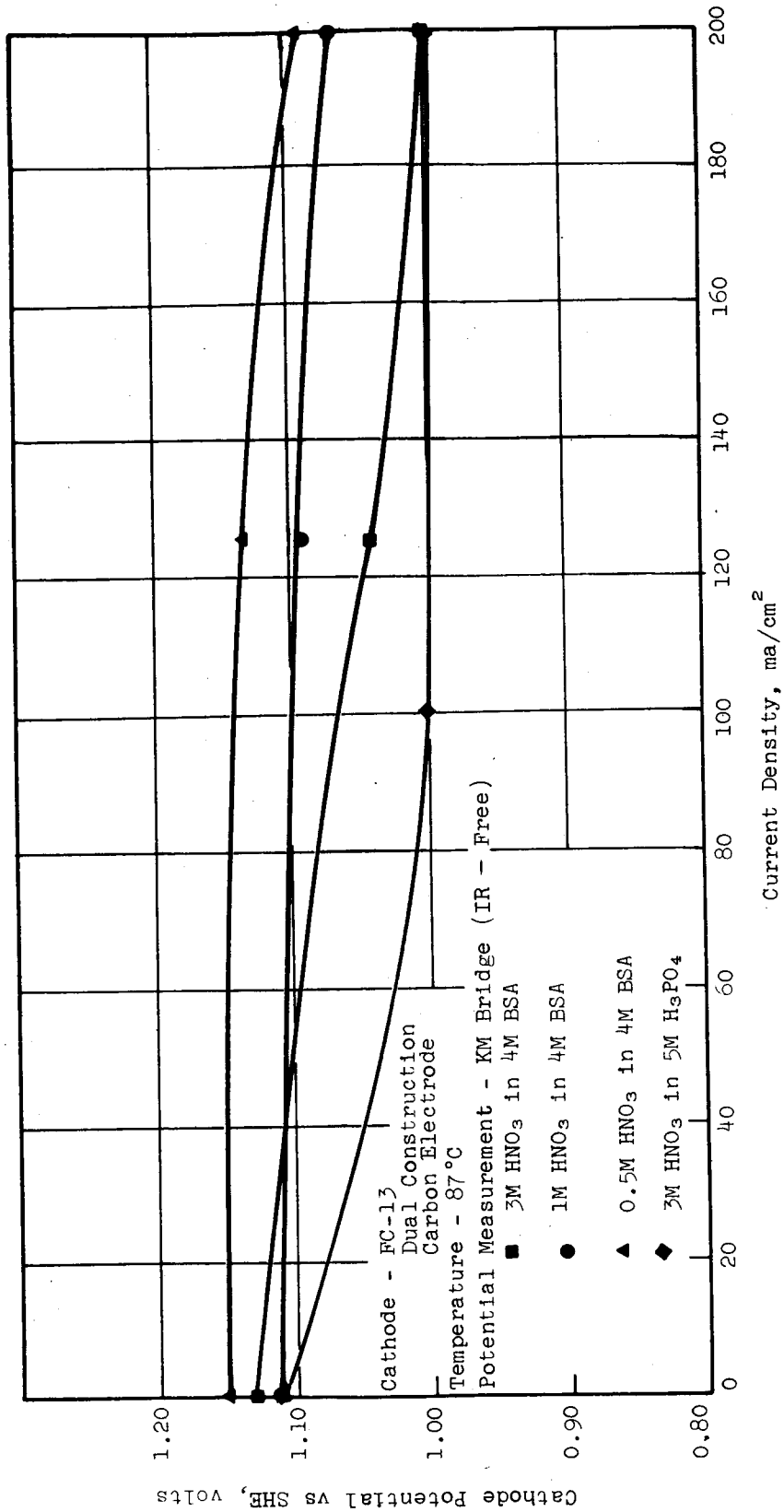

Figure A-63. Cathodic Reduction of HNO_3 in Benzenesulfonic Acid Electrolyte

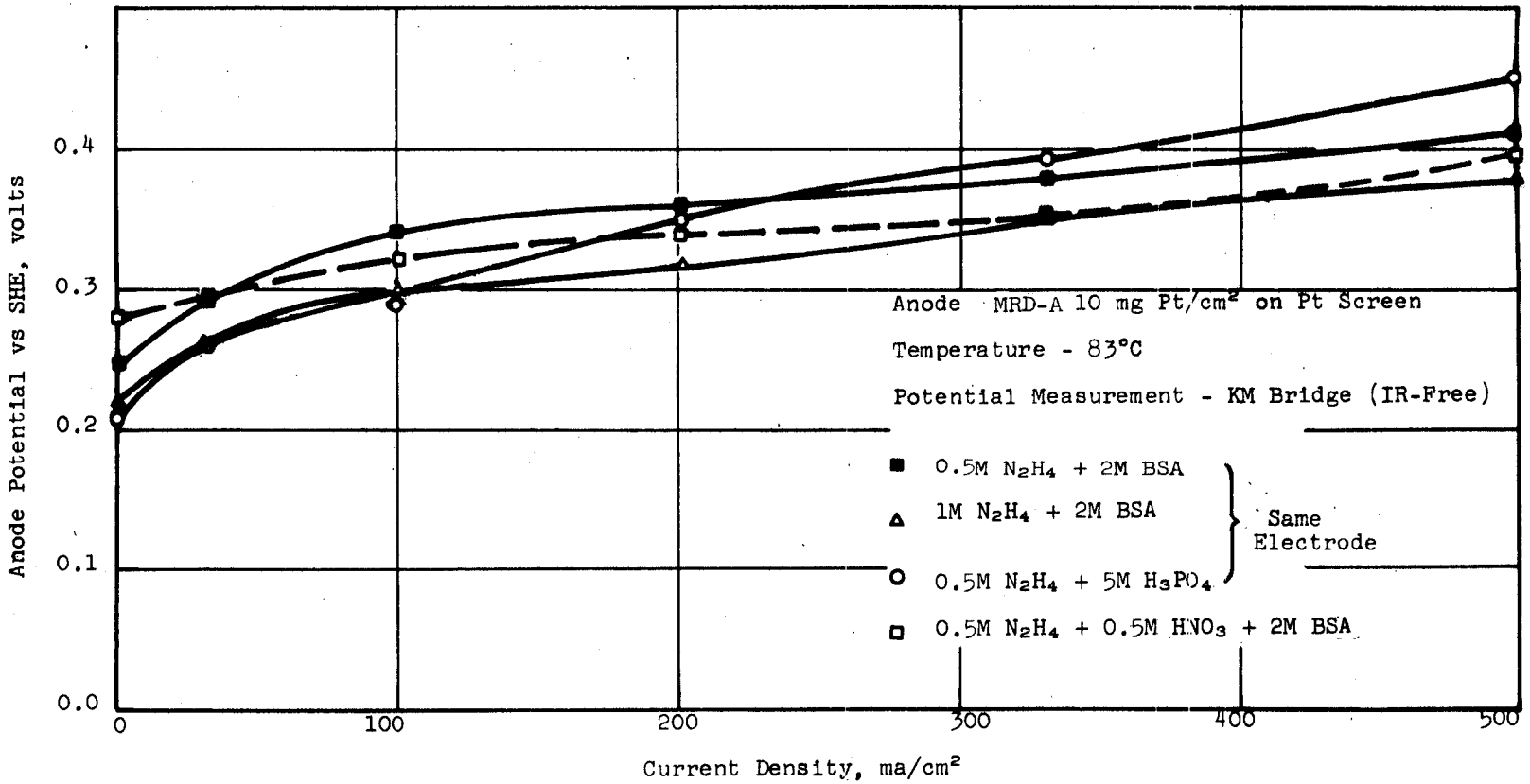

Figure A-64. Anodic Oxidation of N_2H_4 in Benzenesulfonic Acid Electrolyte

APPENDIX VI

ANHYDROUS HYDROGEN FLUORIDE SYSTEMS

A. BACKGROUND

One of the strongest oxidizers known, chlorine trifluoride, is a rocket propellant candidate, and may conceivably be used as an electrochemical oxidant for the production of electrical power in the rocket which is being propelled. Since chlorine trifluoride will react with water and most of the common solvents, only completely fluorinated materials such as hydrogen fluoride or fluoride salts can be considered as solvents or electrolytes. Since such fuels as hydrogen or hydrazine are compatible with hydrogen fluoride, the system ClF_3/HF (KF)/H_2 or ClF_3/HF (KF)/N_2H_4 are logical choices to demonstrate the feasibility of the fluoride cell.

The cell reactions are:

$$\text{(Cathode)} \quad ClF_3\ (g) \longrightarrow Cl^- + 3F^- - 4e^-$$
$$\text{(Anode)} \quad N_2H_4\ (l) \longrightarrow N_2 + 4H^+ + 4e^-$$

$$\text{(Cell)} \quad ClF_3\ (g) + N_2H_4\ (\ell) \longrightarrow N_2 + HCl + 3HF$$
$$\Delta F^\circ = -223\ \text{KCal}$$
$$E^\circ = 2.42\ \text{v}$$

Energy Density = 950 watt-hours/lb

During the first six-month contract, (ref. 1) half-cell polarization tests were used to demonstrate the anodic oxidation of hydrazine and the cathodic reduction of chlorine trifluoride. Current densities up to 5 ma/cm² were attained for 1M N_2H_4 oxidation at a polarization of 0.5 v at 3°C. Current densities of 20 ma/cm² were obtained for chlorine trifluoride reduction at 3°C. In a molten electrolyte of KF·3HF at 85°C, current densities of 5 ma/cm² at a polarization of 0.5 v were supported at platinum cathodes in contact with chlorine trifluoride, and current densities up to 100 ma/cm² were attained at anodes in 1M N_2H_4 at 0.5 v polarization.

The solid palladium electrode was demonstrated as an anode for hydrazine oxidation in anhydrous hydrogen fluoride. Silver, cadmium, and lead fluoride and the palladium-hydrogen reference electrodes were evaluated as reference electrodes in anhydrous hydrogen fluoride at 3°C or potassium fluoride-hydrogen fluoride melts at 85°C.

This section describes the development of porous electrodes for utilizing chlorine trifluoride, hydrazine, and hydrogen as reactants, and the construction and testing of a full cell of the type ClF_3/KF·3HF/H_2. Potentiostatic studies of metal oxidation in anhydrous hydrogen fluoride are presented.

B. REFERENCE ELECTRODES IN ANHYDROUS HYDROGEN FLUORIDE

1. Background

Reference electrodes are required for both half-cell and full-cell studies in anhydrous hydrogen fluoride solutions. Anodic and cathodic polarization curves for fuels or oxidants in anhydrous hydrogen fluoride must be measured against a reference electrode that is compatible with the solvent and electrolyte. Aqueous reference electrodes, such as the calomel electrode, are not satisfactory for use with anhydrous systems because of contamination difficulties and because of the unknown liquid junction (ref. 30). The ideal reference electrode has a reproducible potential, is not readily polarized, returns quickly to its original open-circuit potential after polarization, and does not contaminate the working electrode or its electrolyte.

The silver/silver fluoride, copper/copper fluoride, and lead/lead fluoride electrodes have been suggested as reference electrodes in hydrogen fluoride solutions by Koerber and DeVries (ref. 31).

2. Electrode Preparation

Preparation of reference electrodes for use in anhydrous hydrogen fluoride solutions was accomplished as follows:

a. Silver/Silver Fluoride Electrode

A piece of pure silver wire, 0.14 cm diameter by 10 cm long, was cleaned with fine emery paper (00) and anodized in KF·3HF at 85°C at successively higher current densities (1, 2, 5, 10 ma/cm^2) until a polarization of 0.5 v from the original open-circuit potential occurred.

b. Lead/Lead Fluoride Electrode

A strip of pure lead 10 by 0.2 by 0.5 cm was scraped clean with a knife and anodized in KF·3HF as in a above.

c. Copper/Copper Fluoride

A strip of pure copper wire, 0.10 cm diameter by 10 cm long, was cleaned with fine emery paper and anodized in KF·3HF as in a above.

d. Hydrogen/Palladium Electrode

A piece of 3-mil thick palladium, 0.5 by 1.0 cm, was spot welded to 0.05 cm diameter platinum lead wire and coated with platinum black by cathodizing in 3% $H_2PtCl_6 \cdot 6H_2O$ for two minutes at 20 ma/cm^2 for each side. The electrode was washed and dried in air and cathodized in KF·3HF at 5 ma/cm^2 for 60 minutes.

3. Polarization Potentials of Reference Electrode Candidates

Reference electrode candidates were tested in KF•3HF solution at 85°C by anodic polarization at current densities as high as 100 ma/cm^2. Such high-current densities would not normally be employed for half-cell potential measurement, but if the anodes could withstand severe polarization at such drain rates, they would be good anode candidates as well as reference candidates.

The anodic polarization of hydrogen, lead, silver, and copper electrodes in KF•3HF at 85°C is shown in Figure A-65. The silver, hydrogen, and lead electrodes withstood anodic currents up to 100 ma/cm^2 with little polarization, while the copper electrode was polarized 0.3 volt at this current density. The potential of the lead electrode is about 0.3 v more negative than the hydrogen electrode.

Although reduction to hydrogen would be expected at this potential, none was observed. Apparently lead has a high overvoltage for hydrogen reduction in KF•3HF solutions. The very active potential of lead makes it a better reference candidate than the less active metals, since traces of lead ion would not be reduced at surfaces with a more positive potential and thus contaminate the test electrodes.

C. SOLID PALLADIUM-HYDRAZINE DIFFUSION ELECTRODE

The use of solid palladium for purification of hydrogen and as a hydrogen diffusion anode is well known (refs. 7 thru 12) Previous work at this Laboratory has shown that aqueous hydrazine can be used to charge a palladium membrane with hydrogen, and that the hydrogen can be burned anodically on the opposite side of the membrane after diffusion through the foil. This scheme is attractive for the anhydrous hydrogen fluoride system, since the hydrazine reductant will be restricted from the electrolyte compartment and cannot come into contact with potent oxidizers such as chlorine trifluoride.

Also, the hydrazine may be used either in the anhydrous form or in aqueous solution, since water cannot pass through the palladium membrane to contaminate the anhydrous electrolyte.

A disk of 1-mil thick palladium*, 1 in. in diameter, was plated at 14 ma for 2 minutes for each side in a "Rhodex" proprietary rhodium plating solution.

---

* Englehard Industries Inc., Newark, N. J., 75% Pd, 25% Ag

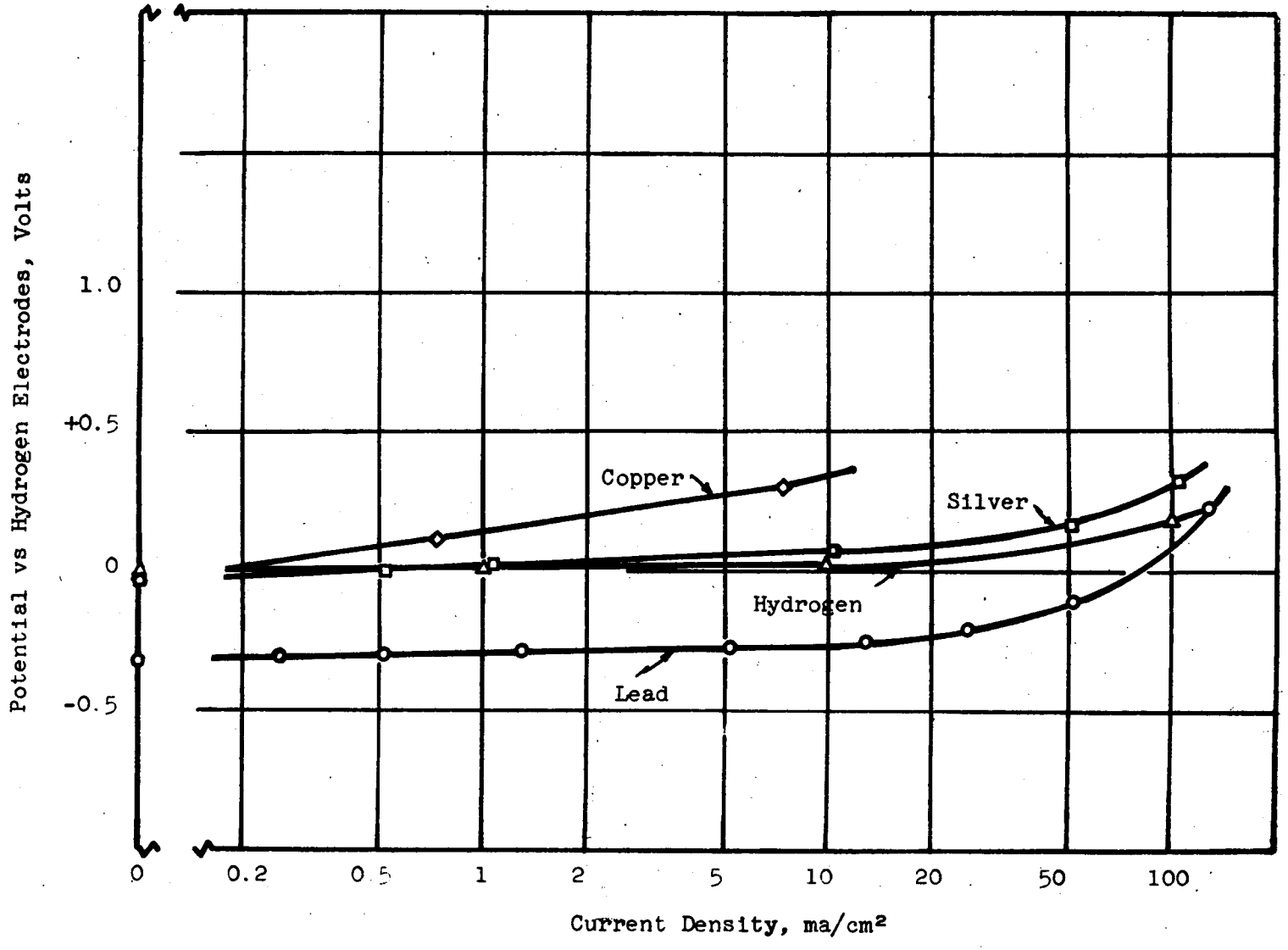

Figure A-65. Anodic Oxidation of Hydrogen, Lead, Copper, and Silver in KF·3HF at 85°C

The rhodinized palladium was mounted in a Teflon holder (Figure A-66) which exposed a disk 0.5 inch in diameter (1.27 cm^2). A lead-lead fluoride reference electrode was placed adjacent to the electrode holder in one side of a Teflon "H" cell, and a lead counter electrode was mounted in the opposite side of the "H" cell. The Teflon electrode holder was filled with a solution of 5M N_2H_4 in 5M KOH and the "H" cell filled with molten KF·3HF. The "H" cell was immersed in a fluidized sand thermostat for temperature control at 85°C. The open-circuit potential of the palladium membrane was measured, and the electrode was anodically polarized at successively increasing currents until drastic potential failure occurred. Potentials against the lead-lead fluoride reference were measured at the end of each 2-minute polarization period with both an electrometer and a Kordesch-Marko bridge. The latter instrument measured polarized electrode potentials without IR drop. Results are tabulated in Table A-35. The open-circuit potential was 0.05 v more positive than that of the hydrogen electrode in the same electrolyte. The electrode withstood a current density of 39 ma/cm^2 before severe polarization occurred. This experiment demonstrated that the palladium-hydrazine electrode can be used in anhydrous hydrogen fluoride systems. To avoid anodic attack of the palladium, the potential must be maintained at a potential less than 0.5 volt positive to the lead electrode (see next section). The normal potential of the electrode in contact with hydrazine is in a suitable region to avoid anodic attack.

D. POROUS NICKEL-HYDROGEN ELECTRODE

A circular piece of porous nickel plaque*, 1 in. in diameter by 25 mil thick, was treated with 25 mg of platinum per square inch by spontaneous deposition from a dilute solution of chloroplatinic acid. The catalyzed disk was mounted in a Teflon holder which exposed 1.27 cm^2 of the electrode surface, as shown in Figure A-66. The back side of the membrane was purged with hydrogen gas and the assembly immersed in KF·3HF at 85°C. A lead-lead fluoride reference electrode was placed adjacent to the electrode holder in one side of the Teflon "H" cell, and a lead counter electrode was placed in the opposite side of the cell. The free space in the assembly was purged with nitrogen gas. The electrode was anodically polarized as previously described for the palladium membrane.

The porous nickel-hydrogen anode withstood a current density of 39 ma/cm^2 before severely polarizing (see Table A-36). The anodic polarization at this loading was more favorable than that of the palladium membrane at the same current density (Table A-35).

---

* Gould National Batteries, Inc., St. Paul, Minnesota

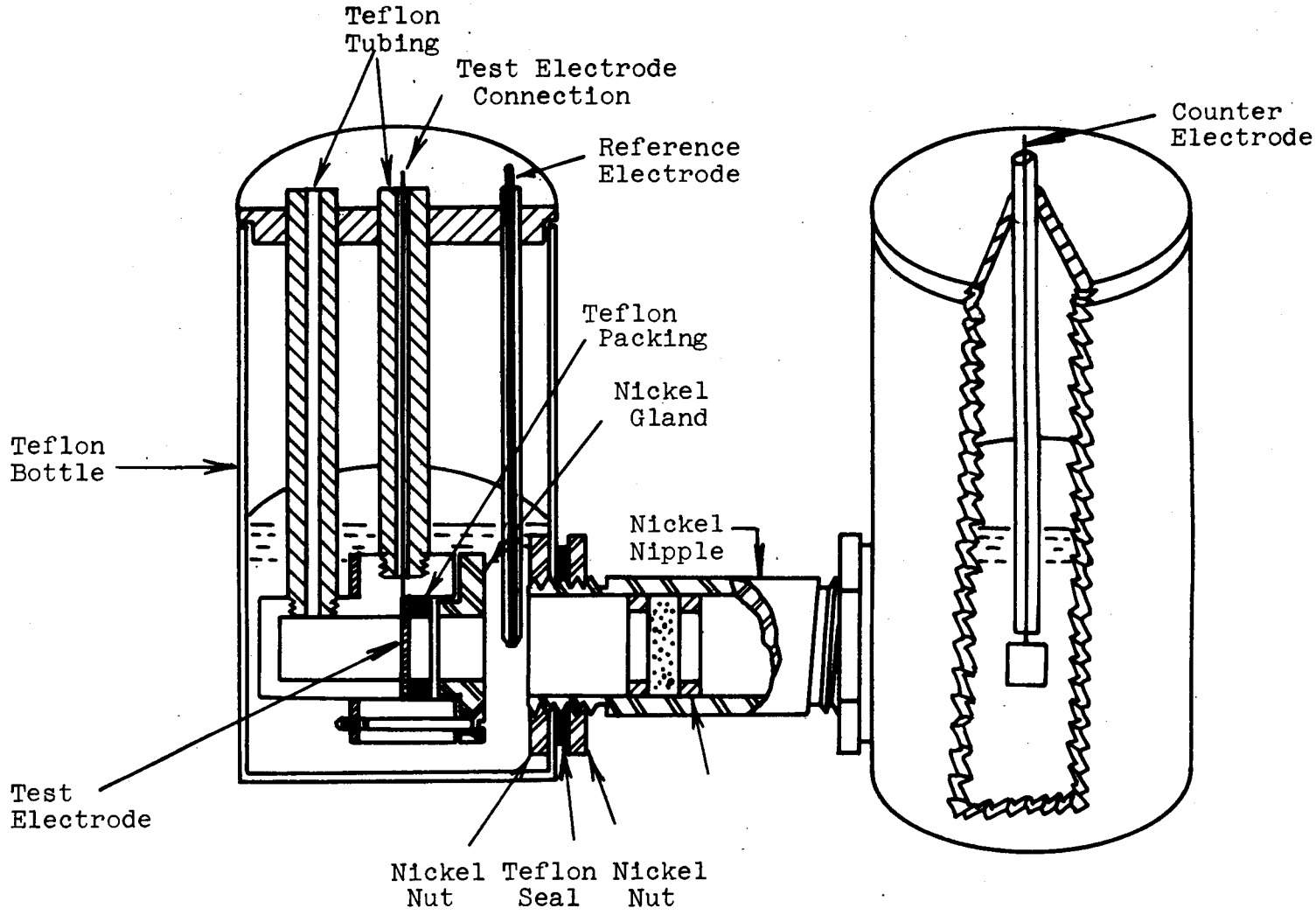

Figure A-66. Polarization Cell for Hydrogen Fluoride Systems

Table A-35

ANODIC POLARIZATION OF PALLADIUM-HYDRAZINE ELECTRODE IN KF·3HF AT 85°C

Fuel - 5M N_2H_4 in 5M KOH

Current Density ma/cm²	Potential vs Hydrogen Electrode After 2 Minutes Polarization, volts*
0	0.05
0.8	0.08
1.6	0.08
3.9	0.10
8.0	0.13
16	0.14
39	0.34

*IR-free

Table A-36

ANODIC POLARIZATION OF HYDROGEN-POROUS NICKEL ELECTRODE IN KF·3HF AT 85°C

Current Density ma/cm²	Potential vs Hydrogen Electrode After 2 Minutes Polarization, volts*
0	0.00
0.8	0.00
1.6	0.00
3.9	0.01
8.0	0.03
16	0.08
39	0.20

*IR-free

E. POTENTIOSTATIC ANODIC POLARIZATION MEASUREMENTS

Potentiostatic anodic polarization measurements have been shown to be useful for evaluating metal corrosion (ref. 8, 32). The degree of anodic protection present as a metal is subjected to gradually increasing anodic potentials is readily apparent by measuring the anodic current accompanying controlled polarization (ref. 33, 34).

1. Method

Solid metal specimens were prepared for anodic polarization measurements by polishing with (00) emery paper and washing in ethylene trichloride, water, and acetone. The total geometric surface area exposed to electrode was measured. The specimens were mounted in one side of a Teflon "H" cell with a lead-lead fluoride reference electrode close to the metal surface. A lead counter electrode was placed in the opposite side of the "H" cell. The cell was filled with molten KF·3HF, and the void space was purged with dry nitrogen gas. The assembly was placed in a fluidized sand bath thermostat maintained at 85°C. Polarization measurements were made with a potentiostat. After the open-circuit potential was measured, with reference to a lead reference electrode, the potential was fixed at successive intervals of 0.04 volt more positive than the open-circuit potential and the current recorded after one minute's polarization at each potential. These measurements were continued to a potential 1.8 volts more positive than the lead reference, and the potential was adjusted in 0.04-volt negative intervals until the current changed from anodic to cathodic. The polarization pattern is shown in Figure A-67 for solid nickel. The current increases steadily as the potential becomes more positive up to a potential 0.65 volt to the reference electrode, after which the current reversed and was relatively constant at 15-25 μa at potentials more positive than 0.8 volt. After reversing the current direction, a constant current region at 8-15 μa occurred at potentials more positive than 0.8 volt, and a small current peak was recorded at 0.7 volt, after which the current fell to zero and became cathodic. The pronounced peaks and regions of small constant anodic currents are evidences of the formation of protective anode fluoride films on the nickel surface. Nickel is known to be a good construction material for fluoride and hydrogen because of its tendency to form tough protective anode films.

A specimen of porous nickel plaque was tested for corrosion in the KF·3HF melt by the same procedure as just described for solid nickel (see Figure A-68). The anodic currents were many times higher for a given geometrical surface area than for the solid nickel specimen because of the much greater surface area of the sintered nickel and possibly a greater specific reactivity. After the initial current peak at 0.7 volt, the current decreased but not to the trivial values for the solid specimen as shown

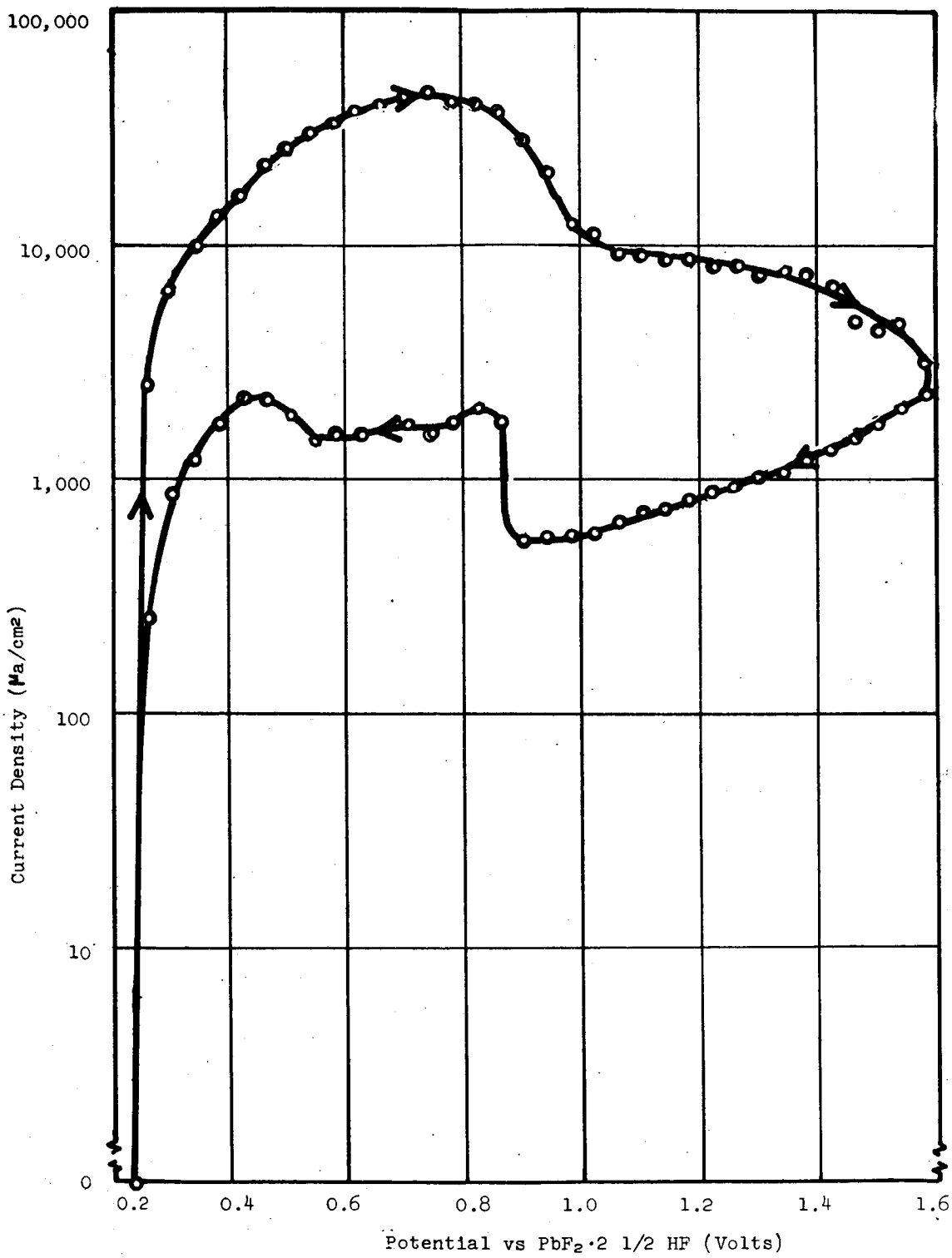

Figure A-67. Potentiostatic Anodic Polarization of Nickel Plaque in KF·3HF at 85°C

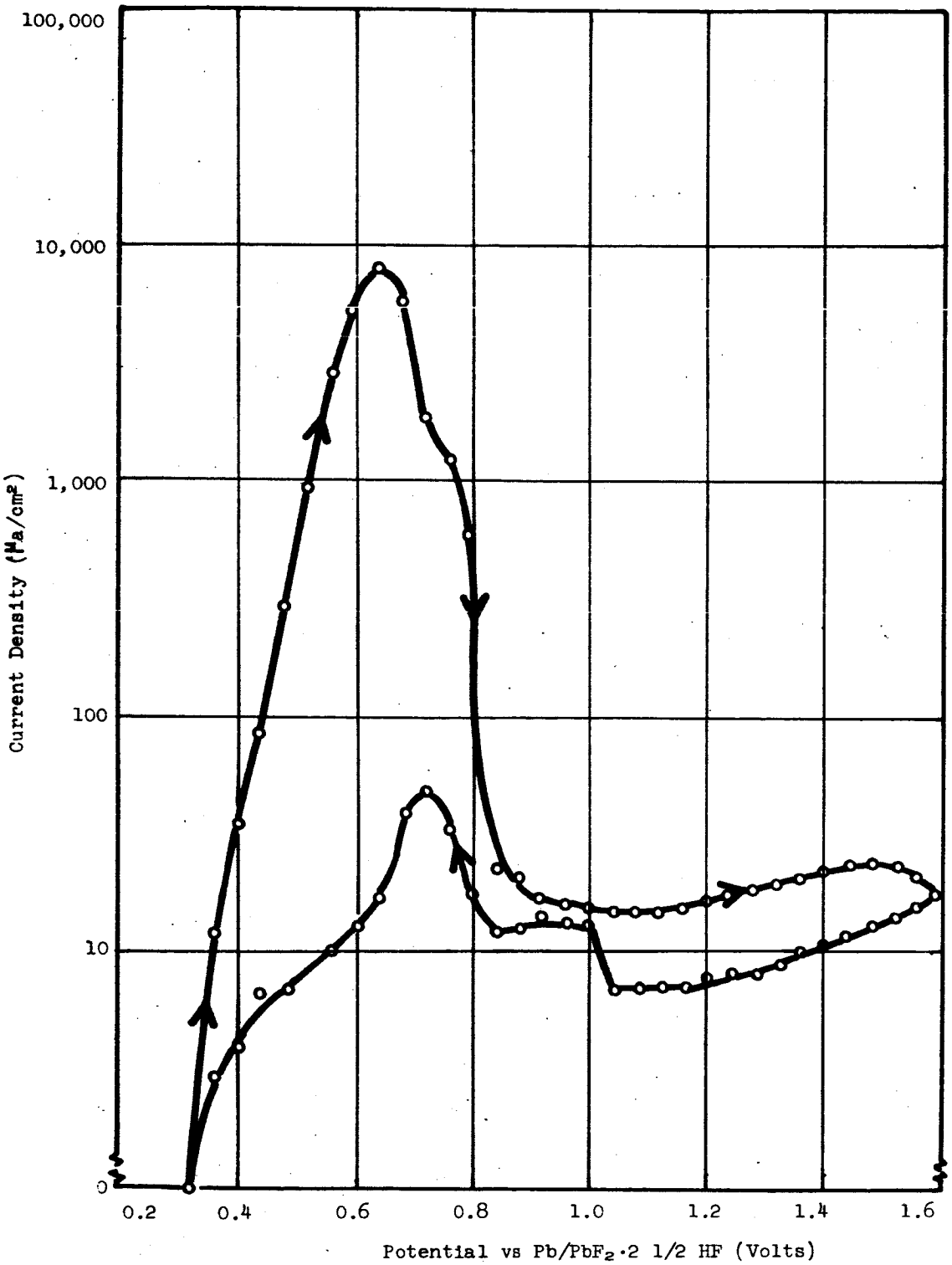

Figure A-68. Potentiostatic Anodic Polarization of Solid Nickel in KF·3HF at 85°C

by Figure A-67. The large anodic currents above 0.8 volt indicated appreciably attack instead of passivation. Additional tests with slower sweeping periods and longer potential spans will be required to further characterize the nickel plaque for use in the KF•3HF melt.

The anodic polarization of copper (Figure A-69) resulted in much greater anodic currents than those incurred during solid nickel polarization (Figure A-67). A maximum in the current-potential curve occurred at 0.8 volt positive to the lead/lead fluoride reference, but the current decreased only slightly at more positive potentials that 0.8 volt. Copper corrodes much more rapidly than nickel in the KF•3HF melt at 85°C and does not become readily passivated at high anodic potentials. Long-term tests would be required to more completely evaluate copper corrosion.

Anodic polarization of palladium (Figure A-70) indicated that this metal is slowly anodically corroded in the KF•3HF melt at 85°C. Unlike nickel and copper, palladium did not show a maximum in the current-potential relation.

As contrasted to the behavior of solid nickel, the anodic current of palladium first increased as the potential became more positive and then was almost constant at about 70 $\mu a/cm^2$ at potentials from 1.0 to 1.7 v to the lead-lead fluoride electrode.

2. Conclusions Regarding Metal Corrosion in KF · 3HF at 85°C

(1) Solid nickel does not dissolve anodically in KF · 3HF at 85°C at potentials more negative than 0.3 v to the lead-lead fluoride electrode. Solid nickel is anodically protected at potentials of 0.9 to 1.6 v at a corrosion rate of about 63 milligrams of nickel per square decimeter per day (mdd) or 0.010 in. penetration per year (ipy). Solid nickel is a potential cathode material for use with chlorine trifluoride.

(2) Highly porous nickel plaque is not anodically oxidized at potentials more negative than 0.25 v but is rapidly corroded at potentials from 0.3 to 1.6 v. The great difference between nickel plaque and solid nickel is the enormous true surface area of the former compared with the geometrical surface area on which current densities were based. The exact composition of the nickel plaque may also be different from that of the solid nickel. Nickel plaque would not be a satisfactory cathode material for use with chlorine trifluoride.

(3) Solid copper is not anodically attacked at potentials more negative than 0.5 v, but the metal corrodes severely at potentials more noble than 0.63 v. This metal would not make satisfactory cathodes for use with chlorine trifluoride but might be used to contain the KF · 3HF melt in the absence of chlorine trifluoride if traces of copper can be tolerated.

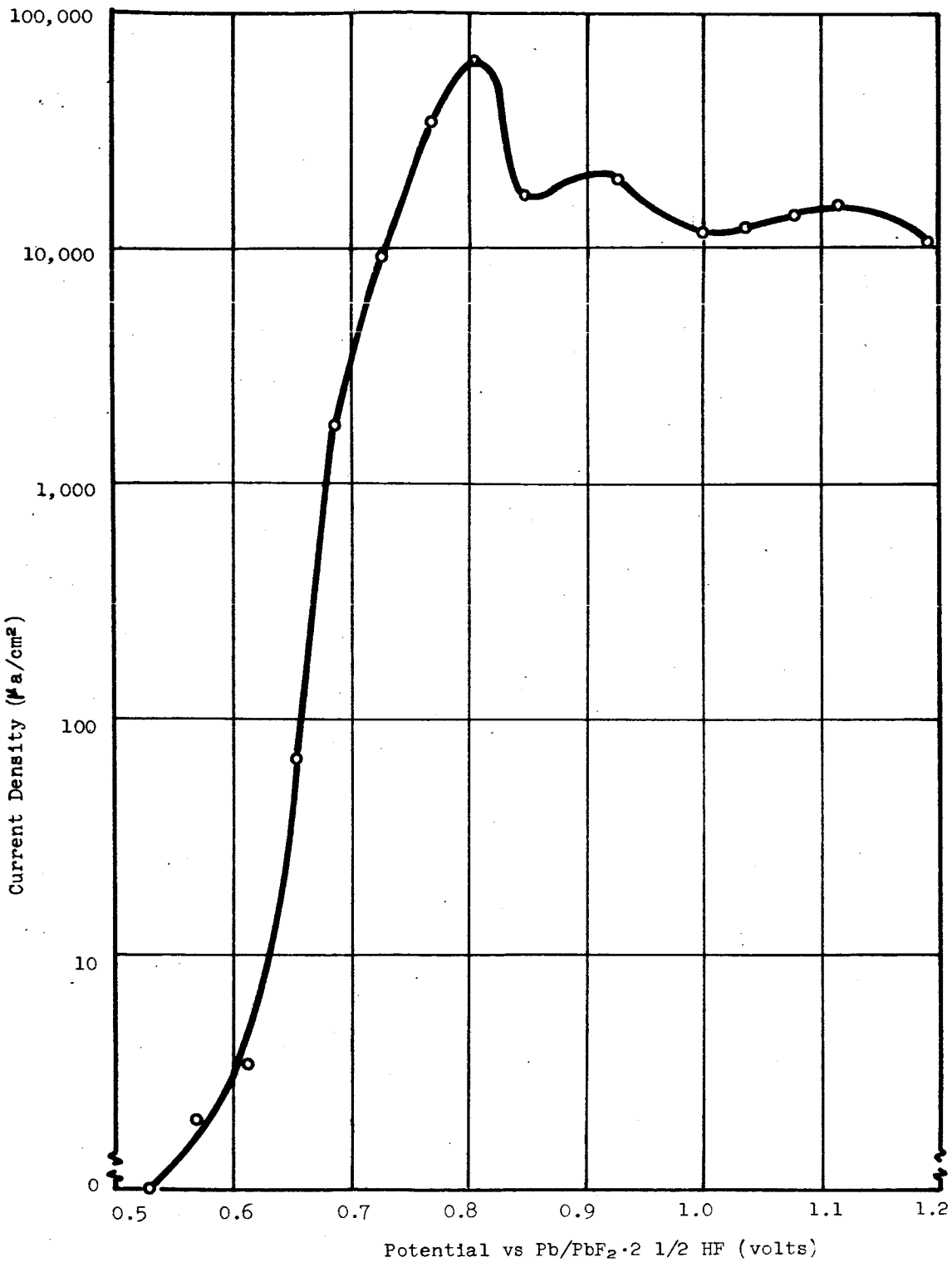

Figure A-69. Potentiostatic Anodic Polarization of Copper in KF·3HF at 85°C

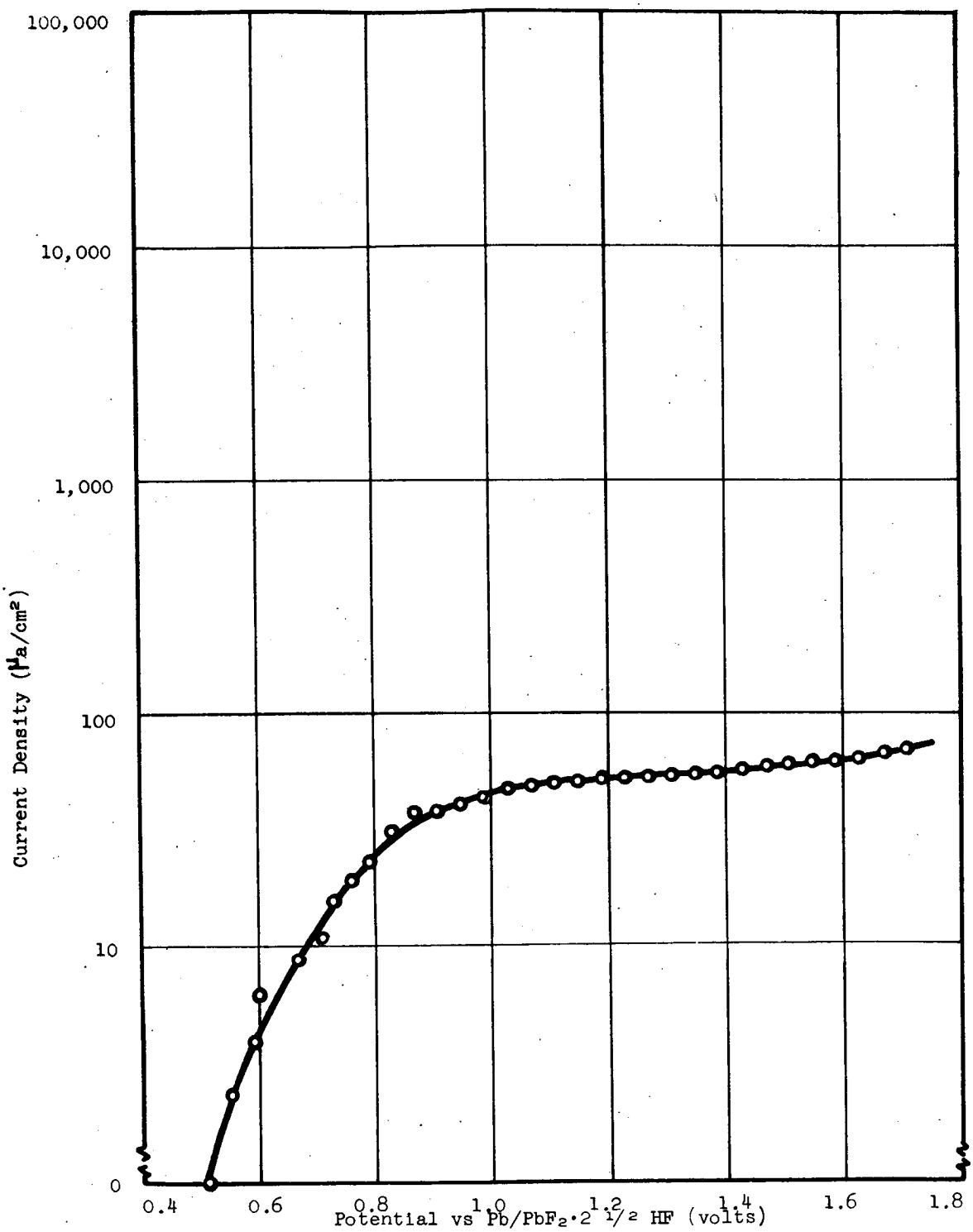

Figure A-70. Potentiostatic Anodic Polarization of Solid Palladium in KF·3HF at 85°C

(4) Assuming that palladium dissolves as Pd^{++}, the anodic current plateau for palladium at about 70 $\mu a/cm^2$ corresponds to a corrosion rate of 334 mdd or 0.040 ipy. This rather high corrosion rate would cause failure of thin palladium membranes. The potential of such anodes should be kept more negative than 0.7 v to prevent rapid dissolution. For example, at 0.7 v, a dissolution current of 11 $\mu a/cm^2$ corresponds to a corrosion rate of 53 mdd or 0.006 ipy.

F. FULL CELLS WITH ANHYDROUS HYDROGEN FLUORIDE

1. Experimental

A full-cell unit was constructed from Teflon and stainless steel, as shown in Figure A-71. The anode and cathode were contained in separate compartments to minimize the chance of violent direct reaction of chlorine trifluoride with anode fuels. Cathodes were disks of porous FC-13 carbon *, 15/16 in. in diameter by 1/8 in. thick with no treatment. Previous half-cell experiments had shown that carbon was the best chloride trifluoride cathode material among those tested (ref. 1). A MD-A type anode with a platinum loading of 10 mg/cm^2 was used as the fuel electrode (ref. 2). The molten electrolyte $KF \cdot 3HF$ at 85°C was used for all runs. A second full cell was constructed with metallic lead replacing the hydrogen anode. Polarization characteristics of the two full cells were determined, both with and without IR drop. Results are shown in Figures A-72 and A-73.

2. Polarization Characteristics of the ClF_3/H_2 Full Cell

The $ClF_3/KF \cdot 3HF/H_2$ full cell had a high open-circuit voltage of 1.83 v at 85°C. The cell polarized severely upon drawing currents higher than 10 ma/cm^2. The polarization was principally caused by IR drop in the high resistance cell, since IR-free measurements with a Kordesch-Marko bridge indicated only reasonable polarization up to current densities of 80 ma/cm^2 (see Figure A-72).

Symmetrical polarization curves for the anode and cathode indicated that the electrodes were well balanced.

3. Polarization Characteristics of the ClF_3/Pb Full Cell

The $ClF_3/KF \cdot 3HF/Pb$ full cell had an open-circuit voltage of 2.10 v at 85°C (Figure A-73). Again, severe resistance polarization was encountered at current densities above 10 ma/cm^2, although IR-free potentials were only moderately polarized at current densities as high as 80 ma/cm^2.

---

* Pure Carbon Co., St. Marys, Pa.

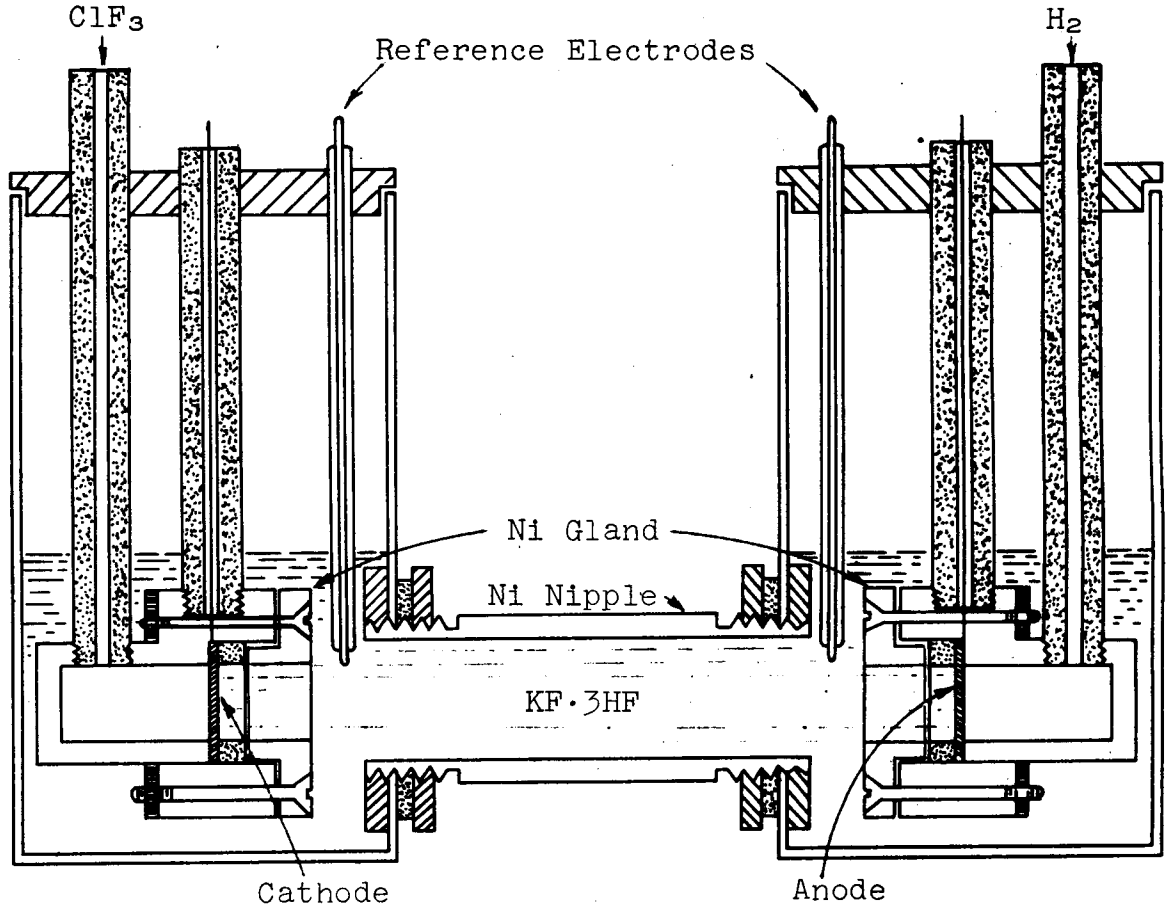

Figure A-71. Full Cell for Anhydrous Hydrogen Fluoride System

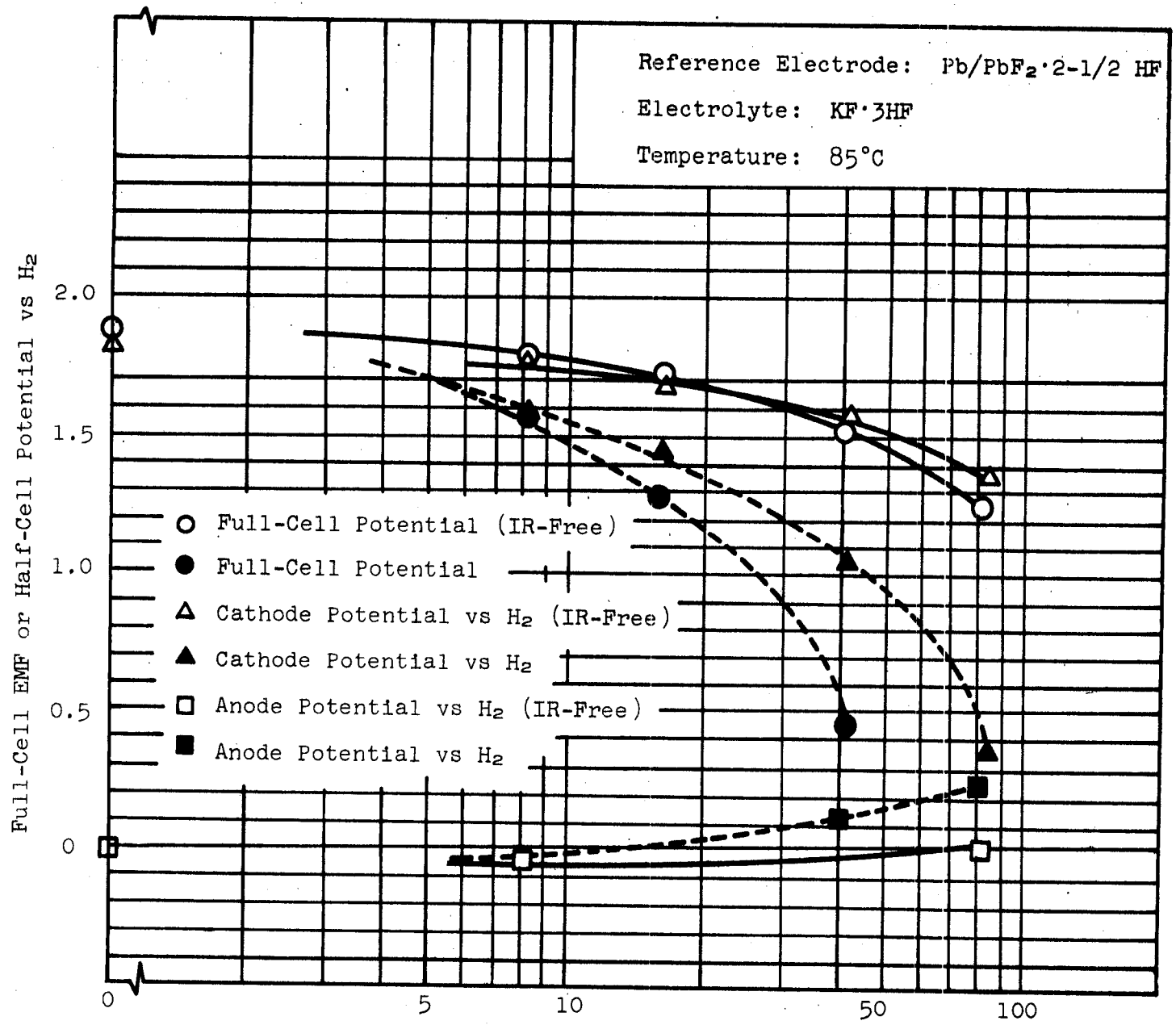

Figure A-72. Polarization Characteristics of Full Cell $ClF_3/KF \cdot 3HF/H_2$

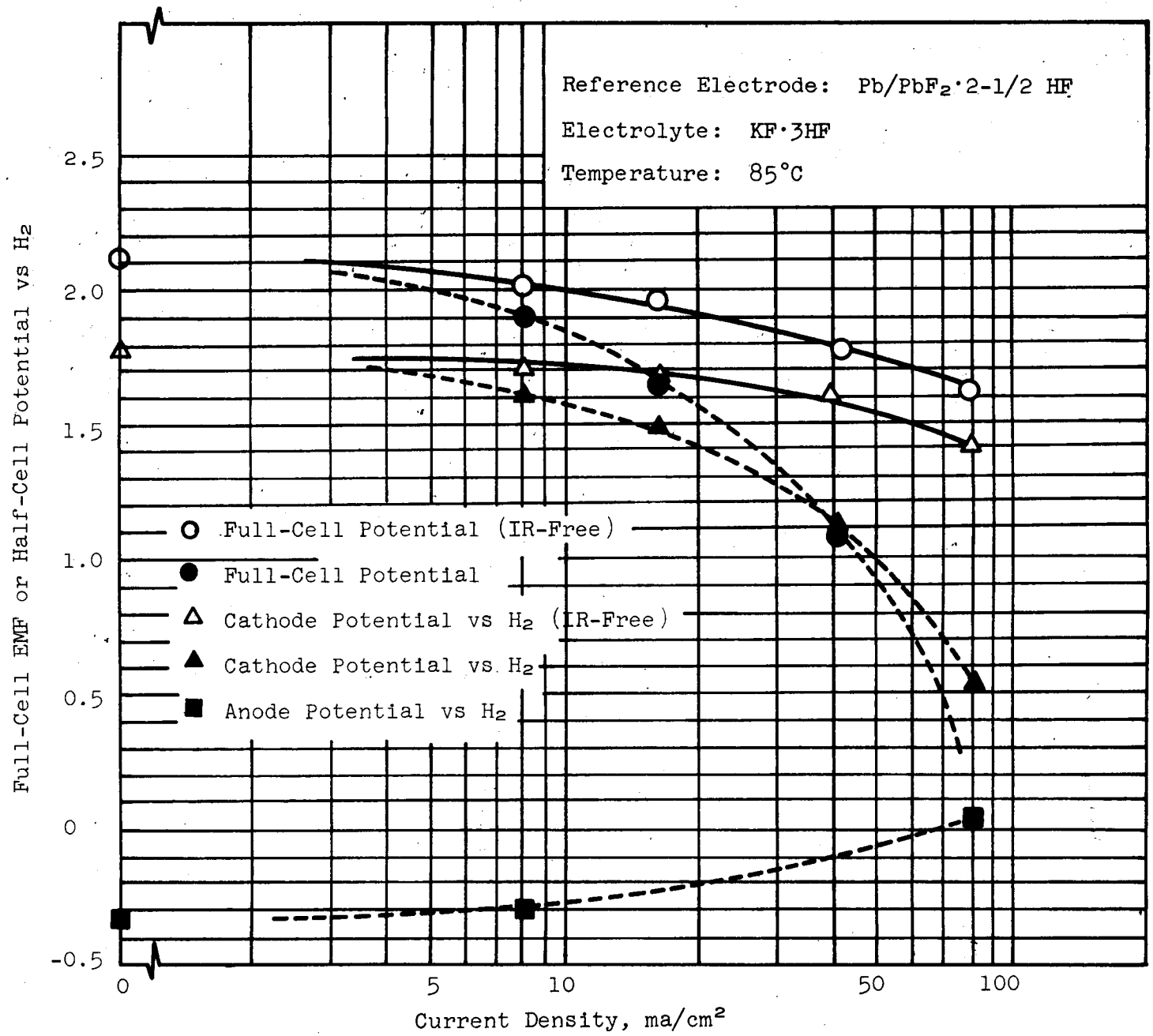

Figure A-73. Polarization Characteristics of Full Cell ClF_3/KF·3HF/Pb

H. CONCLUSIONS

Anhydrous hydrogen fluoride and KF-HF can be employed as electrolytes in cells using such potent reactants as chlorine trifluoride hydrazine, and hydrogen. The operation of both half cells and full cells of this type has been demonstrated. The wide separation between anode and cathode used in full-cell demonstrations for reasons of safety results in a cell that is severely resistance polarized at current densities above 10 ma/cm^2. Any practical cell design awaits the development of electrodes that will efficiently contain the reactants and prevent mixing of the high-energy fuels and oxidant. With such electrodes, cells could be designed with closer electrode spacing and correspondingly lower IR losses. The corrosion of metals in contact with ClF_3 is severe.

APPENDIX VII

A. CALCULATION OF REVERSIBLE HYDROGEN POTENTIALS IN POTASSIUM HYDROXIDE SOLUTIONS

The reversible hydrogen potential for a hydrogen electrode in contact with its ions:

$$H_2 = 2H^+ + 2e^-$$

or the equivalent reaction in base:

$$H_2 + 2\ OH^- = 2H_2O + 2e^-$$

versus the standard hydrogen potential (which is defined as zero at all temperatures) can be calculated for any temperature and concentration of base from the ionization constant of water, K_w, the concentration of base, and the activity coefficient of the base by the relation:

$$E = E^\circ - RT/nF \ln a_{H^+}$$

$$= E^\circ - 2.303 \frac{RT}{nF} (\log K_w - \log a_{OH^-}) \text{(ref. 35)}$$

The ionization constant of water is given as a function of the absolute temperature, T, by Harned (ref. 36).

$$\text{Log } K_w = 4470.99/T + 6.0875 - 0.017060\ T$$

Activity coefficients of potassium hydroxide solutions from Harned (ref. 36) are plotted in Figure A-74.

For example, when $M_{KOH} = 5$, $m_{KOH} = 5.33$.

K_W and A_{OH^-} at 25°C are given in Table A-37, and the hydrogen potential versus the standard hydrogen electrode becomes:

$$E = 0 - \frac{2.303 \times 1.99 \times 298.2}{23{,}060} (-14.00 - 1.013) = 0.886$$

The above potential is positive according to the Electrochemical Society convention. Changing to experimental potentials, the sign of the potential is changed to minus.

Calculations of hydrogen potentials versus the saturated calomel electrode in 5M KOH at the temperatures of the experimental cells are given in Table A-37.

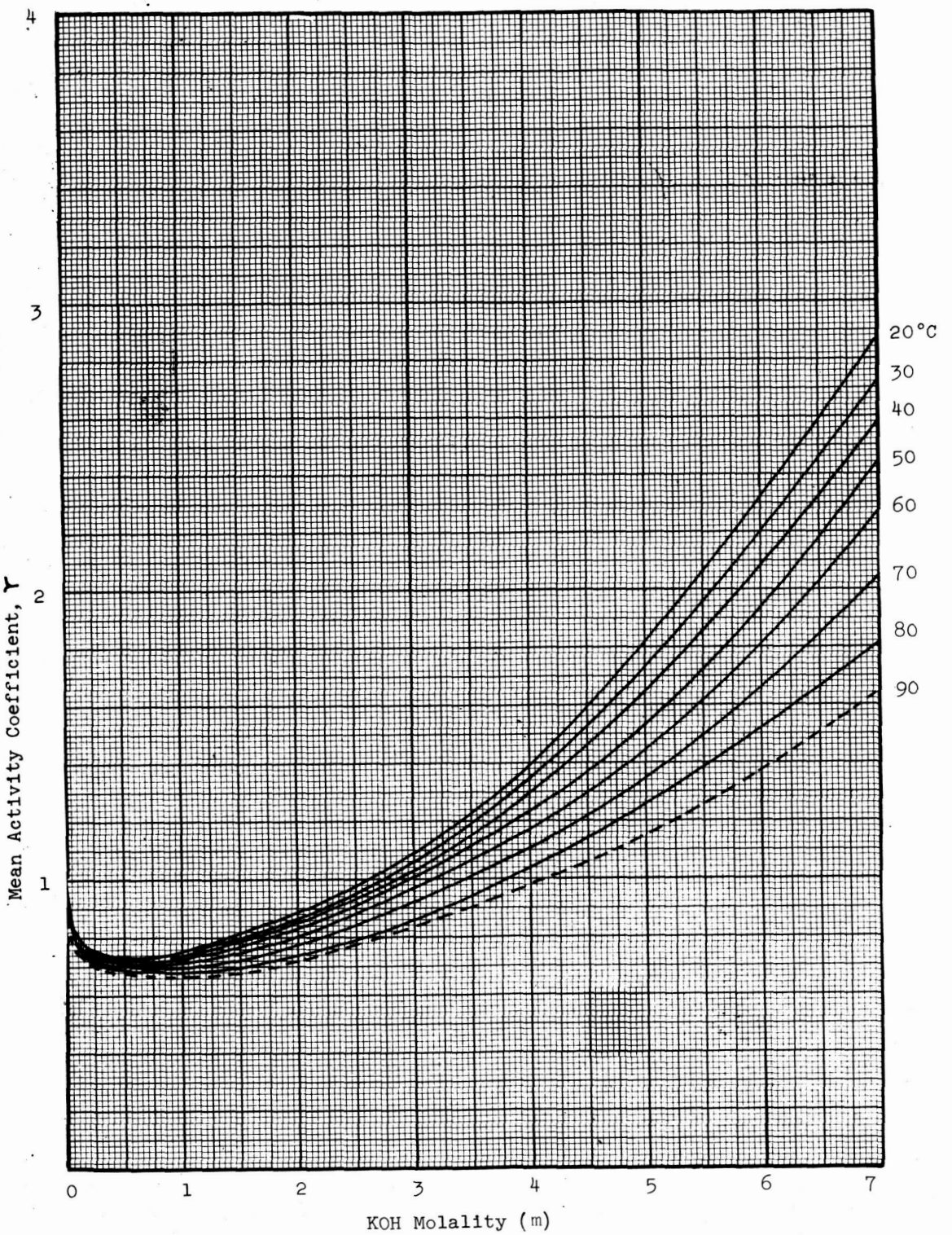

Figure A-74. Mean Activity Coefficients of Aqueous KOH Related to Concentration and Temperature. From Data of Harned (ref. 36) (Curve for 90°C extrapolated.)

Table A-37

CALCULATED DATA FOR HYDROGEN ELECTRODE POTENTIAL VS SCE IN 5M KOH AT 25°C, 60°C, AND 90°C

Temp. °C	log K_W	RT/F	E°_B Volts	γOH^-
25	-14.00	0.0592	-0.828	1.90
60	-13.02	0.0662	-0.861	1.58
90	-12.43	0.0772	-0.900	1.23

Temp. °C	a_{OH^-}	log a_{OH^-}	E_{H_2} Volts	SCE Volts	E_{H_2} vs SCE*
25	10.30	1.013	-0.886	0.24	-1.13
60	8.53	0.930	-0.925	0.22	-1.14
90	6.56	0.817	-0.958	0.20	-1.16

*Without liquid junction potential

VIII. APPENDIX

FUEL CELL SYSTEM REQUIREMENTS

Under the terms of the subject contract, Article I.A.1.h, the NASA Project Manager is to define requirements for a fuel cell system using storable rocket propellants as reactants. This contractual requirement is herewith defined as follows:

(a) Power requirement - 1 kilowatt electrical output; current density, 100 ma/cm^2; operating potential, 28 ± 2 volts.

(b) Environmental conditions - Normal earth atmosphere at 25°C and 1 atmosphere pressure.

(c) Weight and volume restrictions - Electrode area, 60 ± 4 in.^{2} shape approximately square; dimensions may be between approximately 8 in.^{2} and approximately 7 x 9 in. Length as required by the number of cells. The weight shall be smallest practical based upon the most recent data.

(d) Operating duty cycle - Continuous duty at 1 kilowatt with 100% overload (2.0 kilowatts at 21 ± 2 volts) for five minutes once every eight hours. Operating period, 1000 hours.

(e) Special conditions affecting operation (1), (4), (5) and (7). Discuss alternate conditions (2), (3) and (6).

(1) Normal earth gravity
(2) Zero gravity
(3) Recovery of product water
(4) Venting of product water
(5) Venting of gaseous products
(6) Sorption of gaseous products other than nitrogen
(7) Operating temperature: 15-90°C

The subject contract further specifies under Article I.A.1.i that at the end of nine months under the contract, the contractor shall submit to the NASA Project Manager his recommendations to meet the requirements described above in terms of (a) cell design features, (b) reactants and electrolyte selection, (c) size and weight estimate, and (d) storage and feed system recommendations.

APPENDIX IX

STUDY OF OXYGEN ELECTRODE MATERIAL

In low-temperature fuel cells which presently are operating or under development, the cathodic polarization using O_2, H_2O_2 or air is much larger than the anodic polarization using hydrogen or hydrazine for fuel. The resulting loss of operating potential has been one of the limiting functions in the development of a compatible fuel cell system.

Screening tests were carried out on porous Teflon-bonded electrodes using the cathodc polarization sweep technique. These electrodes were made from submicron size powders of the materials listed in Table A-38.

Cathodic polarization curves on these electrodes are shown in Figures A-75 and A-76. The reversible oxygen electrode potential, which was used to calculate the overpotentials, was obtained by adding 1.23 volts to the experimentally measured hydrogen electrode potential in the same solution at the same temperature. According to these results ruthenium, rhodium, platinum, palladium and silver were chosen for further investigation.

2. Catalytic Activities of Metal Oxides

a. Preheat Treatment of Precious Metal Powders

Ru, Rh, and Pd powders were preheated in oxygen atmosphere for one hour at 700°C and Pt was preheated for one hour at 525°C in order to obtain a stable oxide layer on the surface of the metal particles. Preheating did not result in any observable change in Pt powder, but other metal powders showed distinct oxide formation represented by entirely different colors after the heat treatment. During production of the electrodes from these powders it was also noticed that the preheated powders were somewhat coarser than those without treatment. However, no actual measurement of the particle size of the preheated powders was made.

Table A-39 shows the effect of the heat treatment on the polarization characteristics of these metal electrodes, expressed by cathodic current densities at the overpotential of 0.6 volt vs the reversible oxygen electrode potential. Because of the low polarization of Pt, the current density for Pt electrodes were given at the overpotential of 0.35 volt in acid and 0.25 volt in caustic electrolyte vs the reversible oxygen electrode.

Results are summarized as follows:

Table A-38

MATERIALS TESTED IN THE SCREENING EXPERIMENT

Electrolyte	Material	Remarks
Acid (85% H_3PO_4	C	Two different types of submicron size carbon black, produced at Monsanto Research Laboratory.
	Ru	Engelhard black. Average size 150Å. Surface 18≈20 m^2/g.
	Rh	Engelhard black. Average size 150A. Surface area 18≈20 m^2/g.
	Pd	Engelhard black. Average size 125A. Surface area 20≈30 m^2/g.
	Pt	Engelhard black. Average size 100Å. Surface area 23≈28 m^2/g.
	Ta	Supplied by Kawecki Chemical Co., -300 mesh.
Caustic (5M KOH)	C	Shawinigan black. Average size 450Å. Surface area 75 m^2/g.
	Ag	Engelhard catalytic silver. Submicron size.
	Ni	Fisher Chemical Company, -300 mesh.
	Rh, Pd, Pt	Engelhard black. Same as those listed for acid.

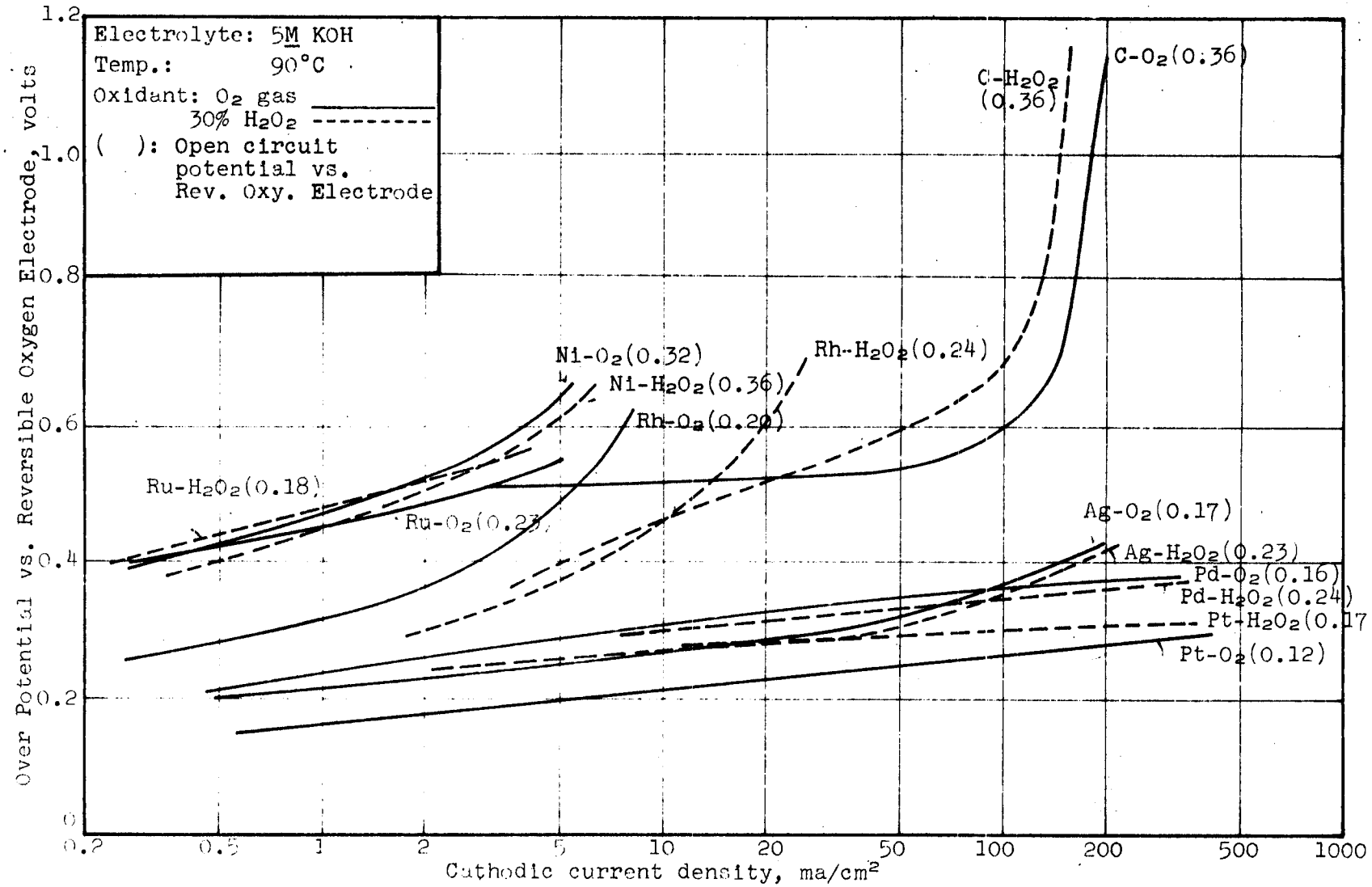

Figure A-75. Cathodic Polarization Curves of MRD Porous Electrode Made of Various Metals in Caustic Electrolyte

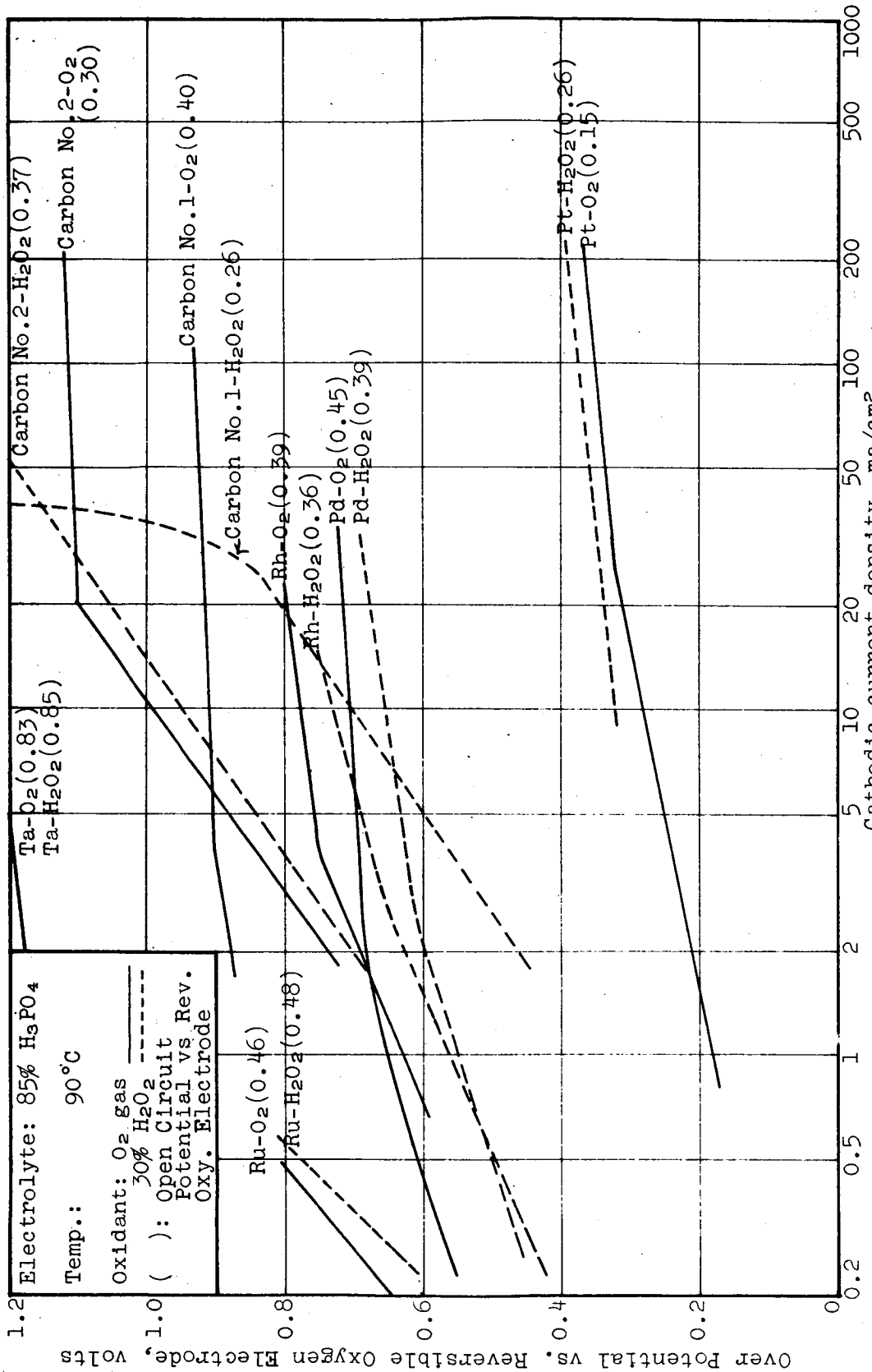

Figure A-76. Cathodic Polarization Curves of MRD Porous Electrode Made of Various Metals in Acid Electrolyte

Table A-39

EFFECT OF PREHEAT TREATMENT OF PRECIOUS METALS ON THEIR POLARIZATION CHARACTERISTICS

Cathodic current densities are in ma/cm² at the overpotential of 0.6 volt vs the reversible oxygen electrode in the acid electrolyte and 0.5 volt in the caustic electrolyte.

Electrolyte: 85% H_2PO_4
Temperature: 90°C
Oxidant: Pure O_2 or 20% H_2O_2

		Ru	Ru-O†	Rh	Rh-O†	Pd	Pd-O†	Pt	Pt-O†
OCP††	O_2	0.46	0.44	0.39	0.39	0.45	0.44	0.15	0.20
	H_2O_2	0.48	0.30	0.36	0.28	0.39	0.39	0.26	0.33
C.D. ma/cm²	O_2	0.17	0.25	0.63	0.04	0.45	0.07	100‡	16‡
	H_2O_2	0.22	9.0	1.5	0.15	2.0	1.4	60‡	8.5‡

† -O indicates pretreatment
†† Open Circuit Potential vs Reversible Oxygen Electrode in the same solution at the same temperature.
‡ Because of the low polarization of Pt, C.D. were taken at the overpotential of 0.35 volt.

Electrolyte: 5M KOH
Temperature: 90°C
Oxidants: Pure O_2 or 30% H_2O_2

		Ru	Ru-O†	Rh	Rh-O†	Pt	Pt-O†
OCP††	O_2	0.23	0.22	0.20	0.26	0.12	0.13
	H_2O_2	0.18	0.33	0.24	0.34	0.17	0.26
C.D. ma/cm²	O_2	2.5	37	5.4	20	35‡	0.6‡
	H_2O_2	1.3	32	13	40	4.5‡	3.5‡

† -O indicates the pretreatment. Ni was oxidized in air for one hour at 700°C.
†† Open Circuit Potential vs Reversible Oxygen Electrode in the same solution at the same temperature.
‡ Because of the low polarization of Pt, C.D. for Pt electrodes are at the overpotential of 0.25 volt vs the reversible oxygen electrode.

(1) Pre-oxidation improved somewhat the open circuit potential in the acid electrolyte (except Pt), but in the caustic solution nearly all pre-oxidized electrodes showed higher overpotential at open circuit than those by electrodes without pretreatment.

(2) Pre-oxidation increased the polarization in the acid electrolyte (except Ru), but decreased significantly those on Ru and Rh electrodes in the caustic electrolyte.

(3) Generally the oxides tested have some catalytic activity, however the improvement of performance obtained by oxidation is limited by other changes in the powder such as electronic conductivity, powder size and surface area. These factors apparently combine in the electrodes tested, resulting in higher polarization.

b. Oxide Catalysts of Transition Metals with Silver

Silver powder of -300 mesh was prepared by reduction of 3% $AgNO_3$ solution with 10% hydrazine. Fine powdery silver precipitate was filtered, washed thoroughly with distilled water, dried and sieved. Electrodes were made from this powder, mechanically mixed with 2% by weight of various catalysts.

Catalysts tested were Ni, Ni alloy containing approximately 10% each of Ti and Al, Th, Ti and Mo, either as received from the chemical supplier or after various preheat treatments to form oxides. These metals were chosen because the results might give us some information on the catalytic activity related to semiconductor characteristics; i.e., p-type semiconductor will be produced by Ni and Ni alloy, n-type by Ti and Th, and amphoteric type by Mo (ref. 16).

Conditions for the heat treatment were the following:

(a) Heating in Argon with a trace of oxygen (approximately 2 ppm) for one hour at 700°C.

(b) Heating in air for one hour or less at 700°C.

It was expected that the first method would give a partial oxidation only on the surface of the powder particles, while the second method would completely oxidize the metal powder.

Table A-40 shows the cathodic current densities on these electrodes at the overpotential of 0.35 volt vs the reversible oxygen electrode in the same solution.

Table A-40

CATHODIC CURRENT DENSITIES, IN MA/CM^2, OF MRD SILVER ELECTRODE CONTAINING VARIOUS TRANSITION METAL OXIDE CATALYSTS AT THE OVERPOTENTIAL OF 0.35 VOLT VS THE REVERSIBLE OXYGEN

Electrode: Ag + 2 wt% of Catalysts in MRD Electrode Structure
Electrolyte: 5M KOH
Oxidants: Pure O_2-gas or H_2O_2 (30%)
Temperature: 90°C

Material*		NO Catalyst	Ni (A)	Ni (C)	Ni-Al-Ti	Ni-Al-Ti (B)	Ni-Al-Ti (C)	Mo (A)	Mo (B)	Mo (C)	Ti (A)	Ti (B)	Ti (C)	Th (A)	Th (B)	Th (D)
OCP**	O_2	0.17	0.17	0.15	0.17	0.13	0.16	0.20	0.22	0.21	0.17	0.17	0.17	0.16	0.15	0.17
	H_2O_2	0.22	0.21	0.22	0.20	0.22	0.20	0.18	0.22	0.21	0.22	0.22	0.20	0.22	0.24	0.22
C.D. ma/cm^2	O_2	8.0	8.4	12	3.0	1.7	1.5	21	34	3.4	24	68	11	52	14	64
	H_2O_2	10	8.6	14	2.2	1.4	1.1	24	48	4.4	29	44	17	58	24	108

* Heat - treatment of metals.
A: No treatment, as received from the supplier.
B: 1 hour is Argon containing about 2 ppm of oxygen, at 700°C.
C: Oxidation in air for 1 hour at 700°C.
D: Oxidation in air for 10 minutes at 700°C.

** Open Circuit Potential vs Reversible Oxygen Electrode in the same solution and temperature.

These results gave reasonably clear evidence that transition metal oxides of n-type or amphoteric type semiconductors (ThO_2, TiO_2) had much higher catalytic activity on the oxygen electrode than those of p-type semiconductor (NiO) and that the catalytic activity was more significant when the metal was partially oxidized rather than fully oxidized.

Full polarization curves of silver electrode without catalysts as a control, of one with nickel oxide (oxidized in air for one hour at 700°C) and of one with thorium oxide (oxidized in air for 10 minutes at 700°C) are given in Figure A-77.

The results are very interesting since among all transition metals thorium and titanium require the highest heat of initial absorption of oxygen on the metal surface and also the highest free energy of formation of the highest oxide as shown in Figure A-35.

3. Development of a Method for Precipitation of Fine Silver Powder

In spite of such a significant improvement obtained by transition metal oxide catalysts, particularly ThO_2, the general performance of these silver electrodes was still not better than the activity given by the platinum electrodes. It may be essentially true that platinum can have a better open circuit potential than silver on the oxygen electrode, because of the less negative free energy of oxide formation of platinum at the operating temperature of the cell. However, the main factors contributing to the difference observed in the polarization characteristics would be: (1) a large difference in the sizes of the powders, and (2) some difference in the kinetic characteristics as an oxygen carrier in the oxygen reduction process. Further effort was made to improve the process of making finer silver powder in order to increase the surface area which should result in increasing an apparent current density.

Methods tried were the following:

(1) Various concentrations of silver nitrate and hydrazine were used.

(2) Ultrasonic agitation* was applied during the reduction process.

*A Sonifier ultrasonic probe by Branson Instrument, Inc., Stanford, Connecticut, was used.

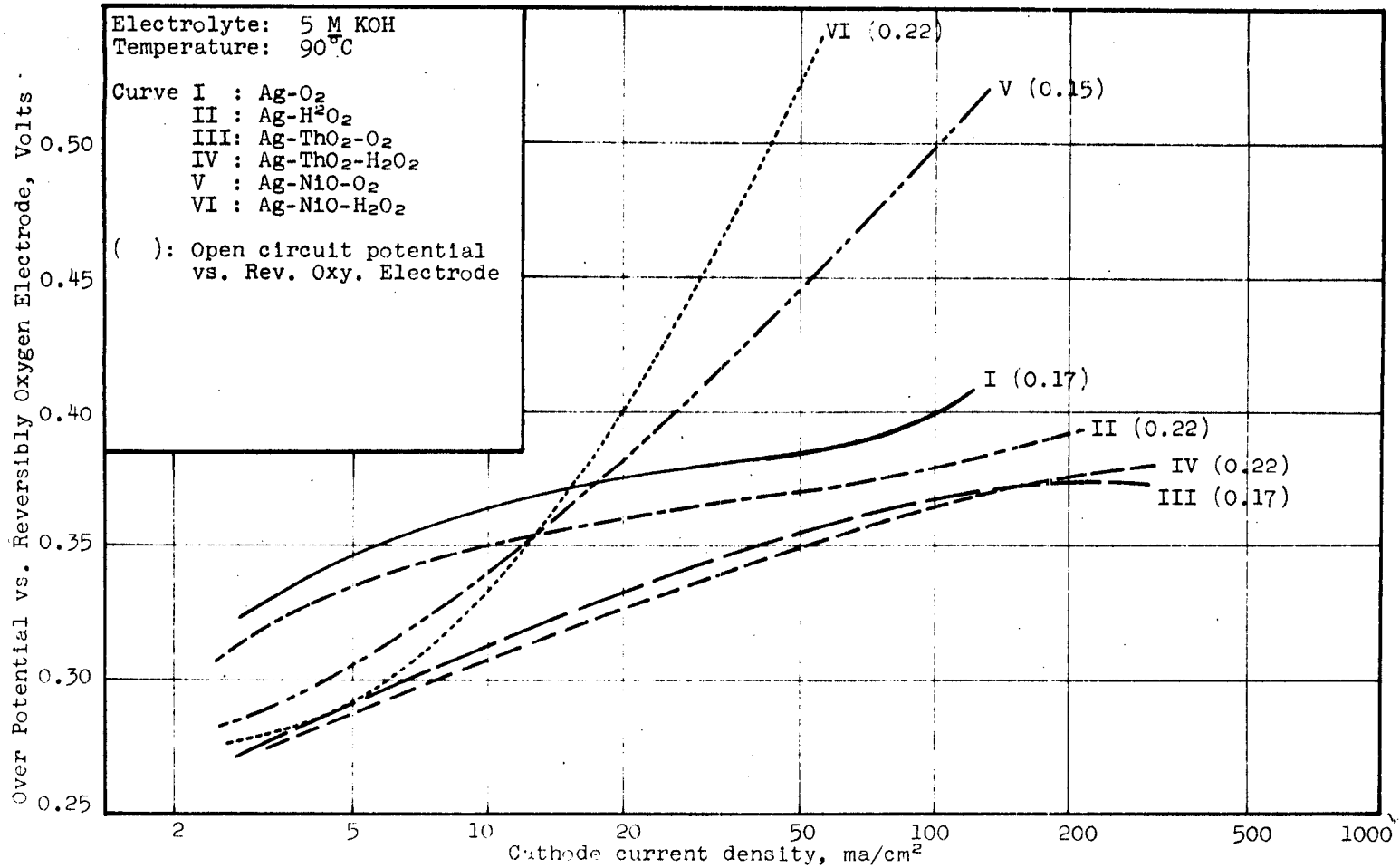

Figure A-77. Typical Cathodic Polarization Curves of MRD Porous Ag Electrodes with Transition Metal Oxide Catalysts

(3) Polyvinylpyrrolidone (PVP), a wetting agent, was added to the solution after the reduction process was completed. The ultrasonic agitation was then applied to disperse agglomerated particles.

(4) Polyvinylpyrrolidone was added to silver nitrate solution before the reduction process was started and the reducing agent was slowly added while the ultrasonic agitation was being applied.

(5) Sodium borohydride, $NaBH_4$, was used as a reducing agent instead of hydrazine.

(6) Various concentrations of silver nitrate and sodium borohydride were used.

Cathodic polarization curves of MRD porous electrodes made of the silver precipitates prepared under various conditions are shown in Figures A-78 and A-79. The various conditions for the precipitations are summarized in Table A-41. Results on Pt electrodes are also shown for comparison.

These results indicate the following:

(1) The ultrasonic agitation and PVP addition produced silver precipitates of higher activities.

(2) Silver precipitated by $NaBH_4$ was more active than that by N_2H_4.

(3) Silver precipitated from more diluted solutions were more active. This was perhaps due to the finer size of the powder as indicated by the color of the precipitate.

(4) The most important fact was that some silver cathodes showed the identical activities with platinum cathode for oxygen gas and even higher activities for H_2O_2.

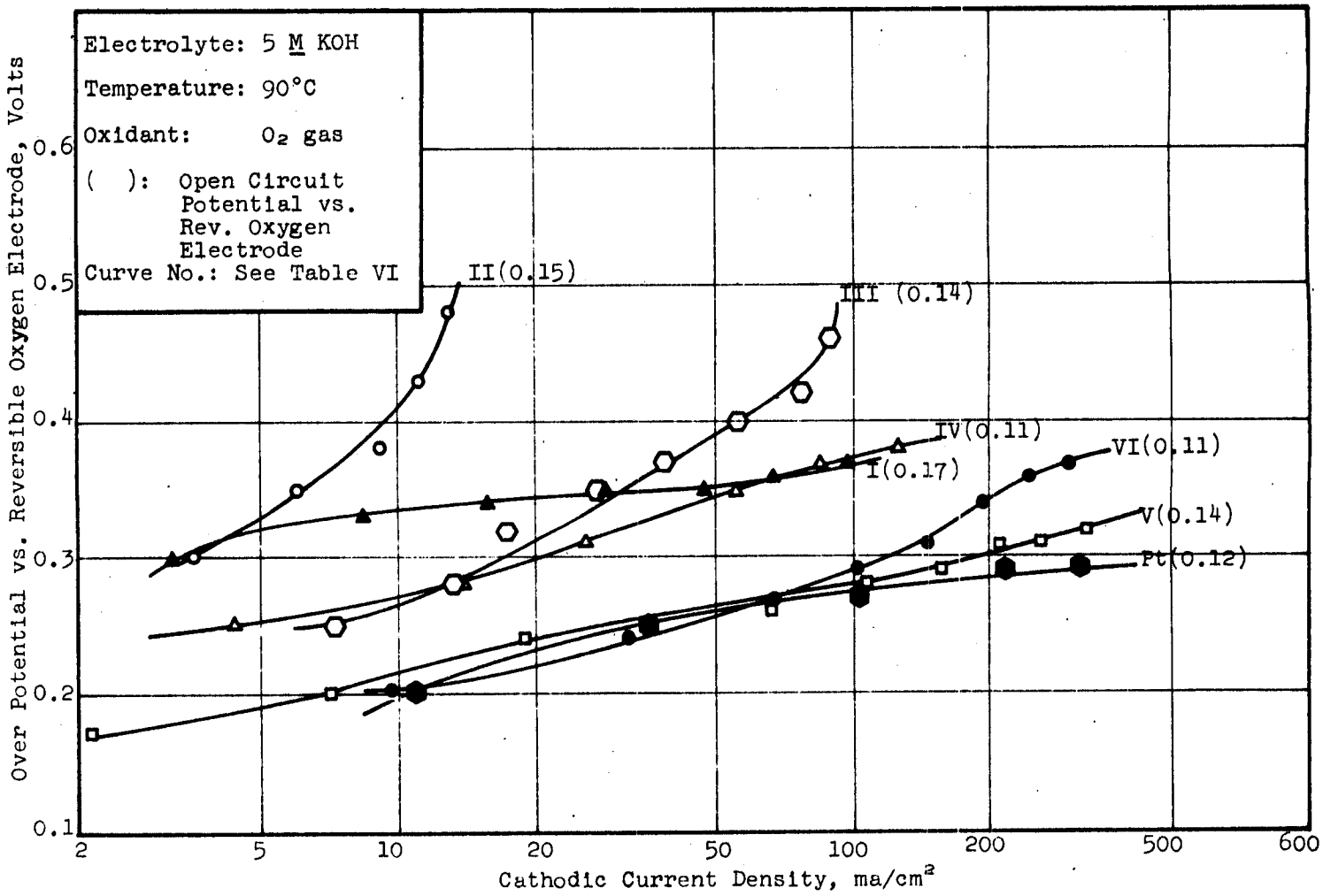

Figure A-78. Cathodic Polarization Curves of MRD Porous Electrode Made of Various Silver Powders

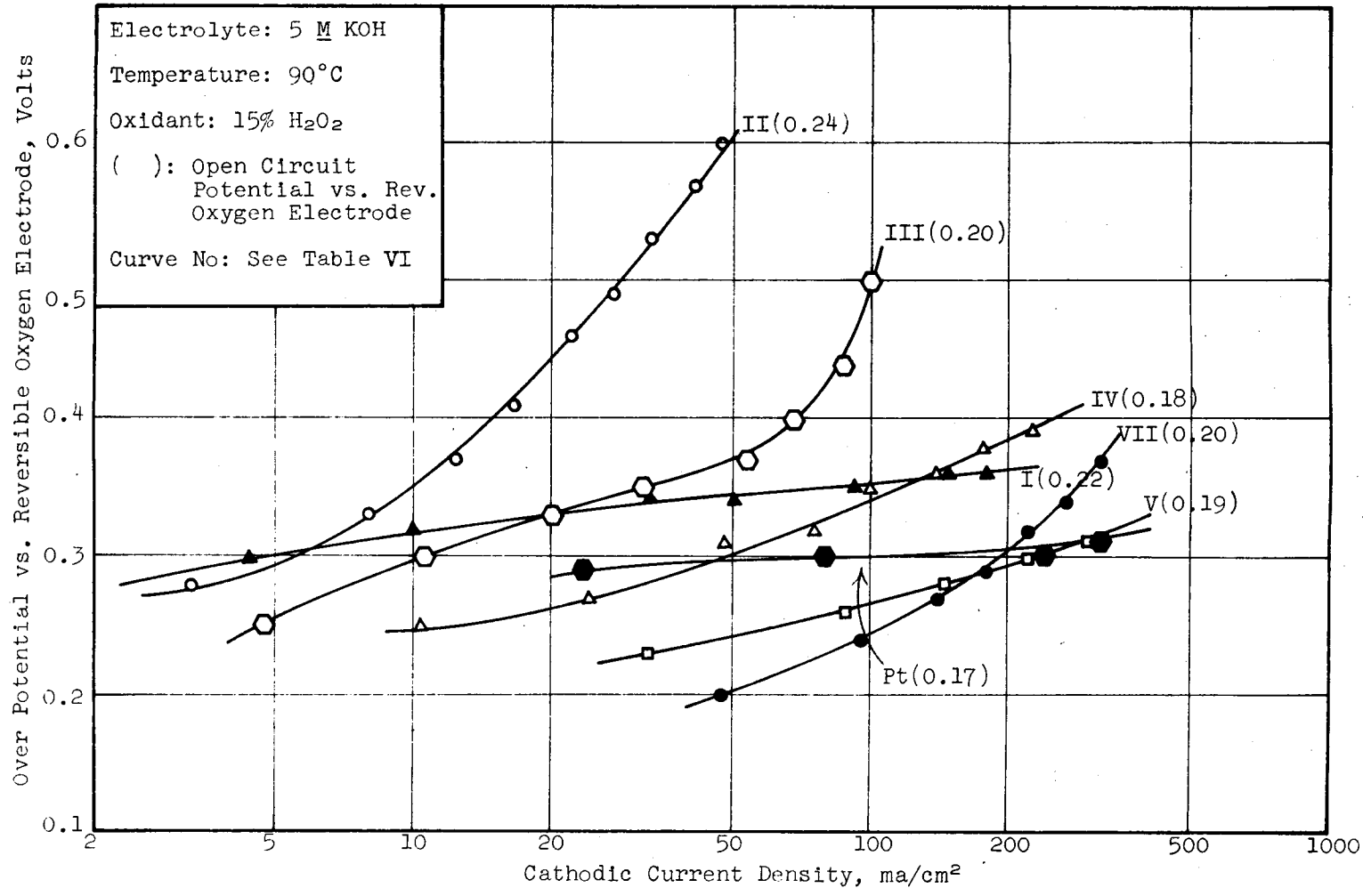

Figure A-79. Cathodic Polarization Curves of MRD Porous Electrode Made of Various Silver Powders

Table A-41

CONDITIONS FOR THE PRECIPITATION OF SILVER POWDERS USED TO PREPARE THE ELECTRODES SHOWN IN FIGURE A-79

Batch No. (Curve No.)	Conc. of $AgNO_3$, %	Reducing Agent	Conc. of Reducing Agent, %	PVP Addition, %		Ultrasonic Aggitation Applied		Color of the Precipitates
				Before Reduction	After Reduction	During Reduction	After Reduction	
I	3	N_2H_4	10	--	--	--	--	greyish yellow green
II	1	N_2H_4	2	--	--	--	--	yellow green
III	1	N_2H_4	2	--	0.5	X	X	yellow green
IV	1	$NaBH_4$	2	--	0.5	X	X	greyish yellow green
V	1	$NaBH_4$	2	1.0	--	X	--	dark greyish green
VII	5	$NaBH_4$	10	1.0	--	X	--	dark greyish green

APPENDIX X

SYSTEM DESIGN

1-KW N_2H_4/N_2O_4 FUEL CELL SYSTEM

Contract No. NAS3-4175

11 December 1964

MONSANTO RESEARCH CORPORATION
BOSTON LABORATORY
Everett, Massachusetts 02149

TABLE OF CONTENTS

LIST OF TABLES

LIST OF FIGURES

I. SYSTEM BASIS

The contractual requirements call for the design of a 1-kw system using storable rocket propellants. In this design, dinitrogen tetroxide (N_2O_4) and hydrazine (N_2H_4) were selected as reactants on the basis of their performance in full cells with Monsanto MD type electrodes. The N_2O_4 is assumed available from tank storage as a gas. The hydrazine monohydrate is metered into 5M H_3PO_4 and used in solution.

Earth environment conditions are assumed. However, exceptions are discussed in later sections.

The design presented in this report is based on the best state-of-the-art developed from a theoretical research program and is an illustration of the potential of the system. An applied research program to optimize the fuel cell module and to develop and prove out the supporting auxiliaries is required for a practical, full-scale working system.

II. DESIGN PROCEDURE

A 3 x 3-inch test cell was constructed and its performance was characterized with respect to temperature, reactant flow rates, and concentrations. The results of these tests have been reported (ref. 1). The cell voltage-current density curves at various temperatures with optimum flow rates and concentrations are shown in Figure 1.

A system design using these data and the system specifications (Appendix A) was attempted, but it was impossible to meet simultaneously the voltage and electrode area specifications at the 1-kw and 2-kw levels in the same module design. Accordingly, an optimum electrode area was calculated and the number of cells was adjusted to meet all the electrical requirements. The design performance of the module is shown in Figure 2.

Energy and mass balances calculated from the design performance and single cell data are presented in Tables 1 through 4. Calculation details are given in Appendix B. Table 4 represents expected conditions with normal optimization of electrodes and other system components. The actual system design was based on the data in Table 4.

The support system design was based on the requirements for best performance found in the experimental program to date. In particular, the high gas velocity of N_2O_4 dictated a recirculation system.

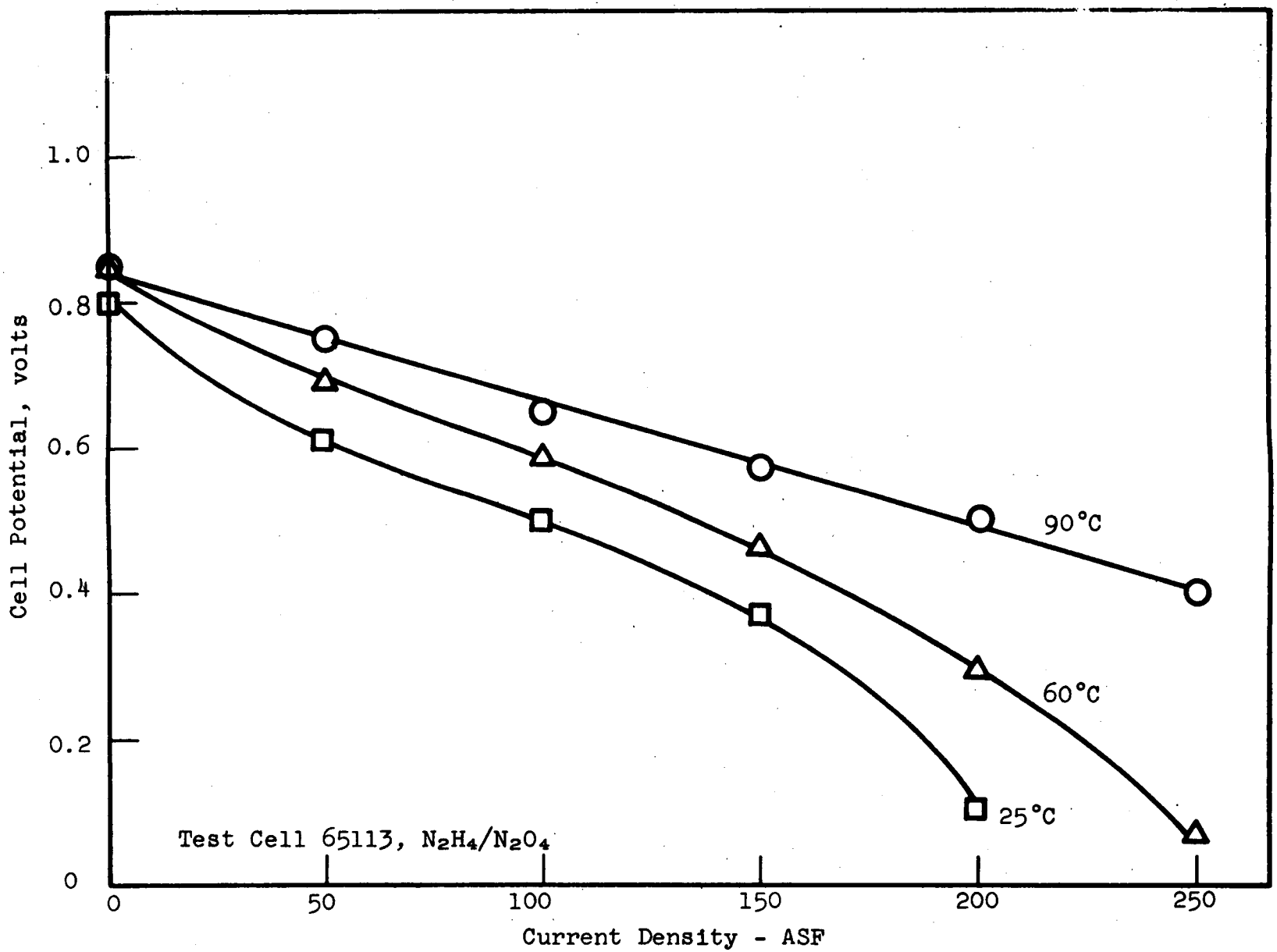

Figure 1. Single-Cell Performance Curve

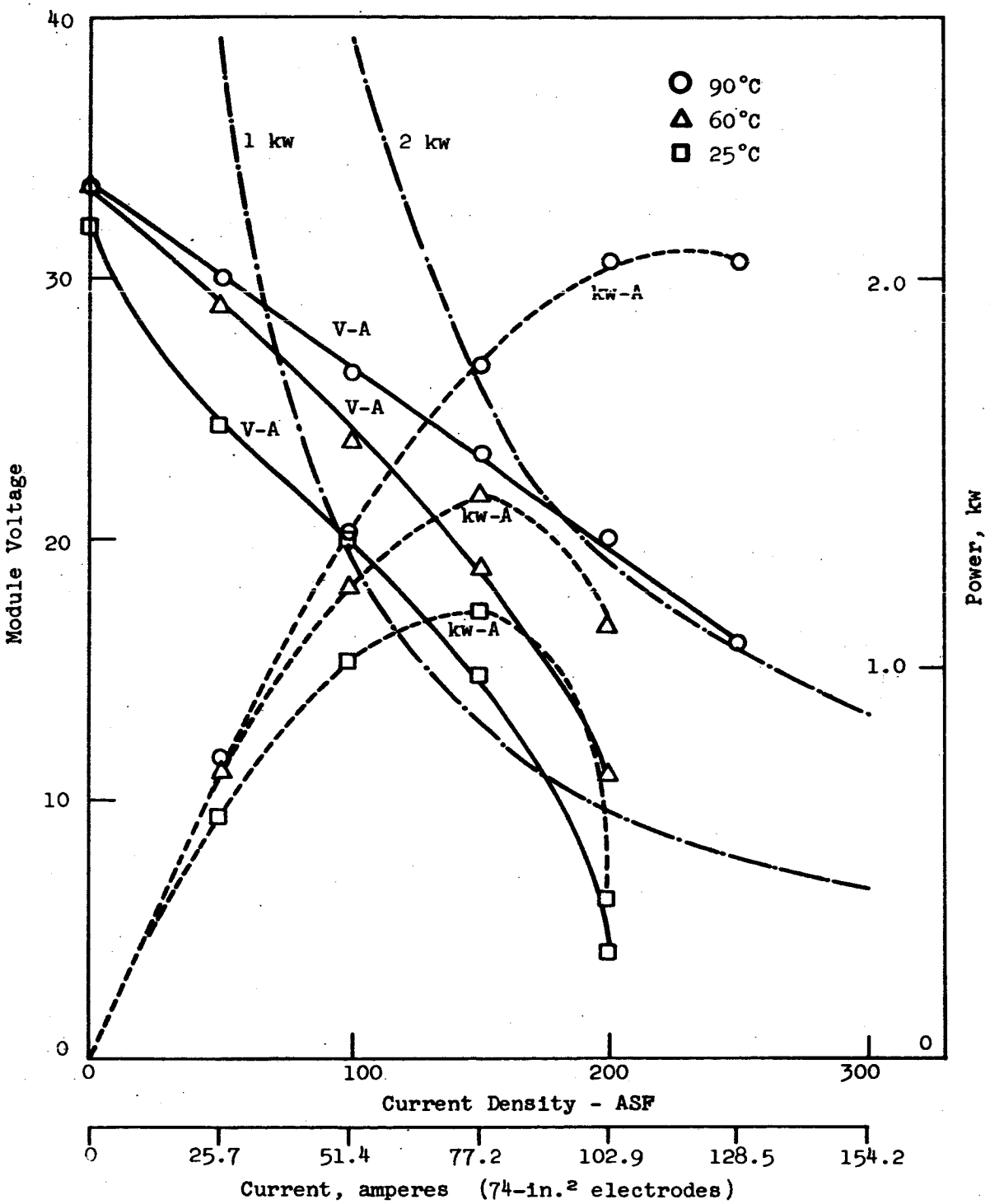

Figure 2. Design Performance, 40-Cell Module, N_2H_4/N_2O_4

Table 1

MASS AND ENERGY BALANCE TABULATION AT 25°C

Reaction $N_2O_4(g) + N_2H_4(L) \quad 2H_2O(L) + 2NO(g) + N_2(g)$

$E° = 1.42$ volts $\quad \Delta H° = -107.73$ kcal/g-mole $\quad \Delta S° = 77.76$ cal/°K g-mole $\quad \Delta F° = -130.90$ kcal/g-mole $\quad -T\Delta S° = -23.17$ kcal/g-mole

		CELL REACTION HEAT REJECTION		HEAT REJECTED BY N_2H_4 DECOMPOSITION	TOTAL HEAT	REACTION AND PRODUCT RATES						WATER BALANCE IN ANOLYTE			
I ASF	Ecell Volts	Kcal g-mole	Btu/hr	Btu/hr	Btu/hr	N_2H_4* Kg/hr	N_2O_4† Kg/hr	NO l/hr	N_2** l/hr	H_2** l/hr	H_2O†† Kg/hr	Input $N_2H_4 \cdot H_2O$ (g/hr)	Output N_2-H_2Gas (g/hr)	System Output KW	Heat Removed‡ Anode Gas (Btu/hr)
50	0.61	51.57	1963	13	1976	0.50	1.76	450	221	12.1	0.52	179	5	0.627	11
100	0.50	61.65	4693	13	4706	0.97	3.53	899	436	12.1	1.04	350	9	1.028	21
150	0.37	73.57	8401	13	8414	1.46	5.29	1,348	652	12.1	1.56	523	14	1.141	32
200	0.10	98.57	15,007	13	15,020	1.94	7.06	1,798	867	12.1	2.08	696	18	0.411	42

(4)

*As $N_2H_4 \cdot H_2O$ - 37% efficiency at 100 ASF at 90°C
†Assuming 50% eff
**Includes decomposition of wasted N_2H_4
††Includes product and hydrazine hydrate water
‡Heat removed by N_2, H_2 and H_2O gases plus evaporation of H_2O

SYSTEM - 1 KW Nominal (67 ASF at 90°C)

40 Cells 74 in.^{2} Electrodes

N_2O_4-N_2H_4 Based on Test No. 65113

Table 2

MASS AND ENERGY BALANCE TABULATION AT 60°C

Reaction $N_2O_4(g) + N_2H_4(L) \quad 2H_2O(L) + 2NO(g) + N_2(g)$

$E° = 1.45$ volts $\quad \Delta H° = -107.27$ kcal/g-mole $\quad \Delta S° = 79.27$ cal/°K g-mole $\quad \Delta F° = 133.6$ kcal/g-mole $\quad -T\Delta S° = -26.40$ kcal/g-mole

		CELL REACTION HEAT REJECTION		HEAT REJECTED BY N_2H_4 DECOMPOSITION	TOTAL HEAT	REACTION AND PRODUCT RATES						WATER BALANCE IN ANOLYTE			
I ASF	Ecell Volts	Kcal g-mole	Btu/hr	Btu/hr	Btu/hr	N_2H_4* Kg/hr	N_2O_4† Kg/hr	NO l/hr	N_2** l/hr	H_2** l/hr	H_2O†† Kg/hr	Input $N_2H_4 \cdot H_2O$ (g/hr)	Output N_2-H_2Gas (g/hr)	System Output KW	Heat Removed‡ Anode Gas (Btu/hr)
50	0.72	40.84	1554	209	1763	0.70	1.76	450	313	196	0.60	0.251	0.080	0.740	204
100	0.59	52.87	4025	209	4234	1.18	3.53	899	528	196	1.11	0.424	0.116	1.213	298
150	0.47	63.96	7303	209	7512	1.66	5.29	1,348	744	196	1.63	0.597	0.148	1.449	380
200	0.27	82.41	12,466	209	12,675	2.14	7.06	1,798	959	196	2.15	0.770	0.182	1.110	466
250	0.06	101.79	19,371	209	19,580	2.62	8.82	2,247	1173	196	2.70	0.942	0.216	0.308	552

*As $N_2H_4 \cdot H_2O$ - 37% efficiency at 100 ASF at 90°C
†Assuming 50% eff
**Includes decomposition of wasted N_2H_4
††Includes product and hydrazine hydrate water
‡Heat removed by N_2, H_2 and H_2O gases plus evaporation of H_2O

SYSTEM - 1 KW Nominal (67 ASF at 90°C)

40 Cells 74 in.^{2} Electrodes

N_2O_4-N_2H_4 Based on Test No. 65113

Table 3

MASS AND ENERGY BALANCE TABULATION AT 90°C

Reaction $N_2O_4(g) + N_2H_4(L) \quad 2H_2O(L) + 2NO(g) + N_2(g)$

$E^\circ = 1.476$ volts $\quad \Delta H^\circ = 106.90$ Kcal/g-mole $\quad \Delta S^\circ = 80.64$ cal/°K g-mole $\quad \Delta F^\circ = 136.17$ Kcal/ g-mole $\quad -T\Delta S^\circ = 29.27$ Kcal/ g-mole

I ASF	Ecell volts	Cell Reaction Heat Rejection Kcal g-mole	Cell Reaction Heat Rejection Btu/hr	Heat Rejected by N_2H_4 Decomposition Btu/hr	Total Heat Btu/hr	Reactant and Product Rates N_2H_4* Kg/hr	N_2O_4† Kg/hr	NO L/hr	N_2** L/hr	H_2** L/hr	H_2O†† Kg/hr	Water Balance in anolyte Input from $N_2H_4 \cdot H_2O$ (Kg/hr)	Water Balance in anolyte Output with N_2 and H_2 Gas (Kg/hr)	System Output KW	Heat Removed‡ from Anode Gas (Btu/hr)
50	0.75	37.73	1,436	1674	3,110	2.32	1.76	450	999	1,568	1.15	0.80	2.29	0.771	5,409
100	0.66	46.03	3,504	1674	5,178	2.71	3.53	899	1,214	1,568	1.66	0.97	2.49	1.357	5,893
150	0.58	53.39	6,096	1674	7,770	3.20	5.29	1,348	1,430	1,568	2.18	1.15	2.67	1.789	6,323
200	0.50	60.74	9,247	1674	10,921	3.68	7.06	1,798	1,645	1,568	2.70	1.32	2.87	2.056	6,777
250	0.40	70.00	13,326	1674	14,990	4.15	8.82	2,247	1,859	1,568	3.22	1.49	3.06	2.056	7,230

* As $N_2H_4 \cdot H_2O$ - 37% efficiency in Electrochemical at 100 ASF

† Assuming 50% efficiency

** Includes decomposition of wasted N_2H_4

†† includes product and hydrate water

‡ Heat removed by N_2H_2, H_2O gas and vaporization of H_2O

SYSTEM - 1 KW Nominal (67 ASF at 90°C)

40 Cells 74 in.^{2} Electrodes

N_2O_4 - N_2H_4 Based on Test No. 65113

Table 4

MASS AND ENERGY BALANCE TABULATION AT 90°C

E° = 1.476 volts ΔH° = -106.90 cal/g-mole ΔS° = 80.64 cal/°K g-mole ΔF° = -136.17 Kcal/g-mole $-T\Delta S^\circ$ = -29.27 Kcal/g-mole

I(ASF)	E(cell) volts	Cell Reaction Heat Rejection Kcal g-mole	Cell Reaction Heat Rejection Btu/hr	Heat Rejected by N_2H_4 Decomposition Btu/hr	Total Heat	Reactant and Product Rates N_2H_4* kg/hr	N_2O_4† kg/hr	NO l/hr	N_2** l/hr	H_2** l/hr	H_2O†† kg/hr	System Output KW	Water Balance in Anolyte Input From $N_2H_4 \cdot H_2O$ kg/hr	Water Balance in Anolyte Output with N_2+H_2 Gas	Heat Removed Btu/hr from Anode Gas‡
50	0.75	37.73	1436	102	1538	0.59	1.76	450	263	95	0.56	0.771	0.21	0.28	659
100	0.66	46.03	3504	102	3606	1.07	3.53	899	478	95	1.07	1.357	0.38	0.48	1143
150	0.58	53.39	6096	102	6198	1.55	5.29	1,348	693	95	1.59	1.789	0.56	0.66	1507
200	0.50	60.74	9247	102	9349	2.03	7.06	1,798	908	95	2.11	2.056	0.73	0.85	2025
250	0.40	70.00	13,326	102	13,428	2.51	8.82	2,247	1,123	95	2.63	2.056	0.90	1.04	2478

*As $N_2H_4 \cdot H_2O$ - 90% Eff. at 100 ASF

†Assuming 50% eff.

**Includes decomp. of wasted N_2H_4

††Includes product and hydrate water

‡Heat removed by N_2, H_2, H_2O gas and vaporization of H_2O

(7)

The weights and volumes of components are catalog values or estimates from the literature. Module weights and volumes were calculated from the proposed design and the electrode separator system used in the test cell.

III. PROPOSED MODULE PERFORMANCE

Test data and the required electrical specifications dictated 90°C operation temperature with 74 in.^{2} electrodes and 40 cells. The anticipated module performance is:

For 1-kw, 67.5 ASF (34.9 amp) at 28.8 volt
For 2-kw, 188 ASF (96.5 amp) at 20.7 volt

The module performance at other current densities and temperatures is shown in Figure 2. As with reactant efficiencies, normal optimization of electrodes, separators, and other system components can be expected to improve the electrical characteristics. Figure 2 does not include power requirements of supporting auxiliaries.

IV. PROPOSED CELL CONSTRUCTION

The module will be constructed in a single series bipolar arrangement. Details of individual cell construction are shown in Figure 3. Principal features of this construction are: a rigid plastic frame containing manifold and feeder provisions molded about the electrodes, cell sealing provided by an irregular "O-ring", gelled electrolyte contained between the electrodes, and a corrugated bipolar plate to provide electrical contact and reactant flow passages.

The molded frame is similar in design to cells presently being investigated at Monsanto Research Corporation. However, because of the nature of the fuel and oxidant, further studies must be made to determine material compatibility. Initial investigation has shown that high density polyethylene should give fully reliable life in excess of 300 hours (ref. 4, and other testing within MRC) with a maximum life well exceeding this figure.

The reactant and product manifold passages in this molded frame were designed to give a low pressure drop inlet and large volume outlet to provide even distribution of the inlet solution and outlet solution and product gases.

The irregular "O-ring" seals will be custom molded of suitable materials. At present, in the 3 x 3-inch test cells used on this contract, the "O-rings" used for sealing have been Parker compound V494-7 for the catholyte and Parker compound E515-8 for the anolyte. These have given suitable service to date and are expected to be suitable in the proposed design.

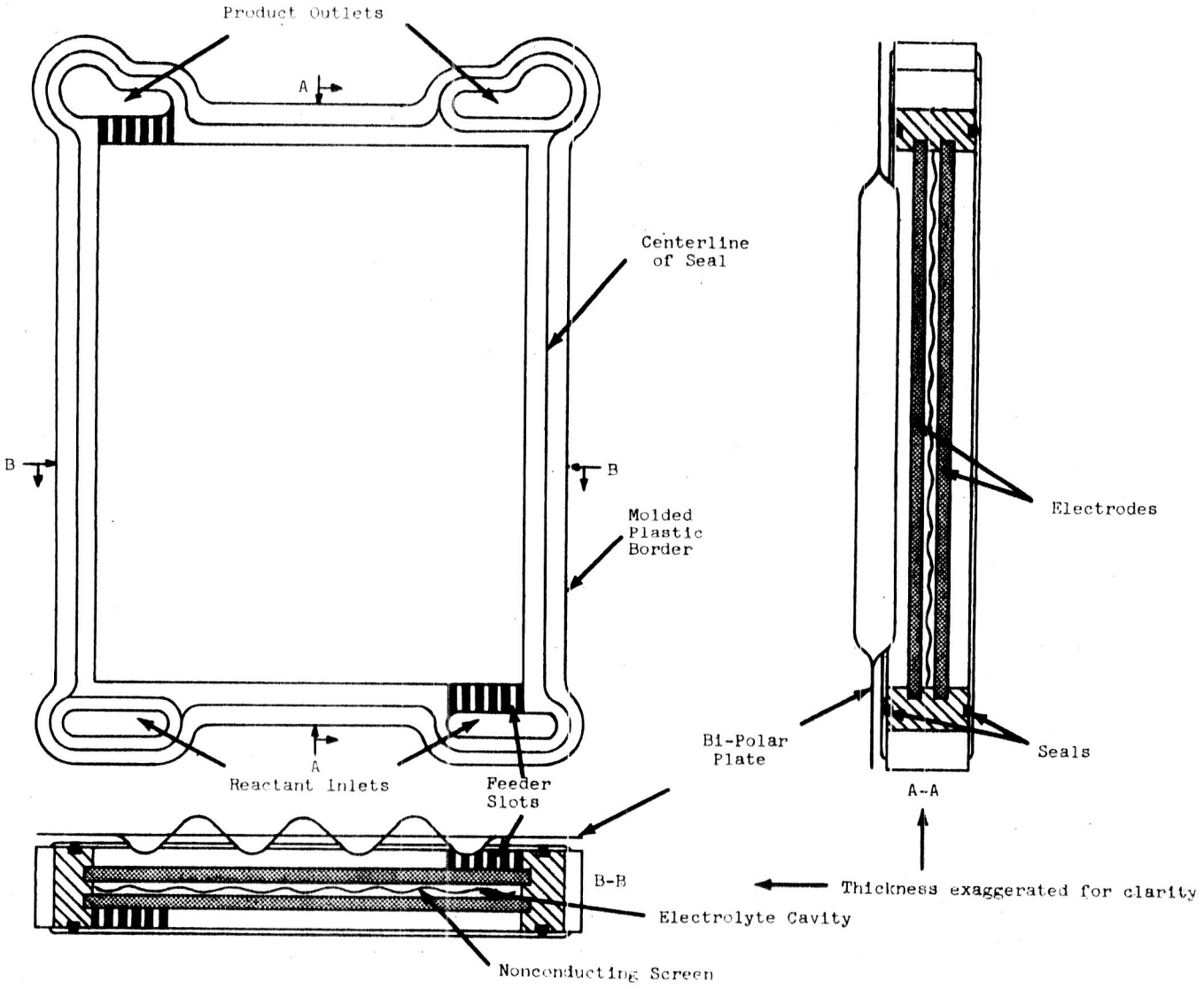

Figure 3. Cell Construction

The electrolyte, a phosphoric acid Santocel® gel, will be injected into the electrolyte cavity after the border is molded. A screen or porous mat of nonconducting material will be included in the electrolyte cavity to prevent shorting of the electrodes in the event of excessive reactant pressure or other malfunction.

V. SYSTEM CONFIGURATION

A schematic diagram of the proposed system is shown in Figure 4.

Hydrazine hydrate ($N_2H_4 \cdot H_2O$) from an outside storage tank is metered at a controlled rate into the anolyte, which is then pumped into the module. The amount of fuel metered is determined mainly by the duty cycle of the module; for a constant power output, a simple calibrated orifice would be sufficient. For an irregular duty cycle, the valve could be controlled by monitoring the N_2 production, N_2H_4 concentration in the anolyte, or the electrical power consumption.

After reaction in the cell, the anolyte and product N_2 are returned to the electrolyte tank where N_2 saturated with water vapor is vented.

N_2O_4 gas is supplied to the recirculation system from external tankage through a controlled metering valve, while the system is simultaneously vented through a purge valve. The metering-venting cycle is adjusted to give at least 50% utilization of N_2O_4. For a constant power output, a simple timer control operating the valves would be sufficient. For irregular power consumption, the valves could be controlled by monitoring the N_2O_4 or NO partial pressures, or the electrical power consumption.

The reactant gases are recirculated through the cell by a compressor at a rate sufficient to insure optimum cathode performance. Product water is condensed and trapped out of the stream.

A radiator is shown dotted in the schematic diagram. Depending on the magnitude of radiative losses from the system and the duty cycle of the module, a separate radiator may not be required. Although the module will not give 2-kw performance at room temperature, 1 kw is easily produced with a substantial heating effect. Thus, the module can be considered self-starting with the time required to realize optimum performance determined by the bulk heat capacity of the system and radiative losses. If shorter times are required, the available electrical power can be used through heating elements or, alternatively, N_2O_4 and N_2H_4 can be burned hypergolically in a special manifold to heat the system.

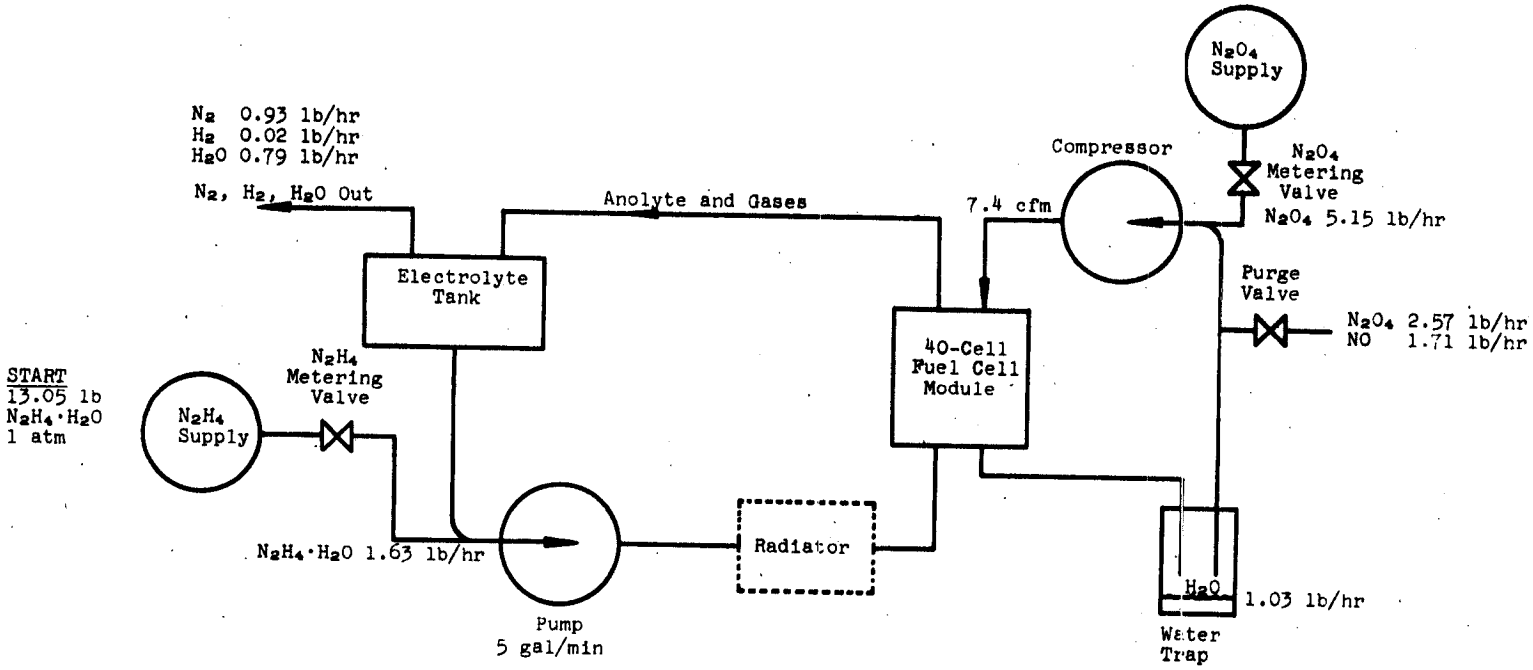

Electrolyte Tank

	Start		Finish
	0.52 lb N_2H_4 (≈3m/l)		0.24 lb N_2H_4
	1.90 lb H_3PO_4 (≈30%)		1.90 lb H_3PO_4
	4.74 lb H_2O		3.48 lb H_2O
Total	7.16 lb	Total	5.62 lb

Overall Material Balance, 8 Hours

In	
$N_2H_4 \cdot H_2O$	13.05 lb
N_2O_4	42.10 lb
Total	55.15 lb

Out + Accumulation	
Tank Exhaust	= 13.75 lb
Purge	= 34.75 lb
Tank Accumulation	= - 1.54 lb
Cathode Water Accumulation	= 8.28 lb
Total	55.24 lb

Figure 4. System Configuration and Mass Balance for 8-Hour Run

VI. MATERIAL BALANCE FOR EIGHT-HOUR OPERATION

An eight-hour mission was arbitrarily selected to provide a basis for a sample material balance. The results are included in Figure 4.

It should be emphasized that with normal development and optimization the fuel cell system is considered potentially applicable to a wide variety of either terrestrial or space mission times, each one requiring separate specification of tankage, waste gas and liquid treatment, recirculation requirements, operating temperature and heat input or output. For this reason, the material balance arrived at here, as well as system weights and volumes, do not represent an operational limit, but serve purely as one specific example. Both module and auxiliary weights and volumes are tabulated in Table 5 for an eight-hour mission. Longer mission times would require some additions of supporting auxiliaries and would tend to increase weight and volume.

VII. WATER REMOVAL AND RECOVERY OF PRODUCT WATER

The present design provides for accumulation of product water from the N_2O_4 stream, and no provision has been made for make-up of water lost from the anolyte. In an eight-hour mission time neither effect causes much concern. However, longer mission times would require provisions to take care of both processes.

For the anolyte, recovery of part of the water from exhaust gas streams by condensation and subsequent return to the anolyte tank is the simplest method. The excess condensed water would have to be purified of traces of N_2H_4 by catalytic decomposition before the water could be used outside the fuel cell module.

The product water trapped from the N_2O_4 stream presents a more difficult problem because of the possibility of its reaction with N_2O_4 to form HNO_3 and NO. In long-term missions, this would put a basic limitation on N_2O_4 utilization efficiency (Appendix C). The problem can be attacked in at least two ways:

(1) Development of less porous electrodes to minimize back diffusion of water vapor into the N_2O_4 stream.

(2) Fast condensation and separation of the condensed water from contact with the N_2O_4 in a time short enough to prevent the reaction from coming to equilibrium.

Table 5

CELL AND MODULE WEIGHT-VOLUME COMPILATION

Cell Component	Wt, g
Anode MRDA-Pt	27.9
Cathode Double MRDC-C	55.8
Bipolar Plate .010 304 stainless steel	180.0
Molded border, high density polyethylene including sealing ring	93.5
Electrolyte, phosphoric acid gel	49.0
Total wt/cell	406.2

Wt. - 40 cells = 16,500 g	= 35.8 lb
End plates	4.2 lb
Tie bolts	1.5 lb
Misc. insulator, etc.	≈1.0 lb
Total Module Wt	42.5 lb

Module Volume

(13 in.)(10 in.)(.170 in./cell)(40 cells) = 876 $in.^3$ = .52 ft^3

Auxiliary Weights and Volumes

	Weight lb	Volume ft^3
Electrolyte tank	2.0	0.2
Water trap tank	1.3	0.1
Pump	1.9	0.05
Compressor	1.0	0.03
Purge valve	0.5	*
N_2H_4 metering valve	0.3	*
Electrolyte shut-off valve	0.5	*
Piping and fittings	≈5.0	*
Support frame	≈5.0	*
Electrical components, leads controls, etc.	≈5.0	*
Access space, tube and wire runways, etc.	-	0.4
Total	22.5	0.78

Total System Wt ≈ 65.0†

Total System Volume ≈ 1.30 ft^3†

*Included in access space

†Does not include cooling auxiliary if required

VIII. ZERO GRAVITY OPERATION

The principal problem associated with this fuel cell system in adapting it for a zero gravity environment is the separation of the gaseous phases from liquid phases. Several solutions to this problem are possible:

1. Certain space missions necessarily involve maintenance of artificial gravity for personnel-manned compartments. In cases of this type the fuel cell with or without tankage, or at least the phase separation portion of the fuel cell system, could be operated under the artificial gravity conditions.

2. Phase separation in rotating centrifugal machines offers some advantage. Here the gas-laden exit stream from the fuel cell is pumped to the powered centrifugal separator. The underflow liquid phase enters the primary electrolyte pump suction and is forced into an accumulator type electrolyte tank. Effectively, then, the electrolyte pump is placed before the electrolyte tank and the entire fuel cell system is internally pressurized on the liquid side.

3. Use of semi-permeable membranes has frequently been suggested as a means of zero gravity phase separation. This idea is equally applicable to a bulk liquid phase fuel cell system such as the N_2H_4 system as it is to all gas phase systems, e.g., H_2/O_2.

The MRD cathodes employed in our fuel cells are semi-permeable and possess excellent mechanical properties when supported on a screen grid. Special formulations of this electrode for use purely as a semi-permeable membrane are possible, and it is believed that effective control of both pore size and distribution and hydrophobic properties can be obtained. We have also had experience with various types of porous Teflon materials, which appear adaptable to this service.

A semi-permeable membrane approach could be particularly attractive for this N_2H_4 system because of the very low operating pressures required, thus simplifying construction and reducing weight of the phase separator device.

APPENDIX A

FUEL CELL SYSTEM REQUIREMENTS

Under the terms of the subject contract, Article I.A.1.h, the NASA Project Manager is to define requirements for a fuel cell system using storable rocket propellants as reactants. This contractual requirement is herewith defined as follows:

(a) Power requirement - 1 kilowatt electrical output; current density, 100 ma/cm^2; operating potential, 28 ± 2 volts.

(b) Environmental conditions - Normal earth atmosphere at 25°C and 1 atmosphere pressure.

(c) Weight and volume restrictions - Electrode area, 60 ± 4 in.^{2} shape approximately square; dimensions may be between approximately 8 in.^{2} and approximately 7 x 9 in. Length as required by the number of cells. The weight shall be smallest practical based upon the most recent data.

(d) Operating duty cycle - Continuous duty at 1 kilowatt with 100% overload (2.0 kilowatts at 21 ± 2 volts) for five minutes once every eight hours. Operating period, 1000 hours.

(e) Special conditions affecting operation (1), (4), (5) and (7). Discuss alternate conditions (2), (3) and (6).

(1) Normal earth gravity
(2) Zero gravity
(3) Recovery of product water
(4) Venting of product water
(5) Venting of gaseous products
(6) Sorption of gaseous products other than nitrogen
(7) Operating temperature: 15-90°C

The subject contract further specifies under Article I.A.1.i that at the end of nine months under the contract, the contractor shall submit to the NASA Project Manager his recommendations to meet the requirements described above in terms of (a) cell design features, (b) reactants and electrolyte selection, (c) size and weight estimate, and (d) storage and feed system recommendations.

APPENDIX B

MASS AND ENERGY BALANCE CALCULATIONS

Operating Conditions:
1 kw (nominal) N_2H_4-N_2O_4 Fuel Cell System

The tabulation of mass and energy balance (Tables 1 to 4) were calculated from the experimental voltage, current, and power curves (Figure 2) and from the thermodynamic data for the fuel cell reaction and chemical species involved. The following section describes the approach used for the calculations.

A. MASS RATES FOR REACTANTS AND PRODUCTS BALANCE

1. N_2H_4

In calculating the $N_2H_4 \cdot H_2O$ (as hydrate) mass rate a current efficiency of 37% at 100 ASF and 90°C was assumed for Tables 1 to 3, which corresponds to the current experimental data. Table 4 shows the fuel cell properties based on expected improvement to 90% efficiency at 100 ASF for N_2H_4. The unused N_2H_4 is assumed to decompose to N_2 and H_2. This decomposition was assumed to be constant at a given temperature regardless of current density.

$$N_2H_4 \longrightarrow N_2 + 2H_2 + \Delta H = 12.05 \text{ kcal/g-mole}$$

Another section of the Appendix will show calculations for decomposition rates at other temperatures.

The total mass flow rate, $\dot{M}$, in grams/hour is:

$$\dot{M} = \frac{I \times 3600 \times MW}{nF} \times N_c \times \frac{100}{\eta_E}$$

where I = total current of module = current density (ASF) x area (ft^2)

MW = gram molecular weight (50 for $N_2H_4 \cdot H_2O$)

n = number of gram equivalents/mole = 4 for N_2H_4

F = Faradays' number - 96,500 coul/gram equivalent

N_c = total number of cells per module = 40

η_E = efficiency in % of the electrochemical reaction

The product of (I x 3600) gives coulombs/hour.

2. N_2O_4

The N_2O_4 usage efficiency was set as 50%. Although this figure has not yet been approached in the unoptimized cells now being built, it is expected to be attained.

$\dot{M}_{N_2O_4}$ in grams/hour is calculated in the same way as for N_2H_4; n = 4 for N_2O_4 also.

3. N_2

In calculating the N_2 mass rate, all the input N_2H_4 was assumed to produce N_2 through either the electrochemical reaction or by decomposition.

Thus, the mass flow rate of N_2 can be calculated from the $N_2H_4 \cdot H_2O$ flow rate:

$$\dot{M}_{N_2} \text{ in liters/hr at STP} =$$

$$\dot{M}_{N_2H_4 \cdot H_2O} \times \frac{1}{M_{N_2H_4 \cdot H_2O}} \left(\frac{\text{g-moles}}{\text{hr}}\right) \times \frac{RT}{P} \left(\frac{\text{liters}}{\text{g-mole}}\right)$$

4. H_2

The H_2 mass rate can be calculated from the decomposition ratio and is assumed constant at a given temperature. Values are expressed as liters/hr at STP.

5. NO

The NO rate is calculated assuming the postulated fuel cell reaction to hold. It can be calculated from the N_2O_4 utilization rate, with the efficiency again 50% and with 2 moles NO formed per mole of N_2O_4 reaction:

$$\dot{M}_{NO} \text{ in liters/hr} =$$

$$\frac{1}{2} \dot{M}_{N_2O_4} \times \frac{1}{MW_{N_2O_4}} \left(\frac{\text{g-moles } N_2O_4}{\text{hr}}\right) \times \frac{2 \text{ g-moles NO}}{\text{g-mole } N_2O_4} \times \frac{RT}{P} \left(\frac{\text{liters}}{\text{g-mole}}\right)$$

6. H_2O

The H_2O mass rate includes the electrochemical production of H_2O and that introduced by the $N_2H_4 \cdot H_2O$.

$$\dot{M}_{H_2} \text{ in grams/hr} = \frac{I \times 3600}{nF} \times N_c \times \left(\frac{\text{g-moles } H_2O}{\text{hr}}\right) \times MW_{H_2O}$$

$$+ \dot{M}_{N_2H_4 \cdot H_2O} \times \frac{MW_{H_2O}}{MW_{N_2H_4 \cdot H_2O}}$$

where n = 2 per mole of H_2O produced.

B. CALCULATION OF THE THERMODYNAMIC QUANTITIES E°, ΔF°, ΔH°, ΔS°, $-T\Delta S^\circ$ FOR THE CELL REACTION AT DIFFERENT TEMPERATURES

Reaction: N_2H_4 (L) + N_2O_4 (g) $\longrightarrow$ 2NO (g) + N_2 (g) + $2H_2O$ (L)

1. ΔH°_T

ΔH°_T was calculated from the ΔH°_f of the reactants and products at the various temperatures used.

$$\Delta H^\circ_T \text{ (reaction)} = \Delta H^\circ f(N_2)$$

$$+ 2\Delta H^\circ f(NO) + 2\Delta H^\circ f(H_2O) - \Delta H^\circ f(N_2H_4) - \Delta H^\circ f(N_2O_4)$$

The ΔH°_f for any temperatures were calculated from heat capacity data, or interpolated from tabulated data.

$$\Delta H^\circ_{fT} = \Delta H^\circ_{f298} + \int_{T_{298}}^{T_1} \Delta C_p dT$$

2. ΔS°

ΔS°_T for the reaction at any temperature was calculated from the entropies of the reactants and products at the various temperatures.

$$\Delta S^\circ_T \text{ (reaction)} = S^\circ_{N_2} + 2S^\circ_{H_2O} + 2S^\circ_{NO} - S^\circ_{N_2H_4} - S^\circ_{N_2O_4}$$

Again, the values were gathered from tabulated data, or calculated from heat capacity data.

$$S^\circ_T = S^\circ_{298} \int_{T_{298}}^{T_1} Cp/T \, dT$$

3. ΔF°

ΔF°_T was calculated from the values of ΔH°_T and ΔS°_T in the previous section.

$$\Delta F^\circ_T = \Delta H^\circ_T - T\Delta S^\circ_T$$

4. E°

The theoretical potential for the reaction (E°) is:

$$E^\circ = \frac{-\Delta F^\circ \text{ (reaction)}}{nF}$$

where ΔF° (reaction) is expressed in joules.

C. ESTIMATION OF DECOMPOSITION EFFECTS AT VARIOUS TEMPERATURES FOR N_2H_4

The efficiency was found experimentally at 90°C and 100 ASF to be 37%. Thus, the amount of decomposition can be calculated:

$$\dot{M} \text{ (decomp)} = \dot{M}_{N_2H_4 \cdot H_2O} \text{ (total)} - \left(\frac{I \times 3600}{nF}\right) \times N_c \times MW_{N_2H_4 \cdot H_2O}$$

This amount is assumed to be caused by the fast flow rate at the back of the electrode, and thus to be constant at all current densities for a given temperature.

For the same flow rate, the value of decomposition at other temperatures was calculated from the general kinetic rate, that is, that a reaction rate doubles for a 10°C increase in temperature.

D. FUEL CELL HEAT REJECTION

The total heat rejection of the cell is equal to the sum of the heat of decomposition of the wasted N_2H_4, the irreversible terms of the fuel cell electrochemical reaction, and the $T\Delta S$ term of the reaction.

$$Q\ (\text{electrochemical}) = \left(1 - \frac{E_T}{E^\circ}\right) \Delta F\ (\text{reaction}) + T\Delta S^\circ$$

per mole of electrochemical reaction, and

$$Q\ (\text{decomp}) = \Delta H\ (\text{decomp})$$

per mole of N_2H_4 decomposed.

Where E_T = operating voltage

E° = theoretical reversible voltage

ΔH (decomp) = ΔH° (reaction) for N_2H_4 (L) $\longrightarrow N_2 + 2H_2$

For the 40-cell module, the rate of heat rejection per hour is:

$$\text{Total } Q\ (\text{Btu/hr}) = Q\ (\text{elect})\ \left(\frac{\text{kcal}}{\text{g-mole } N_2H_4}\right)$$

$$\times \frac{I \times 3600}{nF}\ \left(\frac{\text{g-mole } N_2H_4}{\text{hr}}\right) \times N_c \times 3.97\ \left(\frac{\text{Btu}}{\text{kcal}}\right)$$

$$+ Q\ (\text{decomp})\ \left(\frac{\text{kcal}}{\text{g-mole } N_2H_4}\right) \times \dot{M}\ (\text{decomp})\ \left(\frac{\text{g } N_2H_4 \cdot H_2O}{\text{hr}}\right)$$

$$\times \frac{1}{MW_{N_2H_4 \cdot H_2O}} \times 3.97\ \left(\frac{\text{Btu}}{\text{kcal}}\right)$$

E. H_2O VAPOR REMOVED BY N_2 AND H_2 GASES

The total vapor pressure above the electrolyte tank is 14.7 psia (1 atm). The total pressure is $P_{H_2O} + P_{N_2} + P_{H_2}$. Thus, knowing the vapor pressure of water in 35% H_3PO_4 at various temperatures:

$$\frac{\text{moles } H_2O}{\text{moles } (H_2 + N_2)} = \frac{P_{H_2O}}{1\text{-}P_{(H_2 + N_2)}} = \frac{X_{H_2O}}{X_{(H_2 + N_2)}}$$

where P_{H_2O} is the vapor pressure of water in atm, and

X is the mole fraction.

Knowing the mole fractions of $(N_2 + H_2)$ and H_2O present, the number of moles of H_2O/liter $(N_2 + H_2)$ can be calculated:

$$\frac{\text{gram } H_2O}{\text{liter } (N_2 + H_2)} = \frac{P}{RT} \left(\frac{\text{moles } (N_2 + H_2)}{\text{liter } (N_2 + H_2)}\right)$$

$$x \frac{X_{H_2O}}{X_{(N_2 + H_2)}} \left(\frac{\text{moles } H_2O}{\text{moles } N_2}\right) x \frac{18 \text{ g}}{\text{moles } H_2O}$$

where P is in atm

$R = .082$ atm liter/°K mole

$T = °K$

X_{H_2O} = mole fraction H_2O

$X_{(N_2 + H_2)}$ = mole fraction $(N_2 + H_2)$

This figure multiplied by the combined mass flow rate of $N_2 + H_2$, will give the g/hr H_2O rejected.

F. HEAT REMOVED FROM SYSTEM BY ANODE GAS

Heat removed will occur through a number of routes including:

1. Vaporization of H_2O
2. N_2, H_2, and H_2O vapor
3. System radiation
4. Cathode gas

Only the first two have been calculated, since the amount of heat removed by other sources is not calculable without actual construction of a test module.

1. Heat Removed by Vaporization of Water

$$Q \text{ (vaporization)} = \Delta H \text{ (vaporization)} \left(\frac{\text{kcal}}{\text{g-mole}}\right)$$

$$\times \frac{\text{g}}{\text{hr}} (H_2O) \times 3.97 \left(\frac{\text{Btu}}{\text{kcal}}\right) \times \frac{1}{18} \left(\frac{\text{g-mole } H_2O}{\text{g } H_2O}\right)$$

In practice, the steam tables (Keenen and Keyes) were used.

2. Heat Removed from Heat Content of H_2O, N_2, and H_2 Gases

The rejection of N_2 (gas), H_2 (gas) and H_2O (vapor) at the operating temperature of the fuel cell to the ambient temperature of surroundings will remove:

$$Q_H = \quad CpdT \quad \text{in cal/g-mole}$$

The heat removal in Btu/hr are:

$$Q_{H_2O} = Q_H \frac{\text{cal}}{\text{mole}} \times \frac{\text{g } H_2O}{\text{hr}} \times \frac{1}{18} \frac{\text{mole } H_2O}{\text{g } H_2O} \times 0.00397 \frac{\text{Btu}}{\text{cal}}$$

for H_2 or N_2

$$Q_{N_2} = Q_H \frac{\text{cal}}{\text{mole}} \times \dot{M}_{N_2} \frac{\text{liter}}{\text{hr}} \times \frac{P}{RT} \left(\frac{\text{moles}}{\text{liter}}\right) \times 0.00397 \frac{\text{Btu}}{\text{cal}}$$

APPENDIX C

EFFICIENCY LIMITATIONS DUE TO FORMATION OF NITRIC ACID

Since all the product water of the electrochemical reaction is made and removed at the cathode, it is assumed that back diffusion of water vapor through the electrode causes all product water to be rejected as part of the cathode system.

However, N_2O_4 reacts with water to form HNO_3 and HNO_2 (ref. 2):

$$N_2O_4 + H_2O \longrightarrow HNO_3 + HNO_2 \qquad \text{in cold dilute solution}$$

$$3NO_2 + H_2O \longrightarrow 2HNO_3 + NO \qquad \text{in warm concentrated solution}$$

Either reaction can be reversed under favorable conditions.

At 25°C, the maximum concentration of HNO_3 with atmospheric pressures of N_2O_4 is about 60% (ref. 3). Above 20% HNO_3 virtually no HNO_2 is in solution.

A reasonable guess at the saturation level we will reach in the cathode water is ≈50% HNO_3 by weight.

From the amount of water produced per mole of N_2O_4 reacting, it is possible to calculate the amount of N_2O_4 used to saturate the water, and thus see the effect on the N_2O_4 efficiency.

$$\text{electrochemical-}N_2O_4 + 4H^+ \longrightarrow 2H_2O + 2NO + 4e^-$$

Thus, two moles (36 g) of water are produced per mole of N_2O_4 reacted.

Since the reaction

$$3NO_2 + H_2O \longrightarrow 2HNO_3 + NO$$

forms 2 moles of HNO_3 per mole of H_2O, and 50% HNO_3 results, the following is true:

y = g H_2O unreacted = g HNO_3 formed

$36-y$ = g H_2O reacted

$$y = (36-y)\ \frac{128\ g\ HNO_3}{18\ g\ H_2O}$$

$$y = 32\ g$$

Thus, 4 g of H_2O are reacted, or 0.22 Mole. Since 1.5 moles N_2O_4 are used per mole of water, 0.33 mole is wasted.

This then would limit the possible efficiency to $\frac{100}{1.33} = 75\%$.

However, this is the worst possible condition and 50% HNO_3 might not be formed in the dynamic case.

REFERENCES

1. J. C. Orth, Monthly Progress Report No. 7, "Study of Fuel Cells Using Storable Rocket Propellants", 1-30 November 1964, Monsanto Research Corporation, Boston Laboratory, Contract No. NAS3-4175, 10 December 1964.

2. Hildebrand and Powell, "Principles of Chemistry", Latimer and Hildebrand, "Reference Book of Inorganic Chemistry (combined volume) (1952), The MacMillan Co.

3. Yost and Russell, "Systematic Inorganic Chemistry" (1946), Prentice-Hall, Inc.

4. Bellanca, Salyer, Harris, "Evaluation of Elastomers as O-Ring Seals for Liquid Rocket Fuel and Oxidizer Systems", September 1963, Monsanto Research Corporation, Dayton, Ohio, Contract No. AF 33(616)-8483.

APPENDIX XI

SYSTEM DESIGN

1-KW N_2H_4-O_2 FUEL CELL SYSTEM

Contract No. NAS3-4175

10 November 1964

Submitted by:

MONSANTO RESEARCH CORPORATION
BOSTON LABORATORY
Everett, Massachusetts 02149

TABLE OF CONTENTS

LIST OF FIGURES

LIST OF TABLES

System Basis

For this design, dissolved hydrazine and gaseous oxygen were selected for fuel and oxidant. This selection was made because this system has been fully characterized in the execution of this contract and satisfactory life tests approaching one thousand hours have been performed. Fuel source selected was 100% hydrazine hydrate ($N_2H_4 \cdot H_2O$). Oxidant source was pure oxygen gas either from direct high pressure storage, cryogenic storage, or the decomposition of hydrogen peroxide (H_2O_2).

Design Procedure

Once fuel and oxidant were selected, a 3" x 3" test cell was constructed to present latest state-of-the-art. This cell was then characterized to obtain the basis for the system design.

Voltage-amperage curves at varying temperatures for this cell are shown in Figure 1 (70°C was selected as maximum steady-state operating temperature due to excessive loss of hydrazine - greater than approx. 1.5% - with the nitrogen exhaust above this point). From these data, a system having the specified performance was proposed and electrical performance calculated (Figure 2). Thermodynamic characteristics, reactant and product flow rates, and heat transfer requirements were then calculated for this system (Tables 1,2,3,4). Once the cell module configuration (electrode area and number of cells) was selected from the test cell results, the module construction was designed and weight calculated. The module construction was based on construction techniques used in previous Monsanto multi-cell test modules and on the electrodes and separator used in the test cell.

From these calculations of the characteristics of the basic module, the support system was designed and auxiliaries selected. The system was designed for operation at 25°C ambient temperature, atmospheric pressure and normal earth gravity, and mission time was selected at 8 hours. Conditions differing from these are discussed. Weights and volumes of auxiliaries are either catalog values or estimates from the literature and were selected for minimum weight and volume.

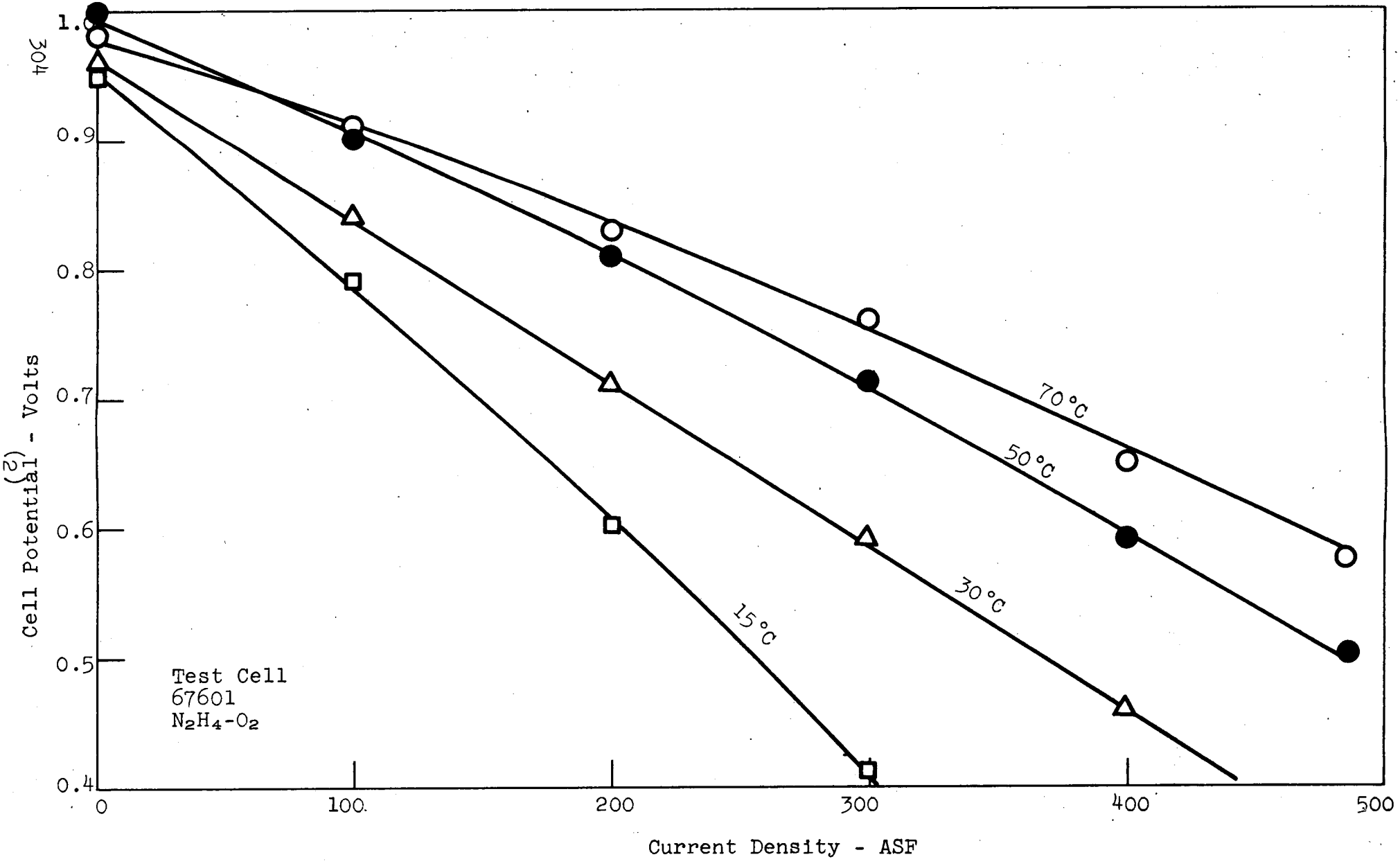

Figure 1. Single Cell Performance Curve

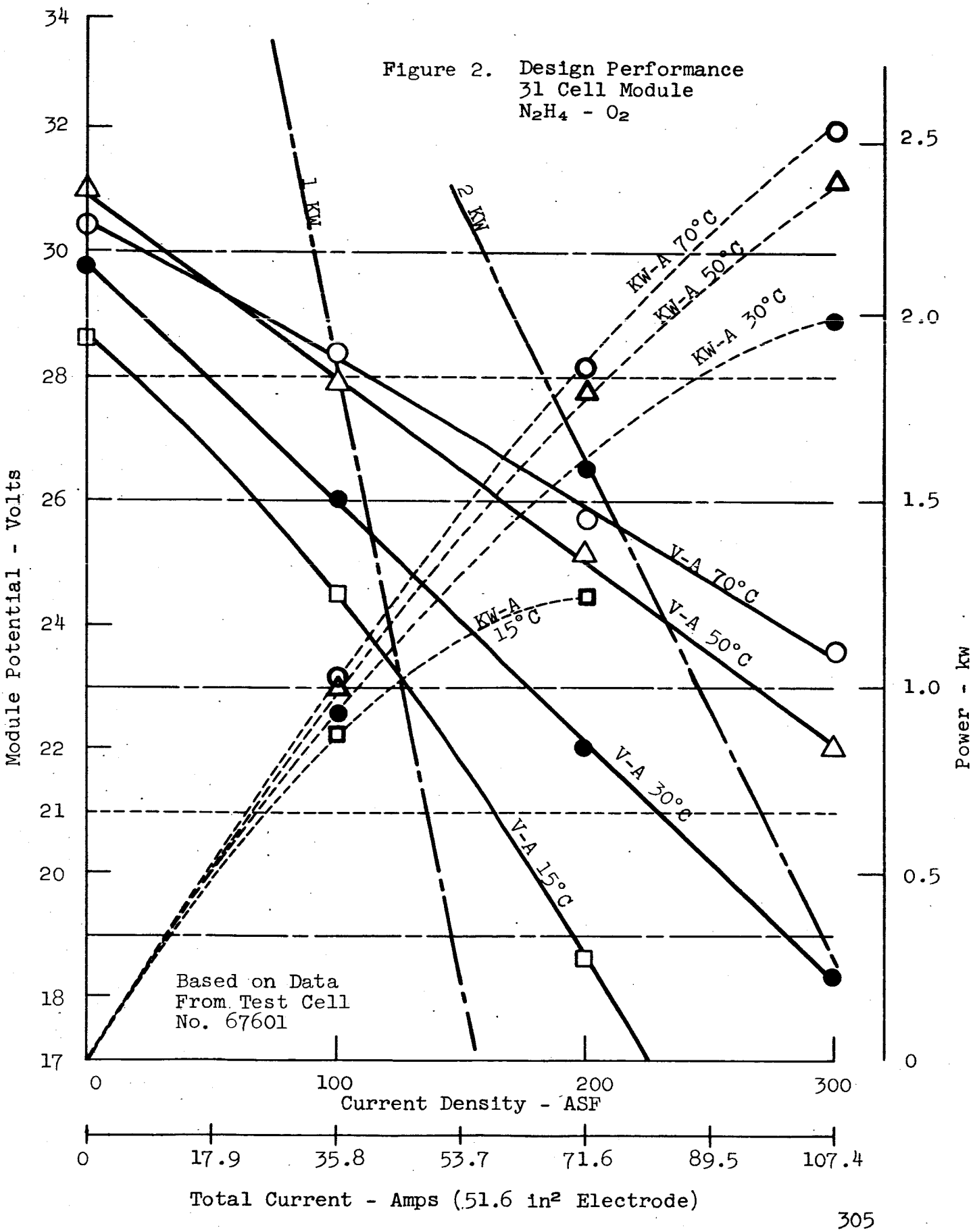
Figure 2. Design Performance
31 Cell Module
N_2H_4 - O_2
1 KW
2 KW
KW-A 70°C
KW-A 50°C
KW-A 30°C
KW-A 15°C
V-A 70°C
V-A 50°C
V-A 30°C
V-A 15°C
Based on Data
From Test Cell
No. 67601
Module Potential - Volts
Power - kw
Current Density - ASF
Total Current - Amps (51.6 in² Electrode)
34
32
30
28
26
24
22
21
20
18
17
2.5
2.0
1.5
1.0
0.5
0
0
100
200
300
0
17.9
35.8
53.7
71.6
89.5
107.4

305

Table 1

MASS AND ENERGY BALANCE TABULATIONS -15°C

$N_2H_{4_L} + O_{2_G} \longrightarrow 2H_2O_L + N_{2_G}$

Temperature 15°C

C° 1.612v ΔH° -148.63 Kcal/mole ΔS° +0.450 cal/gm-mole °K ΔF -148.76 Kcal/mole TΔS 129.69 cal/mole

		HEAT REJECTED		REACTANT AND PRODUCT RATES						HEAT REMOVED	
I ASF	E_{cell} Volts	Kcal g-mole	Btu/hr	N_2H_4* g/hr	O_2 Liters/hr	H_2O** g/hr	N_2 Liters/hr	System Output KW	H_2O Rej W/N_2 g/hr	H_2O sat N_2 Btu/hr	Radiator Btu/hr
50	0.876	67.77	1297.1	252.6	113.2	269.0	110.9	0.486	1.52		
100	0.790	75.65	2895.9	505.1	226.3	537.9	221.7	0.877	3.06		
150	0.695	84.42	4847.4	757.7	339.4	806.8	332.6	1.157	4.59		
200	0.60	93.19	7133.7	1010.2	452.6	1075.7	443.5	1.332	6.13		
250	0.51	101.51		1262.8	565.7	1344.7	554.4				
300	0.41	118.73		1515.4	678.9	1613.7	665.3				

*100% $N_2H_4 \cdot H_2O$
**inc. H_2O Hydrate

SYSTEM - 1 KW Nominal (100 ASF 70°C)

31 Cells 51.6 in.^{2} Electrodes

N_2H_4-O_2 Based on Test Cell No. 67601

(4)

Table 2

MASS AND ENERGY BALANCE TABULATION -30°C

Temperature 30°C

$N_2H_{4_L} + O_{2_G} \rightarrow 2H_2O_L + N_{2_G}$

E° 1.615$_L$ $\quad \Delta H^\circ$ -148.712 Kcal/mole $\quad \Delta S^\circ$ + 0.973 cal/g-mole °K $\quad \Delta F$ -149.007 Kcal/mole $\quad T\Delta S$ 295.01 cal/mole

		HEAT REJECTED		REACTANT AND PRODUCT RATES						HEAT REMOVED	
I ASF	Ecell Volts	Kcal g-mole	Btu/hr	N_2H_4* g/hr	O_2 Liters/hr	H_2O** g/hr	N_2 Liters/hr	System Output KW	H_2O Rej W/N_2 g/hr	H_2O sat N_2 Btu/hr	Radiator Btu/hr
50	0.90	65.72	1,257.9	252.6	113.2	269.0	110.9	0.497	3.89	9.8	
100	0.84	71.23	2,726.7	505.1	226.3	537.9	221.7	0.930	7.78	19.5	
150	0.77	77.79	4,466.7	757.7	339.4	806.8	332.6	1.29	11.67	29.3	
200	0.71	83.21	6,369.7	1010.2	452.6	1075.7	443.5	1.58	15.57	38.9	
250	0.65	88.82	8,500.1	1262.8	565.7	1344.7	554.4	1.81	19.46	48.8	
300	0.59	94.33	10,831.9	1515.4	678.9	1613.7	665.3	1.97	23.35	58.6	

* 100% $N_2H_4 \cdot H_2O$

** inc. H_2O Hydrate

SYSTEM - 1 KW Nominal (100 ASF 70°C)

31 cells 51.6 in.^{2} Electrodes

N_2H_4-O_2 Based on Test Cell No. 67601

Table 3

MASS AND ENERGY BALANCE TABULATIONS -50°C

Temperature 50°C

$N_2H_4{}_L + O_{2_G} \longrightarrow 2H_2O_L + N_{2_G}$

$E°$ 1.619$_L$ $\Delta H°$ -148.838 Kcal/mole $\Delta S°$ + 1.738 cal/gm mole ΔF -149.40 Kcal/mole $T\Delta S$ 561.72 cal/mole

		HEAT REJECTED		REACTANT AND PRODUCT RATES						HEAT REMOVED	
I ASF	E_{cell} Volts	Kcal/ g-mole	Btu/hr	N_2H_4* g/hr	O_2 Liters/hr	H_2O** g/hr	N_2 Liters/hr	System Output KW	H_2O Rej W/N_2 g/hr	H_2O sat N_2 Btu/hr	Radiator Btu/hr
50	0.94	62.19	1190.3	252.6	113.2	269.0	110.9	0.52	12.08	31.0	
100	0.90	65.92	2523.4	505.1	226.3	537.9	221.7	1.00	24.15	62.0	
150	0.85	70.41	4042.9	757.7	339.4	806.8	332.6	1.41	36.25	93.0	
200	0.81	74.14	5675.4	1010.2	452.6	1075.7	443.5	1.80	48.34	124.0	
250	0.76	78.77	7538.3	1262.8	565.7	1344.7	554.4	2.11	60.43	155.1	
300	0.71	80.41	9233.4	1515.4	678.9	1613.7	665.3	2.36	72.52	186.1	

*100% $N_2H_4 \cdot H_2O$
**inc. H_2O Hydrate

SYSTEM - 1 KW Nominal (100 ASF 70°C)

31 cells 51.6 in.^{2} Electrodes

N_2H_4-O_2 Based on Test Cell No. 67601

Table 4

MASS AND ENERGY BALANCE TABULATIONS -70°C

Temperature 70°C

$N_2H_{4_L} + O_{2_G} \longrightarrow 2H_2O_L + N_{2_G}$

E° 1.624 ΔH° -148.970 Kcal/mole ΔS° +2.571 cal/gm-mole °K ΔF -149.85 Kcal/mole TΔS 882.37 cal/mole

		HEAT REJECTED		REACTANT AND PRODUCT RATES						HEAT REMOVED	
I ASF	E_{cell} Volts	Kcal g-mole	Btu/hr	N_2H_4* g/hr	O_2 Liters/hr	H_2O** g/hr	N_2 Liters/hr	System Output KW	H_2O Rej W/N_2 g/hr	H_2O sat N_2 Btu/hr	Radiator Btu/hr
50	0.94	62.35	1193.4	252.6	113.2	269.0	110.9	0.521	40.37	98.55	1094.9
100	0.91	65.05	2507.3	505.1	226.3	537.9	221.7	1.01	80.70	197.0	2310.3
150	0.87	68.65	3941.9	757.7	339.4	806.8	332.6	1.45	121.07	295.5	3646.4
200	0.83	72.40	5542.2	1010.2	452.6	1075.7	443.5	1.84	161.4	394.0	5148.2
250	0.795	75.69	7243.5	1262.8	565.7	1344.7	554.4	2.21	201.8	492.6	6750.9
300	0.76	78.84	9053.1	1515.4	678.9	1613.7	665.3	2.53	242.2	591.2	8461.9

*100% $N_2H_4 \cdot H_2O$
**inc. H_2O Hydrate

SYSTEM - 1 KW Nominal (100 ASF 70°C)

31 Cells 51.6 in.^{2} Electrodes

N_2H_4-O_2 Based on Test Cell No. 67601

(T)

Proposed Module Performance

From the data obtained from the test cell (Figure 1), it was decided to operate the system at 70°C This dictated a 31 cell module having 51.6 sq. in. electrode area per cell to obtain 1 KW at 28 volts at 100 amp/ft^2 current density. The volt-amps curves for this module, based on test cell data, were then plotted in Figure 2. Power output in KW at the test temperatures was calculated and plotted against current. In addition, two lines were added crossing the V-A curves at the 1 and 2 KW points for clarity.

As can be seen from Figure 2, the voltage at 70°C and a power output of 2KW is 25.5 v. This voltage is in excess of the 2 KW design point of 21 $\pm$ 2 volts. It is felt that this is a desirable condition; however, if 21 volts is required at the 2 KW power level, a tap could be installed so that power would be drawn from less than the full 31 cells. In fact, the test cell data show that approximately 3 KW could be obtained at 21 volts. Figure 2 does not include allowance for power drawn by the supporting auxiliaries, pump 25 watts, fans 75 watts. This load would bring the operating voltage at 1 KW down to 28 v from 28.3 v. In the design of the cell construction, electrodes of 56 in.^{2} area were used. This 10% overage was included to allow for any decrease of performance with life and represents a safety factor.

Cell Construction

The module will be constructed in a single series bipolar arrangement. The proposed cell construction is shown in Figure 3. The bipolar plate will be a sheet of 0.010 nickel corrugated to provide flow channels for the anolyte and oxidant and to provide support for and electrical contact with the electrodes. A double manifold is provided for the anolyte in order to provide uniform flow. The anolyte enters from the heat exchanger through the two manifold passages at the bottom and exits with the produced nitrogen through the two passages at the top. Manifolding and electrode sealing is provided by the anode gasket of 0.060 ethylene-propylene rubber. The cathode gaskets seal the sides of the cathode cavity while leaving top and bottom open for gas flow. Corrugated inserts are used to aid in sealing across the O_2 inlet and exhaust.

This cell construction is virtually identical to that used at present in proprietary multi-cell modules undergoing test at Monsanto Research Corporation. The principal difference is that the proprietary cells use a flat bipolar plate with stainless steel screening to provide flow passages, electrode support, and electrical contact.

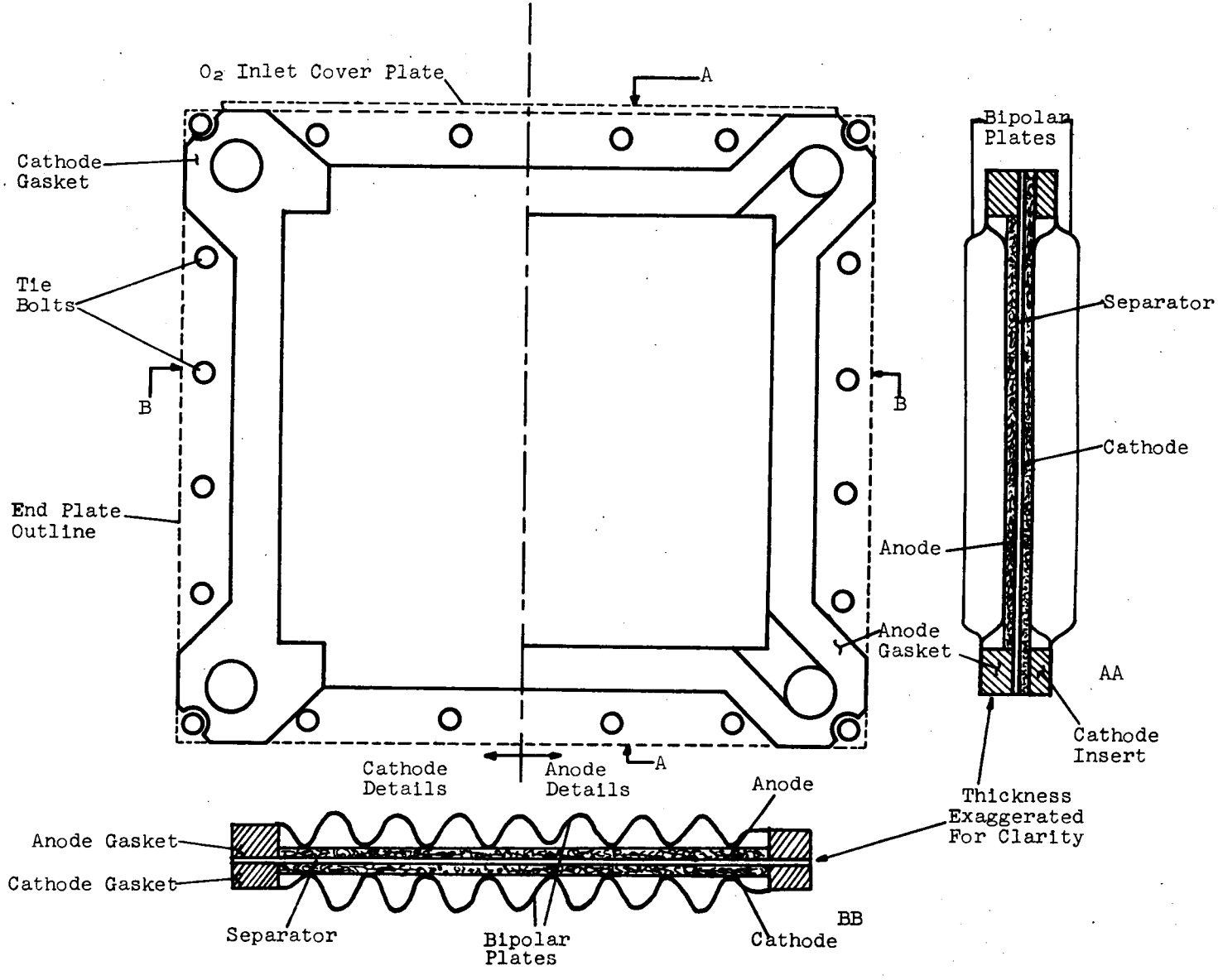

Figure 3. Cell Construction

System Configuration

A schematic diagram of the proposed system is shown in Figure 4. The anolyte enters the suction of the pump through a manual shut off valve from the bottom of the electrolyte tank. It then passes through the heat exchanger before entering the fuel cell module. The anolyte containing the produced nitrogen exits the cell and returns to the electrolyte tank where the nitrogen saturated with water vapor is then vented.

The 100% hydrazine hydrate fuel enters the system through a control valve at the inlet of the pump. The duty cycle of the fuel cell system determines the operation and control of the metering valve. For a constant cell output the valve would be a simple calibrated orifice and shut off valve. For an irregular duty cycle the valve could be controlled by monitoring the nitrogen production, hydrazine concentration in the anolyte, or electrical power consumed.

The oxygen enters the module at a pressure of approximately 1 in. H_2O and exits through a timer controlled purge valve. From experimental evidence it is felt that a one percent purge will be adequate for removal of inerts.

In Figure 4, a catalytic combustor for removal of any hydrazine vapor present in the exhaust nitrogen stream is shown dotted.

Figure 5 shows a phantom view of the proposed component placement. The electrolyte tank and module are arranged so that in the event of pump failure the electrolyte circulation will continue by gas lift from the produced nitrogen.

Weights and volumes of cell components, module and auxiliaries are listed in Table 5.

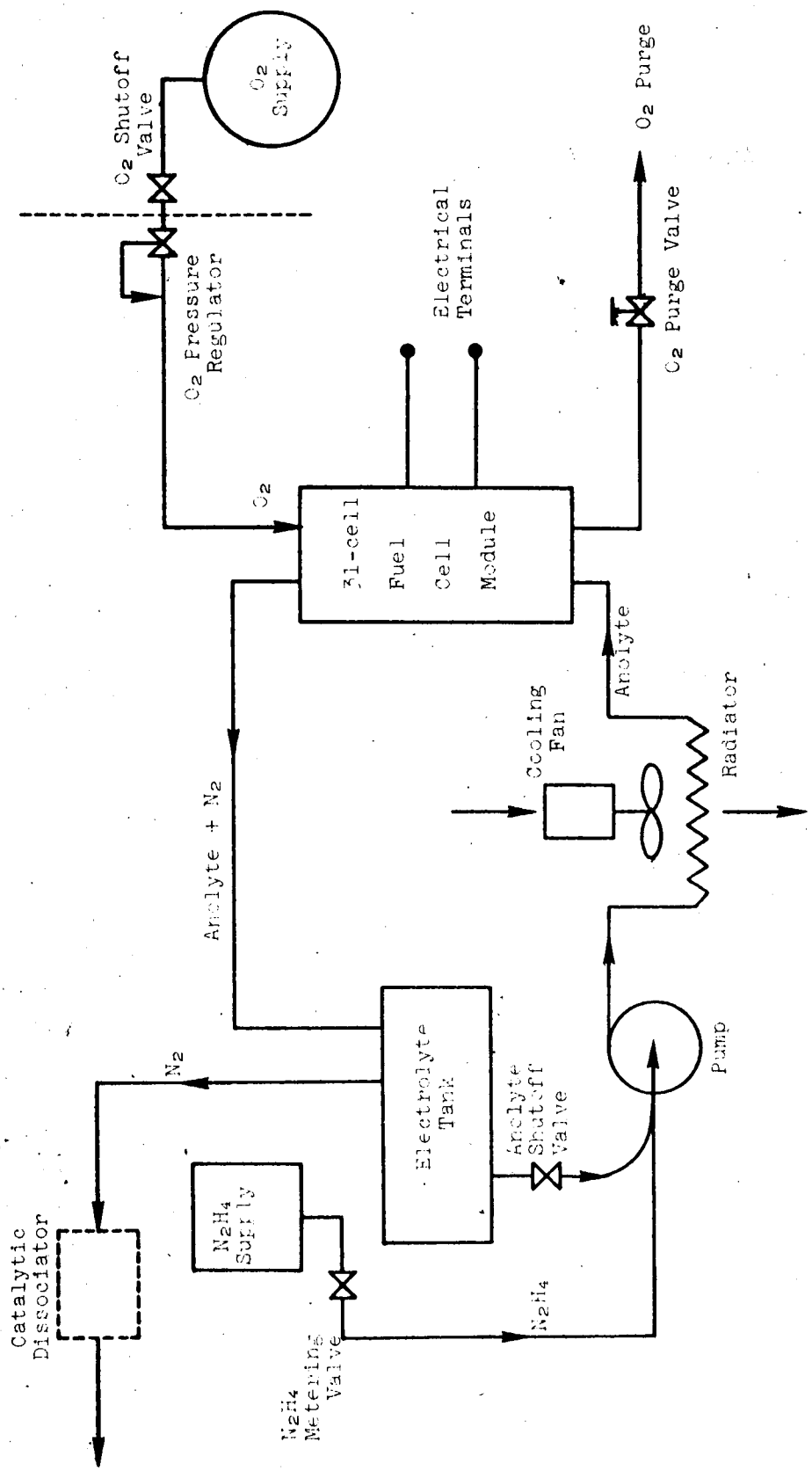

Figure 4. System Schematic

Table 5

Cell and Module Weight-Volume Compilation

Cell Component	Wt, g
Anode	19.5
Cathode with manifolding extensions	23.0
Bipolar plate 0.010 Ni	110.0
Anode gasket 1/16 in. EPR rubber	30.0
Cathode gaskets 1/16 in. EPR rubber (2)	15.0
Separator 0.005 polypropylene mat	3.30
Total Wt/Cell	200.80

Wt. 31 cells = 6224.8 g = 13.7 lb

End Plates (2) 11 1/4 x 10 1/4 in. Ni-Plated Mg	3.4 lb
Tie bolts	1.5 lb
Misc. insulators, etc.	≈1.0 lb
Total Module Wt	19.6 lb

Module Volume

(11 1/4 in.)(10 1/4 in.)(31 cells)/(7 cells/in.) = 511 $in.^3$ = .3 ft^3

Auxiliary Weights and Volumes	Weight lb	Volume ft^3
Electrolyte tank Hydrazine tank	3.1	.52
Pump	1.6	.05
Radiator and fans	5.2	.11
O_2 purge solenoid valve	.5	*
N_2H_4 solenoid valve	.5	*
Electrolyte shut off valve	.75	*
Piping and fittings	≈5.0	*
Support frame	≈5.0	*
Electrical components, leads controls etc.	≈5.0	*
Access space, tube and wire runaways etc.		.4
Total	26.65	1.08

Total System Wt ≈46 lbs

Total System Volume ≈1.3 ft^3

* Included in Access Space

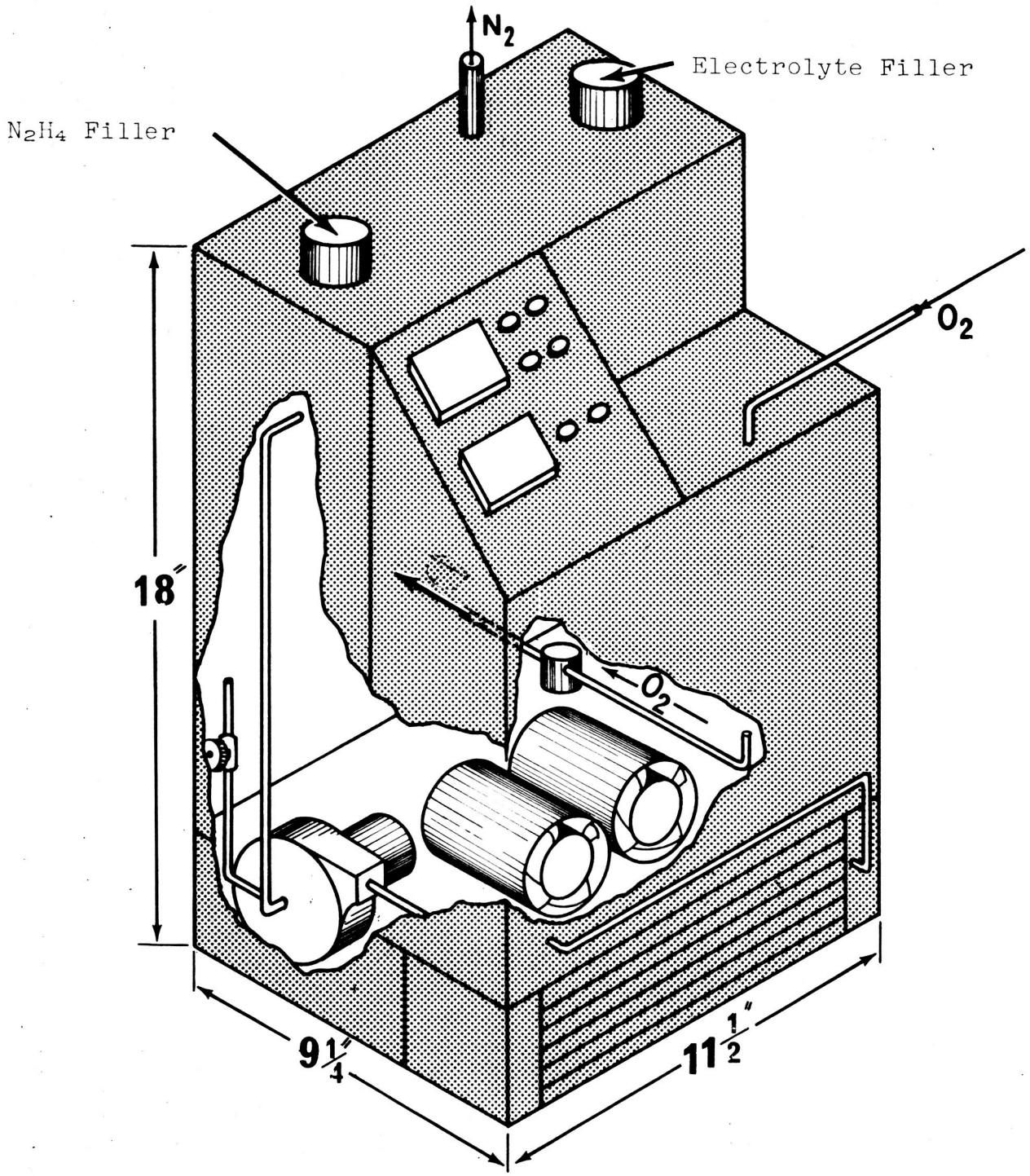

Figure 5. System Assembly

Material Balance for Eight-Hour Operation

An eight-hour mission was arbitrarily selected to provide basis for a sample material balance.

It must be emphasized that the basic fuel cell system is considered readily applicable to a wide variety of either terrestial or space mission times, each one requiring separate specification of tankage, waste gas and liquid treatment, operating temperature and oxygen source - depending on the exact mission requirements.

The material balance arrived at here, then, as well as system weights and volumes, do not represent an operational limit, but rather serve purely as one specific example.

Figure 6 schematically presents the system process design together with operating pressures, temperatures and flow rates. Stream compositions and an overall material balance are also given.

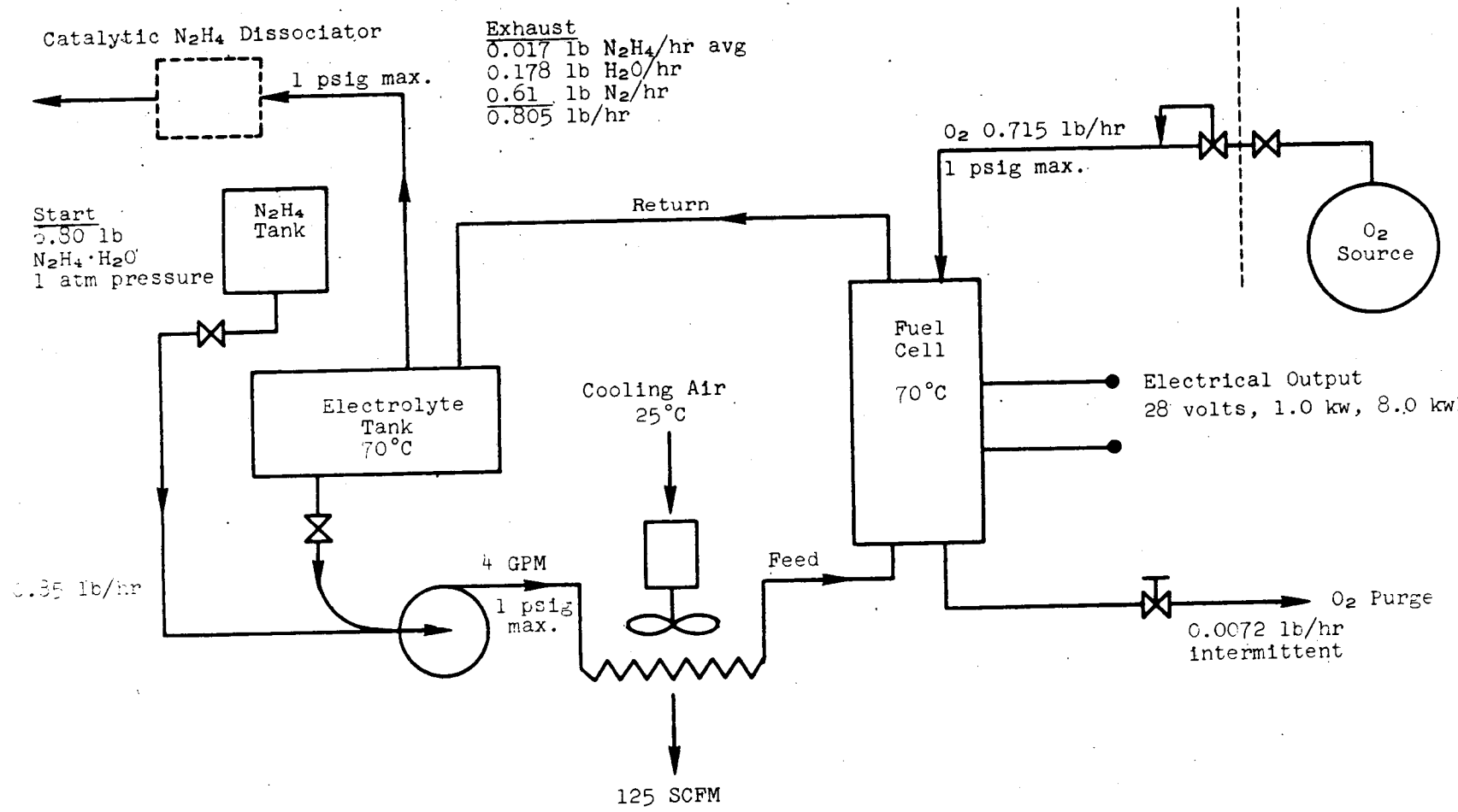

(16)

Electrolyte Tank

Start	Finish
8.0 lb H_2O	15.4 lb H_2O
2.85 lb KOH(≈26%)	2.85 lb KOH(≈15%)
1.93 lb N_2H_4(≈20%)	.58 lb N_2H_4(≈3%)
12.78 lb Total	18.83 lb Total

Overall Material Balance - 8 Hours

In:	$N_2H_4 \cdot H_2O$	6.80
	O_2	5.72
		12.52
Out + Accum:		
	Tank Exhaust	6.45
	O_2 Purge	.06
	Tank Accum.	6.05
		12.56

Figure 6. Material Balance for 8-Hour Run

Electrolyte and Fuel Tankage

Sizing of liquid tankage for this system is based on an 8 hour run at 70°C operating temperature.

The electrolyte tank is sized by assuming that at the end of 8 hours it will hold approximately 2 gal of liquid with a KOH concentration of about 15%, and a vapor space of 1/2 gal volume. Initially the tank will hold about 1.1 gal of liquid KOH, N_2H_4 and H_2O.

A cell and piping liquid internal volume of 0.44 gal was calculated, so that initially the electrolyte tank will hold 1.1-0.4 = 0.7 gal liquid. This will give an initial liquid turnover rate of 3.6 times contents per minute and decreasing to 2 times contents per minute at the finish, with the 4 GPM pumping rate.

Electrolyte tank internal volume, then, is 578 in^3.

Fuel tank is sized on the basis that the electrolyte tank will hold about 20% N_2H_4 at the start and will deplete to 3% N_2H_4 at the end of 8 hours. Based on the cell N_2H_4 consumption, the fuel tank will have to hold 6.8 lbs $N_2H_4.H_2O$, or about 0.8 gal. A 1 gal tank size was selected to allow a slight freeboard above the liquid.

Both electrolyte and fuel tank will be included in a single, 2 compartment tank of molded 1/8" thick polypropylene. Overall tank dimensions are 15.0 in x 11.5 in x 5.25 in or 0.514 ft^3 volume. Tank weight will be 3.1 lb.

Heat Exchanger Design

The heat exchanger was designed for the heat rejection rate required at the operating point, 70°C, 100 ASF (2310 Btu/hr). No allowance was made for radiation or convection losses from the system external to the heat exchanger. This, in effect, provides a safety factor above that used in the calculations.

For the design, a staggered, multitube heat exchanger was selected, a cooling air flow was assumed at 125 SCFM, and the anolyte pumping rate was 4 gpm. A trial and error solution using empirical equations for the film coefficients was then performed. The design indicated a 20 tube unit with 1/4 in. nominal diameter nickel tubes of 0.010 wall thickness stacked in three rows, 7-6-7, with 0.2 in. spacing between tubes in each row.

Two Globe Industries VAX-3-BD blowers were selected to provide cooling air. These will be controlled by a thermostat in the electrolyte tank.

Water Removal and Recovery of Product Water

The system as proposed thus far is designed about an eight hour mission time with accumulation of product water in excess of that removed by the nitrogen exhaust. In some cases continuous operation with only the addition of fuel would be required. To accomplish this, several methods of water removal may be proposed.

The simplest method would be to operate the system at a temperature where the water produced in the reaction and the water removed in the nitrogen stream balance. For normal atmospheric pressure this temperature is 198°F for hydrazine hydrate as fuel and 196.5°F for hydrazine.

If the system were operating in a vacuum environment a pressure regulator could be used to maintain the electrolyte tank at the vapor pressure of the anolyte of the desired concentration. With this system the product water would cause the vapor pressure to increase and the water would vaporize and exhaust through the regulator.

Other possible systems would include the recirculation of some of the product nitrogen continuously through the electrolyte tank and an external condenser and the use of the heat rejected by the hydrogen peroxide decomposer to evaporate the water.

In all systems proposed the water could be recovered from exhaust gas streams, where desired, by conventional condensation techniques. This recovery of product water is complicated by the fact that all gas streams will contain some small percentage of N_2H_4 vapor (N_2H_4 vapor pressure only slightly greater than water) as a contaminant, and conedensation techniques will result in co-sequestering of both N_2H_4 and H_2O in the same liquid phase.

Perhaps the simplest way to handle the N_2H_4 contamination problem is to catalytically dissociate the N_2H_4 vapor before the exhaust gas stream passes to the condenser.

Other approaches which could be investigated are fractional distillation, ion exchange processes, catalytic combustion, absorption or chemical scrubbing.

Zero Gravity Operation

The principal problem associated with this fuel cell system in adapting it for a zero gravity environment is the separation of the gaseous product nitrogen from the liquid anolyte. Several solutions to this problem are possible.

1. Certain space missions necessarily involve maintenance of artificial gravity, for personnel manned compartments. In cases of this type the fuel cell with or without tankage or at least the phase separation portion of the fuel cell system could be operated under the artificial gravity conditions.

2. Phase separation in rotating centrifugal machines offers some advantage. Here the gas laden exit stream from the fuel cell is pumped to the powered centrifugal separator. The underflow liquid phase enters the primary electrolyte pump suction and is forced into an accumulator type electrolyte tank. Effectively then, the electrolyte pump is placed before the electrolyte tank and the entire fuel cell system is internally pressurized on the liquid side.

3. Use of semi-permeable membranes has frequently been suggested as a means of zero gravity phase separation. This idea is equally applicable to a bulk liquid phase fuel cell system such as the N_2H_4 system as it is to all gas phase systems, e.g. H_2/O_2.

The MRD cathodes employed in our fuel cells are semi permeable and possess excellent mechanical properties when supported on a screen grid. Special formulations of this electrode for use purely as a semi permeable membrane are possible, and it is believed that effective control of both pore size and distribution and hydrophobic properties can be obtained. We have also had experience with various types of porous Teflon materials, which appear adaptable to this service.

A semi-permeable membrane approach could be particularly attractive for this N_2H_4 system because of the very low operating pressures required, thus simplifying construction and reducing weight of the phase separator device.

Appendix A

Oxygen Generation from Hydrogen Peroxide

Oxygen for this fuel cell system in either space or terrestial applications can be supplied by the catalytic decomposition of storable hydrogen peroxide (H_2O_2).

Extensive technology exists in the design and manufacture of H_2O_2 catalytic generator systems which is readily adaptable to production of a unit to satisfy this fuel cell design. This technology is available both within NASA (e.g. NASA Technical Note, D-480, October 1960, on H_2O_2 catalytic reaction control rockets) and from H_2O_2 manufacturers, such as Becco Chemical Division, Food Machinery and Chemical Corporation, New York. No attempt will be made here to specify a design for the oxygen generation system. Production rates and conditions and expected thermal output of the generator are tabulated below.

For the purposes of this evaluation it is assumed that 98% H_2O_2 will be used. For an 8 hour duty cycle, then, a total of 12.4 lbs of H_2O_2 will be required to produce oxygen enough to operate at 100 ASF, 70°F, with a 1% purge rate.

Table A-1 Reactant, Product and Thermal Rates for Oxygen Generator

Gross Fuel Cell System Electrical Output at 70°C (kw)	O_2 Rate (lb/hr)	98% H_2O_2 Rate (lb/hr)	Heat Rate (btu/hr)	H_2O Production (lb/hr)
0.52 (50 ASF)	0.36	.78	940	0.42
1.01 (100 ASF)	0.72	1.55	1880	0.83
1.45 (150 ASF)	1.08	2.32	2820	1.24
1.84 (200 ASF)	1.44	3.10	3760	1.66
2.21 (250 ASF)	1.80	3.87	4700	2.07
2.53 (300 ASF)	2.16	4.65	5650	2.49

O_2 Delivery Pressure - 1 psig max
O_2 Delivery Temperature - 70°C Saturated max.

Evaluations of direct H_2O_2 utilization in this type fuel cell have been made and the performance obtained has corresponded approximately to that of O_2 usage, indicating that no electrochemical advantage is gained from the use of H_2O_2. Further, spontaneous decomposition of peroxide in the cell and consequent loss of unreacted O_2 by venting are prohibitively large. Changes in the cathode catalyst system would be required to correct this.

From the standpoint of heat and water balance, it appears that the separate peroxide decomposer is the most favorable approach.

The heat of H_2O_2 decomposition, 1880 btu/hr at system design point, could be used in a compact cell water removal system. In this system a heat exchange between hot decomposer gases and a portion of the electrolyte stream, with an electrolyte-water vapor phase separator, could effect re-concentration of electrolyte and partial cooling of H_2O_2 decomposition products.

APPENDIX B

MASS AND ENERGY BALANCE CALCULATIONS

Operating Conditions: 1 kw (nominal) N_2H_4-O_2 Fuel Cell System.

The tabulation of mass and energy balance (Tables 1 to 4) were calculated from the experimental voltage, current and power curves (Figure I) and from the thermodynamic data for the Fuel Cell reaction and chemical species (N_2H_4, H_2O, N_2, O_2) involved. The following section shows the approach used for these calculations.

A. MASS RATES FOR REACTANTS AND PRODUCTS AND BALANCE

1. N_2H_4

In calculating the N_2H_4 mass rate a current effeciency of 98% was assumed. The calculation is:

$$\dot{M}_{N_2H_4} \text{ (mass flow rate in g/hr)} = \left(\frac{I \times 3600 \times Mwt}{nF}\right) \frac{100}{98}$$

where I = total current of module
= current density (ASF) x area in ft^2

Mwt = gram molecular weight

n = number of gram equivalents/gram mole = 4 for N_2H_4

F = Faraday's number = 96,500 coul/gram equivalent

The combination of (I x 3600) giving coulombs/hr. Thus, the mass rate is tabulated for total currents.

2. Oxygen

The conditions for oxygen include 100% current efficiency and a 1% purge rate. The calculation is:

$$\dot{M}_{O_2} \text{ (mass flow rate in liters/hr)} = \left(\frac{I \times 3600}{nF}\right) \frac{\text{mole}}{\text{hour}} \times \left(\frac{RT}{P}\right) \frac{\text{liter}}{\text{mole}} \times \frac{101}{100}$$

where R = gas constant = .082 atm-liter/°K mole

T = standard temperature in °K

P = standard pressure in atm

Note that the mass flow rate is tabulated for standard temperature and pressure, and not for operating conditions.

3. H_2O and N_2

These calculations are of the same type as for N_2H_4 and O_2.

For N_2, 100% current efficiency was assumed and mass flow rate is at STP.

For H_2O the fact that N_2H_4 is added as 100% $N_2H_4 \cdot H_2O$ must be taken into account.

B. CALCULATION OF THE THERMODYNAMIC QUANTITIES E°, ΔF°, ΔH°, ΔS°, $T\Delta S^\circ$ FOR THE CELL REACTION AT DIFFERENT TEMPERATURES

$$\text{Reaction: } N_2H_4(L) + O_2(g) \longrightarrow 2H_2O(L) + N_2(g)$$

1. ΔH°_T

ΔH°_T was calculated from the ΔH°_f at the various temperatures used.

$$\Delta H^\circ_{T(\text{reaction})} = \Delta H^\circ_{f(N_2)(g)} + 2\Delta H^\circ_{f(H_2O)(L)} - \Delta H^\circ_{f(N_2H_4)(L)} - \Delta H^\circ_{f(O_2)(g)}$$

where ΔH°_f is the free energy of formation at that temperature in kcal/g mole.

The ΔH°_f for $N_2H_4(L)$ for any temperature was calculated from the known ΔH°_f at 298°K and the heat capacity as a function of temperature.

$$\Delta H^\circ_{fT} = \Delta H^\circ_{f\ 298^\circ K} + \int_{T_o}^{T_1} C_p dT$$

The ΔH°_f for $H_2O(L)$ was interpolated from tabulated data.

2. ΔS°

ΔS° reaction for any temperature was calculated from the entropies of the reactants at the various temperatures.

$$\Delta S^\circ_{(\text{reaction})} = S^\circ_{(N_2)} + 2S^\circ_{(H_2O)(L)} - S^\circ_{(N_2H_4)(L)} - S^\circ_{(O_2)(g)}$$

where ΔS° is in cal/g mole.

Again for $H_2O(L)$ the entropies were interpolated from tabulated data.

For $N_2(g)$, $O_2(g)$, and $N_2H_4(L)$ the entropies at various temperatures were calculated from values at 298°K and heat capacity functions.

$$S^\circ_T = S^\circ_{298} + \int_{T_0}^{T_1} \frac{C_p}{T} dT$$

3. ΔF° and ΔS°

ΔF° reaction is calculated from the values of ΔH° reaction and ΔS° reaction from the previous section.

ΔF° reaction = ΔH° reaction - TΔS° reaction for the temperature in question.

4. E°

The theoretical potential for the reaction (E°) is:

$$E^\circ = \frac{-\Delta F^\circ (\text{reaction})}{nF}$$

where $\Delta F^\circ_{(\text{reaction})}$ is expressed in joules,

n = g equivalent/g mole,

F = 96,500 coul/equivalent

C. FUEL CELL HEAT REJECTION

The amount of heat rejection of the cell is equal to the sum of the TΔS term and the irreversible terms. In general:

$$Q = \text{heat rejection, } \left(\frac{\text{kcal}}{\text{g mole of } N_2H_4 \text{ reacting}}\right)$$

$$= \left(1 - \frac{E_T}{E^\circ}\right) \Delta F_{(\text{reaction})} + T\Delta S_{(\text{reaction})}$$

for each temperature and current in tabulation.

where E_T = operating voltage of one cell,

and E° = theoretical reversible voltage of one cell.

For the 31-cell module, the rate of heat rejection per hour:

$$\text{heat rejection (btu/hr)} = Q\left(\frac{\text{kcal}}{\text{g mole } N_2H_4}\right)$$

$$\times \left(\frac{I \times 3600}{nF}\right) \frac{\text{g mole } N_2H_4}{\text{hr}} \times 3.97 \text{ btu/kcal}$$

D. H_2O VAPOR REMOVED BY N_2

The total pressure above the reservoir tank is 14.7 psia or 1 atm. The total pressure = $P_{H_2O} + P_{N_2}$. Thus, knowing the vapor pressure of water at various temperatures, the ratio of:

$$\frac{\text{moles } H_2O}{\text{moles } N_2} = \frac{P_{H_2O}}{1-P_{H_2O}} = \frac{XH_2O}{XN_2}$$

where P_{H_2O} is the vapor pressure of water in atm and

X is the mole fraction.

Thus, knowing the mole fractions of N_2 and H_2O present, the number of moles of H_2O/liter N_2 can be calculated.

$$\frac{\text{g } H_2O}{\text{liter } N_2} = \left(\frac{P}{RT}\right) \frac{\text{moles } N_2}{\text{liter } N_2} \times \left(\frac{X_{H_2O}}{X_{N_2}}\right) \frac{\text{moles } H_2O}{\text{moles } N_2} \times 18 \frac{\text{g}}{\text{moles } H_2O}$$

where P is in atm

R = .082 atm liter/°K mole

T = °K

X_{H_2O} = mole fraction H_2O

X_{N_2} = mole fraction N_2

This figure, times the mass flow rate for $N_2(\dot{M}_{N_2})$ will give the g/hr H_2O rejected.

E. HEAT REMOVED FROM SYSTEM

Heat removal will occur through a number of routes including: the heat carried out by N_2 and water vapor, the heat of vaporization of the water removed, and the heat removed through the system radiation.

1. Heat Removed by Vaporization of Water

$\Delta H_{(vaporization)}$ of H_2O which saturates the N_2 exit gas will remove:

$$Q_{(vaporization)} = \Delta H_{(vaporization)} \left(\frac{kcal}{mole}\right) \times \frac{g}{hr} (H_2O)$$

$$\times 3.97 \text{ btu/kcal} \times \frac{1}{18} \frac{\text{mole } H_2O}{\text{g } H_2O}$$

This gives $Q_{(vaporization)}$ in btu/hr.

2. Heat Removed from Heat Content of H_2O Vapor and N_2 Gas

The rejection of N_2 (gas) and H_2O (vapor) at the operating temperature of the fuel cell to the ambient temperature of surroundings will remove:

$$Q_H = \int_{T_o}^{T_1} CpdT$$

where Q_H is in cal/mole.

For H_2O,

$$Q_H\left(\frac{btu}{hr}\right) = Q_H\left(\frac{cal}{mole}\right) \times \frac{\text{g } H_2O \text{ vapor}}{hr} \times \frac{1}{18} \frac{\text{mole } H_2O}{\text{g } H_2O} \times 0.00397 \text{ btu/cal}$$

For N_2,

$$Q_H\left(\frac{btu}{hr}\right) = Q_H\left(\frac{cal}{mole}\right) \times \frac{\text{liters } N_2}{hr} \times \left(\frac{P}{RT}\right)\frac{\text{moles}}{\text{liter}} \times 0.00397 \text{ btu/cal}$$

where the value of liters N_2/hr is at STP,

thus $\left(\frac{P}{RT}\right)$ also is at STP.

$Q_{(vaporization)} + Q_H$ are listed together in the tabulation as heat removal by H_2O sat. N_2.

3. Heat Removed by Radiator

The heat removed by the radiator is the heat necessary to complete the overall heat balance between the heat rejected (i.e., formed) by the fuel cell, and the heat removed by the water vapor and N_2 (gas). Since the actual expected operating temperature of this system is 70°C, the radiator is designed to meet the requirements of the system at this temperature.

SUMMARY

This report describes work undertaken to develop fuel cell systems operating on storable rocket propellants as reactants. The following reactants are of interest in this work:

(a) hydrazine, cryogenic H_2, and H_2-rich reformer gases as fuels; and

(b) cryogenic O_2, HNO_3, N_2O_4, H_2O_2, and ClF_3 as oxidizers.

Electrodes have been developed and demonstrated in a number of different systems for each reactant. Hydrazine has been extensively used as a dissolved fuel in strong caustic with a Pd-catalyzed, porous nickel plaque anode. Hydrazine fuel has also been used with an MRD-A Pt electrode (a thin, screen-supported membrane electrode developed at MRC) in strong acid electrolytes.

Hydrogen gas has been demonstrated as a fuel in both acid and alkaline electrolytes with the MRD-A Pt electrode. Both H_2 and N_2H_4 were successfully used with a special Pd-25%Ag hydrogen diffusion anode.

The MRD-C carbon/Pt electrode has been used extensively in this work as an O_2 electrode in alkaline electrolytes, and its activity with acid electrolytes and with H_2O_2 as the oxidant has been confirmed. The best electrode developed for HNO_3 or N_2O_4 oxidizer was a double MRD-C carbon electrode (no Pt). Both solution cathodes (porous carbon or Pt screen) and porous Teflon vapor diffusion electrodes were investigated for this application.

Four full cell systems were investigated. For the $N_2H_4/KOH/O_2$ cell, the hydrazine was used as a dissolved fuel in the KOH electrolyte. A porous nickel plaque anode, asbestos separator, MRD-C carbon/Pt cathode were used with this cell. Over 2285 hours of life at 100 ma/cm^2, 25°C, was obtained with a cell voltage of 0.6-0.7 v. Oxygen at atmospheric pressure was used with only a slight purge.

For the $N_2H_4/H_3PO_4/N_2O_4$ cell a flow-through MRD-A Pt anode, silica-gel/H_3PO_4 separator, and double MRD-C carbon cathode were used. The N_2H_4 fuel was dissolved in the H_3PO_4 electrolyte. Cell voltages of 0.65-0.74 v were realized for over 645 hours at 100 ma/cm^2, 60°C.

In the N_2H_4/ion exchange membrane/HNO_3 cell, both the fuel and oxidant were dissolved in H_3PO_4 electrolyte. Carbon block cathodes and flow-through MRD-A anodes were used with a cation exchange membrane. This system was operated for 30 hours at 100 ma/cm^2, 60°C, with a potential of about 0.5 v. The increased

polarization was due to IR losses through the membrane. The use of an acid/base cell with an ion exchange membrane was investigated but not found to be promising.

The $ClF_3/HF(KF)/H_2$ system was demonstrated as an unoptimized full cell. However, materials problems prevented complete cell testing.

The most promising results were obtained with the $N_2H_4/KOH/O_2$ and $N_2H_4/H_3PO_4/N_2O_4$ systems, and system designs for 1-kw units were developed for these cells. For the alkaline-O_2 cell system, weight and volume are 45 lb and 1.3 ft^3, respectively, for 1 kw. The corresponding figures for the acid-N_2O_4 cell are 67 lb and 1.3 ft^3.

The feasibility of steam reforming unsymmetrical dimethylhydrazine and monomethylhydrazine, both potential storable propellants, has been demonstrated. A gas stream containing approximately 42 mole-% H_2 was obtained used MMH-H_2O feed stock and precious metal catalysts.